Mathematical modelling of epithelium homeostasis

Elisa Domínguez Hüttinger

DEPARTMENT OF BIOENGINEERING,
IMPERIAL COLLEGE LONDON

Supervisors: Reiko J Tanaka and Mauricio Barahona

May 27, 2015

Submitted in partial fulfilment of the requirements for the degree of Doctor of Philosophy and the Diploma of Imperial College London

Abstract

The body and organs of all animals are covered by epithelial tissues, such as the epidermis and the airway epithelium. Epithelial tissues play a key role in protecting the body from environmental aggressors. Failure to maintain a competent epithelium can lead to the onset of many diseases, including Atopic dermatitis (AD) and infection by *Streptococcus pneumoniae*. Treatment of AD is currently restricted to the relief of symptoms, mainly because the underlying mechanisms remain elusive. Antibiotic resistance threatens the effectiveness of the prevalent treatments for infection. Devising new and effective therapeutic strategies that halt the progression of these diseases requires an understanding of the different disease mechanisms that can cause loss of epithelial homeostasis in different patients. Intricate regulatory networks of several biochemical and cellular interactions maintain epithelium homeostasis in healthy individuals, but can also propagate different disturbances, resulting in a wide spectrum of possible disease phenotypes. In this thesis, we propose mathematical models of these regulatory networks to analyse the mechanisms that lead to the onset and progression of AD and pneumococcal infection from a systems-level perspective. Our mathematical model of AD reproduced, for the first time, the different stages of the disease that have been observed in the clinic. Moreover, we proposed different pathogenic mechanisms, triggered by different genetic and environmental risk factors that are known to predispose to AD. By assessing the effects of common treatments for AD, we suggested effective treatment strategies that can prevent the aggravation of the disease, in a patient-specific way. Our data-driven mathematical model of pneumococcal infection identified four qualitatively different mechanisms by which co-infection can drive the pathogenic process. They can be counteracted by distinctive treatment strategies that only partially involve antibiotics. Our work provides a theoretical framework for the integration and analysis of clinical and experimental data describing epithelial homeostasis.

Contents

List of Figures

List of Tables

Statement of Originality

This thesis and the research that is here presented, are product of my own work. Any ideas from the work of other people are fully acknowledged and appropriately referenced.

Elisa Domínguez Hüttinger
Department of Bioengineering
Imperial College London

Copyright Declaration

This thesis is dedicated to my parents,
Christine Hüttinger and Raúl Domínguez Martínez.
We are a family of story-tellers.
The language of this narrative is mathematics,
its subject, biology,
and the plot, a process.

Acknowledgements

I would like to express my most sincere gratitude and admiration to my supervisor, Dr Reiko J Tanaka, for her constant support, motivation, guidance, encouragement and commitment during this research project. It has been a privilege and pleasure to have been part of this process.

To my co-supervisor, Prof Mauricio Barahona (Department of Mathematics, Imperial College London) for his support, fruitful discussions and fundamental inputs to this research.

To my collaborators: Dr Masahiro Ono (University College London), Dr Georgios Stamatas (Johnson and Johnson), Dr Thomas B Clarke (Department of Medicine, Imperial College London), Dr Mariko Okada (RIKEN), Prof Alan Irvine (Trinity College Dublin), Dr Diego Oyarzún (Department of Mathematics, Imperial College), Dr Alejandro Colman-Lerner (Universidad de Buenos Aires), Dr Marina Macías-Silva (Universidad Nacional Autónoma de México) and Dr Yuzuru Sato (visiting researcher at Imperial College London), for enriching this research with their knowledge and expertise.
To William Nightingale and George Buckle, for their interest, motivation and valuable inputs to this research project.
To all my colleagues from the Biological Control Systems Lab., particularly to the members of the ”epithelium-team”, Panayiotis Christodoulides, Mark van Logtestijn, Dr Neville J Boon and Matthias Malagó. It has been a real pleasure to work with you guys! Also to Alejandro Adrián Granados Castro and to Sang Y Lee for very insightful discussions. Thanks also to past members of the group, particularly to Dr Andrea Y Weiße and to Dr Paula Freire-Pritchett.
I am thankful for advice and discussions with Dr Heather Harrington, Dr Mariano Beguerisse Diaz, Dr Michael Schaub, Dr Borislav Vangelov, Dr Claire Higgings, Dr Martina Wicklein, Dr Kit Longden (Janela Research Campus), Dr Osbaldo Resendis Antonio (INMEGEN), Dr Juan Carlos Martínez García (Cinvestav) and Dr María Elena Álvarez-Buylla (UNAM).
I am grateful for the support provided by my mentor, Dr Emmanuel Drakakis.

This thesis benefited strongly from the insightful comments and discussions with my examiners, Dr Stan Marée (John Innes Centre) and Dr Krishnan (Department of Chemical Engineering, Imperial College London).

The constant support and love from my family have been vital for accomplishing this task. Thanks to all the members of my ”family - sets”: Hüttinger (Christine, Helmut, Alexander, Ariane, Carolina, Julia, Gabriel, Paul, Angie and Pao), Domínguez (Raúl, Malú, Pepe, Mariana, Gabriela, Alejandro and Lulú) and Kronberger (Michi, Anna, Matilda and Maciej).

I want to thank my family in London: Alonso Castillo Ramírez (a.k.a. the ”real” Uri Alon), Daniela Franco Bodek (my official guru), Maria Fernanda Jiménez Sólomon (Sra M.F. - my big sister!) -for being my family in London.

Thanks to my ”fellow-expats” Lorena Segura Morán and Olga Beatriz Zurita Rendón, for all the ”cronopian” adventures that gave me a burst in life, energy and motivation throughout this process.
I want to express my appreciation to my friend Victor Hugo Jiménez Sánchez for being on my side all these years. To Elena Phoka, Dan Cook and Aleksandra Berditchevskaia for all the sunny moments that illuminated this research project. To Pável Hernández Ramírez, for all the motivation and encouragement. To Edgar Salomón García Treviño, for promoting a lyrical view of engineering research.

I am very grateful to Filotheos Bezerianos, who supported me enormously during a substantial part of these years.

I want to give a special thanks to Léna Tanaka-Jammes, who motivated the beginning of this research project.

This work was founded by CONACyT (scholarship 212800) and supported by a EPSRC grant (through a Career Acceleration Fellowship to Reiko J Tanaka) and by the Santander Mobility Award 2013.

Acronyms and terminology

AD Atopic dermatitis.

AJ Adherens Junctions.

AMP Anti-Microbial Peptide.

BALF Broncheo-alveolar lavage fluid.

BD-2 β-defensin (type of AMP).

CDS Corneodesmosome (intercellular junction between corneocytes).

CFU Colony Forming Units.

DC Dendritic cell.

DDE Delay Differential Equations.

HAE Human Airway Epithelial cell culture.

HBE Human Broncheal Epithelial cell culture.

IBD Inflammatory Bowel Disease.

IL-1 Interleukin 1.

KLK Kallikrein (a protease).

NHEK Normal Human Epidermal Keratinocytes.

OD Optical Density.

PAMP Pathogen-Associated Molecular Pattern.

PAR2 Protease-activated Receptor.

PPI Protein-Protein Interactions.

PWA Piecewise Affine Function.

QSSA Quasi-steady state approach.

RHE Reconstructed Human Epidermis.

SC Stratum corneum.

SG Stratum Granulosum.

SNP Single Nucleotide Polymorphism.

T84 Human Colonic adenocarcinoma cell line.

TEER Trans-Epithelial Electrical Resistance (directly related to permeability barrier function of epithelial monolayers).

TEWL Trans-Epidermal Water Loss (inversely related to epidermal permeability barrier function).

TF Transcription Factor.

TJ Tight Junctions.

TLR Toll-Like Receptor (Innate immune response receptor).

TSLP Thymic Stromal Lympho-Poietin.

Chapter 1

Introduction

The body and the organs of all animals are covered by a tissue type termed epithelium [1]. For example, the outermost layer of the skin is enacted by the epithelial tissue called epidermis, and the respiratory tract is covered by airway epithelium [1]. Being directly in contact with the environment, one of the main functions of the epithelium is to regulate the exchange of substances between the self and the environment [2]. It plays a pivotal role in protecting the body from environmental aggressors, such as pathogens or chemicals, and also mediates the exchange of water and nutrients [1].

Accordingly, loss of epidermal function is associated to a wide variety of diseases, including infection [3, 4, 5, 6], allergies [7, 8, 1, 9, 10, 11, 12, 13], and cancer [14, 15]. Despite the high prevalence of these diseases [16, 17, 18, 19, 20, 18, 21, 22], the different mechanisms that can cause many of them have not yet been clarified, hindering the effectiveness of treatment and preventive strategies [23, 24, 25, 12].

The epithelium protects against environmental aggressors by two means: First, it enacts a physical permeability barrier that hinders the penetration of external substances. Second, epithelial cells are able to mount immune responses that eradicate environmental aggressors that have infiltrated through the epithelial barrier [14].

Interestingly, while a competent epithelial barrier function prevents the onset of unnecessary immune responses [10, 26, 13, 27], immune responses can lead to tissue-damaging inflammation that impair barrier function [28, 29, 30, 31, 32]. Given this complex interplay between barrier function and immune responses, a *coordinated* and *balanced* action of these two protective properties is necessary to maintain a competent epithelium that prevents the onset of diseases [14, 1, 8].

Coordination between barrier function and immune responses is achieved through strongly interconnected regulatory networks between the different biochemical and cellular components of the epithelium that enact barrier function and immune responses, respectively [33]. For example, both barrier components and anti-microbial substances are simultaneously produced in

response to physical damage to the epidermis [34] or to the colon [35]. Also, pro-inflammatory cytokines reduce the expression of epithelial barrier components in the airway epithelium [28] and in the epidermis [36]. The integrity of intercellular junctions that determine the permeability of epithelial tissues is affected by immune cells [30, 31] and signalling pathways that mediate the immune responses [37, 38, 26]. In contrast, disruption of intercellular junctions activates signalling pathways that trigger immune responses [10] and triggers the recruitment of pro-inflammatory cytokines to the epithelium [13, 27, 39].

A myriad of genetic and environmental *predisposing risk factors* can impair the functioning of individual components of these regulatory networks, eventually triggering a pathogenic process [40, 41, 42, 11]. Genetic risk factors include mutations or polymorphisms that impair the levels of expression of components of the epithelial barrier [43], of protease inhibitors controlling barrier function and inflammation [44], of cellular receptors that sense the competence of the epidermal barrier function [45], and of cellular receptors that sense the pathogen load [46]. Environmental risk factors include an abnormal exposure to pathogens [14, 47, 48] or chemicals [49] and the immoderate use of soaps and detergents [50, 8].

Thus far, the links between these predisposing risk factors and the development of diseases have been studied mainly by experimental and clinical methods that assess how individual risk factors affect individual components of the regulatory networks. However, loss of epithelial homeostasis often emerges from impaired *interactions* between the strongly entangled network components, and can seldom be attributed solely to the malfunction of an individual network component [51, 52, 53]. Hence, understanding how risk factors result in the development of disease requires a systems-level view, that considers the *interplay* between the different components of the regulatory networks of biochemical and cellular interactions that control epithelial function.

In this thesis, we analyse the mechanisms responsible for the maintenance of epidermal homeostasis from a systems- biology perspective. Particularly, we propose mathematical models of the regulatory networks of entangled biochemical and cellular interactions that control epithelial function, and analyse the impact of predisposing risk factors on the functioning of these networks.

We use the mathematical model to describe and understand the transition form a healthy epithelium to a pathological state. This requires a *dynamic description* that considers the multiple time-scales in which the different biochemical and cellular processes that underlie the *pathogenic process* operate.

To achieve this, we represent the regulatory interactions controlling epithelial homeostasis in the form of coupled systems of Ordinary Differential Equations (ODE) that operate at different time-scales. This mathematical framework assumes spatial homogeneity of the reactions

modelled. We [54] and others [55, 56, 57, 58, 59, 60, 61] have analysed different aspects of the spatial regulation of epithelial function, but the interplay between barrier function and immune responses has not been addressed within a spatial framework. Among other clinically relevant questions, spatial assessment of the epithelial function in the context of AD or pneumococcal infection could help to address the conditions required for the spread of infection and inflammation when epithelial homeostasis is lost. This analysis could be done using compartment models, as in [54], Partial Differential Equations (PDEs) as in [59, 61], or agent-based models as in [56, 57, 58]. However, for simplicity, in this thesis, such a spatial analysis is neglected, and left for future work.

Here, we first build and characterize mechanistic models of the sub-networks that determine the activity of the main biochemical and cellular effectors that enact the immune responses and the epithelial barrier function, respectively. They correspond to *regulatory modules* that control the levels of pro-inflammatory cytokines, of immune cells and of structural components of the epithelium. We find that these regulatory modules can be grouped into different *network motifs* that display distinctive qualitative behaviours that can be described in a simpler, phenomenological manner. We then re-assemble and analyse the regulatory networks controlling epithelial homeostasis by connecting the individual, phenomenologically represented regulatory modules. This mesoscopic and qualitative description of the reaction network allows us to analyse and extract the main control mechanisms that are responsible for the maintainance of epithelial homeostasis.

With our multi-scale and modular approach, we are able to obtain a mechanistic and quantitative description of pathological processes related to the loss of epithelial homeostasis.

Our mathematical models serve as frameworks for the integration and analysis of scattered experimental and clinical data, and reveal several potential mechanisms that are responsible for the maintenance of epithelial homeostasis.

We focus on two diseases: Atopic dermatitis (AD), an allergic skin disease, and infection of the airway epithelium by *Streptococcus pneumoniae*. Both of these diseases represent a important social burden, given by their high incidence [19, 18, 20, 21] and ineffectiveness of current treatment strategies that can be attributed to the lack of understanding of the causes of AD [17, 11, 62, 24, 25, 63, 64, 65, 66] and the incipient threat of antibiotic resistance of evolving strains of *Streptococcus pneumoniae* [23].

It is thus urgent to devise new therapeutic strategies that effectively prevent and cure AD and pneumococcal infection. This requires a understanding of the different pathogenic mechanisms that underlie the development of these diseases.

AD and infection by *Streptococcus pneumoniae* result from a loss of homeostasis of the epidermis [7, 8, 67] and the airway epithelium [68, 69, 38], respectively.

In both cases, loss of epithelial function results from an imbalance between the two protective properties of the epithelium. i.e. permeability barrier function and immune responses to invading pathogens [7, 70, 71, 72, 30]. In the epidermis and in the airway epithelium, these two protective properties are co-regulated by an intricate network of biochemical and cellular interactions [34, 36, 37, 28, 30, 38, 26]. Understanding the interplay between these two protective properties, given by the entangled regulatory networks that control barrier function and immune responses, is pivotal to elucidate the disease mechanisms of AD and pneumococcal infection.
Further, both in the epidermis [43, 73, 74, 75, 76, 47, 77, 40, 11, 47, 48, 49, 50] and in the airway epithelium [69, 78, 21], loss of epithelial homoeostasis can be triggered by different mechanisms. Elucidating mechanism-dependent pathogenic process is essential to propose effective, patient-specific treatment strategies.
Given these common structural features, we believe that the mechanisms that underlie the onset and progression of these apparently disparate diseases can be uncovered by our mathematical modelling framework, based on the analysis of the dual interplay between immune responses and permeability barrier function.

1.1 Atopic dermatitis is a complex and socially relevant disease for which effective treatment strategies are required

AD is a skin disease characterized a defective epidermal permeability barrier function that appears as dry and scaly skin, and by aberrant immune responses to environmental insults, manifested as excessive inflammation and allergy [17]. AD affects approximately 15% of infants worldwide (20% in the United Kingdom [19], 15% in Germany [18] and 10% in Nigeria [20]), and its incidence has been rapidly increasing [18, 19, 18]. Moreover, patients with a clinical history of AD have a strong predisposition for developing other atopic diseases, such as asthma and allergic rhinitis [17, 11, 62].
In terms of its economic impact, the average costs of treating AD per patient per year has been estimated to represent up to 4,480 USD in the United States of America [79] and 1425 EUR pro patient per year in Germany [18]. These costs are increasing with the augmenting prevalence of AD [80].
Despite its clear socio-economic relevance, the mechanisms leading to AD have not been fully elucidated, limiting the treatment options to the relieve of symptoms [17, 24, 25]. For instance, emollients enhance the permeability barrier function [40], steroids decrease the inflammation [66], and antibiotics reduce the infection that results from a defective epithelial function [81]. However, long term treatment does not guarantee remission of the disease [63], and can even

lead to aggravation of the AD condition by further affecting the epidermal structure [64, 65, 66]. The complexity of understanding and treating AD is further increased by the facts that *several* different predisposing genetic [43, 73, 74, 75, 76, 47, 77] and environmental [40, 11, 47, 48, 49, 50] risk factors have been linked to the development of AD, and that the pathogenesis of AD comprises several different phases, characterized by distinctive epidermal phenotypes of increasing severities [25, 81]. Together, these two observations suggest that effective treatment strategies must account for the risk-factor and disease-stage dependent, patient-specific pathogenic process of AD. Hence, devising effective treatment for AD is a challenging task that requires a mechanistic and clear understanding of the full pathogenic process of AD.

AD results from dysfunction of the regulatory networks of biochemical and cellular interactions that control epidermal homeostasis [43, 73, 74, 75, 76, 47, 77, 40, 11, 47, 48, 49, 50], leading to the impaired immune responses and barrier function that characterize the damaged epidermis of AD patients. In fact, the pathogenic effects of the predisposing risk factors for AD have been attributed to the impact of these genetic or environmental conditions on the regulatory networks controlling epithelial homeostasis [43, 74, 47, 40, 50]. However, due to the strong connectivity of these regulatory networks, the disturbances elicited on them by individual risk factors can propagate [8, 36, 13], gradually affecting the whole regulatory network controlling epithelial homeostasis and resulting in disease phenotypes of increasing severities [25, 82]. Thus, understanding the relative contributions of the individual risk factors on the pathogenesis of AD requires a systems-level framework, that considers the interplay between the co-regulated network components that control epithelial function.

Here, we propose such a systems-level framework, in the form of a mathematical model of the regulatory mechanisms that control epithelial function and that are affected by the different risk factors that predispose to AD. Through mathematical modelling, we aim to uncover the mechanisms that underlie pathological dynamics, as proposed in [83].

In this thesis (chapters 2, 3, 4, 5 and 6), we build on the previous research from our group [84] to propose the first mathematical model of AD. The focus of our model is the analysis of the complex interplay that exists between the permeability barrier function and the immune responses to invading pathogens. For this, we consider different time-scales to simultaneously describe the slow, cellular level processes and the fast, biochemical reactions that, together, maintain epidermal homeostasis.

The resulting mathematical model provides a coherent explanatory framework for different pathogenic mechanisms that can result in an AD condition.

1.2 Reducing the prevalence of infection by *Streptoccoccus pneumoniae* requires new treatment strategies

Yearly, 14.5 million severe cases of infection and 820 000 deaths are caused by *Streptoccoccus pneumoniae* [21]. Further, the effectiveness of treating infection by *Streptoccoccus pneumoniae* and other bacterial pathogens is threatened by the incipience of antibiotic resistance [23]. Thus, new therapeutic strategies for preventing and treating infection by *Streptoccoccus pneumoniae* are required. For this, a mechanistic and quantitative understanding of the infectious process is necessary.

Steptococcus pneumoniae is a bacteria that normally resides in the upper airway epithelium as a commensal organism that does not cause infection. However, circumstances such as colonization of the airway epithelium by other pathogens including *Haemophilus influenzae*, can trigger an infectious process by *Steptococcus pneumoniae*, eventually developing into a severe infection [21, 69].

Systemic infection by *Steptococcus pneumoniae* starts by impaired host-pathogen interactions between the upper airway epithelium and *Steptococcus pneumoniae*. This disruption is often triggered by the presence of a second pathogen [78, 69], but the exact pathogenic mechanisms are not clear.

An appropriate host response that prevents infection requires a competent epithelial barrier function and immune responses. However, these two protective properties of the epithelium inhibit each other. On the one hand, a competent barrier not only restricts bacterial invasion [85, 68, 38], but also limits the access of components of the immune systems to the site of infection [30, 86, 71, 87]. On the other hand, while reducing the pathogen load [88, 89], immune responses also damage the epithelial barrier [30, 86, 71, 87].

Thus, infection results from an unbalanced host-response to the invading pathogen [90]. Understanding the mechanisms by which co-pathogenesis triggers infection hence requires a quantitative systems-level framework that considers the complex interplay between barrier function, immune responses and pathogen load.

In this thesis (chapter 8), we propose a mathematical model of the host pathogen interactions between *Streptococcus pneumoniae* and the upper airway epithelium.

Our model builds on previous models of pneumococcal infection [91, 92, 93, 94], and considers, for the first time, the role of the epithelial barrier in mediating the infectious process, as well as the complex interplay between barrier function and immune responses.

Our data-driven mathematical model was calibrated with experimental data, and uncovered different potential mechanisms that can result in infection.

1.3 Previous mathematical models of epithelium homeostasis

The mathematical models proposed in this thesis correspond to dynamical descriptions of the regulatory networks controlling epithelial homeostasis.
We focus on the interplay between the two protective properties of the epithelium, namely the immune responses and permeability barrier function. In our models, we represent the interconnected processes that control the biochemical and cellular mediators of the immune response and barrier function by coupled systems of ODEs that operate at different time-scales.

Many of the previous mathematical models of epithelium function consider *either* permeability barrier function, *or* the immune responses to infiltrating pathogens. Only a handful of models explore how epithelium homeostasis is maintained through a controlled interplay between immune responses and the permeability barrier function.

Two types of models explore permeability function of epithelial tissues.
The first type encompasses the *pharmacokinetic models*, which assess the relation between structure and composition of epithelial barriers (particularly, the skin barrier) with the permeability barrier function. These models are commonly used to gain a quantitative understanding of the penetration of substances (such as topical drugs) through the epidermis [95].
The second type of models focuses on exploring how the *structure* of epithelial tissues (particularly, epidermis [56, 57, 58, 59] and the intestine [60, 61]), is regulated. The dynamics of the epithelial cells are represented by multi-scale models, that consider the interplay between birth, death, migration and differentiation of sub-populations of cells in the tissue, and the biochemical processes that operate within the individual cells. The mathematical formalisms used for the construction of these models comprise deterministic rule-based representations of the cellular kinetics [56, 57, 58], stochastic agent-based models [96] and PDEs [61, 59],allowing the analysis of the spatial regulation of epithelial tissues. These modes were used, for example, to understand the mechanisms responsible for the self-renewal of healthy epidermis [56, 57, 58], as well as diseases such as psoriasis [96, 97], tissue damage by Human Papilloma Virus (HPV) [59], and colorectal cancer [60, 61].

Some other mathematical models have focused on the immune responses that occur on epithelial tissues. For example, the ODE-based model of [98] considers the immune responses elicited by macrophages in response to cholesterol that leaks through a disrupted endothelium. This model could capture the early stages of atherosclerosis, although it neglects the effects of chronic, tissue-damaging inflammation on the endothelial barrier function, although a impaired

permeability barrier function is also a characteristic feature of this disease [98].
The ODE-based mathematical model of [99] describes how dose-response curves of cytokines are affected by different micro-environments. The different dose-response behaviours are obtained by simulating the interplay between different populations of cytokine-producing cells that occur in healthy or in psoriatic epidermis.
Most of the mathematical models of host-pathogen interactions that occur at epithelial surfaces focus on the relation between different pathogens and the immune responses. For example, the ODE model proposed in [100] explores the host response to *E coli* to understand mastitis. Also, the model in [101] considers the mechanisms leading to infection in the stomach by *Helicobacter pylori*. Mechanisms leading to pneumonia, a infection that results from impaired host response between *Steptococcus pneumoniae* and the airway epithelium, have been analysed in the models proposed in [91, 94] and [92] that do not consider the permeability barrier function. More abstract models [102, 103] have focused on the dual effect of immune responses on pathogen load. On one hand, immune responses can lead to effective elimination of the pathogen, and on the other, persistent immune responses result in tissue damage that promotes further pathogen growth.
Several mathematical models of viral infection consider the role of the epithelium mediating viral replication, but neglect its permeability barrier function that hinders the infection of the blood stream or other organs [5]. Examples include the models of infection by Influenza A virus [104, 105], by Epstein Barr virus [106], and of the dynamics of foot-and-mouth disease [107].

Previously, two mathematical models that consider the role of the dual interplay between the the permeability barrier function and the immune responses have been used to uncover the mechanisms that are responsible for the development of diseases associated to the loss of epithelium homeostasis, namely Inflammatory Bowel Disease (IBD) [108] and colon cancer [109].
The mathematical model of IBD proposed in [108], considers the interplay between pathogens, epithelial barrier function and the immune responses. IBD is characterized by a recurring inflammatory response to commensal bacteria of the gut, caused by a decreased amount of anti-inflammatory immune response mediators that lead to a increased propensity of inflammation in IBD patients. In their ODE model, IBD is represented by setting a non-zero rate of production of immune cells that both amplify the inflammation and also damage the epithelium. Simulations of a nominal interaction network reproduces the characteristic, transient immune response and barrier damage that results from a bacterial challenge observed in healthy patients. In contrast, simulations of the IBD condition results in a chronic decrease in the epithelial barrier function and unresolved inflammation, typical of IBD patients. Thus, their model successfully

reproduces the IBD phenotype.
The mathematical model of [109] explores the chronic inflammation associated to colon cancer by representing and analysing the interplay between inflammation, tumour growth, and barrier function. In their ODE model, inflammation induces tumour growth, and is counteracted by a competent barrier function. The tumour suppressor $p53$ increases the production of barrier components (mucin), and the oncogene *APC* increases the growth rate of the tumour. Simulation of oncogenic mutations (loss of function of $p53$ or gain of function of *APC*) appear as a increased tumour size.

These two mathematical models are useful to understand the mechanisms that lead to the loss of homeostasis of *intestinal* epithelium. However, to explore if AD and upper airway infections result of a imbalanced dual relation between barrier function and immune responses, mathematical models of the epithelium that are tailored specifically to the epidermis and the upper airway epithelium, respectively, are necessary.

The first mathematical model of AD was proposed in [84]. It consists of a mechanistic characterization of the protease networks that control both barrier function and epidermal inflammation. Simulations of the ODE model, assuming genetic (low expression of a protease inhibitor) or environmental (increased pH) risk factors known to predispose to the disease, effectively reproduces the increased propensity of inflammation that is typical of AD patients. This mathematical model, however, does not consider the tissue-level effects of active proteases, given by a decreased epidermal permeability and increased immune responses that result from protease-dependent skin desquamation [110] and cytokine expression [111, 112]. The pivotal role of these proteases in the development of AD is attributed to these two tissue-level effects [113, 114, 111, 115], that must be considered in a multi-scale framework that relates the interplay between protease activity, barrier function and immune responses. In this thesis, we build on the mathematical model of [84] (described in more detail in section 3.2.3), and explicitly consider, for the first time, how increased protease activity can lead to tissue damage in the form of loss of epithelial homeostasis.
Very few mathematical models of host-pathogen interactions occurring at epithelial surfaces explicitly consider the role epithelial permeability barrier function in mediating the outcome of the infection. The model proposed in [93] considers, for the first time, the role of the epithelial barrier in mediating infection by *Steptococcus pneumoniae*, although it does not consider the interplay between barrier function and immune responses.

This interplay is given by the tissue-damaging effects of immune responses, and by the inhibition of the neutrophil transmigration by a competent epithelial barrier [30, 86, 71, 87]. The

tissue-damaging effects of neutrophil transmigration are major determinants of the pathology of infection [31, 30]. Therefore, we believe that it is important to explicitly consider the dual relation between immune responses and barrier function.
The mathematical model of the host-pathogen interactions between *Streptococcus pneumoniae* and the upper airway epithelium proposed in this thesis (chapter 8) builds on the models proposed in [93, 91, 94, 92] and explicitly considers, for the first time, the dynamic interplay between the epithelium barrier function and the immune responses.
Taking together, in this thesis, we propose the first mathematical models of AD (chapters 2-7) and upper airway infection (chapter 8) that consider the dual interplay between barrier function and inflammation. Our models are conceptually similar to the models of Wendelsdorf et al (2010) [108] and Lo et al (2013) [109], but are specifically tailored to different types of epithelium (epidermis and upper airway epithelium). Further, as will be discussed in coming chapters, our modelling approach is based on modularity and time-scale separation of different model components, rather than being a explicit representation of the entangled biochemical reactions controlling epithelial function, as in the models of Wendelsdorf et al (2010) [108] and Lo et al (2013) [109].

1.4 Motivation of the thesis

The research presented in this thesis is motivated by the clinical and social importance of uncovering the mechanisms that underlie the onset and progression of diseases associated to the loss of epithelial homeostasis.
These diseases include infections [3, 4, 5, 6], allergies [7, 8, 1, 9, 10, 11, 12, 13], and cancer [14, 15], affecting a wide proportion of the population worldwide [16, 17, 18, 19, 20, 18, 21, 22]. The high prevalence of these diseases can partly be attributed to the lack of understanding of the underlying pathogenic mechanisms, that limits the effectiveness of the current treatments and of preventive strategies [23, 24, 25, 12]. It is therefore urgent to uncover the pathogenic mechanisms that result in loss of epithelial homeostasis, to find new ways to effectively prevent and cure these clinically, socially and economically important diseases. In this thesis, we focus on the analysis of one allergic (AD) and one infectious (pneumonia) disease. However, we believe that the theoretical framework proposed in this thesis can be used to explore the mechanisms that lead to the development of many other diseases that involve loss of epithelial function, such as asthma [39], viral infections [5] and several forms of cancer [116, 14].

These diseases result from impaired networks of cellular and biochemical interactions that control epithelial homeostasis. Particularly, alterations in the interplay between the two protective properties of the epithelium, namely the immune responses to environmental aggressors

and the permeability barrier function, play a major role in driving these diseases. Thus, a systems-level framework that allows the simultaneous consideration of the immune responses and permeability barrier function, and serves as a tool to integrate and analyse experimental and clinical data describing different regulatory components is required.
Currently, there exists no such a theoretical framework to represent the regulatory networks that underlie epithelial homeostasis. It is therefore timely to develop such a theoretical and integrative framework that allows the analysis of the mechanisms that are responsible for the loss of epidermal homoeostasis, associated to the onset of many socially relevant diseases.

1.5 Aims and objectives

The general objective of the thesis is to gain a mechanistic understanding of the regulatory networks that control epithelial homeostasis, and its role in the development of diseases that involve loss of epithelial function, using a systems biology approach.
Particularly, the work presented in this thesis has following aims:

- To *integrate* scattered experimental and clinical data on the regulatory networks controlling epithelial homeostasis that underlie the pathogenic mechanisms of Atopic dermatitis and infection of the upper airway by *Streptococcus pneumoniae*. *Addressed in chapter 2 and section 8.3*.

- To develop a mathematical modelling framework to represent the regulatory networks controlling epithelial homeostasis. *Addressed in chapter 3 and section 8.4.2.*

- To uncover plausible patient-specific mechanisms that underlie the pathogenic process of AD. *Addressed in chapters 4 and 6.*

- To use the insights gained from the mathematical model of AD to assess different patient-specific treatment strategies for this complex disease. *Addressed in chapter 5.*

- To reach a qualitative agreement between the AD model simulations and experimental data on the pathogenesis of the disease. *Addressed in section 6.2.*

- To apply the modelling framework, based on the analysis of the reaction networks underlying epidermal homeostasis, to another disease that involves loss of epithelial function. *Addressed in chapter 8*

- To clarify different potential mechanisms that can lead to infection of the upper airway epithelium by the commensal bacteria *Streptococcus pneumoniae*. *Addressed in chapter 8*.

- To calibrate a model of the regulatory mechanisms that underlie epithelial homeostasis with quantitative experimental data. *Addressed in appendix B*.

1.6 Main findings

The main findings of this thesis are as follows:

- The reaction network controlling epidermal homeostasis, reconstructed from existing experimental and clinical data (figure 2.3), contains the biochemical and cellular processes from which the pathogenesis of AD can be reconstructed by *in vitro* simulations. These modelling results suggest that the disease (AD) can emerge from the complex interactions between the components of the reaction network that have been previously described in the literature (chapters 4 and 6).

- The host-pathogen interactions between *Streptococcus pneumoniae* and the upper airway epithelium that underlie the infection by this bacterium can be described by the reaction network presented in figure 8.2. The validity of this model is supported by the qualitative agreement between the *in silico* simulations and experimental *in vivo* data (figure 8.4), and by the qualitative description of different infectious processes that have been observed in the clinic (section 8.6).

- The epithelial barrier function components describe a self-recovering dynamical behaviour that arises from the underlying feedback control structure (section 3.3).

- The immune cells affecting epithelial inflammation can act as a frequency filter that discriminates between different sporadic and recurrent events of cytokine release (section 3.4).

- The reaction networks controlling *epithelial* homeostasis can be decomposed into three elementary building blocks, representing the self-recovering determinants of the permeability barrier function, the switch-like release of pro-inflammatory cytokines, and the persistence of immune cells (chapter 3). The control structure that underlies homeostasis of the epidermis (figure 3.1) and the airway epithelium (figure 8.3) can be represented by interplay between these regulatory modules.

- The mathematical modelling framework proposed in this thesis, based on modularity and time-scale separation, can be used to qualitatively (epidermis) and quantitatively (upper airway epithelium) describe the regulatory networks controlling epithelial homeostasis.

- The interplay between the two protective properties of the epithelium (barrier function and immune responses) must be tightly controlled by the underlying regulatory networks of biochemical and cellular interactions to prevent the onset of diseases associated to the loss of epithelial homeostasis. Indeed, our model analysis suggests that inherited or environmentally determined weak barrier function or immune response can result in the development of AD (figures 4.5 and 6.5 A) or infection (figures 8.12 and 8.13).

- Our mathematical model of AD is consistent with the clinical observation that this complex disease can result from both genetic as well as environmental predisposing risk factors (figure 6.5).

- Our mathematical model of AD provides a plausible mechanistic explanation of the preventive effect of emollient treatment (figures 5.3 and 6.5).

- Our mathematical model of AD explains why different cohorts of AD patients could benefit from different pharmacological treatment (chapter 5).

- Simulations of our mathematical model of AD agree with different pathogenic mechanisms that have been reported in the literature (section 6.2).

- Analysis of our mathematical model of the host pathogen interactions between the upper airway epithelium by the commensal bacteria *Streptococcus pneumoniae* identified different mechanisms leading to loss of homeostasis (section 8.5)

1.7 Publications

- Elisa Domínguez-Hüttinger, Masahiro Ono, Mauricio Barahona, and Reiko J Tanaka. Risk factor-dependent dynamics of atopic dermatitis: modelling multi-scale regulation of epithelium homeostasis. *Interface Focus*, 3:20120090, February 2013.
  Reproduced in chapter 4.

- A mathematical model that uncovers disease mechanisms of Atopic dermatitis: *in silico* reproduction of the disease dynamics from early to advanced stages of the pathogenic process. *In preparation; results from chapters 5 and 6.*

- Mathematical modelling of host pathogen interactions reveals patient-specific mechanisms leading to infection. *In preparation; results from chapter 8.*

1.8 Structure and overview of the thesis

This thesis is organized as follows: The mathematical model of the pathogenic mechanisms that drive AD is presented in chapters 2-7.
Particularly, in chapter 2 we describe the regulatory network controlling epidermal homeostasis. For this, we integrate clinical and experimental data from the literature that describe different individual components of the reaction network. We also describe different risk factors that predispose for AD, as well as the clinical features of this disease, in the context of the regulatory networks controlling epidermal homeostasis.
In chapter 3, we decompose the reaction network controlling epidermal homeostasis described in chapter 2 into different regulatory modules. Using a combination of mathematical models previously proposed in the literature, and new models that are proposed for the first time in this thesis, we characterize each of these individual regulatory modules. We find that all of the regulatory modules considered in this thesis can be categorized into three types of network motifs that can be distinguished based on their qualitative behaviours. The mathematical modelling approach used in this thesis is briefly described in appendix A.
In chapters 4 and 6, using the network motif description developed in chapter 3, we re-assemble the reaction network controlling epidermal homeostasis into mathematical models that describe the cellular and biochemical interactions that underlie early (chapter 4) and late (chapter 6) stages of AD. We analyse each of these two mathematical models, by asking how the risk factors that predispose to AD affect the functioning of the regulatory network controlling epithelial homeostasis, eventually leading to the onset (chapter 4) and progression (chapter 6) of AD.
In chapter 5, we use the mathematical model that reproduces the early stages of AD to assess the impact of different treatments, commonly used by AD patients, on the regulatory networks controlling epidermal homeostasis that have been disrupted by a particular risk factor.
The general conclusions and future work of the results derived from the mathematical model of AD (chapters 3-6) are presented in chapter 7.

The mathematical model of the host-pathogen interactions between *Streptococcus pneumoniae* and the upper airway epithelium that underlie pneumococcal infection is introduced, presented, analysed and discussed in the self-contained chapter 8. Details on the parameter estimation for the pneumococcal infection model are given in appendix B.

The concluding remarks of this thesis are given in chapter 9.

Enjoy!

Chapter 2

Reaction network controlling epidermal homeostasis: the biology of Atopic dermatitis

2.1 Introduction

This section is devoted to the description of the reaction network controlling epidermal homeostasis. We integrated scattered clinical and experimental data on the individual reactions controlling epidermal function into a *systems-level representation*, which we call the reaction network controlling epidermal homeostasis. Proper functioning of this reaction network is required for healthy epidermal functioning, and loss of epidermal homeostasis, resulting from deregulation of this reaction network, underlies Atopic dermatitis (AD). In subsequent chapters, we will propose mathematical models of AD by representing (parts of) this reaction network.
This chapter is organized as follows:
First, in section 2.3, we will give a *clinical* description of AD, by giving an overview of the hallmarks of AD skin, the predisposing risk factors, and the main treatments for this disease.
Next, in section 2.4 we provide a more detailed description of the reaction networks controlling epidermal homeostasis (i.e. the underlying *biology*). We will focus on the keratinocyte, because: (1) it is the most abundant cell type of the epidermis, and the epidermis enacts the epithelial constituent of the skin, (2) it enacts both barrier and immune regulatory functions, corresponding to the two regulatory properties of the epithelium we are interested in, and (3) it is in direct contact with the environment, and must therefore constantly integrate and respond to changing environmental conditions, via its reaction networks.
While describing the reaction network controlling epidermal homeostasis, we will pinpoint the components of the network that are affected by the risk factors predisposing for AD. Identi-

fying the risk factors in the context of the complex, strongly interconnected reaction networks that they affect, will evidence the need of a mathematical model of AD to uncover the disease mechanisms triggered by the different risk factors.

2.2 Structure and function of the epidermis

AD is a disease that affects mainly the epidermis, which is a type of stratified epithelium that enacts the upper layer of the skin (figure 2.1). The epidermal tissue is mainly composed by keratinocytes at different levels of differentiation [17]. The basal layer is composed by undifferentiated and proliferative keratinocytes (basal cells). Upward movement towards the granular layer is accompanied by expression of differentiation markers, such as components of the skin barrier, intercellular junctions (the desmosomes), proteases, immune receptors and lipid modifying enzymes. The granular layer forms the last and most differentiated viable layer of keratinocytes. For simplicity, in figure 2.1, only the basal and the granular layers are represented. The uppermost layer of the epidermis is the skin barrier. It is formed by dead keratinocytes [117] that are held together by inter-cellular junctions, called desmosomes, and are embedded in a lipid matrix. This "brick and mortar" like structure [33] hinders the penetration of environmental aggressors, including pathogens, into the viable layers of the epidermis. A competent barrier is also essential to prevent excessive loss of water that can lead to dehydration [118]. Accordingly, a leaky barrier, resulting, for example, from excessive protease activity that leads to increased desquamation of inter-cellular junctions and inhibits the formation of the lipid matrix [119], leads to invasion of the viable epidermis by environmental factors [33]. Infiltrated pathogens are recognized at the granular layer by immune receptors, triggering immune responses that decrease the pathogen load but also can lead to the activation of adaptive immune responses via Dendritic cells (DC) [67, 7, 49]. Together, barrier function and immune responses to infiltrating pathogens provide the protective function that characterizes the epidermis [33].

In this research, we pay special attention to the keratinocytes that form the granular layer, because these are the uppermost cells in the *viable* epidermis and are hence closest to the environment. As such, these keratinocytes play a central role in mediating, responding and adapting to changing environmental conditions. This complex signal processing is achieved by the **biochemical networks of regulatory interactions** that are explained in detail later in this chapter.

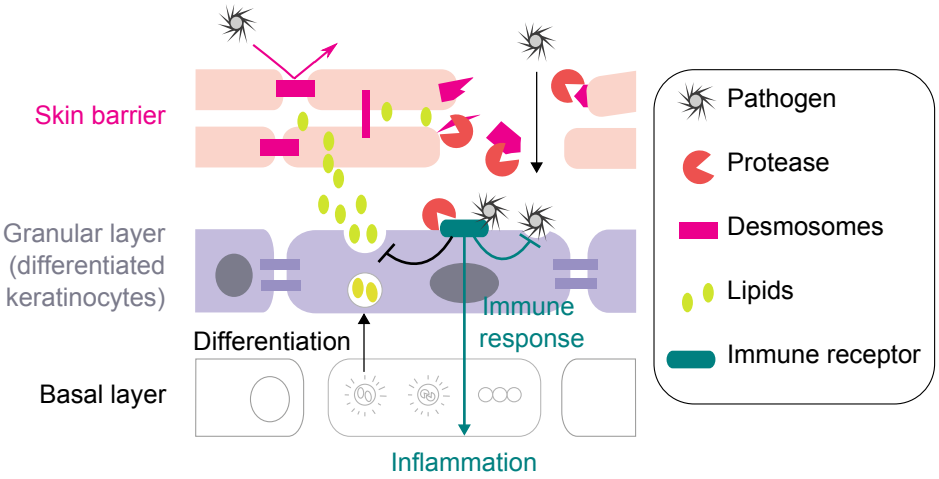

Figure 2.1: **Structure and protective functions of the epidermis.** The epidermis is a stratified epithelium composed by keratinocytes at different levels of differentiation: Cells in the basal layer gradually differentiate until forming the granular layer. Eventually, cells in the granular layer release their lipids and die to form the skin barrier. One of the main functions of the skin barrier is to hinder the penetration of environmental aggressors, including pathogens, into the viable layers of the epidermis. Accordingly, a leaky barrier, resulting from excessive desquamation and reduced skin barrier formation, caused in part by over-active proteases, leads to invasion of the viable epidermis by pathogens. Infiltrated pathogens are recognized at the granular layer by immune receptors, triggering immune responses that decrease the pathogen load but eventually also lead to tissue-damaging inflammation.

2.3 Symptoms and predisposing risk factors for Atopic dermatitis

AD is a complex disease. First, because it has a complex phenotype, given by several symptoms such as a dysfunctional skin barrier [7], infection [6], increased inflammation [81, 120] and allergy [121]. Second, because several genetic [77, 6, 47, 122, 75, 74, 76, 123] and environmental [47, 124] predisposing risk factors for AD have been identified as potential triggers of the disease. These include mutations or polymorphisms affecting skin barrier components [43, 73, 125, 126, 127] and immune responses [77, 6, 47, 122], prolonged use of hard water [124], increased [49] or decreased [47] exposure to environmental aggressors, and excessive use of soaps and detergents [124, 128], among others.

The pathological process of AD is further complicated by the fact that the impaired AD epidermis can lead to the emergence of further risk factors. For example, chronic inflammation can impair the genetic expression levels of barrier components, and and a weak barrier function can alter the micro-environmental conditions of the epidermis (increase in pH). This dual interplay

between AD risk factors and symptoms is responsible for a gradual worsening of the disease and the intricate disease mechanisms that characterize AD.

2.3.1 AD characteristics

The epidermis of AD patients is characterized by following symptoms [17] (figure 2.2A):

- Dysfunctional *skin barrier*, leading to a increased permeability to environmental aggressors, such as pathogens and allergens. Loss of barrier function also results in skin dehydration, leading to a dry and scaly skin [7].
- Propensity for *infection* by bacteria such as *Staphylococcus aureus* [6, 129].
- Frequent [81] and long-lasting [120] *inflammation* that is sometimes accompanied by allergic reactions to ubiquitous environmental insults [121].

The pathological process of AD is further complicated by the fact that the impaired AD epidermis can lead to the emergence of further AD characteristics. For example, a chronic inflammation can impair the genetic expression levels of barrier components, and and a weak barrier function can alter the micro-environmental conditions of the epidermis (increase in pH). This dual interplay between AD risk factors and symptoms is responsible for a gradual worsening of the disease and the intricate disease mechanisms that characterize AD. The causal relations between these AD sympoms is given by (figure 2.2):

(1) Dysfunctional skin barrier leads to an increased permeability to environmental factors, such as pathogens, thus, increasing the susceptibility for infection [7, 13].

(2) Increased pathogen load in the viable epidermis weakens the skin barrier by the interference of the pathogens with the barrier repair mechanisms of the host [130, 119].

(3) Augmented pathogen load further promotes inflammation [13].

(4) Excessive inflammation weakens the pathogen-eradicating innate immune responses, further increasing the propensity for infection [6].

(5) Sustained inflammation further impair barrier function by interfering with gene expression programs that control the barrier remodelling process [36].

This interplay, depicted in figure 2.2B, has two important consequences.
First, it can lead to a *gradual worsening* of the disease. While early stages of AD are characterized by occasional flares of barrier damage and innate immune responses to infiltrating

pathogens [49], during late stages of the disease, AD skin suffers from unresolved inflammation [81], sustained barrier defects [131, 132], secondary infection [133] and tissue remodelling [134, 135]. It is hence clear that gaining a mechanistic understanding of the early phases of the disease process is clinically relevant, since this will help to devise early therapeutic interventions that can prevent the onset of late, severe forms of the disease.

Second, this strong connectivity between the above mentioned symptoms suggests that there are several different *potential triggers* of the disease process. Indeed, as we will see in the next section, there are different genetic and environmental risk factors that predispose for AD that directly affect either pathogen load, immune responses or barrier function. Once initiated the pathogenic process, any of these risk factors can lead to the development of a full AD phenotype, i.e. to the (progressive) impairment of pathogen load, immune responses and barrier function.

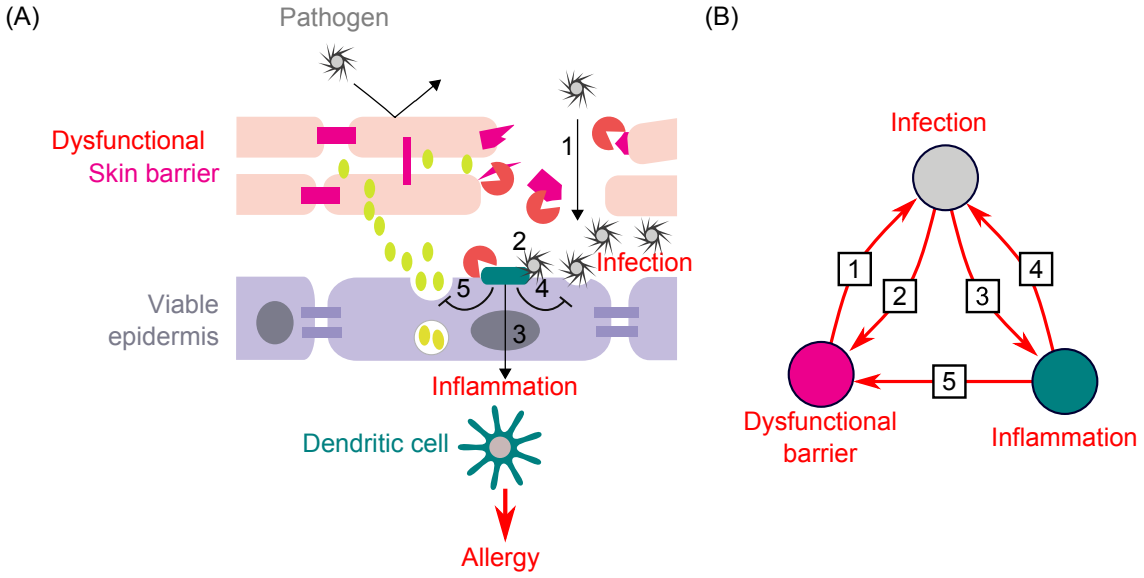

Figure 2.2: **Causal interplay between the symptoms of Atopic dermatitis** Cartoon **(A)** and network **(B)** representation of the interplay between the different symptoms of AD. **(1)** A dysfunctional skin barrier leads to an excessive penetration of environmental aggressors. **(2)** Infiltrated pathogens trigger further barrier damage by interfering with skin barrier repairing programs. **(3)** Increased load of infiltrated pathogens induce immune responses, eventually leading to inflammation and allergy. **(4)** Inflammation weakens the pathogen-eradicating innate immune responses. **(5)** Tissue-damaging inflammation interferes with the barrier formation process.

2.3.2 Genetic and environmental risk factors for AD

AD is a complex disease, because there are **several different genetic and environmental risk factors** that predispose to this disease [124]. These risk factors can be divided into three main categories, depending on which aspects of the epidermis they affect (summarized in table 2.1):

- **Risk factors affecting skin barrier function.** These risk factors affect the levels of expression of structural components of the skin barrier, most notably the protein filaggrin [43, 73, 125]. Filaggrin is responsible for cross-linking between the extracellular lipid envelope and the intercellular cytoskeleton of the keratinocytes that form the skin barrier [136], and has been identified as a key determinant of the permeability barrier function of the epidermis [73]. Changes in gene expression of filaggrin and other components of the skin barrier can be driven by genetic risk factors, such as polymorphisms [126, 127] or mutations [73], but also by a long-term exposure to pro-inflammatory cytokines [137, 29, 138] and by changes in barrier function [139, 140]. It has been suggested that expression of barrier components can also be affected by prolonged use of hard water [124], likely due to the interference of the high calcium concentrations contained in hard water with the regulation of terminal differentiation of the keratinocytes [141, 45, 142, 140].

- **Risk factors affecting immune responses.** These risk factors affect the functioning of the signalling cascades that determine the *innate* immune reactions that occur in response to infiltrated pathogens [143]. Alterations in these signalling cascades can result from genetically (polymorphisms) [77, 6] or environmentally [47] determined changes in the levels of expression of innate immune receptors (TLR4 [47]), cytokines (Interleukin 1 (IL1) [122]), anti-inflammatory cytokines (IL1 receptor antagonist [77]), and endogenous antibiotics termed Anti-microbial peptides (AMPs) [6]. Also environmental factors can affect the functioning of the signalling cascades. Particular attention has received the so called *hygiene hypothesis*, which states that that a defective development of the innate immune system, responsible for reduced levels of immune system components, can also result from the lack of contact with pathogens in very early stages of life [47].

- **Risk factors affecting protease activity.** The protease kallikrein (KLK) affects both the immune responses [111, 112, 144] and the skin barrier function [113, 144, 145]. Increased KLK activity can result from frequent use of soaps and detergents [124] that rise the pH, increasing the catalytic activity of these enzymes [128], from genetically determined decrease in the expression of the protease inhibitor LEKTI [75, 74], or from the increased expression and activity of the protease [76, 123]. The role of the levels of expression of the protease inhibitor LEKTI on the development of AD is further supported by the strong resemblance between the phenotype of Netherton Syndrome, a mendelian

disease caused by a loss of function mutation of SPINK5 gene (that encodes LEKTI), and severe forms of AD [74]. Also, the key role of the activity of the protease KLK on the development of AD is evidenced by transgenic mice in which the overexpression of KLK leads to the development of an AD- like phenotype [123].

Not only the pathogenic process of AD can be triggered by several genetic and environmental risk factors, but there is also a synergy between them, because the presence of two or more risk factors dramatically increases the susceptibility to develop AD [146, 132].
Once the pathogenic process has been triggered by any of these risk factors, the AD condition can be further aggravated. This is because dysfunctional epidermis displays an altered micro-environment that can trigger the emergence of further risk factors. For example, persistent inflammation and altered barrier function that characterizes AD skin (see section 2.3.1) can lead to the decrease in the expression of filaggrin [138] and AMPs [47]. This causal relation between risk factors is responsible for the gradual disease aggravation discussed in section 2.3.1.
To assess the impact of the different risk factors on the epidermal function, how they contribute to the onset of the pathogenic process, what causes the synergy between them, and what are the mechanisms that underlie the gradual aggravation of the AD condition, it is necessary to pinpoint the exact biochemical targets of these risk factors within their regulatory context, to showcase how these impaired biochemical components are related among them. For this, in the next section, we give a detailed description of the reaction network controlling epidermal function.

2.4 Reaction network of biochemical interactions controlling epidermal homeostasis

A healthy epidermis is given by a low pathogen load, a competent skin barrier, and infrequent immune responses that resolve easily. To maintain this homeostatic condition, intricate regulatory networks of biochemical interactions control barrier function, immune responses, and pathogen load (figure 2.3 A).
Proteases (figure 2.3 B) play a key role in the maintenance of epidermal function [147], particularly kallikreins (KLK) [144], because they affect both immune responses [130, 112] and barrier function [110, 113]. They are activated by infiltrating pathogens [130, 148] and by changes in barrier function [149], acting both as sensors and modulators of epidermal function. Changes in the pH of the skin, driven by soaps or detergents, can increase the catalytic activity of KLKs [128]. Changes in the gene expression of the gene encoding for KLK [76] or its inhibitor LEKTI [75] can also increase the activity of KLK.

Table 2.1: Major genetic and environmental risk factors predisposing to the development of AD

Genetic (Mutations, polymorphisms)	**Environmental (including an altered micro-environment)**
Risk factors affecting skin permeability barrier function	
Mutations or polymorphisms of the Filaggrin gene [43, 73]	Prolonged use of hard water (impaired epidermal calcium gradient) [124] Pro-inflammatory micro-environment [137, 29, 138] Impaired barrier function [139, 140]
Risk factors affecting immune responses	
Polymorphisms in the gene encoding for the IL1 receptor antagonist [77] Decreased expression of TLR2 [37]	Lack of contact with pathogens in early stage of life, associated to the impaired development of innate immune system (Hygiene hypothesis) [47]
Risk factors affecting protease activity	
Polymorphisms in the *SPINK5* gene [75, 74] Polymorphisms affecting protease expression [76, 123]	Prolonged use of soaps and detergents, which increase skin pH [124]

A competent barrier (figure 2.3 C), achieved by the combination of extracellular lipids, intracellular junctions (corneodesmosomes, CDS), and intercellular structural proteins such as filaggrin, hinders the penetration of external pathogens. Its function can be affected by external aggressors, such as tape strip or acetone treatment, as well as by the expression of its constituents, most notably, filaggrin [127]. Barrier function is modulated by KLKs [110, 113], pro-inflammatory cytokines [137, 29, 138] and by changes in the epidermal calcium gradient that results from skin barrier disruption [139, 150, 151]. Barrier function is commonly measured by Transepidermal Water Loss (TEWL), that quantifies the permeability of the epidermis and is hence negatively related to barrier function [152].

Infiltrated pathogens (figure 2.3 D) trigger immune responses by activating signalling pathways induced by TLR [153] (figure 2.3 E), Interleukin IL1 [154] (figure 2.3 F), and proteases [155, 130] (figure 2.3 B). Once activated, these signalling pathways trigger immune responses in the form of release of AMPs [114, 34], recruitment of neutrophils [156, 144] and phagocytosis [157] that, together, reduce the pathogen load.

Excessive activation of innate immune responses can lead to the activation of Th2 mediated adaptive immune responses (figure 2.3 G). Pro-inflammatory cytokines, such as TLSP, are induced by innate immune response signalling cascades [111], and trigger the migration of dendititic cells (DC) to the lymph nodes (figure 2.3 A,II). There, DC induce the differentiation of

naïve T cells into Th2 cells [158] via the IL4 dependent activation of the Gata3 pathway [159]. This process, known as allergic sensitization [160, 161, 9], is responsible for the allergic component of AD, as well as for the establishment of the pro-inflammatory micro-environment in the skin that further interferes with barrier function [137].
This regulatory interplay between pathogen load, immune responses, barrier function and protease activity is depicted in figure 2.3 A; a overview of the connectivity is represented in the inset of figure 2.3 A. Detailed description of the individual modules (figures 2.3 B-F) is given below.

2.4.1 Protease networks: Regulation of kallikrein (KLK) activity

The activity of the protease KLK must be tightly controlled to maintain a proper epidermal function, because active KLK (KLK* in figure 2.3 B) and its target receptor, the protease activated receptor PAR2, play major regulatory roles in the determination of barrier function [110, 113] and immune responses [130, 112]. Particularly, active KLK controls the desquamation of the skin barrier via the pH-dependent degradation of CDS [113, 128, 145]. Activated PAR2 (denoted by PAR2* in figure 2.3 B) inhibits the deposition of lipids into the skin barrier [113], and increases the expression of pro-inflammatory cytokines, such as IL1a, IL6, IL8, TNF-α [130], ICAM2 [112] and TSLP [111, 162]. Active PAR2 also mediates the immune responses to infiltrating pathogens, by increasing the expression of AMPs such as hBD-2 [130, 114], inducing keratinocyte phagocytosis [157] and triggering neutrophil recruitment [156].
The regulation of KLK activity involves several processing steps and different mediators. First, inactive KLK must be expressed and packed into LB (figure 2.3 B,1) and released into the extracellular space (figure 2.3 B,2). These processes are mediated by barrier function (via changes in TEWL [163, 149] and in the epidermal calcium gradient [164]), and by infiltrated pathogens (via TLR signalling [148]).
Once released into the extracellular space between skin barrier and granular layer, the inactive KLK cleaves itself, in a auto-catalytic, pH dependent manner [128] (figure 2.3 B,3). Active KLK can be inhibited by LEKTI, via the formation of an inactive heterodimer [165] (figure 2.3 B,4). Also this process is pH dependent [166]. The epidermal pH can be affected by immoderate use of soaps and detergents [124]. All the pH dependent reactions are represented by red arrows in figure 2.3 B. Active KLK [111] and also exogenous proteases from infiltrated pathogens such as *S. aureus* [130, 162] cleave and activate PAR2 (figure 2.3 B,5, active PAR2 denoted by PAR2*).
Noteworthy, the activity of KLK is increased in the disrupted skin of many AD patients, suggesting that KLK activity plays also a clinically important role in the maintenance of epidermal

homeostasis. Partly, this high KLK can be attributed to alterations in the levels of expression of the key components of the KLK regulatory network (KLK [76], PAR2 [112] and LEKTI [75]). In some (but not all) patients, these alterations are caused by genetic variants termed Single Nucleotide Polymorphisms (SNPs) [75, 76] (represented by green arrow in figure 2.3 B). The catalytic KLK activity can also be increased by the excessive use of soaps and detergents that increase the epidermal pH [124] (represented by red arrows in figure 2.3 B).

2.4.2 Skin barrier function

The permeability barrier function of the epidermis is enacted by the skin barrier, also known as stratum corneum, which is the uppermost layer of the epidermis. It is formed by death keratinocytes (the corneocytes), embedded in a lipid matrix termed "corneal envelope", and hold together by strong intercellular junctions (the corneodesmosomes, CDS) [33]. Strong cohesion between the corneocytes is further provided by filaggrin, a protein that is responsible for cross-linking between the extracellular corneal envelope and the intercellular cytoskeleton [136]. Together, corneosomes [167, 113], lipids [168, 169], and filaggrin [73] are the key biochemical determinants of the permeability barrier function.
Regulated production and formation processes of these three skin barrier components are hence pivotal for maintaining a competent barrier. The expression of CDS (figure 2.3 C,1) and of the unprocessed and inactive filaggrin precursor pro-filaggrin (figure 2.3 C,2) are decreased by pro-inflammatory cytokines, including IL4 [170, 138], IL13 [137], and IL22 [29] The *de novo* production of lipids and packing into LB (figure 2.3 C,3) requires the expression of lipid-modifying enzymes [169, 171]. The levels of expression of pro-filaggrin [140, 138, 163, 172, 142], CDS [173] and lipid-modifying enzymes [173] are further affected by changes in the permeability barrier function (via changes in TEWL and the epidermal calcium gradient). To become part of the lipid matrix, lipids must be released from their containing LB into the extracellular space [174] (figure 2.3 C,4). This process is induced by skin barrier disruption [174, 150, 140, 175] and inhibited by active PAR2 [113]. To become a functional part of the skin barrier, filaggrin must be post-translationally modified (figure 2.3 C,5), a process that is mediated by several proteases, including Caspase 14 (Casp-14) [176], SASPase [177], and ELA2 [178]. Casp-14-mediated activation of pro-filaggrin is induced by barrier damage, via changes in TEWL [139], enacting a negative feedback control mechanism.
The key determinant in the desquamation of the skin barrier is active KLK, by cleaving the CDS (figure 2.3 C,6) in a pH dependent manner [113, 128, 145].

2.4.3 Regulation of infiltrated pathogen load

The pathogen load in the viable epidermis is controlled by the two protective properties of the epithelium: the permeability barrier function and the immune responses. The infiltration of pathogens from the environment to the viable epidermis is determined by the permeability barrier function [7, 132] (figure 2.3 D,1). The rate of infiltration of external aggressors is also dependent on the amount of stimuli in the environment [49].
Elimination of the pathogen is triggered by immune responses (figure 2.3 D,2) in the form of AMPs [6, 144, 179, 114, 133] neutrophil recruitment [144, 180] and phagocytosis of by epidermal cells [157]. Neutrophil recruitment to the site of infection in response to activation of immune response pathways is a cellular level process, represented in figure 2.3 A,I. The rate of elimination of invading pathogens can also be increased by antibiotics [129, 81, 24].

2.4.4 IL1 and TLR mediated immune responses

The focus of this thesis is on KLK-mediated immune responses, due to the pivotal role KLK activity in mediating *both* immune responses and barrier function, the two protective properties of the epithelium that must be tightly co-regulated to maintain homeostasis.
However, also the signalling pathways triggered by Interleukin-1 (IL1) and Toll-Like receptor (TLR) activation, respectively, seem to play important roles in mediating the innate immune responses in AD skin, since their activity is often impaired in AD patients [181, 77, 182, 183].
TLR signalling is triggered by a broad range of infiltrated pathogens, via the association of Pathogen-Associated Molecular Patterns (PAMP) to the TLR [184] (figure 2.3 E,1). Upon activation, TLR pathway induces the activation of the Transcription Factor (TF) NFκB (figure 2.3 E,2), which results in the increased expression of AMPs [153] and pro-inflammatory cytokines such as IFN-γ [122] (figure 2.3 E,3).
Infiltrated pathogens lead to the expression of inactive, pro-IL1 (figure 2.3 F,1) via the induction of TLR signalling by PAMPs [122]. PAMPs also trigger the activation of pro-IL1 into IL1* by inducing its inflammasome- mediated cleavage (figure 2.3 F,2). Active IL1 forms a binds to IL1 receptor (IL1R) to form the heterodimer IL1*1R (figure 2.3 F,3), which results in the activation of a NFκB-dependent signalling pathway (figure 2.3 F,4), resulting in the release of pro-inflammatory cytokines and a further increase in pro-IL1 expression (positive feedback loop). The receptor antagonist IL1Ra inhibits IL1 signalling by associating with IL1 receptor, forming an inactive complex (figure 2.3 F,5) [154].
In many AD patients, SNPs affect the expression of IL1 [182] and of IL1Ra [77] (represented by green arrows in figure 2.3 F).

2.4.5 Adaptive immune responses drive Th2 polarization

The differentiation of naïve T cell into Th2 cells, a process known as Th2 polarization [39], plays a major role in the pathogenesis of AD, particularly during the advanced stages of the disease. Polarization of Th2 cells (1) triggers the onset of allergic reactions through a process termed *allergic sensitization* [160, 161, 27], (2) leads to the establishment of a pro-inflammatory environment in the epidermis, and (3) contributes to the chronic inflammation that is typical of AD lesions from patients at severe stages of AD [185, 186]. Moreover, the pro-inflammatory micro-environment interferers with the epidermal differentiation programs, further inflicting on the epidermal function [137, 138, 29, 125].

Polarization of Th2 cells involves two steps: First, cytokines released by keratinocytes in the viable epidermis [143] activate DC [187]. Particularly, active-PAR2- induced TSLP [39, 111], but also TNF-α [130] and IFN-γ, induced by TLR2 [122], stimulate the migration of DC to the lymph nodes [187], where they expose previously internalized antigen and increase the levels of the cytokine IL4 [188]. This cellular level process of activation and migration of DC to the lymph nodes in response to rise in cytokine levels is represented in figure 2.3 A,II.

The second step occurs in the lymph nodes, where active DCs increase the production of the cytokine IL4 [9, 39, 12]. This triggers the differentiation from naïve T cells into polarized Th2 cells via the activation of the Jak-Stat6-signalling pathway (figure 2.3 G,1) which controls the production of the TF Gata3 [159, 189] (figure 2.3 G,2). The TF Gata3 acts as a master regulator that orchestrates the T cell differentiation process from from naïve T cells to Th2 cells [190] (figure 2.3 G,3). This TF also increases its own expression [191] (figure 2.3 G,4), as well as the production of more IL4 [122], enacting two positive feedback loops.

Once polarized, Th2 cells migrate back to the epidermis (figure 2.3 A,III). There, Th2 cells contribute to the establishment of a pro-inflammatory micro-environment by increasing the production of cytokines such as IL13 [9, 29], IL22 [137] and IL4 [122]. Th2 cells also elicit allergic reactions by releasing IgE and TARC that activate Mast cells that then release histamine in response to environmental insults [158, 9].

2.5 Conclusions

In this chapter, we integrated and organized scattered experimental and clinical data into a reaction network controlling epidermal homeostasis (figure 2.3). In the following chapters, we will represent this reaction network by mathematical models, and analyse the impact of different risk factors on its functioning. Such a formal description of the entangled biological processes controlling epidermal homeostasis is necessary to uncover the pathogenic mechanisms leading to the onset of AD.

Due to the modular, input-output representation of the reaction network controlling epidermal homeostasis, further biological processes could easily be incorporated. A extension of the model would require the identification of the components of the current version of the reaction network that affect and are affected by newly added molecules or cell types.

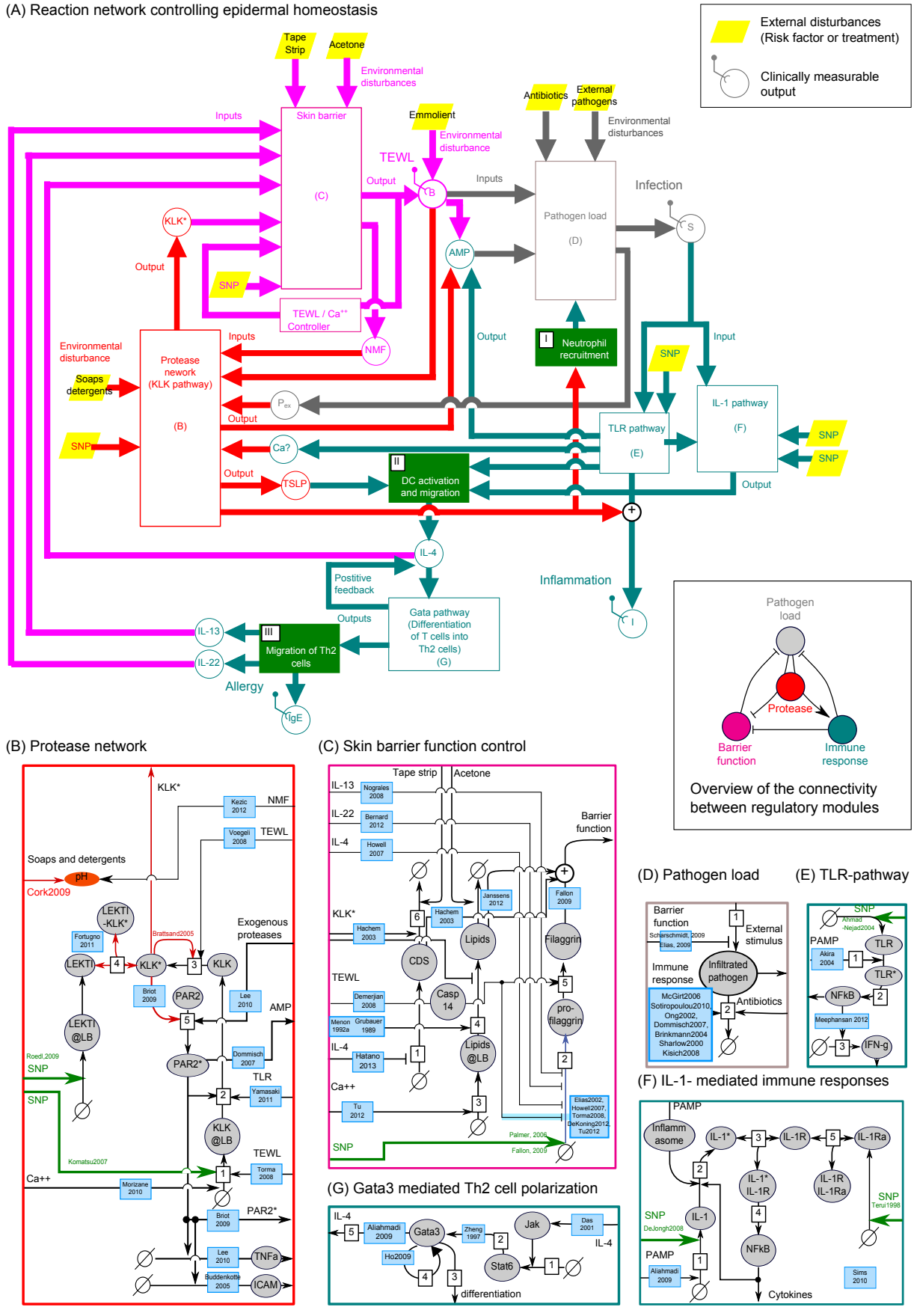

Figure 2.3: *(Caption on next page).*

Figure 2.3: (Previous page.) **Control structure of the reaction networks regulating epidermal homeostasis**. **[A]** Systems-level representation of the control structure regulating epidermal homeostasis, given by the interplay between modules mediating skin barrier function (magenta), pathogen load (grey), protease activity (red) and immune responses (cyan). Each of these modules is affected by inputs, environmental and genetic disturbances (SNPs) and a regulatory sub-network that is detailed in sub-figures **[B-F]**. The inset is a simplified representation of the detailed control structure depicted in the main figure. With the exception of the cellular processes described in the three green boxes (labelled I, II and III in figure **[A]**), all the reactions correspond to biochemical interactions. Sub-figures **[B-F]** represent the biochemical reactions controlling **[B]** protease networks, **[C]** Skin barrier function, **[D]** Pathogen load, **[E]** TLR-mediated immune responses, **[F]** IL1 mediated immune responses, and **[G]** Gata3-mediated adaptive immune responses. The key reference for each of the individual reactions is denoted by a blue box. Green arrows denote SNPs. Incoming and outgoing arrows correspond to inputs and outputs, respectively (equivalent to those in figure **[A]**). Grey circles denote biochemical species. An arrow entering and exiting a grey box represents a production, conversion or degradation processes. Positive or negative modulations of these biochemical reactions are denoted by spiky or blunt end arrows, respectively. For description of the individual reactions, please refer to the main text.

Chapter 3

Regulatory modules: Decomposition of the reaction network into network motifs

3.1 Introduction

In the previous chapter, we gave a detailed description of the reaction networks controlling epidermal homeostasis that are considered in this thesis. In this chapter, we present our mathematical modelling approach, which consists in decomposing the reaction network (depicted in figure 2.3) into elementary building blocks, termed regulatory modules. These regulatory modules can be divided into following three categories:

- Regulatory modules controlling **skin barrier components**. They correspond to the *biochemical* networks controlling lipid and filaggrin content depicted in figure 2.3 C.
- Regulatory modules controlling the **cytokine release**. These include the *biochemical* networks controlling innate immune responses triggered by the protease KLK (figure 2.3 B), the active TLR pathway (figure 2.3 E), the cytokine IL1 (2.3 F), as well as the Gata-3 signalling pathway mediated the adaptive immune reaction to IL4 (figure 2.3 G). For simplicity, we will focus on protease- and IL4 mediated cytokine release.
- Regulatory modules controlling the **cellular immune effectors** in response to biochemical mediators. These include protease-dependent neutrophil recruitment to the epidermis (figure 2.3 A,I), the protease-dependent migration of DC to lymph nodes (figure 2.3 A,II), and the mobilization of differentiated Th2 cells (figure 2.3 A,III).

Previous characterization of these regulatory modules show that they display following three *characteristic qualitative behaviours*:

- Upon perturbation, skin barrier components, particularly lipids [151, 150, 174, 173, 140] and fillaggrin [176, 139], follow a **self-recovering dynamical behaviour**.

- The induction of cytokine release upon stimulation [192, 193, 194] follows a **switch-like dose response behaviour**. Particularly, previous research suggests that protease-dependent innate immune responses [84] (figure 2.3 B), and the IL4 dependent adaptive immune responses [195] (figure 2.3 G), represented by yellow boxes in figure 3.1, represent such a switch-like dose response behaviour. Noteworthy, also the innate immune response pathways that are triggered in response to TLR [194] (figure 2.3 E) and IL1 activation [196] (figure 2.3 F) seem to display a switch-like dose response behaviour.

- The **cellular immune effectors**, namely neutrophils (2.3 A,I), DC neutrophils (2.3 A,II) and Th2 cells (2.3 A,III) that are activated and mobilized upon a biochemical (cytokine) stimulation, **persist** even after the cytokine levels have ceased [116, 144] (represented by green boxes both in figure 3.1 and in figure 2.3 A).

Accordingly, we classify the regions of the regulatory network controlling epithelial homeostasis (figure 2.3) controlling barrier components (figure 2.3 C), cytokine release (figure 2.3 B.E,F,G) and cellular immune effectors (figure 2.3 AI-III) into three different classes of regulatory modules displaying a switch-like dose response behaviour, self-recovery, and persistent dynamics, respectively (figure 3.1). In this chapter, we will first introduce a mathematical representation of the above mentioned regulatory modules. For those regulatory modules for which a mathematical model exists in the literature, we will describe the regulatory module using the existing mathematical representation. Particularly, we will use the mathematical description of the switch-like innate immune responses induced by KLK proposed in [84] (yellow "KLK" box in figure 3.1), the IL4-dependent signalling pathways that mediate Th2 cell polarization described in [195] (yellow "IL4" box in figure 3.1), and the mathematical model of the self-recovering filaggrin dynamics proposed in [197] (blue "filaggrin" box in figure 3.1). For the remaining regulatory modules considered in this thesis (persistent cellular immune mediators, represented as green boxes in figure 3.1 and self-recovering lipid content, represented by the blue "lipid" box in figure 3.1), we will propose, for the first time, simple mechanistic models that are able to reproduce the desired qualitative behaviour described in the experimental literature. For all of the mathematical models considered (both from the literature and proposed in this thesis), we will show example simulations displaying the characteristic qualitative behaviours.

To model each of the regulatory modules considered in this thesis, we will chose the simplest mechanistic representation, in which the desired qualitative behaviour emerges from the underlying biochemical and cellular control structure. This will allow us to pinpoint the most relevant network properties that are responsible for the three different qualitative behaviours displayed by the individual regulatory modules. These control- and feedback structures are the three *network motifs* that are responsible for the three qualitative behaviours displayed by the

epithelial regulatory modules. Particularly, we will see that a combination of *positive feedback and cooperativity* can lead to a switch-like dose response behaviour, self-recovery dynamics are achieved by a *negative feedback*, and persistence results from *time-scale differences* between the fast, biochemical processes that mediate cytokine production, and the slow dynamics of the cellular level effectors.
Finally, having identified the underlying mechanisms, we will introduce simpler, *phenomenological mathematical representations* of these three different qualitative behaviours.
In our qualitative modelling approach, experimentally observed behaviours of the individual regulatory network elements robustly emerge from the underlying control structure, without the need of fine-tuning of parameters. This allows us to integrate scattered experimental and clinical data, for which no detailed quantitative information is available, into a quantitative and systems-level framework. With this, we can systematically analyse the role of individual regulatory modules in the maintenance of epithelial homoeostasis, without neglecting their regulatory context.

In subsequent chapters, we will use the resulting modular representation of the regulatory modules to re-construct and analyse the reaction network presented in figure 2.3, as shown in figure 3.1.

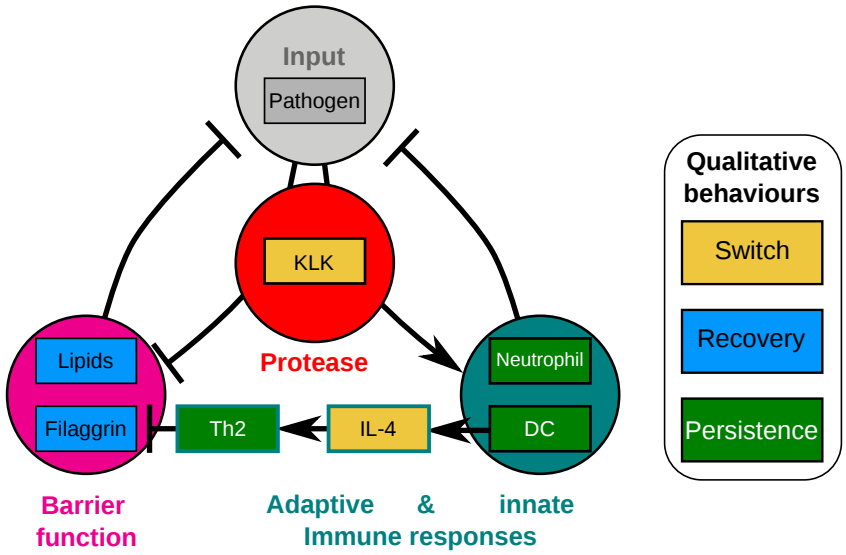

Figure 3.1: **Decomposition of the reaction network controlling epidermal homeostasis into regulatory modules.** Barrier function components filaggrin and lipids are characterized by a self-recovering dynamics. Release of cytokines triggered by proteases or by the IL4 display a switch-like dose response behaviour. The dynamics of cellular immune effectors persists even after the cease of their biochemical triggers.

3.2 Switch-like dose response behaviour characterizes the release of cytokines

3.2.1 Bistability is a switch-like dose-response behaviour with memory

A switch-like dose response behaviour refers to the relation between a input (commonly, a ligand) and the steady state concentrations of an output, where small changes in the input can drive large changes in the output [198]. A particular class of switch like behaviour is *bistability*, in which this abrupt change in output concentration is also *history-dependent*. In such a bistable dose-response behaviour, the critical concentration of the input at which the abrupt switching from low to high values occurs (denoted by S^+ in figure 3.2 A) is different from the critical input concentration that triggers the switching from high to low values (S^- in figure 3.2 A). Hence, the *onset* of production of the output occurs at the threshold concentration S^+, while the *cease* of output production occurs at the threshold concentrations S^+. The region between the two threshold values S^+ and S^- is termed **bistable region**, because the output can have two possible values, high or low, depending on the *previous* values of the output; if previous values are low, then the system remains at the low branch, and vice versa. This property confers the system with **memory**, also termed as *hysteresis*, since the current state depends on past values (figure 3.2 A).

3.2.2 Bistability characterizes immune responses

Bistable dose-response behaviour has been repeatedly observed across different immune response pathways. For example, it has been observed for the response of DC to stimulation with the PAMP LPS [193], in the release of pro-inflammatory cytokines in psioratic lesions [99], activation of T-cell receptor [199], the terminal differentiation of lymphocytes [200], and NFκB dependent response to mechanical stress [201].

Particularly, immune responses that control epidermal homeostasis have also been found to display a bistable switching behaviour. These include the dose-response behaviour describing the pathogen-mediated release of cytokines induced by proteases [84], IL1 [196], and TLR2/4 [194] (corresponding to the innate immune response pathways, figure 3.2 B) as well as the the release of pro-inflammatory cytokines induced by Gata3 in response to rises in IL4 [195] (corresponding to a adaptive immune response pathway, depicted in figure 3.2 B).

Here, we will consider two of these immune response pathways: innate immune responses triggered by KLK in response to infiltrated pathogens (figure 3.2 C), and adaptive immune responses triggered by the pro-inflammatory cytokine IL4 (figure 3.2 D). We acknowledge that the activation of other *innate* immune response pathways, particularly those involving IL1 and TLR2, also play a important role in the pathological process of AD, since long-term changes

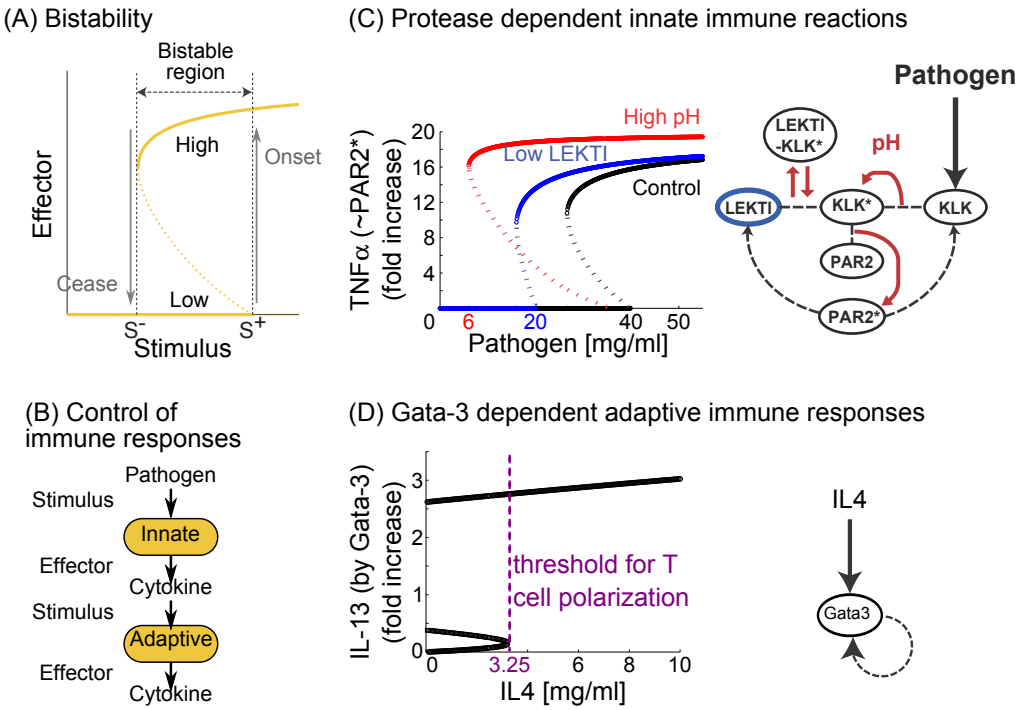

Figure 3.2: **Bistable switching characterizes the dose-response behaviour of cytokine release by active immune response pathways. [A]** Schematic representation of a bistable dose-response (bifurcation) behaviour describing the relation between the concentration of the input (stimulus) and the steady state concentration of the output (effector). Effector concentrations remain at low values until a critical threshold S^+ in the stimulus concentration is reached, triggering the abrupt activation of the effector. High effector values can be decreased only if the ceasing threshold $S^- < S^+$ is reached. The history-dependent region comprised between S^- and S^+ is termed bistable region. Figure adapted from [84]. **[B]** Innate and adaptive immune responses are triggered by pathogens or cytokines, respectively, and result the release of cytokines in a bistable dose-response manner. **[C]** *Left:* Protease-dependent innate immune reactions display a bistable dose response behaviour that is affected by environmental (high pH) and genetic (low LEKTI) risk factors. *Right:* Reaction network of biochemical interactions controlling protease activity. Figure adapted from [84]. **[D]** *Left:* Gata-3 dependent adaptive immune responses to stimulation with the pro-inflammatory cytokine IL4 displays a bistable switching behaviour that is responsible for the *irreversible* polarization of individual T cells. It results from a underlying reaction network controlling Gata-3 activity that displays positive feedback and cooperativity. Figure adapted form [195].

in the activation levels of components of the IL1 [32, 154, 182] and TLR [81, 47, 6, 183] signalling pathways have been associated to the loss of epidermal homeostasis. However, given that they display the same qualitative dose-response behaviour as KLK-mediated immune responses, namely bistability [84, 196, 194], in our qualitative modelling framework, the role a

switch like dose-response behaviour in mediating epithelial innate immune responses can be enacted by any of these innate immune response pathways. We chose to focus particularly on KLK signalling, because KLK activation not only affects innate immune responses, but also has a major impact barrier function and the onset of adaptive immune responses, representing a major hub in the regulatory network controlling epidermal homeostasis.
In the following sections, we will introduce the mathematical descriptions of the regulatory modules controlling KLK- and Gata3- mediated cytokine release. They correspond to the ODE models proposed in [84] and [195], respectively, and were chosen because they are simple yet mechanistic descriptions of the switch-like dose response behaviour that characterizes these immune responses.

3.2.3 Protease dependent innate immune reactions: KLK model

In this section, we describe the mathematical model of the control of KLK activation, proposed by Tanaka et al [84].
In [84], Tanaka *et al* proposed the first mathematical model of the regulatory module controlling the activity of the protease KLK. It describes the biochemical interactions regulating KLK activity, detailed in section 2.4.1 and represented in figure 2.3 B. Particularly, it considers the interplay between the key mediators of KLK activation, namely inactive (KLK) and active (KLK^*) protease, inactive (PAR2) and active ($PAR2^*$) protease receptor, unbound protease inhibitor (LEKTI), and the inhibitory complex (KLK^*LEKTI). The reactions considered are auto-catalysis of KLK (first positive feedback), reversible formation of the inhibitory complex, activation of PAR2 by active KLK5, and active PAR2- mediated production of KLK5 (second positive feedback) and LEKTI. The input to the network is represented by infiltrated pathogens (S) that induce the production of inactive KLK5. The connectivity between the network components is reproduced in figure 3.2 C (right). The corresponding mathematical model is given by the system of equations 3.1:

$$\frac{d[\mathrm{KLK^*LEKTI}]}{dt} = k_\mathrm{a}[\mathrm{KLK^*}][\mathrm{LEKTI}] - k_\mathrm{d}[\mathrm{KLK^*LEKTI}] - \delta_{\mathrm{LK}}[\mathrm{KLK^*LEKTI}], \tag{3.1a}$$

$$\frac{d[\mathrm{LEKTI}]}{dt} = -k_\mathrm{a}[\mathrm{KLK^*}][\mathrm{LEKTI}] + k_\mathrm{d}[\mathrm{KLK^*LEKTI}] + t_\mathrm{L}(m_\mathrm{L} + f_\mathrm{L}[\mathrm{PAR2^*}]) - \delta_\mathrm{L}[\mathrm{LEKTI}], \tag{3.1b}$$

$$\frac{d[\mathrm{KLK^*}]}{dt} = -k_\mathrm{a}[\mathrm{KLK^*}][\mathrm{LEKTI}] + k_\mathrm{d}[\mathrm{KLK^*LEKTI}] + k\frac{[\mathrm{KLK^*}][\mathrm{KLK}]}{[\mathrm{KLK^*}] + C_\mathrm{K}} - \delta_{\mathrm{K^*}}[\mathrm{KLK^*}], \tag{3.1c}$$

$$\frac{d[\mathrm{KLK}]}{dt} = -k\frac{[\mathrm{KLK^*}][\mathrm{KLK}]}{[\mathrm{KLK^*}] + C_\mathrm{K}} - \delta_\mathrm{K}[\mathrm{KLK}] + f_{\mathrm{KS}}S + f_\mathrm{K}[\mathrm{PAR2^*}], \tag{3.1d}$$

$$\frac{d[\mathrm{PAR2}]}{dt} = -k_\mathrm{P}\frac{[\mathrm{KLK^*}][\mathrm{PAR2}]}{[\mathrm{KLK^*}] + C_\mathrm{P}} - \delta_\mathrm{P}[\mathrm{PAR2}] + m_\mathrm{P}, \tag{3.1e}$$

$$\frac{d[\mathrm{PAR2^*}]}{dt} = f_{\mathrm{PS}}S[\mathrm{PAR2}] + k_\mathrm{P}\frac{[\mathrm{KLK^*}][\mathrm{PAR2}]}{[\mathrm{KLK^*}] + C_\mathrm{P}} - \delta_{\mathrm{P^*}}[\mathrm{PAR2^*}]. \tag{3.1f}$$

The model was analysed in terms of its steady state solutions, neglecting its fast transient dynamic behaviour. It displays a robust bistable dose response behaviour that can be attributed to the presence of the two positive feedbacks (auto-catalysis of KLK activation and active PAR2- dependent production of KLK) in the network. Example simulations of this bistable dose-response behaviour using the nominal parameter values in [84] are reproduced in figure 3.2 C (left).

Two of the risk factors that affect the reaction network controlling epidermal homeostasis have a direct impact on KLK activity: Increased epidermal pH dramatically increases the catalytic activity of active KLK [128], as well as its affinity for LEKTI [166]. This environmental risk factor was represented in the model by increasing the catalytic rates of KLK* (parameters k and k_P in equation 3.1) and the affinity between active KLK and LEKTI (parameters k_a and k_d in equation 3.1). Similarly, the lower expression of the KLK inhibitor LEKTI is a genetic risk factor that is represented in the model of [84] by decreasing the LEKTI production rate (parameter t_L in equation 3.1).

Simulating these risk factors dramatically alters the dose response behaviours, decreasing the thresholds of onset and cease of the protease-mediated immune responses (S^+ and S^-) which leads to a increased sensitivity to pathogen load (lower S^+) and a more persistent immune response (lower S^-), as shown in figure 3.2 C.

We follow the notation of [84] and refer to these two conditions as ”low LEKTI” and ”high pH”, respectively, as opposed to the healthy ”control” (figure 3.2 C).

We refer to this model as the KLK model, and use it in the next chapters with the nominal parameters proposed in [84].

3.2.4 Gata-3 mediated Th2 cell polarization

In this section, we describe the mathematical model of the activation of Gata-3 production, proposed by Höfer et al [195].

In [195], Höfer *et al* proposed the first mathematical model of irreversible Th2 polarization in response to the activation of the Transcription Factor (TF) Gata-3 by IL4. This simple mathematical model describes the dynamics of the Gata-3 activity in the undifferentiated T cells that reside in the lymph nodes, in response to stimulation with IL4. It comprises a positive feedback term that describes the Gata-3 mediated Gata-3 expression, as well as a non linear term that represents the post-translational modifications that the TF Gata-3 has to overcome before enacting the positive feedback (figure 3.2 D, right). The resulting one-dimensional ODE (equation 3.2) displays a irreversible, bistable dose-response behaviour (given by a threshold value $S^- < 0$) that characterizes the irreversible polarization of individual Th2 cells, as shown in the simulations of equation 3.2, using the nominal parameter values proposed in [195] (reproduced in figure 3.2 D, left).

In the following chapters (particularly, chapter 6), we use this mathematical model with the nominal parameter values proposed in [195] to describe the IL4 dependent activation of Gata-3.

$$\frac{d[\text{Gata3(t)}]}{dt} = \alpha[IL4] + \frac{\kappa_G[\text{Gata3(t)}]^2}{1+[\text{Gata3(t)}]^2} - \kappa[\text{Gata3(t)}]. \tag{3.2}$$

3.2.5 Network motifs that result in bistability: positive feedback and cooperativity

As we have seen in the two examples above, bistability can result from biochemical networks displaying positive feedback with cooperativity. In fact, it has been suggested [202, 203], that in many different reaction networks, the presence of these two network properties are required for a bistable dose-response behaviour. Thus, the combination of positive feedback and cooperativity represents a class of *network motifs* that can be enacted by different mechanisms [204, 205, 206], including the auto-catalysis controlling KLK activity (equations 3.1) and the self-regulated transcription that enhances Gata-3 expression (equation 3.2).

3.2.6 Phenomenological representation of bistable dose response behaviour by a perfect switch

In addition to *mechanistic* mathematical models (such as equations 3.1 and 3.2) in which bistability emerges from the underlying reactions (as shown in figures 3.2C and D, respectively),

the bistable-dose response behaviour (figure 3.2 A) can be mathematically described and simplified with Piecewise-affine (PWA) functions [207].
In brief, the PWA approximation gives a phenomenological (as opposed to mechanistic) rule that relates the input (stimulus) to the output (effector) (figure 3.2 A).
Assuming a perfect switch, the effector can be approximated by two constant values, E_{low} and E_{high}, representing the "low" or "high" branches of the bifurcation diagram, respectively.
Assuming that the input changes dynamically in the time-scale τ, then the relation between the time-dependent input $S(\tau)$, the current output $E(\tau)$ and the previous output values $E(x<\tau)$ can be approximated as follows:

- If $S(\tau) < S^{-}$, then $E(\tau) = E_{low}$ (effector is low if the stimulus concentration is low).
- If $S(\tau) > S^{-}$, then $E(\tau) = E_{high}$ (effector is high if the stimulus concentration is high).
- If $S(\tau) \in [S^{-}, S^{+}]$, then:
  - if $E(x<\tau) = E_{low}$, then $E(\tau) = E_{low}$, or
  - if $E(x<\tau) = E_{high}$, then $E(\tau) = E_{high}$,

  corresponding to the history-dependent determination of the effector value when the stimulus is in the bistable region.

More formally, these conditions can be represented by the PWA given in equation 3.3 (adapted from [208]):

$$E(\tau) = \begin{cases} E_{low} & \text{if } (S(\tau) < S^{-}) \text{ or } \{S(\tau) \in [S^{-}, S^{+}] \text{ and } E(x<\tau) = E_{\text{low}}\} \\ E_{high} & \text{if } (S(\tau) > S^{+}) \text{ or } \left\{S(\tau) \in [S^{-}, S^{+}] \text{ and } E(x<\tau) = E_{\text{high}}\right\}. \end{cases} \tag{3.3}$$

Note that equation 3.3 implicitly assumes two time-scales:

- A **fast** time-scale t that governs the stabilized biochemical interactions that underlie the bistable dose-response behaviour (typically involving a positive feedback and cooperativity, as discussed in section 3.2.5). These biochemical reactions can be represented by a system of ODEs $\dot{\mathbf{E}}(t, S, \mathbf{E})$ (corresponding, for example, to the mathematical model describing KLK activation represented in equations 3.1) that operates at time-scale t and has a input S that does not change significantly ($S(t) \approx constant$) while $E(t)$ reaches its equilibrium value (given by E_{low} or E_{high}, respectively).
- A **slow** time-scale τ that determines the dynamics of the input $S(\tau)$ by the governing equation $\dot{S}(\tau) = F(\tau, S)$.

A special case of the system 3.3 occurs when the slowly changing input $S(\tau)$ is itself determined by its quickly stabilizing output $E(t)$ (and vice-versa). In such a case, also the dynamics of $S(\tau)$ (that depend on $E(\tau)$) can be descried by the PWA given in equation 3.4 (adapted from [208]):

$$\dot{S}(\tau) = \begin{cases} F_{low}(S) & \text{if } E(\tau) = E_{low} \\ F_{high}(S) & \text{if } E(\tau) = E_{high}, \end{cases} \tag{3.4}$$

where F_{low} and F_{high} are the two *governing equations* that determine the dynamics of S when $E(\tau) = E_{low}$ or $E(\tau) = E_{high}$, respectively.
Accordingly, the long term behaviour of S is given by the *focal points* S_{ss}^{low} and S_{ss}^{high}, corresponding to the steady state values given by the solution to $F_{low} = 0$ and $F_{high} = 0$, respectively [208].
The coupling between equations 3.3 and 3.4 represents a hybrid system that has been extensively discussed and analysed in [207, 208]. The authors conclude that the long term behaviour of the coupled variable $S(\tau)$ and $E(t)$ is determined by the relative position of the focal points S_{ss}^{low} and S_{ss}^{high} respect to the threshold values S^- and S^+, as follows (figure 3.3):

- A resting, homeostatic ("low") steady state occurs when $S_{\text{ss}}^{low} \leq S^+$ and $S_{\text{ss}}^{high} < S^-$.
- A chronically inflamed steady state occurs when $S_{\text{ss}}^{low} > S^+$ and $S_{\text{ss}}^{high} \geq S^-$.
- Bistability in the two-time-scale dynamical system occurs when $S_{\text{ss}}^{low} \leq S^+$ but $S_{\text{ss}}^{high} \geq S^-$.
- Oscillations occur when $S_{\text{ss}}^{low} > S^+$ and $S_{\text{ss}}^{high} < S^-$.

In conclusion, this methodology allows the derivation of analytical conditions required for different qualitative behaviours of a complex dynamical system that operates in two time-scales, reducing the need for numerical methods. Note however that the agreement between the dynamical behaviour that is analytically derived from the hybrid system representation and the numerical simulations of the model must be verified for the particular mathematical model that is analysed using this approach, to ensure that neither the discontinuities of the hybrid representation of the system, nor the transient behaviour that is not captured by the focal point analysis detailed above, affect the dynamics of the unsimplified mathematical model.
As we will see in sections 4.2.5, 5.3 and 8.5, the PWA approximation and the briefly described dynamical analysis proposed in [208], are useful for the analysis of the reaction network controlling epithelial homeostasis, characterized by the interplay between slow, cellular level processes and fast, biochemical reactions.

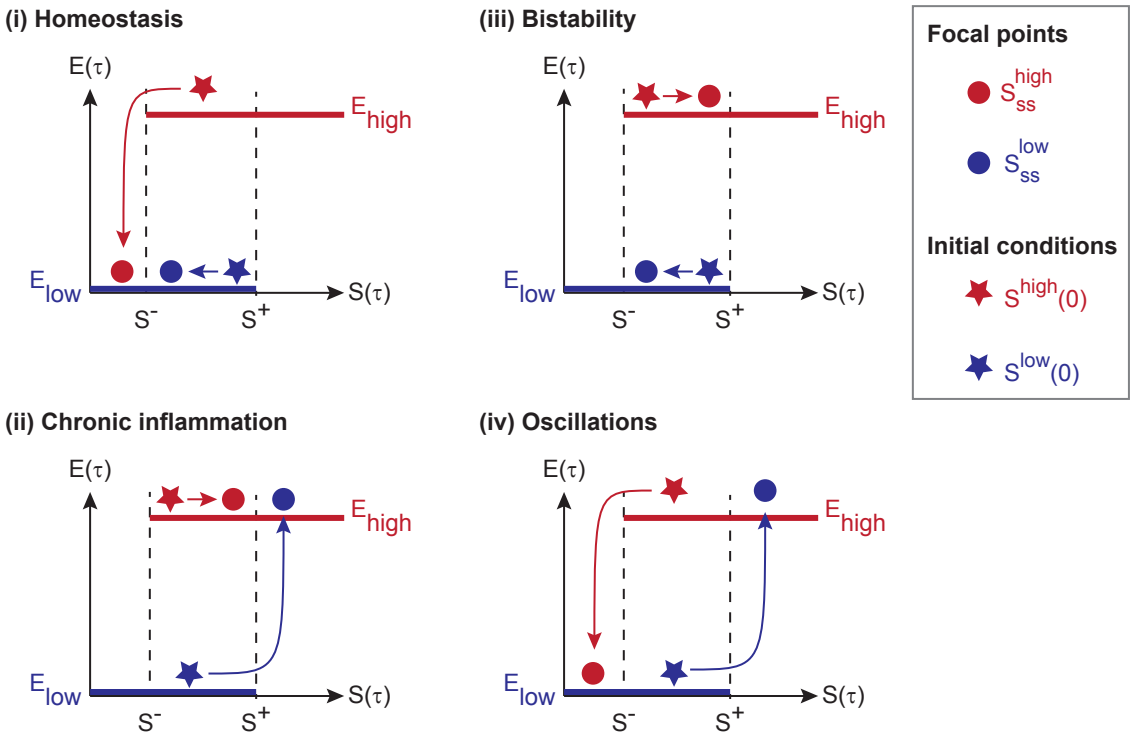

Figure 3.3: **Schematic representation of the qualitative dynamic behaviours of the hybrid system described in the coupled equations 3.3 and 3.4.** The long term dynamical behaviour of the hybrid system 3.3 and 3.4 is determined by the position of the focal points S_{ss}^{low} and S_{ss}^{high} respect to the threshold values S^- and S^+. (i) $S_{ss}^{low} \leq S^+$ and $S_{ss}^{high} < S^-$ lead to homeostasis, (ii) chronic inflammation occurs when $S_{ss}^{low} > S^+$ and $S_{ss}^{high} \geq S^-$, (iii) Bistability arises from $S_{ss}^{low} \leq S^+$ but $S_{ss}^{high} \geq S^-$, and (iv) Oscillations result from $S_{ss}^{low} > S^+$ and $S_{ss}^{high} < S^-$.

3.3 Self-recovery characterizes the barrier function components and is achieved by negative feedback control

A system displays a self-recovering dynamic behaviour if it can recover and maintain a nominal value, even in the presence of perturbations that alter its functioning, both in terms of initial conditions of the system's variables, and of its parameters [209, 210] (figure 3.4 A).

In the epidermis, the skin barrier components lipids and filaggrin display such self-recovering behaviour [211] (figure 3.4 B,C). Disturbances occur in the form of changes in initial conditions -inflicted by environmental triggers such as tape stripping, acetone treatments, or desquamation-, or by constant changes in kinetic parameters, particularly production rates that are affected by pro-inflammatory cytokines [137, 29, 138].

This robustness of skin barrier components to (micro) environmental perturbations is fundamental for the maintenance of a healthy skin. Skin barrier forms the first contact with the environment, and is hence prone to many different perturbations, such as pathogen load, chemicals

including soaps and detergents, physical disruption by scratching, and changes in humidity. Despite these environmental disturbances, skin barrier must maintain a nominal value to maintain its pivotal role in providing **protection** against these environmental conditions, by acting as a semi-permeable (selective) membrane that controls the flux of substances [33] (see figure 3.4 A, *top*).

The self-recovering dynamical behaviour of a biochemical determinant of the barrier function (X) is represented in figure 3.4 A, bottom. Upon a perturbation that alters its initial condition and its production rate , the barrier function transiently drops, but then recovers again to its nominal value $\tilde{X}$. We call the time required for the barrier function component $X(t)$ to restore its nominal value "recovery time".

Such a self-recovering dynamic behaviour that confers robustness to environmental perturbations in the form of parameter changes in the system results from negative feedback control mechanisms that regulate the production of skin barrier components [150, 33].

In the skin barrier, negative feedback control seems to be mediated by an epidermal calcium gradient that is altered upon perturbation of the skin barrier and subsequently triggers several barrier-reparation processes [141, 142, 212].

Indeed, the role of negative feedback in mediating recovery dynamics upon perturbations (*robustness*) has been observed for many different biochemical networks [210], including the synthetic Tet-repressor system in *E. coli* [213, 214], the pheromone response pathway controlled by Fus3 in *S. cerevisiae* [215, 216], the BMP4 signalling pathway modulated by the pseudoreceptor BAMBI in *X laevis* [217], the hyperosmotic stress response in yeast [218, 219], and signalling networks underlying bacterial chemeotaxis [220, 221].

Mathematical models have identified the key role of negative feedback in determining the self-recovering dynamic behaviour of epithelial cell volume [222] and filaggrin content in the epidermis [197].

Negative feedback can thus be regarded as the key network motif that is responsible for the self-recovering dynamic behaviour. In fact, this has been theoretically proven, both by analytical [223] and computational [224] methods.

In the following, we will introduce mathematical models that represent the regulatory modules that are responsible for the self-recovering dynamical behaviour of the skin barrier components, lipids and filaggrin. These regulatory modules correspond to network motifs comprising a negative feedback control structure (figures 3.4 B,C, left). We will show simulations that exemplify the self recovering dynamical behaviour upon changes in production rates that result from these network structures (figures 3.4 B,C, right). Finally, we will introduce a phenomenological representation of the self-recovering dynamics (figure 3.4 D).

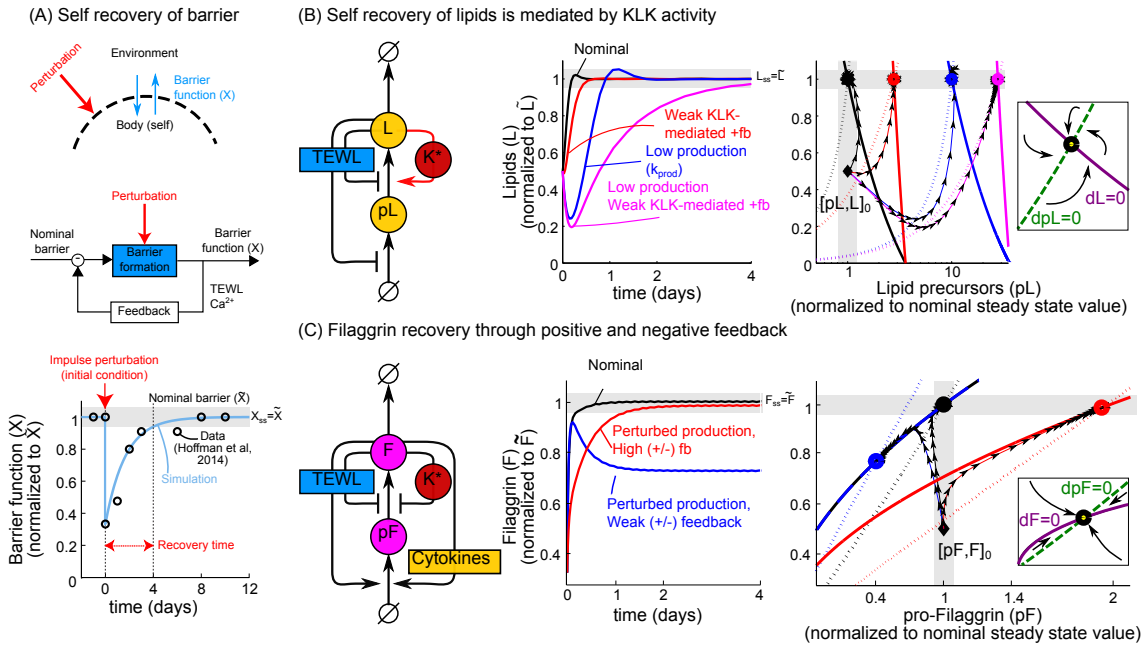

Figure 3.4: **Self-recovery characterizes the barrier function components and is achieved by negative feedback control (A)**, *Top:* Skin barrier regulates the exchange of substances with the environment even in the presence of perturbations. *Center:* Self-recovery of the skin barrier is achieved through negative feedback. *Bottom:* Barrier function (X) shows a self-recovering dynamic behaviour, characterized by a return to its nominal steady state $\tilde{X}$ upon a perturbation. This self-recovery has been characterized experimentally [225] and can be simulated by equation 3.7. **(B) Self recovery of lipid content in the skin is mediated by KLK activity** *Left* The lipid content in the skin barrier is controlled by two TEWL- driven negative feedback loops and a KLK-mediated positive feedback loop. *Center* Lipid concentration recovers to a nominal value even after step changes in the basal production rate. The speed of recovery is increased by the KLK-mediated positive feedback. *Right* In the presence of perturbations, lipid precursors are over-produced to maintain a nominal lipid concentration. **(C) Filaggrin recovery is achieved through the interplay between positive and negative feedbacks** *Left* Filaggrin content in the skin is controlled by a double negative feedback, mediated by TEWL and KLK activity, and a double positive feedback, mediated by TEWL and pro-inflammatory cytokines. *Center* An interplay between a strong positive and a strong negative feedback mediate the recovery of filaggrin upon perturbations in initial conditions and basal expression rate. *Right* Upon perturbation, maintenance of a nominal filaggrin steady state is achieved by the feedback-mediated increase in pro-filaggrin expression.

3.3.1 Lipid content in the skin barrier is controlled by a double negative feedback and modulated by KLK activity

In this section, we propose a novel mathematical model of the regulatory networks controlling the self-recovery of the skin barrier lipids.

Already early studies characterizing barrier function have shown that the rate of synthesis of lipids is directly proportional to loss of permeability barrier function, measured by TEWL [151]. Further, this increased rate of lipid release upon barrier disruption does not take place if the skin is occluded [150, 174]. More recent studies using high throughput analysis of gene expression dynamics upon barrier disruption also show that genes associated to lipid metabolism tend to be up-regulated upon disruption [173].

Recovery upon disruption is achieved by the barrier-damage-induced release of previously synthesized lipids that are contained in the LB of differentiated keratinocytes [140] (denoted by "Lipids@LB" in figure 2.3 C), a restoration process that is inhibited by active proteases (KLK) [113]. Given that KLKs are also activated by barrier damage [149], this KLK-mediated inhibition of lipid production corresponds to a positive feedback from barrier function to barrier restoration that constrains the negative feedback control mediating lipid homeostasis (see figure 3.4 B, *left*).

In equation 3.5, we propose a simple model of this regulatory module mediating lipid concentrations. It represents the coupled dynamics between the lipid component of the barrier (L, corresponding to "Lipids" in figure 2.3 C), and the lipid precursors contained in the LB (pL, corresponding to "Lipids@LB" in figure 2.3 C) depicted figure 3.4 B, *left*. We assume that barrier function is directly proportional to L and negatively regulates the synthesis of pL (first negative feedback, denoted by "TEWL-mediated -fb" in equation 3.5b) and the release of pL into L (second negative feedback, denoted by "TEWL-mediated -fb" in equation 3.5a). The inhibitory effect of active proteases (K^*) on the release of LB lipids is modelled in the simplest possible way, by assuming that the rate of pL release is proportional to L, with rate f_{KLK}. This *positive feedback* enacted by KLK results from the fact that activation is *induced* by barrier damage, but *inhibits* LB release, comprising two negative feedbacks that together give a positive feedback (denoted by "KLK-mediated +fb" in equation 3.5a). No degradation for pL is assumed, representing the fact that the precursors are consumed mainly during the barrier production process. Simulations of equations 3.5, using the parameters in table 3.1, are shown in figure 3.4 B, right.

In these simulations, we consider two perturbations: A step-like (ten-fold) decrease in the barrier production rate k_{prod}, and a decrease in the initial condition (50% reduction from the nominal steady state value L_{ss}). The effect of KLK-mediated positive feedback was assessed by considering a nominal and a low (100-fold decreased) positive feedback strength f_{KLK}. To

asses the effect of a stronger negative feedback, we considered a 10-fold increase in f_{release}.
The resulting recovery behaviours are shown in figure 3.4 B, *center* (dynamic trajectories) and *right* (nullclines). Upon perturbation in the initial condition, all of the simulated conditions display a self-recovering dynamical behaviour, where $L(t)$ returns to its nominal steady state $\tilde{L}$, even in the presence of an additional perturbation in the production rate. As shown by the displacement of the nullclines in the presence of perturbations (figure 3.4 B, right), the maintenance of a nominal lipid concentration is achieved by the compensating increase in the concentration of lipid precursors. A strong KLK-mediated positive feedback accelerates the speed of recovery to a nominal, healthy value while producing an overshoot in the $L(t)$ dynamics. In contrast, weakening the positive feedback strength (red and magenta trajectories in figure 3.4 B) or increasing the negative feedback strength (not shown) compensates these effects, resulting in over-damped convergence to the nominal steady state value.
Taking together, this preliminary analysis of this toy model representing the regulatory mechanisms controlling lipid concentration suggests that the underlying network motif structure, based on the interplay between two negative feedback loops and one positive feedback enacted by KLK, is capable of displaying a recovering dynamic behaviour upon perturbations both in initial conditions and in production rates.

$$\frac{d\mathrm{L(t)}}{dt} = \overbrace{k_{\text{prod}} \underbrace{(1 + f_{\text{KLK}}\mathrm{L(t)})}_{\text{KLK-mediated +fb}} \underbrace{\frac{1}{1 + f_{\text{release}}\mathrm{L(t)}}}_{\text{TEWL-mediated -fb}} \mathrm{pL(t)}}^{\text{lipid production from precursors}} - \overbrace{k_{\text{deg}}\mathrm{L(t)}}^{\text{lipid degradation}} \quad , \tag{3.5a}$$

$$\frac{d\mathrm{pL(t)}}{dt} = \underbrace{\frac{1}{1 + f_{\text{production}}\mathrm{L(t)}}}_{\text{TEWL-mediated -fb}} - k_{\text{prod}} \frac{1 + f_{\text{KLK}}\mathrm{L(t)}}{1 + f_{\text{release}}\mathrm{L(t)}} \mathrm{pL(t)}. \tag{3.5b}$$

3.3.2 Filaggrin content is regulated by the interplay between a fast negative feedback and a delayed positive feedback

In this section, we describe the mathematical model of the regulatory networks controlling the filaggrin content in the skin barrier, originally proposed in [197] but further analysed in this thesis to explore the relation between the feedback structure and the resulting self-recovery dynamical behaviour.
The filaggrin content in the skin barrier is controlled by a intricate control structure that involves the interplay between two negative and two positive feedback loops (shown on figure 3.4 C *left*):

- A damaged barrier leads to a *reduction* of filaggrin expression [140, 138, 163, 172, 142].

Table 3.1: Parameters of the regulatory module controlling lipid dynamics (dimensionless and arbitrarily chosen parameters for simulating equations 3.5)

Symbol	Name	Nominal value
k_{prod}	Barrier production rate	7.5 (nominal) 0.75 (perturbation)
f_{KLK}	Positive feedback strength, enacted by KLK*	25 (nominal feedback) 0.25 (weak KLK*-mediated feedback)
f_{release}	Negative feedback strength from barrier function to release of LB lipids	1
$f_{\text{production}}$	Negative feedback strength from barrier function to *de novo* production of *pL* (LB lipids)	5 (nominal feedback) 50 (strong negative feedback)
k_{deg}	Lipid degradation rate	10

This positive feedback is further accentuated by the presence of pro-inflammatory cytokines. High cytokine levels are characteristic for a chronically damaged skin barrier, and further interfere with filaggrin expression [226, 137, 227, 137].

- Barrier damage *induces* the post-translational processing of filaggrin into a active form [176, 139], a process that is further accentuated by active KLK [139]. Recall that also KLK activity directly depends on permeability barrier function, hence, this modulation corresponds to a further negative feedback loop.

Based on this reaction network structure, Panayiotis Christodoulides proposed in [197] a mathematical model of filaggrin control, represented by a coupled system of Delay Differential Equations (DDE) describing the dynamics of the filaggrin precursor pro-filaggrin (pF, corresponding to "pro-filaggrin" in figure 2.3 C) and filaggrin (F, corresponding to "Filaggrin" in figure 2.3 C). To explore if this system displays a self-recovering dynamical behaviour, we performed further simulations of a simplified version of the original model [197], neglecting the delay describing the *de novo* production of filaggrin precursors. Note that, in general, the delay can affect the transient, but not the steady state value of the system. Further, as shown in [197], delay does not affect the stability of equations 3.6. Hence, to roughly explore if the control structure depicted in figure 3.4 C, *left* can eventually lead to the recovery of a nominal filaggrin content ($\tilde{F}$) upon a perturbation, it is enough to consider the ODE version of the equations proposed in [197]. The model (equations 3.6) considers a *de novo* production term for pro-filaggrin that comprises a nominal production rate (k_e) that is further enhanced by a com-

petent barrier. The positive feedback is enacted by TEWL and, indirectly, by pro-inflammatory cytokines ("$+fb$" in equations 3.6). It also represents the post-translational modifications that convert pro-filaggrin into filaggrin. This process is inhibited by a competent barrier (directly by TEWL and indirectly by active KLK), representing a negative feedback ("$-fb$" in equations 3.6).

$$\frac{d\mathrm{F(t)}}{dt} = \underbrace{\mathrm{pF(t)}k_{\mathrm{P}}\overbrace{\frac{1}{1+f_{\mathrm{L}}\mathrm{F(t)}}}^{\text{-fb}}}_{\text{post-translational modification}} - \delta_{\mathrm{L}}\mathrm{F(t)}, \tag{3.6a}$$

$$\frac{d\mathrm{pF(t)}}{dt} = \underbrace{k_{\mathrm{e}} + \overbrace{f_{\mathrm{p}}\mathrm{F(t)}}^{\text{+fb}}}_{\textit{de novo}\text{ production}} - \mathrm{pF(t)}k_{\mathrm{P}}\frac{1}{1+f_{\mathrm{L}}\mathrm{F(t)}} - \delta_{\mathrm{pL}}\mathrm{pF(t)}. \tag{3.6b}$$

Simulations of this model, using the nominal parameters reported in [197], are shown in figure 3.4 C *center* (dynamic trajectories) and *right* (nullclines). They show the dynamical behaviour of filaggrin content in response to perturbations in the initial conditions (half the nominal, steady state value $\tilde{F}$). Under nominal conditions (black), filaggrin recovers to its nominal level. Upon a step like decrease in the basal expression rate (to half the nominal value of k_e), fillagrin levels do not recover completely when the two positive and negative feedback strengths are weak (blue, using the nominal parameter values f_P and f_L). We mimicked the onset of the two further feedback arms, driven by KLK and cytokines, by increasing the strength of the negative (2.5 fold in the nominal f_P value) and the positive (two-fold increase in the nominal f_L) feedback strengths. The resulting dynamics, shown in red, are able to display a self recovering behaviour to perturbations in both the initial condition and the step-like decrease in the production rate.
These results suggest that the regulatory module controlling filaggrin concentration, consisting on the interplay between two positive and two negative feedback arms, is responsible for the self-recovering behaviour that characterizes filaggrin content in the skin barrier.

3.3.3 Network motifs that result in self-recovering dynamical behaviour: The key role of negative feedback

As shown in the previous section, the skin barrier components lipids and filaggrin display a self-recovering dynamic behaviour in terms of robustness of its steady state values to perturbations both in the initial condition and in step (constant) changes in nominal production rate of barrier precursors.

Both for filaggrin and lipid content, the mechanism by which this self-recovering behaviour is achieved is though the presence of a negative feedback that controls the barrier formation process. This negative feedback is further modulated by positive feedback loops enacted by KLK (in the case of lipids, figure 3.4 B) and by the TEWL- and cytokine-mediated *de novo* expression of pro-filaggrin (figure 3.4 A).
These results are in congruence with numerous previous findings in the literature [210, 213, 214, 215, 216, 217, 218, 223, 219, 220, 221, 222] (discussed in section 3.3), that have identified negative feedback as the key mechanism responsible for the self-recovering dynamical behaviour.
Intriguingly, the self-recovering dynamical behaviour of the skin barrier components (figures 3.4 B,C) seems to depend not only on a negative, but also on a positive feedback structure. Few publications (for example, [228] and [197]) have discussed the role of positive feedback in stabilizing biological circuits controlled by a negative feedback. However, further research is needed to clarify the role of positive feedback in the determination of the self-recovering dynamical behaviour of the skin barrier components.

3.3.4 Phenomenological description of the self-recovering dynamical behaviour

The self-recovering dynamical behaviour upon perturbations in the initial conditions (impulse perturbation, figure 3.4 A, bottom) and on the production rate can be described in a phenomenological way with the equation 3.7:

$$\dot{X}(t) = \alpha(1 - \frac{X(t)}{\tilde{X}}). \tag{3.7}$$

Defining $\tilde{X}$ as the homeostatic steady state value of X, it can be seen directly from inspection of equation 3.7 that the steady state $X_{ss} = \tilde{X}$, regardless of the value of the parameter α. Indeed, variations in the parameter α affect the recovery time, but do not lead to deviations from the nominal steady state $\tilde{X}$. Furthermore, given that equation 3.7 has a unique steady state $\tilde{X}$, X is also perfectly robust to changes in initial conditions, it will always return to its steady state value after any impulse perturbation. This self-recovering dynamical behaviour of equations 3.7 (with $\alpha = 0.5$), and its agreement with the experimentally observed self-recovering dynamical behaviour of the barrier function of healthy human volunteers upon perturbation with soap [225] is shown in figure 3.4A (bottom).
For simplicity (reduction in number of parameters and state variables), in the remainder of the thesis, the mathematical models representing the network motifs responsible for the homeostatic behaviour of the skin barrier components (lipids and filaggin) are approximated by the equation 3.7.

3.4 Persistence of inflammation: Storing the memory of cytokine dynamics

Inflammation is a *cellular-level process* that involves the activation and migration of cells of the immune system, such as DC, polarized Th2 cells, or neutrophils, in response to *biochemical mediators* such as cytokines or antigens [116, 229].
Thus, inflammation is a process that involves two time-scales: fast dynamics of the biochemical species regulate cytokine production, and slow cellular level dynamics describe the migration, activation and death of immune cells.
Mathematically, this corresponds to an (uncoupled) Quasi-Steady State(QSS) state system, in which some of the variables are assumed to stabilize much (infinitely) faster than the other slower dynamic components of the system. Here, the variable triggering the slow immune cell migration process is the cytokine concentration (C), assumed to be in QSS because it is controlled by fast biochemical processes that mediate cytokine release (C_{ss}). In contrast, the level of migrated immune cells (I_P), changes dynamically in a slow time-scale τ. As depicted in figure 3.5 *left*, the dynamics of the cellular immune response mediators I_P can be described by a cytokine-dependent migration, and a natural death rate.
This simple network motif, depicted in figure 3.5 *left*, can be described by the ODE:

$$\dot{I_P}(\tau) = k_{\text{migration}} C_{\text{ss}}(\tau) - I_P(\tau) k_{\text{death}}. \tag{3.8}$$

As we have seen in section 3.2, the cytokine levels (output of immune responses) can be approximated by two discrete values, C_{high} and C_{low}, corresponding, respectively, to the upper and lower branches of the bifurcation diagrams (see also figure 3.2 *left*). Thus, an abrupt rise in the cytokine levels from C_{low} to C_{high}, will be followed by a steady, but slower, rise in the immune responses. Similarly, sudden decrease in the cytokine levels will lead to a eventual, but slower, decline in the inflammation. This qualitative dynamical behaviour is exemplified in figure 3.5. It shows the experimentally measured number of macrophages that migrate to the nasal epithelium of mice in response to a bacterial challenge that triggers cytokine release within hours of epithelial infection [230], as well as simulations of equation 3.8, setting $k_{migration} = 0.4$, $C_{high} = 100\%$, $C_{low} = 0\%$, and the time of high cytokine exposure, to 8 days.
This dynamical behaviour implies that (1) the cytokine levels that trigger the inflammation must remain high for a extended period of time for a full (maximal) induction of the inflammation to be triggered, and (2) inflammation *persists* for some time after the cytokine levels have been cleared (figure 3.5 *left*). Thus, although simple, this network motif confers *memory* to the system, because the inflammation levels depend on previous exposures to cytokines.

A transient rise in cytokine levels is mirrored by a transient but slow increase and decrease

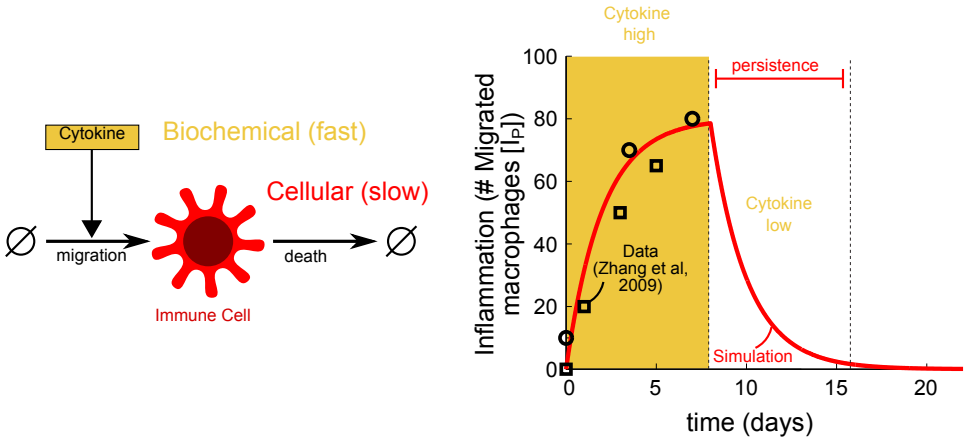

Figure 3.5: **Persistence of inflammation results from time-scale separation between fast cytokine dynamics and slow, cellular processes that involve mobilization of immune cells, triggered by cytokines** An abrupt rise in the cytokine levels from *low* to *high* is followed by a steady, but slower, rise in the immune response, as exemplified by the slow macrophage recruitment to the airway epithelium in response to a bacterial invasion [231] that triggers cytokine release within hours of epithelial infection [230]. Similarly, sudden decrease in the cytokine levels lead to a eventual, but slower, decline of the inflammation, which persists for some time even after cytokine levels have dropped.

in inflammation (figure 3.6 A). Similarly, low-frequency, recurrent exposure to cytokines is followed by oscillating inflammation that is able to resolve between two episodes of high cytokine exposure (figure 3.6 B). However, in a high frequency scenario, in which the time between two episodes of high cytokine exposure is too short for the inflammation to resolve, the persisting inflammation gradually adds up on each new event of cytokine exposure, constantly increasing until eventually stabilizing at oscillations with a higher amplitude than in the low-frequency scenario shown in figure 3.6 B. Under these conditions, the inflammation gradually stores the history of cytokine exposure, acting, effectively, as a capacitor (figure 3.6 C). Chronic exposure to cytokines leads to persistent inflammation that increases monotonically until eventually reaching its maximum amplitude, corresponding to the steady state value of equation 3.8 with $C_{ss} = C_{high}$ (figure 3.6 D).

Taking together, figure 3.6 shows that inflammation described by equation 3.8 is able to store the history of cytokine dynamics, characterized by a given frequency and amplitude.

This persistent network motif has has been observed in other biological systems. For example, it seems to play a important in mediating the context-dependent induction of gene expression by TF NFκB [232, 233], a master regulator that controls the gene expression of many target genes in a context-dependent way [234].

In the context of the reaction network controlling epidermal function, this network motif plays

a key role in the induction of cellular level immune responses by cytokines. Particularly, it is enacted by the migration of DC to the lymph nodes in response to TSLP stimulation [111], the PAR2-mediated recruitment of neutrophils from the blood to the epidermis [156], and the IL4-induced migration of differentiated Th2 cells from the lymph nodes to the epidermis [159, 189, 158].
Equation 3.8 can also be represented by its analytical solution, shown in equation 3.9:

$$I_{\mathrm{P}}(\tau) = k_{\mathrm{migration}} \int_0^{\tau} \mathrm{C_{ss}(t)} e^{k_{\mathrm{death}}(\tau - t)} \, \mathrm{d}t. \tag{3.9}$$

For simplification, in the next chapter, we will use this approximation to describe the persisting cellular level immune responses to cytokines.

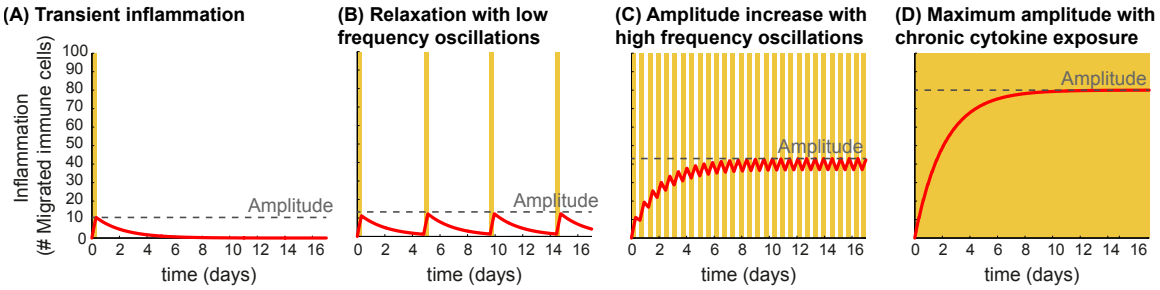

Figure 3.6: **A persistent network motif can act as a capacitor, by storing the history of cytokine dynamics with a given frequency and amplitude of cytokine exposure.** *(A)* transient rise in cytokine levels is mirrored by a transient increase and decrease in inflammation. *(B)* Similarly, low-frequency, recurrent exposure to cytokines is followed by a oscillating inflammation that is able to resolve between two episodes of high cytokine exposure. *(C)* In contrast, in a high frequency scenario in which the time between two episodes of high cytokine exposure is too short for the inflammation to resolve, the persisting inflammation gradually adds up on each new event of cytokine exposure, stabilizing at oscillations with a higher amplitude. *(D)* Chronic exposure to cytokines leads to persistent inflammation that increases monotonically until eventually reaching its maximum, steady state value.

3.5 Multi-scale structure of the reaction network controlling epidermal homeostasis

In this chapter, we decomposed the reaction network controlling epidermal homeostasis presented in the previous section into individual regulatory modules. These elementary building blocks can be grouped into three different network motifs, operating at two different timescales:

- A switch-like dose-response behaviour that characterizes *fast* biochemical interactions that mediate the release of cytokines in response to infiltrated pathogens (innate immune responses) or other pro-inflammatory cytokines (adaptive immune responses). They correspond to the regulatory modules represented in figures 2.3 B and G and in the yellow boxes in figure 3.1.

- Self-recovering dynamics characterizing epidermal barrier components (figure 3.4). These dynamics are driven by barrier restoration processes that involve both *de novo* production of skin barrier precursors (pL and pF) as well as and post-translational modifications resulting in the active barrier components (L and F). They correspond to the regulatory modules represented in figures 2.3 C), corresponding to the blue boxes in figure 3.1.

- Persistent levels of cellular immune mediators that are activated and migrate in response to rises in cytokine levels. They correspond to the regulatory modules represented in figures 2.3 A,I-III, corresponding to the red boxes in figure 3.1.

The switch-like dose-response behaviour is driven by biochemical interactions that mainly involve Protein-Protein Interactions (PPI), which occur at a comparatively much faster time-scale than the *slower* processes of barrier restoration (involving *de novo* synthesis of barrier components) and and mobilization of immune cells (involving migration and extravasation between body sites).
Hence, the network motifs that are considered here can be distinguished depending on in which time-scale they operate: network motifs leading to a switch-like dose-response behaviours operate quickly, stabilizing almost immediately as compared with the slower network motifs that result in homeostasis or persistent dynamics.
Together, the reaction network controlling epidermal homeostasis (figure 2.3) corresponds to a regulatory structure that comprises different modules (figure 3.1) and time-scales (fast PPIs controlling the switch-like cytokine production, intermediate *de novo* formation of barrier components, and slow migration and death dynamics immune cells).

3.6 Conclusions

Here, we decomposed the reaction network controlling epidermal homeostasis (figure 2.3) into individual regulatory modules, corresponding to three elementary building blocks characterized by a distinctive qualitative behaviour.
Each of the regulatory modules is associated to a particular qualitative behaviour, that can be mathematically represented either by simple mechanistic models from which the behaviour emerges, or by phenomenological descriptions described in this chapter.

For the mathematical representation of the switch-like release of cytokines characterizing innate and adaptive immune responses controlling epidermal function, we used mathematical descriptions that were previously proposed in [235] and [195], respectively.
To describe the dynamical behaviours of lipids and filaggrin (figures 3.4 B and C, respectively), we identified for the first time the reaction network structures that mediate the self-recovery dynamics of these skin barrier components, and proposed the first mathematical model that reproduces the self-recovery dynamics of skin lipids (equation 3.5). Another contribution of this chapter is that the recovery dynamics that characterize skin barrier components can be described in a phenomenological way by equation 3.7.
Regarding the persistence motif, in this thesis we identified the regulatory modules and the underlying network motif structure, and proposed a simple mathematical model that displays this persistent behaviour of the immune cells (figure 3.5). We show how this simple motif can act as a frequency filter that distinguishes between different types of cytokine dynamics (figure 3.6).
Each of these network motifs represents hence a distinctive **module** of the reaction network controlling epidermal homeostasis, characterized by particular inputs, outputs, genetic and environmental disturbances, feedback control and, importantly, a plant that operates at given time-scale (figure 2.3 A).
The **modular** and **multi-scale** representation of this detailed network is given in figure 3.1. In the coming chapters, we will analyse multi-scale, modular mathematical models that represent (parts of) this re-assembled reaction network.
First, in chapter 4 we will consider only the interplay between innate immune responses and barrier function. This is a valid and clinically meaningful simplification of the reaction network, since the adaptive immune responses are activated only during late stages of the disease. The model that we examine in chapters 4 and 5 corresponds thus to the early stages of the disease progression.
Then, in chapter 6, we will explore the conditions leading to activation of adaptive immune responses that are responsible for late and severe stages of the disease.
This gradual step - by step re assembly of the reaction network will allow us to reproduce the full pathological dynamics of AD, characterized by a onset phase described in chapter 4 and a disease aggraviation phase described in chapter 6.

Chapter 4

Modelling the early phases of AD: Interplay between protease-dependent innate immune responses, barrier function and infiltrating pathogens

The contents of this chapter are reproduced from our paper [236], that was published under a Creative Commons licence in February 2013. The original article can be found under `http://rsfs.royalsocietypublishing.org/content/3/2/20120090.full`.
The chapter consists of the Author Generated Postprint of the paper [236], preceded by a introduction that locates the paper in the context and terminology of this thesis.

4.1 Introduction to the published paper in the context of the thesis

In the previous chapter, we decomposed the reaction network controlling epidermal homeostasis (figure 2.3) into elementary building blocks (the regulatory modules) that can be grouped into three different network motifs (figure 3.1).
This chapter comprises the first step in the re-assembly of the decomposed reaction network. We consider the interplay between protease-dependent innate immune responses, barrier function and infiltrating pathogens that is disrupted during early phases of AD (figure 4.1). We neglect in this chapter the adaptive immune responses, which are activated only during the later stages of the pathogenic process.
The aim of this chapter is to understand how risk factors that are known to affect the functioning of these network motifs impair the reaction network, triggering the onset of the pathogenic

process. For this, we considered the genetic risk factors that lead to the reduction in the expression levels of the barrier component filaggrin (*"low FLG"*), the protease-inhibitor LEKTI (*"low LEKTI"*) and the immune response mediators AMP (*"low AMP"*). We also consider the environmental risk factor *"high pH"*, responsible for the pH-dependent increase in the catalytic capacity of the proteases.
The reaction network and the risk factors is given in figure 4.1, and was represented by the mathematical model that results from coupling following mathematical representations of the regulatory modules described in chapter 3:

- The concentrations of protease (KLK) and protease-activated receptor (PAR2) are described by the QSS variables $[\mathrm{KLK}^*]_\mathrm{s}$ and $[\mathrm{PAR2}^*]_\mathrm{s}$ in equations 4.1 b and 4.2. These QSS values are the steady state solutions to the system of equations 3.1 [84] for different values of S (equation 4.1 A).

- The dynamics of the barrier function is described in equation 4.1 B by a production term that corresponds to the phenomenological representation of the self-recovering dynamical behaviour of the barrier described in equation 3.7. We further assumed that the rate α in equation 3.7 (corresponding to the term $\frac{b_\mathrm{pre}}{1+k_\mathrm{L}[\mathrm{PAR2}^*]_\mathrm{s}}$ in equation 4.1) is negatively affected by $[\mathrm{PAR2}^*]_\mathrm{s}$. We also added a $[\mathrm{KLK}^*]_\mathrm{s}$-dependent degradation term.

- The immune reactions in equation 4.2 correspond to the solution to equation 3.8, given in equation 3.9, with $k_\mathrm{migration} = k_\mathrm{death} = 1$ and $C_\mathrm{ss}(\tau) = [\mathrm{PAR2}^*]_\mathrm{s}$.

Additionally, we added a dynamical description for the pathogen S (equation 4.1 A), assumed to increase by the infiltration through the skin barrier, and decrease by the immune responses.

Simulations of the resulting mathematical model of this sub-network (figure 4.1, represented in more detail in figure 4.2) with different risk factors, resulted in following three qualitatively distinct dynamic behaviours that correspond to the dynamical behaviours of the hybrid system described in section 3.2.6 (figure 3.3):

- **Homeostasis**: Return to a nominal, healthy steady state level after a transient decrease in barrier function and a single flare of innate immune responses.

- **Recurrence**: Cycles of barrier destruction and recovery and recurrent flares of innate immune responses.

- **Chronic damage**: Persistent barrier damage and unresolved immune responses.

As we can see in figures 4.5 and 4.6, the risk factors *"low AMP"* and *"high pH"* tend to trigger a chronic loss of homeostasis, while *"low LEKTI"* and *"low FLG"* are associated to recurrent flares of barrier damage and immune responses, of different amplitudes (figure 4.6, low) and

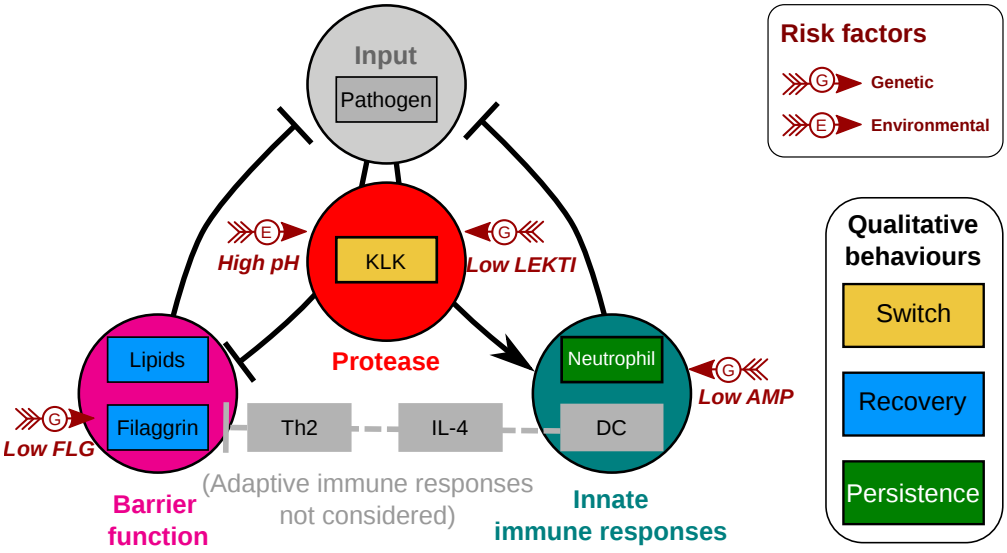

Figure 4.1: **Reaction network mediating the early phases of AD: Interplay between protease-dependent innate immune responses, barrier function and infiltrating pathogens.** Early phases of the pathogenesis of AD are characterized by the aberrant interplay between the regulatory modules controlling protease activity, filaggrin and lipid barrier components, and innate immune responses mediated by infiltrating neutrophils and release of AMPs. These regulatory modules can be grouped into three types of network motifs: switch-like dose-response behaviour characterizing protease activation, self recovery of barrier components, and persistence of the cellular mediators of the immune responses. Input of the multi-scale system is given by the amount of infiltrated pathogens, that is negatively affected by barrier function and by innate immune responses. The **G** (genetic) and **E** (environmental) risk factors considered here are represented by red arrows.

frequencies (figure 6.4).
We also used the model to explore the synergism between risk factors. Consistent with clinical observations, it was found that the combined action of risk factors leads to a significant increase in disease severity.
From these simulation results, following specific predictions can be derived:

1. The severity of the symptoms of the AD epidermis [171] can be classified into three qualitatively different dynamical behaviours of the skin barrier function that changes in response to a pathogenic challenge (figure 4.4):

    - In a healthy skin, the skin barrier quickly recovers to its homeostatic level (figure 4.4 A).
    - Mild forms of AD appear as recurrent flares of barrier damage (figure 4.4 B). In the clinic, this oscillatory behaviour is manifested as the sub-clinical barrier damage

that is characteristic of non-lesional AD skin.

- Severe forms of AD are manifested as a chronic loss of barrier function (figure 4.4 C) that is characteristic of lesional AD skin.

2. Alone, intermediate levels of the protease inhibitor LEKTI (modelled as the risk factor *"low LEKTI"*) or of the barrier component Filaggrin (modelled as the risk factor *"low FLG"* lead to recurrent loss of epidermal homeostasis.

3. A *"low pH"* or weak immune responses (*"low AMP"*) increase the frequency of these oscillations, eventually leading to a chronic damage.

In conclusion, in this chapter, we proposed mechanisms by which risk factors can lead to the loss of epidermal homeostasis, mediated by impaired balance in the interplay between barrier function and innate immune responses. With this, we could reproduce the early phases of the pathogenic process of AD.
In section 5, we use the insights obtained from the analysis of the early phases of AD obtained in this chapter, particularly the risk-factor dependency of the loss of epidermal homeostasis, to envision possible patient-specific treatment for the early phases of AD.
In chapter 6, we evaluate the impact of an impaired epidermis described in this chapter on the onset of *aberrant adaptive immune responses*. With this, we aim to uncover the mechanisms that underlie the severe phases of AD, characterized by an aberrant immune response that interferes with epithelial remodelling.
Combining the insights obtained in sections 5 and 6 can inform new and more efficient patient-specific early treatment strategies for AD that can prevent the onset of advanced and severe forms of the disease while minimizing the unwanted side effects of pharmacological treatments.

4.2 Risk-factor dependent dynamics of atopic dermatitis: Modelling multi-scale regulation of epithelium homeostasis

Authors:
Elisa Domínguez Hüttinger[1], Masahiro Ono[2], Mauricio Barahona[3], Reiko J. Tanaka[1 4]

Author-generated postprint of paper [236],
found under `http://rsfs.royalsocietypublishing.org/content/3/2/20120090.full`.

4.2.1 Abstract

Epithelial tissue provides the body with its first layer of protection against harmful environmental stimuli by enacting the regulatory interplay between a physical barrier preventing the influx of external stimuli and an inflammatory response to the infiltrating stimuli. Importantly, this interdependent regulation occurs on different time scales: the tissue-level barrier permeability is regulated over the course of days, whereas the cellular-level enzymatic reactions leading to inflammation take place within minutes. This multi-scale regulation is key to the epithelium's function, and its dysfunction leads to various diseases. This paper presents a mathematical model of regulatory mechanisms in the epidermal epithelium that includes processes on two different time scales at the cellular and tissue levels. We use this model to investigate the essential regulatory interactions between epidermal barrier integrity and skin inflammation and how their dysfunction leads to atopic dermatitis (AD). Our model exhibits a structure of dual (positive and negative) control at both cellular and tissue levels. We also determined how the variation induced by well-known risk factors for AD can break the balance of the dual control. Our model analysis based on time-scale separation suggests that each risk factor leads to qualitatively different dynamic behaviours of different severity for AD, and that the coincidence of multiple risk factors dramatically increases the fragility of the epithelium's function. The proposed mathematical framework should also be applicable to other inflammatory diseases that have similar time-scale separation and control architectures.

Keywords: Multi-scale modelling, epithelium, time-scale separation, atopic dermatitis, risk factors

[1]Department of Bioengineering, Imperial College London, London SW7 2AZ, United Kingdom
[2]Institute of Child Health, University College London, 30 Guilford St, London WC1N1EH
[3]Department of Mathematics, Imperial College London, London SW7 2AZ, United Kingdom
[4]Correspondence: r.tanaka@imperial.ac.uk

4.2.2 Introduction

Most physiological processes are tightly controlled by regulatory interactions across different temporal and spatial scales. An important example of such multi-scale regulatory interactions is found in the epithelium, the tissue covering the organs and cavities of animal bodies. The epithelium provides the first layer of protection against harmful environmental stimuli such as bacteria, chemicals or pollen through a tightly controlled interplay between the regulation of the physical barrier permeability to the environmental stimuli and the immune reaction to the infiltrating stimuli [34, 237, 39, 238]. Importantly, while the regulation of the physical barrier permeability results from the orchestration between growth, differentiation, and apoptosis of different cell types on the order of hours or days [139, 173], the phenotype of each cell within the epithelium is determined locally based on the concentration of local effectors (such as enzymes and gene transcripts) regulated through protein-protein interaction (PPI) networks on the order of minutes [239, 128]. In turn, the strength of the inter-epithelial stimulus depends on epithelial permeability, a tissue-level property determined by the epithelium's homeostasis. Therefore, regulation of epithelium function involves an interplay of fast inflammation-inducing PPIs with slow barrier-reconfiguring processes in an archetypical example of multiple-scale regulatory feedback.

Defects in this multi-scale feedback regulation may lead to the loss of epithelial homeostasis, inflammation and the development of diseases, including atopic diseases such as asthma [39], allergic rhinitis (hay fever) [12], and atopic dermatitis (AD) [7]. These diseases are typically characterised by two strongly interconnected symptoms (loss of barrier function and exacerbated inflammatory reactions to environmental stimuli) that occur at different spatio-temporal scales.

Epidemiological and biochemical studies have established the relevance of a variety of risk factors that predispose persons to atopic diseases, although the exact causes of these diseases are not fully understood. Risk factors include genetic polymorphisms, as well as environmental factors (such as exposure to allergens or pollutants) [127, 75, 182, 27]. However, the role of individual risk factors in epithelial function is difficult to pinpoint experimentally due to the complexity of the highly interconnected, multi-scale epithelium regulatory network. Indeed, loss of regulation triggered by a risk factor may be the result of imbalances between different processes across cellular and tissue levels. Furthermore, clinically relevant studies are hampered by the interference between multiple risk factors, often observed in patients with atopic diseases [181]. This paper presents a mathematical framework to analyse systems-level mechanisms for atopic diseases. Our framework allows us to systematically assess the effects of single

or multiple risk factors on epithelium function; study how the coincidence of multiple risk factors severely increases the propensity to develop atopic diseases; and deepen our understanding of the underlying mechanisms that lead to pathological conditions.

Several mathematical models have been proposed for studying the *spatial dynamics* of epithelial cells, including migration, proliferation, differentiation and death of gut cells in relation to colorectal cancer [60, 61], or reorganisation of the epidermis during wound healing [240, 56]. However, these models do not explicitly consider the regulatory interplay between the two defensive mechanisms of the epithelium, although the skin barrier integrity and the inflammatory response mediated by PPIs have been modelled in isolation [152, 99]. Our framework builds upon a mathematical model of the *cellular-level* regulatory mechanisms leading to AD that focuses on the activity of proteolytic enzyme kallikreins (KLKs) responsible for both skin desquamation and inflammation [84]. Although this cellular model successfully captures key clinical features of AD and their dependence on some risk factors, it does not consider the intertwined, multi-scale feedback regulation across cellular and tissue levels.

This paper proposes an ordinary differential equation (ODE) model of epithelium function that includes the essential regulatory interplay between the two protective properties that operate on different time scales: physical barrier integrity (on slow scales) and immune reactions to eradicate the stimulus (on fast scales). We focus on the disruption of homeostasis in the epidermis leading to AD, an archetypical example of atopic diseases that affects nearly 30% of the paediatric population worldwide [27]. AD is characterised by an abnormal hypersensitivity to environmental stimuli and a loss of skin barrier function and is commonly manifested as dry, scaly skin and a rash. Note, too, that the essential features of complex regulatory mechanisms clarified by our multi-scale model can be used to broaden our understanding of other pathophysiological processes related to the loss of epithelial homeostasis, particularly in asthma and hay fever, given the confirmed association between AD and other atopic diseases [27].

Crucially, it is the slow, tissue-level behaviour that is observable and used for treatment in clinical settings, yet such long-term dynamics are intricately interlinked with the fast, cellular PPIs. To study the slow dynamics, we assume a separation of time scales and consider quasi-stationarity at the cellular-level, leading to a system of differential-algebraic equations. Our model (Fig. 4.2) is constructed based on the view that overall homeostasis is achieved by mainly two types of regulated balance: one between activation and inhibition of KLKs at the cellular level and another between positive and negative feedbacks from inflammation-inducing signalling pathways to the strength of stimulus at the tissue level. The interplay between the fast cellular-level reactions [84] and the much slower tissue-level dynamics controlling the concentration of the inter-epidermal stimulus is needed in order to understand AD as being a result of the disruption of epithelium homeostasis: excessive skin desquamation weakens the skin barrier, allowing more stimulus to penetrate and trigger PPIs that result in immune reactions

capable of eradicating the stimulus and also lead to inflammation (Fig. 4.2A). Furthermore, our model allows us to identify particular terms and parameters that disrupt these balances at the cellular and tissue levels, which naturally correspond to well-known AD risk factors.

Our model reproduces several key clinical features of AD. In particular, it clarifies the relationship between risk factors and specific dynamical responses to external stimuli. The model also predicts, in a quantitative manner, the increase in the susceptibility of the epidermis to developing atopic conditions given multiple risk factors. These results contribute to the identification of the key underlying regulatory interplay between skin barrier homeostasis and inflammation in AD, and may lead to a more accurate characterisation of the disease symptoms required for personalised treatment. Moreover, our modelling approach, based on the time-scale separation and the view that the disease occurs as a result of loss of balance between dual (positive and negative) feedbacks, provides a theoretical framework for the study of multi-scale regulatory interactions in many other physiological systems. We discuss the generality of our modelling approach for studying the regulatory interactions between the cellular-level inflammatory response and tissue-level regulation of epithelial homeostasis.

4.2.3 Multi-scale model for atopic dermatitis

Our multi-scale model of epidermal homeostasis builds upon a recent cellular-level model for regulation of KLK activities [84], which we couple to a model of tissue-level regulation. The input and output of the cellular-level model are the stimulus and the resultant inflammation, respectively, which, in turn, become the output and input of the tissue-level model (Fig. 4.2C). The biological processes considered in the multi-scale model are explained below, while a complete model description, together with the nominal parameters used in the simulation, is found in the Appendix. The corresponding processes in the model (Fig. 4.2A) are indicated by the same labels (a)-(f) in Fig. 4.2C.

Modelling the tissue-level processes

Healthy skin with high barrier integrity prevents exacerbated penetration of environmental stimuli into the inner epidermal layers (Fig. 4.2A(g)) [132]. Our model considers the skin barrier integrity determined by a combination of the amount of corneocytes [113], their cohesion [43] and the lipid content [34] in the skin barrier. Accordingly, high barrier integrity is preserved by an appropriate balance between the production and desquamation rates of terminally differentiated keratinocytes and by maintenance of high lipid content. Skin barrier integrity is weakened as a result of cellular-level responses. Excessive activation of KLKs leads to increased skin barrier desquamation by degrading the inter-cellular junctions (Fig. 4.2A(a)) [113], while activation of Protease Activated Receptor 2 (PAR2) by active KLKs (Fig. 4.2A(c)) leads to enhanced

inhibition of the lamellar body lipid release into the skin barrier (Fig. 4.2A(b)) [139]. Upon disruption, the skin barrier triggers self-restoring mechanisms, in the forms of gene expression, lipid release and proliferation [34, 173].

A defective skin barrier with low barrier integrity allows more exogenous stimuli to invade the inner epidermal layers (Fig. 4.2A(d)), forming a positive feedback loop from active KLK and PAR2 (denoted by KLK* and PAR2* hereafter) to the stimulus concentration. For the inflammatory states, a large amount of PAR2* is induced and internalized, which then transduces stronger canonical signalling cascades and increases the expression of pro-inflammatory genes (Fig. 4.2A(e)) [112]. The inflammatory level in our model is accordingly represented by the level of PAR2*. These signalling cascades also trigger PAR2*-mediated immune reactions which persist even after the inactivation of PAR2* [116]. PAR2*-induced immune reactions eradicate the accumulated stimulus in the inner epidermal layers (Fig. 4.2A(f)) by mediating the release of antimicrobial peptides or the induction of keratinocyte phagocytosis [34, 157], forming a negative feedback loop from PAR2* to the stimulus concentration. The concentration of stimulus that penetrates the inner epidermal layers is thus determined by the balance between the positive and negative feedback regulations, whose strengths respectively depend on the skin permeability and the capacity of stimulus eradication (Fig. 4.2D).

The activities of the KLKs are regulated by the cellular-level PPI network (Fig. 4.2B), which is induced by the internalised stimulus, as modelled in [84]. Our model considers infiltrated stimuli, such as *Staphylococcus aureus*, which promote the production of KLK via the activation of pattern-recognition receptors [148, 37]. Stimulus-triggered release of KLKs and its inhibitor LEKTI into the extra cellular space (Fig. 4.2B(a)) is followed by auto-activation of KLKs (Fig. 4.2B(b)), inhibition of KLK* by LEKTI (Fig. 4.2B(c)), and activation of PAR2 through KLK* by proteolysis (Fig. 4.2B(d)). All of these protein interactions occur in a pH-dependent manner. The model also includes positive feedback from PAR2* to the expression of KLKs and LEKTI (Fig. 4.2B(e)). The activities of the KLKs are thus determined by the balance between their activation and inhibition rates (Fig. 4.2D).

We represent this multi-scale system of regulatory interactions as a system of integral-differential equations with the time-scale separation by assuming that the steady states of the cellular-level enzymatic reactions (attained in minutes to hours [128]) affects the tissue-level changes in the skin barrier (in days after perturbation by the external stimulus [139]).

Modelling the effects of risk factors for atopic dermatitis

We consider four risk factors that break the balanced regulation at each level, that is, the balance between the activation and inhibition of KLK* at the cellular level and the balance between the positive and negative feedback controls at the tissue level. They correspond to the following four main genetic and environmental elements known to predispose persons to AD.

High pH: Increased pH in the epidermis (pH around 6.5 in AD patients compared to 4.5 in healthy skin) leads to increased catalytic activity of KLKs [128, 113].

Low LEKTI: A decrease in the basal expression rate of LEKTI, a KLK inhibitor, leads to compromised inhibition of KLK activity [75].

High permeability: Increased skin barrier permeability, for example by a genetically determined decrease in the expression of filaggrin (an essential protein for maintaining strong cohesion between epithelial cells) [43], allows increased penetration of stimulus, leading to strong positive feedback from PAR2* and KLK* to the stimulus concentration. It is modelled with increased nominal skin permeability, $\widetilde{P}$, which corresponds to the permeability of the unaffected skin.

Weak stimulus eradication: Decreased capacity of the immune reactions to eliminate the infiltrating stimuli [6, 241] leads to compromised negative feedback from PAR2* to the stimulus concentration.

We investigate the effects of the risk factors (in isolation and combination) on the development of AD by altering the corresponding parameters in the model. The parameters corresponding to the cellular-level risk factors, "high pH" and "low LEKTI", are taken from [84]. New parameters corresponding to the tissue-level risk factors, "high permeability" and "weak stimulus eradication", are varied to see the effects of the balance between the positive and negative feedbacks on the development of AD.

4.2.4 Bistable switch with hysteresis at the cellular level

We are interested in the steady states of PAR2* and KLK* (denoted hereafter as $[\text{PAR2}^*]_\text{s}$ and $[\text{KLK}^*]_\text{s}$, with the subindex s indicating steady states), since we assume that $[\text{PAR2}^*]_\text{s}$ and $[\text{KLK}^*]_\text{s}$ are reached quickly compared with the overall tissue dynamics which they affect.

Figure 4.3A shows the bifurcation diagram for PAR2* (inflammation) described in [84] with the inter-epidermal stimulus concentration as a bifurcation parameter. This dose-response curve exhibits bistability, with *low* and *high branches* corresponding to the non-inflamed and inflamed states, respectively. Therefore, the state switches to the high branch when the stimulus increases above the *inflammation threshold* S^+ and remains there until the stimulus decreases below the *recovery threshold* $S^- < S^+$, at which point it goes back to the low branch and the inflammation stops. This classic hysteretic behaviour induced by the bistability of the model captures the characteristic features of AD, namely the outbreak and persistence of inflammation [84]. We note that similar bistability and hysteresis is observed for $[\text{KLK}^*]_\text{s}$ with the same S^+ and S^- values as for $[\text{PAR2}^*]_\text{s}$.

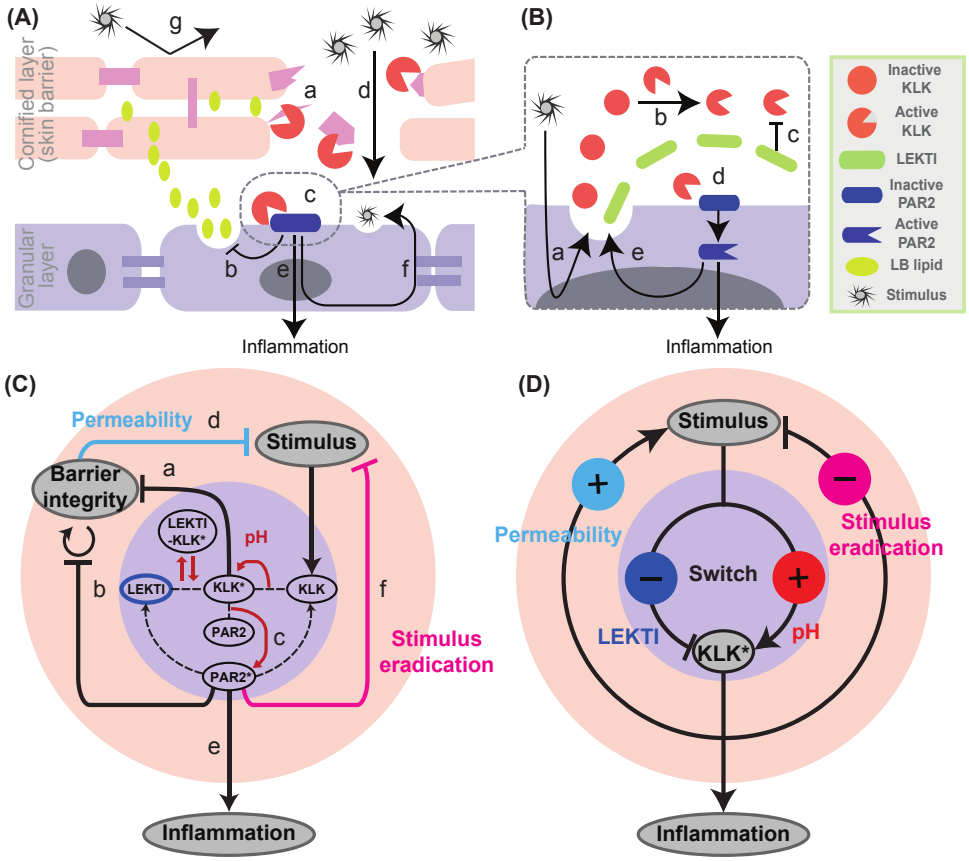

Figure 4.2: **Multi-scale model of Atopic dermatitis.** (A) Tissue-level reactions considered. (a) Skin desquamation by KLK* (active KLK), (b) inhibition of LB lipid release by PAR2* (active PAR2), (c) PAR2 activation by KLK* (at the cellular-level), (d) penetration of the environmental stimuli into the inner layers of the epidermis, (e) inflammation triggered by PAR2* (at the cellular-level), (f) eradication of stimuli by immune reactions, and (g) protection against environmental stimuli by healthy skin barrier. (B) Cellular-level reactions considered. (a) Release of inactive KLK and its inhibitor LEKTI enhanced by inter-epidermal stimulus, (b) auto-activation of KLK by proteolysis, (c) inhibition of KLK* by LEKTI, (d) activation of PAR2 by KLK*, leading to inflammation, and (e) increased release of KLK and LEKTI upon PAR2 activation. (C) Schematic representation of the multi-scale model for epidermal function, consisting of the tissue-level regulation for skin barrier integrity (beige circle) and the cellular-level PPI leading to inflammation (violet circle). (D) Core structure of our model and the risk factors. Switch behaviour of inflammation occurs through stimulus-induced PPI at the cellular level (violet circle) mediated by a combination of positive (KLK* activation) and negative (KLK* inhibition by LEKTI) controls. The concentration of the inter-epidemal stimulus is controlled at the tissue level (beige circle) by a combination of positive (via skin barrier permeability) and negative (via stimulus eradication) feedbacks from KLK*-activated PAR2* leading to inflammation. We consider four risk factors for AD, "high pH", "low LEKTI", "high permeability", and "weak stimulus eradication", each of which breaks the balanced control at the cellular and tissue levels.

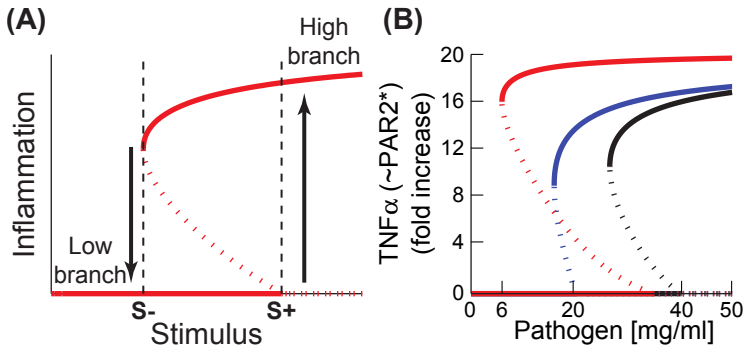

Figure 4.3: **Cellular-level switch-like behaviour.** Reproduced from [84]. (A) Schematic representation of the dose-response behaviour of PAR2* (inflammation) represented by bistability in the bifurcation diagram with varying concentrations of stimulus. The inflammation is on the low branch (no inflammation) until the stimulus increases to the inflammatory threshold S^+, at which point the inflammation switches to the high branch and persists until the stimulus falls below the recovery threshold S^-. (B) Cellular-level risk factors increase the severity of inflammation compared to healthy condition (black). "Low LEKTI" (blue) decreases S^+, increasing the sensitivity to the stimulus. "High pH" (red) decreases S^-, resulting in more sustained inflammation.

The effects of two risk factors, low LEKTI and high pH, on the development of AD have been investigated in [84], and they are in good agreement with clinical data from AD patients. Both risk factors increase the severity of the inflammation (Fig. 4.3B) but in different ways: A low LEKTI condition (blue) results in a lower S^+, corresponding to more susceptibility to the stimulus, as it requires less stimuli for inflammation to occur. A high pH condition (red) leads to a more persistent inflammation with lower S^-, as it requires a further decrease in the stimuli for the inflammation to stop.

4.2.5 Dynamical behaviours in the multi-scale model

This section presents a numerical characterisation of the slow, tissue-level dynamical behaviour of the full system in response to external stimuli, especially the dynamical behaviour of the skin barrier integrity, B, and the inter-epidermal stimulus concentration, S, which was a bifurcation parameter in the previous section. They both depend on $[\text{PAR2}^*]_s$ and $[\text{KLK}^*]_s$ (Fig. 4.2C, Eq. (4.1)). The skin barrier integrity is a clinically relevant variable as an indicator of epidermis health and can be measured by non-invasive methods. We can also follow the dynamic behaviour of PAR2*-mediated inflammation, which is induced when the barrier is damaged and ceases when the barrier starts to recover in the absence of PAR2*.

All the simulations presented below correspond to the response of the system to an external stimulus in sufficiently large concentration such that S rises above the inflammation threshold

S^+, moving the system onto the high branch in the bifurcation diagram for both cellular-level risk factors with a nominal barrier permeability (Fig. 4.3B).

Classification of dynamical behaviours in the slow time

For different sets of parameters, our model exhibits three qualitatively different dynamic behaviours for the skin barrier integrity when responding to environmental challenges of the stimulus (Fig. 4.4), in order of increasing severity of the AD manifestation:

Homeostasis: Complete recovery to the homeostatic level, typical for a healthy epidermis,

Oscillation: Periodic loss of homeostasis, often found in moderate AD skin, and

Persistent damage: Incapability of recovery to the homeostatic level, often observed in severe AD skin.

These three behaviours can be understood in terms of the interplay between the slow and fast dynamics leading to a quasi-static sweep of the bifurcation curve of the fast system.

In the case of homeostasis, the stimulus S is eradicated via immune reactions and falls below the recovery threshold S^-, at which point the inflammation stops as it jumps to the low branch (Fig. 4.4A, right). The barrier integrity then recovers to its homeostatic value with no inflammation (Fig. 4.4A, left). This behaviour is observed when the stimulus eradication is strong enough to decrease S below S^- through negative feedback, although the skin barrier suffers from transient damage while the inflammation is on the high branch, leading to the increase in S through positive feedback.

In some cases, however, S can increase again to S^+ after it transiently falls below S^-, thus re-triggering inflammation that again decreases S below S^- through the same mechanism. This cycle leads to an oscillation of the skin barrier integrity (Fig. 4.4B). Whether S re-increases to S^+ or not is determined by its steady state concentration, S_s, when the inflammation is on the low branch (no inflammation). If S_s is higher than S^+, then S eventually exceeds S^+. A high S_s reflects a weak barrier which cannot keep S low enough without the inflammation causing negative feedback on S.

Under other conditions, S cannot be decreased below S^-, for example, when the stimulus eradication is not strong enough (weak negative feedback) or when the barrier permeability is too high (strong positive feedback) (Fig. 4.4C). Such conditions lead to persistent damage of the skin barrier integrity with the complete loss of barrier integrity, as the inflammation cannot be resolved.

In addition to the qualitative nature of the dynamical behaviour, the severity of the transient barrier damage can be quantitatively evaluated in terms of two clinically relevant measures: the recovery time required for the barrier integrity to recover to its homeostatic level and the

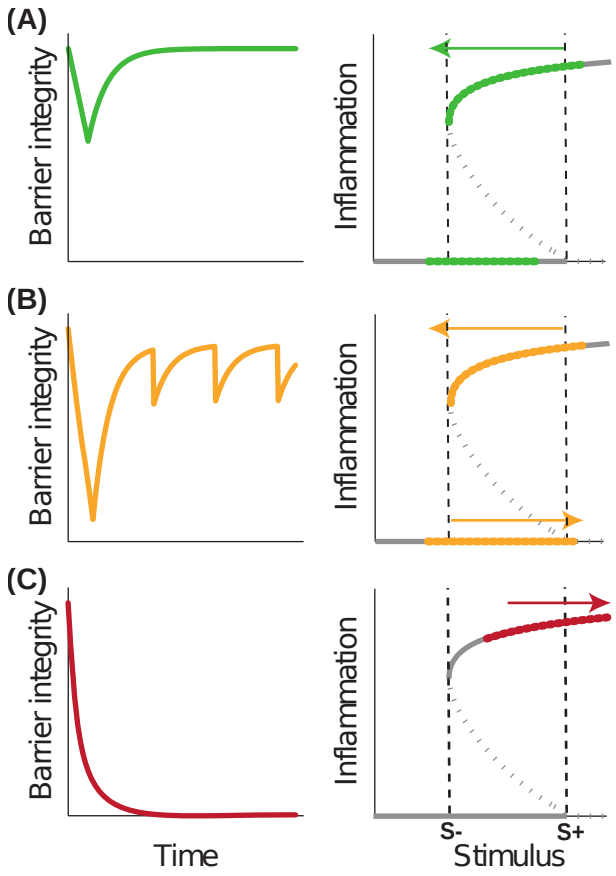

Figure 4.4: **Schematic representation of the three qualitative dynamic behaviours of skin barrier integrity after environmental challenges.** (A) Homeostasis: observed when the stimulus is decreased to S^- and the inflammation stops. (B) Oscillation: observed when the stimulus is repeatedly decreased to S^- (inflammation stops) and then re-increased to S^+ (inflammation reoccurs). (C) Persistent damage: observed when the stimulus fails to decrease to S^-.

maximum amplitude of the damage to the skin barrier. These two measures are usually not independent: the maximum amplitude of the barrier damage depends on the recovery time, since the longer the recovery takes, the heavier the damage is to the barrier.

Risk-factor dependent of dynamical behaviours in the slow time

Our model predicts the risk-factor dependence of the observed behaviour for the skin barrier integrity classified above, based on the different effects of each risk factor on the tissue-level dynamics of S, the value of S_s, which is a solution of the multi-scale model, and the threshold values S^+ and S^- determined by the cellular-level PPI (Fig. 4.5A).

Since the low LEKTI condition leads to a decrease in the inflammatory threshold S^+ (Fig. 4.3B, blue), S is more likely to increase to S^+ after it transiently decreases below S^-, thereby leading to an oscillation of the epidermal integrity (Fig. 4.5B, blue). The high pH condition with a lower

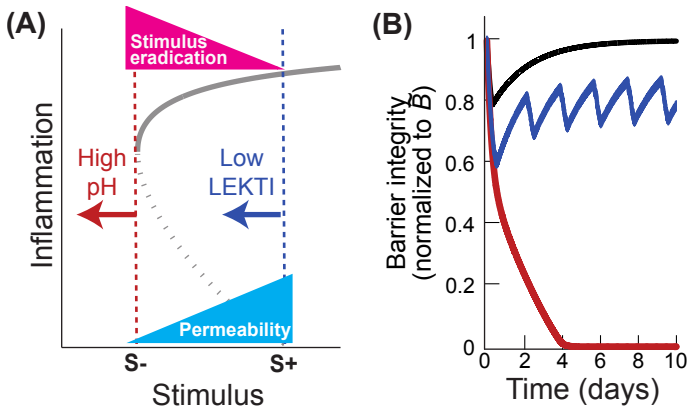

Figure 4.5: **Effects of risk factors.** (A) Schematic representation of the effects of single risk factors on the cellular-level bifurcation diagram. "High pH" decreases S^- and "weak stimulus eradication" prevents the decrease of S, resulting in difficulty in lowering S below S^-. "Low LEKTI" decreases S^+ and "high permeability" increases S, facilitating S to go above S^+. An increase of S by "high permeability" makes it more difficult to reach S^-. (B) Risk-factor dependent behaviour of barrier integrity. While healthy (black) shows homeostasis, "high pH" (red) leads to persistent damage, whereas "low LEKTI" (blue) results in oscillation. The effects of the tissue-level risk factors are shown in Fig. 4.6.

recovery threshold S^- (Fig. 4.3B, red) leads to persistent damage (Fig. 4.5B, red), because it is more difficult to decrease S below S^-.

The high permeability increases S by allowing more of the external stimulus to penetrate (Fig. 4.5A). The larger S is, the more easily S^+ is reached, leading to the oscillation, and the more difficult S is decreased to S^-, leading to the persistent damage. Increasing the degree of the high permeability risk factor (Fig. 4.6A, blue arrow) leads to a qualitative transition from homeostasis (green) to oscillation (yellow), and further to persistent damage (red). This transition is accompanied by a continuous increase in the maximum amplitude of the barrier damage. Note that the external stimulus does not penetrate enough to induce the inflammatory response ("non-responsive") if the permeability is very low (Fig. 4.6A, grey).

When the capacity of stimulus eradication is weak, S cannot be decreased even with high inflammation (Fig. 4.5A). Decreasing the capacity of stimulus eradication (Fig. 4.6A, pink arrow) results in a qualitative transition from homeostasis (green) to persistent damage (red) directly, with a continuous increase in the maximum amplitude of barrier damage. Weakening the stimulus eradication capacity by itself does not lead to the onset of oscillation, since it does not affect either of the two oscillation determining factors, i.e., S_s (determined by the non-inflamed state) or S^+ (determined by the cellular-level PPI).

Our quantitative analysis of the proposed model suggests that the severity of the (transient) damage to the skin barrier is significantly increased by the concurrence of multiple risk factors,

as is often the case for AD [127, 43, 42]. Concurrence of the two tissue-level risk factors ("high permeability" and "weak eradication") makes the transition from homeostasis to oscillation and persistent damage occur by a smaller increase in the degree of each risk factor, resulting in more frequent occurrences of oscillation and persistent damage with a larger maximum amplitude of barrier damage (Fig. 4.6A, grey arrow). Additional presence of cellular-level risk factors ("low LEKTI" (Fig. 4.6B) or "high pH" (Fig. 4.6C)) further increases the skin vulnerability, with a lower occurrence of "non-responsive" (grey) and "homeostasis" (green) and a higher proclivity towards "oscillation" (yellow) and "persistent damage" (red) with a larger maximum amplitude of barrier damage.

4.2.6 Discussion

The regulatory structure of the model leads to distinct dynamic signatures for different risk factors

We have proposed a multi-scale model of the epidermis as a means to investigate the regulatory interplay between the tissue-level skin barrier integrity and cellular-level inflammation with an intrinsic separation of time scales. As a result of a combination of the cellular-level switching and the tissue-level feedback control (Fig. 4.2D), our model displays three qualitatively different dynamic responses for skin barrier integrity: homeostasis, oscillations and persistent damage (Fig. 4.4). These behaviours emerge from a combination of balanced feedback regulation at the cellular level and tissue level.

Our multi-scale model allowed us to assess the impact of several risk factors on the epidermal function and suggests that each risk factor has its own specific dynamic signature (Fig. 4.6). These features could be used to characterise patient-specific causes of AD from the observed dynamic behaviours of the epidermis and to improve the personalised treatment of AD. Importantly, the risk-factor dependent qualitative behaviours do not depend on the particular choice of system parameters, but rather on the general structure of the multi-scale regulatory network model and how the different terms are affected by the risk factors. The $PAR2^*$-induced inflammation is regulated by a dual (positive and negative) control at the cellular level: negative control with inhibition of KLK^* by LEKTI and positive control with pH-dependent activation of KLK^* and $PAR2^*$. The concentration of stimulus at the tissue level is also controlled in a dual way: negative control to decrease it through its eradication and positive control to increase it by degrading the skin barrier. A balance between the two dual controls acting at the cellular and tissue levels is essential to maintaining the healthy homeostasis. The risk factors in this paper correspond to disturbed feedback strengths that cause an imbalance of the dual control (Fig. 4.2D), leading to either oscillatory or persistent loss of homeostasis. The concurrence of multiple risk factors, each of which affects the dual control, dramatically increases the fragility

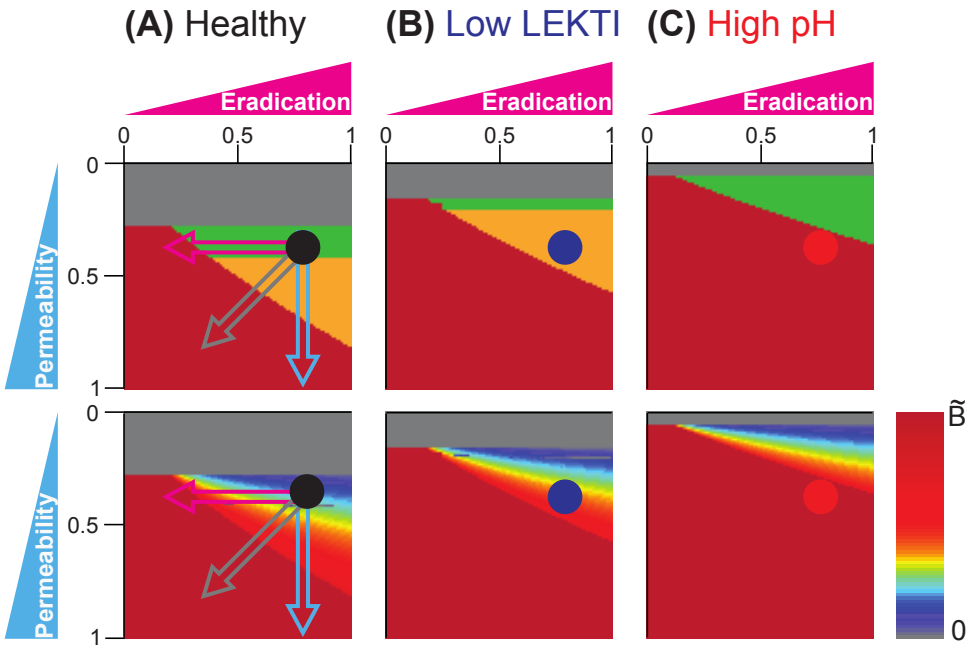

Figure 4.6: **Increase in skin vulnerability caused by the presence of multiple risk factors.** The figure presents a summary of the bifurcations and dynamical behaviours observed for different combinations of tissue-level risk factors ("high permeability" and "weak stimulation eradication") for (A) healthy (high LEKTI and low pH), (B) low LEKTI, and (C) high pH conditions. The black, blue and red circles in (A), (B), and (C) respectively correspond to the nominal values used for the simulation in Fig. 4.5B. Increase in AD severity is represented (top panel) by transition of the dynamical behaviours of the epidermal integrity from homeostasis (green) to oscillations (yellow) and further to persistent damage (red) accompanied (bottom panel) by increases in the maximum amplitude of the skin damage. The grey area indicates "non-responsive" due to the strong skin barrier integrity. (A) Increasing permeability (blue arrow) leads to a qualitative transition from homeostasis to oscillation, and further to persistent damage, accompanied by a continuous increase in the maximum amplitude. Decreasing the capacity of stimulus eradication (pink arrow) results in a direct transition from homeostasis to persistent damage. Concurrence of the two tissue-level risk factors accelerate this transition (grey arrow). Additional presence of cellular-level risk factors ("low LEKTI" (B) or "high pH" (C)) increases the skin vulnerability with a smaller region of "non-responsive" and "homeostasis" but with a larger region of "oscillation" and "persistent damage", compared to healthy (A).

of the regulatory system of epithelial function, even if the system is robust enough to buffer out disturbances caused by single risk factors.

Applicability to other inflammatory diseases

One of the main features of our model is the presence of a switch at the cellular level realised by the bistability in the bifurcation diagram of the inflammation (Fig. 4.3A), coupled with a slower regulatory system. This structure makes our model resemble an 'on-off' hybrid system [242], in which switching between two dynamic control regimes (depending on whether the inflammation is 'on' or 'off') determines the global behaviour of the system.

Pathogen-induced signalling cascades play a key role in protecting the body from infection by triggering immune reactions that contribute to the eradication of the stimulus. However, these signalling cascades also trigger tissue-damaging inflammation, since the induction of stimulus-eradicating mechanisms often concurs with the release of pro-inflammatory mediators [114, 130, 154]. The switch mechanism prevents unnecessary and inefficient immune reactions to be triggered, since the activation of the signalling cascades occurs only when the stimulus concentration is high enough (above the inflammation threshold) to endanger the tissue, and the immune reactions persist until the stimulus falls significantly below the inflammation threshold. This ensures that inflammation does not re-occur through random fluctuations of the stimulus concentration.

Unnecessary and ineffective immune reactions are accompanied by inflammation that can cause the destruction of tissues and has a significant impact on the epithelial function by affecting morphology [238, 157], composition [138], abundance [243] and micro-environment [34] of epithelial cells, without contributing to eradicating pathogens [244, 245]. Indeed, this constitutes a major part of pathology in many inflammatory and infectious conditions including atopic dermatitis [244, 245, 246]. Therefore, fast resolution of the inflammation is essential for the restoration of homeostasis, and relies on a balance between negative (via stimulus eradication) and positive (via tissue damage) feedback from the inflammation to the stimulus concentration.

The bistability of the cellular-level inflammatory responses together with the dual feedback on a longer time scale constitute a biologically reasonable architecture in terms of efficiency and robustness, and it has been found in many inflammation-inducing PPI networks [201, 247]. For example, bistability has been found in the multi-scale regulatory networks of the inflammatory response induced by cytokine interleukin 1 (IL1), another system of interest as regards AD [182, 248]. This system is similar in structure to the KLK system discussed in this paper, since PPI leading to IL1 activation is also triggered by stimuli that infiltrate through the skin barrier [122], including several biotic and abiotic allergens [49, 154], and active IL1 affects the stimulus concentration by initiating immune reactions that eliminate the stimulus [154] and by altering skin barrier formation [226]. Our model can also be applied to the other two atopic

diseases, asthma and hay fever, since the regulation of bronchial and nasal epithelium function occurs though a similar interplay between the tissue-level barrier and cellular-level inflammatory response in the epidermis, bronchial epithelium, and nasal epithelium [12, 27].

Clinical significance

Despite its clinical importance, the epidermal function has seldom been studied from a systems-level perspective. Conventional experimental approaches have not fully revealed the relationships between the barrier dysfunction and inflammatory response in the development of AD [241, 8]. Our model provides a platform to analyse the bi-directional interplay between skin barrier dysfunction and aberrant inflammatory response (Fig. 4.2D).

Our model suggests that the measurement of the barrier integrity over time can predict the type of clinical course a particular patient is expected to follow (Fig. 4.4). This is also compatible with clinical findings: the long-term prognosis of atopic patients may be related to the type of behaviour observed; whereas persistent inflammation is associated with a poor prognosis, patients with periodic inflammation have better chances for resolution of the disease, indicating there may be a correspondence between these behaviours to increasing severities of atopic diseases [249].

An empirical validation of our model predictions, particularly the association between the four risk factors and dynamic model behaviours (Fig. 4.6), and implementing the prediction in dermatological practice will require an empirical system-level investigation of the epithelium to measure the barrier integrity and inflammation over time for different phenotypes and environmental conditions. For this purpose, it is essential to develop a new way to continuously measure the barrier integrity over several hours to a day, for example by non-invasive measurement of transepidermal water loss and skin hydration measurements for the skin from AD patients [250] or by use of organotypic cultures, which allow temporal and spatial quantitative characterisation of the skin [251]. Validation of our results through such studies will contribute to a more efficient, patient-specific treatment of AD and other atopic diseases, since the risk factor triggering the disease condition in a particular patient can be deduced from the time course of the barrier integrity.

Possible extensions of the model and future work

Our model considers the essential processes and reactions that contribute to the regulatory interplay between tissue- and cellular-level dynamics at different time scales from the viewpoint of dual controls. This framework could be extended to include another level with an even slower time scale corresponding to the proliferation and differentiation of epithelial cells. The regeneration of the skin barrier requires skin barrier precursors, i.e., correctly differentiated cells at the

lower layers of the epithelium [171]. Our model assumes a constant concentration b_{pre} of skin barrier precursors. However, formation of these barrier precursors is in fact a dynamic process that is orchestrated among differentiation, proliferation and apoptosis of epithelial cells, and is further affected by inflammatory signals [226, 252]. Describing such dynamics of the epithelial cells at an even slower time scale and coupling it to the multi-scale model proposed here would allow us to explore the interplay between inflammation and epithelial tissue renewal, and to address interesting, open questions regarding deregulation of epithelium renewal in the context of inflammation, which plays an important role not only for AD [171], but also for the development of tumors [253].

The skin immune system can interact with the systemic immune system in AD, which may be incorporated into the model in the future. It has been widely observed that AD patients are more prone to develop asthma and hay fever, leading to the so-called atopic march [27, 62]. It is thought that allergic reactions occur in different organs due to *allergic sensitisation*, which is the induction of allergic reaction and the establishment of immunological memory by repeated exposure of inter-epithelial cells to antigen [27]. This sensitisation usually occurs at the systemic level, and the exposure to the allergen in other organs, after the establishment of sensitisation in the skin, can initiate allergic reactions and subsequent immunopathology there, although local factors such as the integrity of epithelium may be also important for the development of allergic diseases [254]. Incorporation of the allergic reaction in the model would allow us to explore not only the mechanisms of the atopic march but also the allergic diseases of strong clinical relevance [121, 255], while our model considers early events in the pathogenesis of AD that occur before adaptive immune responses to the stimuli, such as histamine release by primed mast cells, are initiated.

Concluding remarks

We proposed a multi-scale model for epithelial function which predicts that the underlying risk factors for AD can be inferred from the clinically observable dynamic response of the skin barrier to environmental challenges. Our model analysis using time-scale separation reveals the effects of AD risk factors on the epidermal function regulated by the dynamic interplay between inflammation and skin barrier permeability. Our results may lead to a better understanding of the design principles of the regulatory systems for epithelial homeostasis and inflammation and may be able to be extrapolated to other atopic diseases. Our modelling approach provides a theoretical framework for studying multi-scale regulatory interactions, characteristic of nearly all physiological systems.

Atopic diseases represent an important and unresolved health problem, mainly because their causes have not yet been elucidated due to the complex nature of the underlying regulatory networks across different scales. Clinical research will benefit from our systems-level mathemat-

ical framework for studying epithelium function, as it will allow systematic evaluations of the effects of risk factors and different treatments, such as corticosteroids or emollients, on clinically observable epithelium markers such as the barrier function. We expect our research will contribute to a deeper understanding, more accurate description, and patient-specific treatment of atopic diseases.

Acknowledgments

EDH thanks the Mexican Council for Science and Technology (CONACyT) for a PhD scholarship. MO is a Human Frontier Science Program Long-Term Fellow. MB acknowledges partial support from the BBSRC through grants BB/F005210/2 and BB/G020434/1. RJT acknowledges funding from the EPSRC through a Career Acceleration Fellowship.

4.2.7 Appendix

Multi-scale KLK model description

Our multi-scale model is a combination of the cellular-level model proposed in [84] (Model 1 with positive feedback from $[\mathrm{PAR2}^*]$ to LEKTI production) and a tissue-level model described as:

$$\frac{dS}{d\tau} = S_{\mathrm{out}}\,\frac{\widetilde{P}}{B+\varepsilon} - S\,(f_{\mathrm{IP}} I_{\mathrm{P}} + I_0)\,, \tag{4.1a}$$

$$\frac{dB}{d\tau} = \frac{b_{\mathrm{pre}}}{1+k_{\mathrm{L}}[\mathrm{PAR2}^*]_{\mathrm{s}}}\left(1-\frac{B}{\widetilde{B}}\right) - d_{\mathrm{K}}[\mathrm{KLK}^*]_{\mathrm{s}} B, \tag{4.1b}$$

where τ corresponds to the slow time scale, S is the concentration of the inter-epidermal stimulus and B is the barrier integrity.

The inter-epidermal stimulus, S, increases by the penetration of external stimulus, S_{out}, through the barrier, hence its rate is proportional to S_{out} and inversely proportional to the skin barrier integrity, B (Fig. 4.2C(d)). The minimum barrier integrity, ε, reflects the fact that even very severe cases of AD [44] do not lead to a complete destruction of the skin barrier and ensures that the model is always well-defined. Eradication of S occurs by the combination of $\mathrm{PAR2}^*$-independent (I_0) and -dependent (I_{P}) immune reactions (Fig. 4.2C(f)) represented by

$$I_{\mathrm{P}} = \int_0^{\tau} [\mathrm{PAR2}^*]_{\mathrm{s}} e^{-\tau+x}\,\mathrm{d}x, \tag{4.2}$$

where the convolution with a decaying exponential captures the persistence of the immune reactions even after inactivation of $\mathrm{PAR2}^*$ [116].

The barrier integrity, B, is determined by the balance between the production and degradation of the barrier. The barrier is produced from precursors, which are assumed to be constantly available with a fixed concentration, b_{pre}, and lipids, whose release is inhibited by PAR2* (Fig. 4.2C(b)). The capacity of the barrier to self-restore the nominal barrier integrity, $\widetilde{B}$, following its disruption [34, 173] is represented by a logistic term. The degradation of the barrier occurs as a result of desquamation mediated by KLK* (Fig. 4.2C(a)).

Note that $[\text{PAR2}^*]_{\text{s}}$ and $[\text{KLK}^*]_{\text{s}}$ are the stable steady state concentrations of PAR2* and KLK* obtained from the ODE model [84] for the cellular-level PPI reaction network which describes the dynamic behavior of the concentration of six species, including PAR2* and KLK*, as a six-dimensional system of ODEs with 21 parameters.

Parameter values and robustness of the model outcomes

The nominal values of the parameters for the cellular-level model are taken from [84]. For the tissue-level model, we chose nominal values (Table 4.1) that are consistent with available experimental data. Since the experimental data to date is qualitative rather than quantitative, our model predictions are concerned with the qualitative effects of the risk factors, in terms of a loss of balance of the dual control, on the system's behaviour.

Such results are largely robust to the parameter choices, as confirmed by a detailed analysis of the sensitivity of the parameters on the model behaviours. Our numerics show that the qualitative behaviour is preserved when the parameters are changed 10-100 fold. More specifically, the PAR2*-independent immune reactions (I_0) and the nominal skin barrier integrity ($\widetilde{B}$) are scaling factors for S_{s}. The concentration of skin barrier precursors (b_{pre}) affects the skin barrier recovery time, but does not alter the qualitative behaviours. The strength of lipid release inhibition by PAR2* (k_{L}) and the rate of desquamation by KLK* (d_{K}) scale the concentrations of $[\text{KLK}^*]_{\text{s}}$ and $[\text{PAR2}^*]_{\text{s}}$, thus affecting the propensity for persistent loss of homeostasis but not the qualitative behaviours.

The other two parameters of the model encapsulate the effects of particular risk factors. The skin permeability ($\widetilde{P}$) was varied from $\widetilde{P} \approx 0$ (no influx of the stimulus) to $\widetilde{P} = 1$ (100 % permeable barrier) to assess the effects of the "high permeability" risk factor on the model behaviours (Fig. 4.6). The effects of the "weak stimulus eradication" risk factor were assessed through varying the corresponding parameter (f_{IP}) from 0.01 (weak stimulus eradication) to 1 (healthy stimulus eradication) (Fig. 4.6). Varying f_{IP} for orders of magnitude higher and lower did not show qualitatively different results.

Table 4.1: Parameters of the mathematical model of the early stages of AD

Parameter	Description	Nominal value	Units
S_{out}	Concentration of external stimulus	95	mg/ml
$\widetilde{P}$	Nominal skin permeability	0.4	1/day
f_{IP}	Strength of stimulus eradication by PAR2*-mediated immune reactions	0.8	1/day
I_0	PAR2*-independent immune reactions	1	1/day
b_{pre}	Concentration of skin barrier precursors	0.5	1/day
k_{L}	Strength of lipid release inhibition by PAR2*	10	none
$\widetilde{B}$	Nominal skin barrier integrity	1	none
d_{K}	Rate of desquamation by KLK*	0.1	1/day
ε	Minimum barrier integrity	0.01	none

Model analysis

$[\text{PAR2}^*]_{\text{s}}$ and $[\text{KLK}^*]_{\text{s}}$ were calculated by solving the fixed point for algebraic equations of the cellular-level model [84] using Maple 13 (Maplesoft, Waterloo, Ontario, Canada). These were used for the dynamic simulations of the multi-scale model using the ODE solver `|ode23t|` in Matlab Version R2010a (The MathWorks, Inc., Natick, MA, USA). The solver `|ode23t|` was chosen to increase the accuracy of the numerical simulations of our stiff multi-scale model, in which abrupt changes in the QSS variables $[\text{KLK}^*]_{\text{s}}$ and $[\text{PAR2}^*]_{\text{s}}$ dramatically change the dynamical behaviour. At each iteration of the solver, the values of $[\text{PAR2}^*]_{\text{s}}$ and $[\text{KLK}^*]_{\text{s}}$ were updated according to the history of S, by using the `|odeset|` command in the function declaration.

Chapter 5

Modelling the effects of treatment of AD: Towards optimal patient-specific treatment for the early phases of AD

5.1 Introduction

In this section, we use the insights obtained in chapter 4 on the disease mechanisms underlying early phases of AD to explore the effects of possible treatments on the pathogenic process. With this, we aim to contribute to the design of patient-specific therapeutic interventions that can prevent the aggravation of the disease (discussed in chapter 6).

We focus on three treatments commonly prescribed to AD patients: antibiotics, emollients and corticosteroids. They directly affect the infiltrated pathogens, the barrier function and the immune responses, respectively [24, 25, 256].

Intriguingly, different treatments benefit only a fraction of AD patients [24]. Likely, this patient-specific effectiveness of the individual treatments can be attributed either to the patient-specific cause (risk factor) or to the patient-specific stage (early vs. late) of the disease [25]. Effective, personalized treatment thus requires an understanding of the underlying mechanisms of these different treatments, and how their impact on the restoration of epidermal homeostasis depends on particular causes and stages of the disease process.

Further, prolonged treatment in the form of antibiotics, emollients and corticosteroids can have adverse long term effects on epidermal homeostasis. For example, frequent use of high doses of antibiotics can lead to antibiotic resistance [23], long term use of emollients can impair barrier restoration mechanisms due to its occlusive effects [150, 174], and extended use of corticosteroids impairs barrier function [64], due to its interference with keratinocyte proliferation and differentiation programs [65]. It is hence clinically relevant to minimize the strength and dura-

tion of the treatment [63]. Our quantitative analysis proposed here corresponds to a first step towards this optimization of the treatment strategy.
To achieve this goal, we explore possible mechanisms responsible for differential effects of these treatments in the context of the model proposed here. This quantitative framework allows the investigation of potential patient-specific causes of AD [236], contributing towards the development of personalized treatment strategies.
The results presented here are preliminary, and are being further investigated in collaboration with Dr Yuzuru Sato (visiting researcher at Imperial College London) and William Nightingale (undergraduate student at the Department of Bioengineering, Imperial College London).

5.2 Mathematical model of the treatments

To model the risk-factor dependent effects of the three different treatments on loss of epidermal function that occurs in early phases of AD, we add following terms to equation 4.1, corresponding to the effects of antibiotics, corticosteroids and emollients, respectively:

- **Antibiotics** increase the rate of elimination of infiltrated stimulus. They are modelled by adding a second degradation term in equation 5.1.
- **Emollients** increase the barrier function. They are modelled by adding a constant term to the barrier production rate (green term in equation 5.1).
- **Corticosteroids** have opposing effects on the functioning of the epithelium. First, they decrease the strength of the immune responses [66]. This mitigates the barrier damaging effects of inflammation (desired therapeutic effect), but can also lead to a increased infection due to reduction of pathogen-eradicating immune responses (adverse effect) [65]. Moreover, sustained use of corticosteroids lead to a decrease in barrier function by interfering with the barrier formation process, an adverse effect known as skin atrophy [65]. We model these effects by the blue terms in equation 5.1, namely:
  - Decreasing the rate of immune-response-dependent barrier degradation, with rate $\kappa_{\text{degradation}} \in [0,1)$. This represents the corticosteroid-induced mitigation of inflammation-induced barrier damage.
  - Decreasing the rate of immune-response-dependent pathogen elimination, with rate $\kappa_{\text{pathogen}} \in [0,1)$. This represents one adverse effect of corticosteroids.
  - Scaling the interference of PAR2-mediated inflammation with the barrier production rate, by the term $C(t)\kappa_{\text{production}}$. Values for $\kappa_{\text{production}} < 1$ reduce the barrier damaging effects of PAR2-dependent inflammation (desired therapeutic effect),

while values of $\kappa_{\text{production}} > 1$ represent a increase in the interference with barrier formation processes (adverse effects).

For simplicity, we chose to model the effects of corticosteroids on epidermal homeostasis by this phenomenological approximation. In an alternative, mechanistic representation of the effects of corticosteroids on the inhibition of immune responses, we modelled the effects of the corticosteroids by assuming that $C(t)$ decreased the rate of activation of the PAR2-mediated immune response pathway. Particularly, we assumed that the corticosteroids decrease the rate of PAR2 activation of the model proposed in [235] (k_{P} in equation 3.1). The resulting simulations are shown in figure 5.1. Clearly, the corticosteroids affect the stimulus-dependent onset of PAR2-mediated immune responses by simply decreasing (linear scaling) the strength of the PAR2-mediated immune responses, but do not significantly affect the threshold parameters S^- and S^+. These results suggest that a mechanistic representation of the effects of corticosteroids on the $PAR2-$ mediated immune responses (by scaling the PAR2 activation rate, as in figure 5.1) can be reasonably approximated by the phenomenological representation in equations 5.1 (scaling of immune responses I_P, barrier damage mediated by active KLK^*_{s}, and inhibition of barrier production meditated by active PAR2^*_{s} effects).

The mathematical model used for the quantitative analysis of the risk-factor dependent effects of treatments is given in equation 5.1:

$$I_{\text{P}} = \int_0^{\tau} [\text{PAR2}^*]_{\text{s}} e^{-\tau+x}\,\text{d}x, \tag{5.1a}$$

$$\frac{dS}{d\tau} = S_{\text{out}}\frac{\widetilde{P}}{B+\varepsilon} - S(t)\,C(t)\kappa_{\text{pathogen}}\,(f_{\text{IP}}I_{\text{P}} + I_0) - S(t)Antibiotics(t), \tag{5.1b}$$

$$\frac{dB}{d\tau} = Emollient(t) + \frac{b_{\text{pre}}}{1+k_{\text{L}}C(t)\kappa_{\text{production}}[\text{PAR2}^*]_{\text{s}}}\left(1-\frac{B}{\widetilde{B}}\right) - d_{\text{K}}C(t)\kappa_{\text{degradation}}[\text{KLK}^*]_{\text{s}}B. \tag{5.1c}$$

A healthy epidermis is modelled by assuming the nominal parameters of the model 3.1 (HC in [84]), with $S_{\text{out}} = 95$, $\tilde{P} = 0.4$, $f_{\text{IP}} = 0.8$ and $b_{\text{pre}} = 0.5$ in equation 5.1. High protease activity induced by *high pH* is modelled by increasing the catalytic rates of KLK in model 3.1 (High pH in [84]). The other parameters used for the model simulations (figures 5.2 and 5.1) are given in table 5.1.

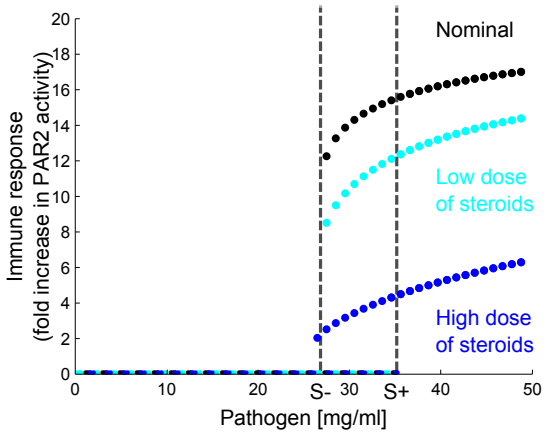

Figure 5.1: **A mechanistic representation of corticosteroid treatment results in a simple scaling of the dose response diagram describing protease mediated inflammation** A mechanistic model of corcorticosteroid treatment (decrease in the PAR2- activation rate k_P in equation 3.1) results in a almost-linear decrease in the steady state levels of PAR2 activity ("Inflammation"), without significantly changing the threshold parameters S^+ and S^-. Hence, this effect can be approximated by simply scaling the steady state levels of $PAR2^*$ and KLK^* on epidermal function, as in equations 5.1.

5.3 Qualitative analysis of patient -specific treatment strategies for the early phases of AD

In sections 4.2.5 (particularly, figure 4.5) and 3.2.6, we determined the two different mechanisms by which risk factors can lead to the loss of epidermal homeostasis. It occurs by differentially affecting the relative position of the steady state values of the infiltrated stimulus when immune responses are low (S_{ss}^{low}) or high (S_{ss}^{high}) respect to the threshold values S^- and S^+.
Recall that a homeostatic epidermis requires $S_{ss}^{low} \leq S^+$ and $S_{ss}^{high} < S^-$ (figure 3.3).
Risk factors such as *"low LEKTI"* or *"low FLG"* preferentially impair the first of these conditions. By *decreasing* S^+ (*"low LEKTI"*) or *increasing* S_{ss}^{low}, these risks factors propitiate $S_{ss}^{low} \leq S^+$, resulting in a recurrent events of barrier damage and inflammation (figure 5.3 A,B)
Risk factors such as *high pH* or *low AMP* preferentially impair the second of these conditions for homeostasis. The risk factor *high pH decreases* S^-, and *low AMP increases* S_{ss}^{high}, resulting in a persistent loss of epidermal homeostasis (figure 5.2 A,B). Accordingly, treatment can propitiate the recovery of epidermal homeostasis by restoring $S_{ss}^{low} \leq S^+$ or $S_{ss}^{high} < S^-$.
Antibiotics and emollient treatments decrease both S_{ss}^{low} and S_{ss}^{high}. Therefore, they can potentially counteract epidermal loss of homeostasis regardless of the mechanism that triggers the disease.
In contrast, corticosteroid treatment interferes with the effects of immune responses on epider-

Table 5.1: Parameters of the model of the treatment of the early phases of AD (dimensionless and arbitrarily chosen parameters for simulating equations 5.1)

Symbol	**Name**	**Nominal values**	
	Treatment parameters		
		no treatment	treatment
$Emollient$	Emollient treatment	0	1 (low), 5 (high)
$C(t)$	Corticosteroid treatment	1	0.1
$\kappa_{\text{degradation}}$	Inflammation-dependent barrier degradation	1	0.1
$\kappa_{\text{production}}$	Inflammation-dependent inhibition of barrier production	1	0.1
κ_{pathogen}	Inflammation-dependent pathogen elimination	1	0.05
$antibiotic$	Strength of emollient treatment	0	1
	Phenotype parameters		
		healthy	disease
f_{IP}	Strength of immune response	0.8 (HC)	0.1 (low *AMP*)
$\tilde{P}$	Skin barrier permeability	0.4 (HC)	0.7 (low *FLG*)

mal function, and can therefore only affect S_{ss}^{high}. Hence, corticosteroid treatment might lead to remission only when the loss of epidermal homeostasis is driven by $S_{\text{ss}}^{low} > S^{+}$.

Figure 5.2 C exemplifies a scenario in which loss of epidermal homeostasis is caused by *low AMP*, resulting in $S_{\text{ss}}^{high} > S^{-}$ (figure 5.2 B), even though $S_{\text{ss}}^{low} \leq S^{+}$ (bistability discussed in section 3.2.6). In this case, a single dose of antibiotics, which reduces $S(\tau)$ below S^{-} (figure 5.2 C), results in total remission (figure 5.2 D). Analogous results are obtained for a scenario in which loss of epidermal homeostasis is caused by *high pH* (figure 5.2 E).

In these examples, a single dose of treatment are sufficient to trigger total remission. The treatment has to be sufficiently strong to drive $S(\tau)$ below S^{-}. Once reached S^{-}, the infiltrated pathogen will stabilize to a homeostatic value of $S_{\text{ss}}^{low} \leq S^{+}$ (as shown in figure 5.2 C). In the case of antibiotics treatment, the stronger the dose, the more likely $S(\tau)$ can be driven below S^{-}. For corticosteroids, however, a optimal dose that leads to remission corresponds to a intermediate concentration of corticosteroids, because of the dual effects of corticosteroids on barrier function and pathogen load.

Figure 5.3 shows a scenario in which use of emollients alleviate the recurrent flares of barrier damage and inflammation (figure 5.3 A) caused by the combination of $S_{\text{ss}}^{low} > S^{+}$ and $S_{\text{ss}}^{high} > S^{-}$ (figure 5.3 B). Specifically, we consider the cases in which emollients compensate the damaging effects of *"low LEKTI"* (figure 5.3 C) and *"low FLG"* (figure 5.3 D) by increasing S_{ss}^{low}.

In the absence of emollients, *"low LEKTI"* or *"low FLG"* induce recurrent flares of inflam-

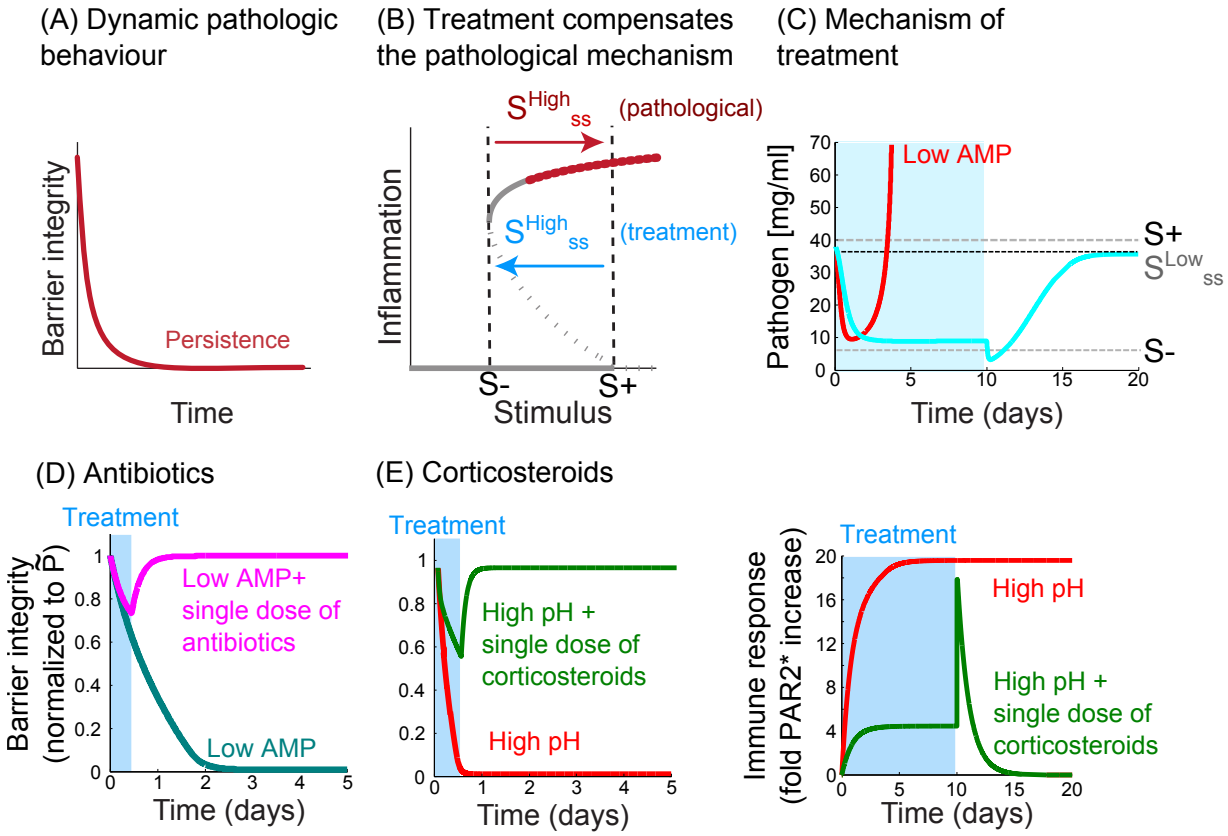

Figure 5.2: **Complete remission of AD can be achieved by treatment that drives the transition from a unhealthy to a healthy steady state** The qualitative dynamic behaviour "persistence" *(A)*, resulting from a inability to reach the recovery threshold value S^- in the bifurcation diagram *(B)*, can be compensated by a single dose of treatment that enables the decrease of $S(\tau)$ in equation 5.1 until surpassing S^-. Once reached S^-, the treatment can be suspended, and $S(\tau)$ (now on the low branch) stabilizes to $S_{ss}^{low} < S^+$ *(C)*. Two examples of these treatments include antibiotics *(D)* and and corticosteroids **(E)**, that can lead to restore epidermal homeostasis that is lost by low AMP and or high pH, respectively.

mation with a high amplitude and frequency (figures 5.3 C and D, red lines). Low doses of emollient decrease both amplitude and frequency of these oscillations (figures 5.3 C and D, blue lines), by accelerating the decrease of $S(\tau)$ to S^- ($\dot{S}$ in equation 5.1 b is larger in the presence of emollients), even if the dose is not strong enough to decrease treated S_{ss}^{low} below S^+. Emollients can lead to a complete remission if the dose is sufficiently high to decrease S_{ss}^{low} below S^+ (black lines in figures 5.3 C and D).

Note that when loss of homeostasis is caused by $S_{ss}^{low} > S^+$, a constant use of emollients is necessary to alleviate the loss of epidermal homeostasis. As soon as the treatment is stopped, S_{ss}^{low} will return back to its original, high steady state, re-setting the pathogenic phenotype given by the recurrent flares of inflammation.

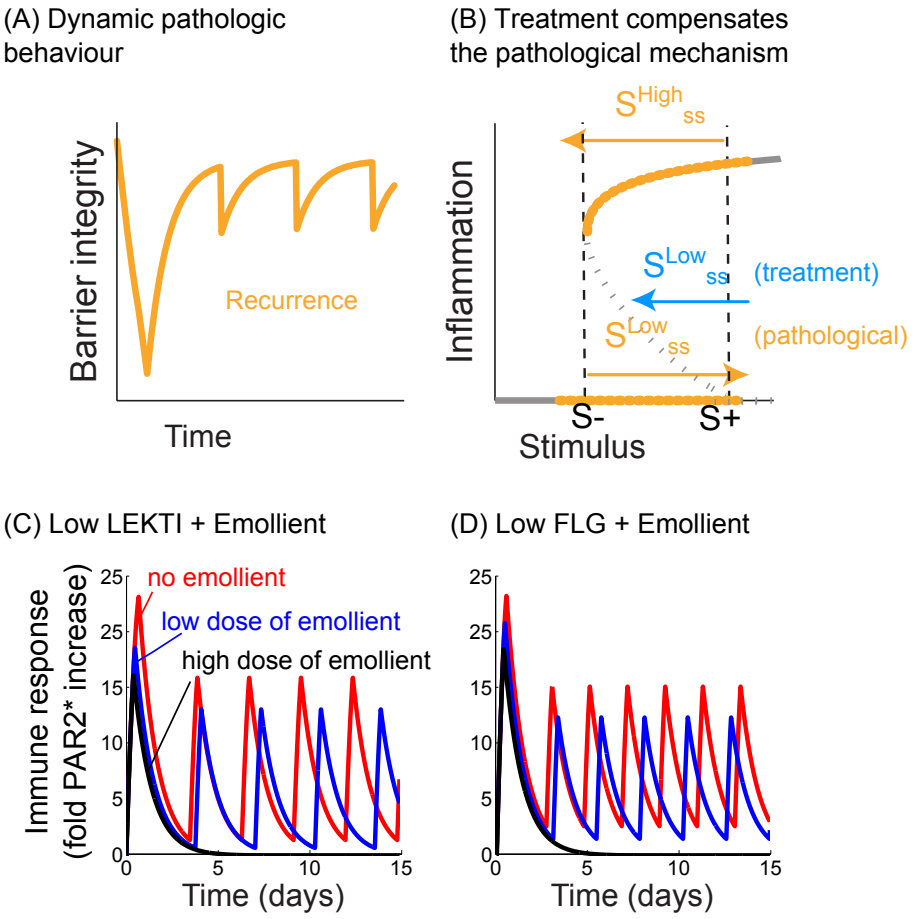

Figure 5.3: **Emollients decrease the frequency and amplitude of recurrent inflammation in a dose-dependent way.** The qualitative dynamic behaviour "recurrence" **(A)**, results from a increase in S_{ss}^{low} to a value above S^{+} that is caused by risk factors such as *"low LEKTI"* **(C)** or *"low FLG"* **(D)**. This loss of homeostasis can be alleviated by emollients, which reduce S_{ss}^{low} in a dose-dependent manner. Low doses of emollients reduce the amplitude and magnitude of the recurrent inflammation, while high doses of emollients lead to a recovery of epidermal homeostasis.

5.4 Conclusions and future work

In this section, we presented a qualitative analysis of the effects of three common treatments, namely antibiotics, emollients and corticosteroids, on the early development of AD.

We explored how different treatments can differentially affect epidermal function that has been lost in a risk-factor dependent way. These results contribute to understanding the patient-specific effects that characterize the treatment of AD [24].

So far, our results rely on a *qualitative* analysis that is based on the hybrid systems approach, proposed in [207, 208] and discussed in section 3.2.6. It helped us to pinpoint different mechanisms by which treatment can lead to the recovery of homeostasis. We exemplified these

mechanisms by considering the effects of antibiotics on a virtual patient in which AD is impaired due to a low expression of AMPs (figure 5.2 D), simulated treatment of patients where the skin is disrupted by high pH corticosteroids (figure 5.2 E), and different doses of emollients on virtual patients where the skin is disrupted by low levels of expression of LEKTI (figure 5.3 C) and filaggrin (figure 5.3 D).
However, a systematic analysis of the effect of treatments on different virtual patients, each of them characterized by a particular risk factor and parameter combination, is required to derive quantitative and clinically relevant model predictions.
We will also use the mathematical model to explore different treatment regimes which combine emollients, antibiotics and corticoseroids that are administrated with particular frequencies and magnitudes.
This will help us to devise a optimal treatment that effective induces epithelial remission but requires only a minimal dose and frequency of drugs, reducing the adverse effects of AD treatments.
Finding optimal treatment to restore epidermal homeostasis that characterizes early phases of AD is particularly important in the context of preventive, patient specific medicine, because treating early phases of AD has the potential to prevent the onset of advanced, severe and irreversible phases of the disease that will be discussed in the next chapter.

Chapter 6

Modelling advanced stages of AD: The onset of adaptive immune responses

6.1 Introduction

In chapter 4, we investigated the role of different risk factors on the early development of AD, characterized by a aberrant interplay between *innate* immune responses and barrier function. During this phase of the disease, mild forms of epithelial dysfunction, appearing as recurrent cycles of barrier damage and inflammation, can be reversed as soon as the risk factor is counteracted [25].
This situation is exemplified in figure 6.1. It corresponds to simulations of equations 4.1 (explained in chapter 4) for three different phases: During the first phase of the simulations (I in figure 6.1), the permeability barrier function is set to its nominal value, corresponding to a healthy system with a nominal filaggrin content ($\tilde{P} = 0.4$). Then, in phase II (red area in figure 6.1), we simulated a decrease in filaggrin content (by setting $\tilde{P} = 0.7$, corresponding to the genetic condition "*low FLG*" discussed in section 4.2.3). As discussed previously (section 4.2.5), a decreased filaggrin content is associated to loss of epidermal homeostasis that appears as recurrent events of loss of barrier function, characteristic of early phases of AD. In the third phase (III), we increased again the fiaggrin content (by re-setting $\tilde{P} = 0.4$). As seen in figure 6.1, restoration of the nominal conditions leads to a recovery of homeostasis. This suggests that mild forms of loss of epidermal homeostasis, appearing as recurrent flares of barrier damage, can be reversed to a healthy phenotype as soon as the risk factor that causes the loss of homeostasis (low FLG expression in figure 6.1) is counteracted.

This reversibility is further discussed in chapter 5. As shown in figures 5.3 and 5.2, during the early phases of the disease, it is possible to attain transient or even complete remission (i.e. restoration of epidermal homeostasis) upon administration of treatments such as emollients, corticosteroids and antibiotics that counteract the triggers of the disease.

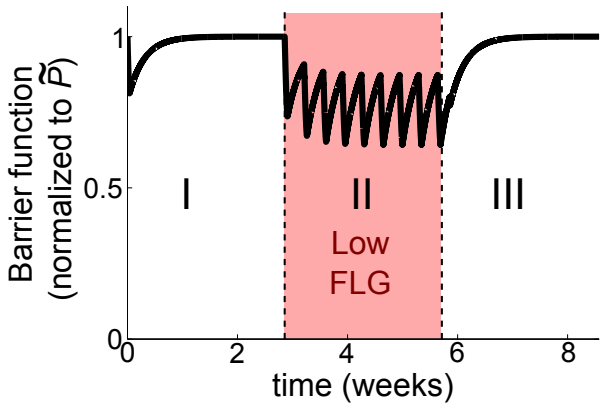

Figure 6.1: **Reversibility of mild and early forms of AD** The plot shows simulations of the model of the early phases of AD, described by equations 4.1. The simulations start with nominal parameters characterizing a healthy epidermis (I), followed by window of time (II) in which filaggrin expression is decreased (by setting $\tilde{P}$ from 0.4 to 0.7) and ending with a restoration of the nominal, healthy conditions (by re-setting $\tilde{P}$ from 0.7 to 0.4) in phase III. Low expression of filaggrin induces a mild form of early AD (appearing as recurrent cycles of barrier damage) that can be reversed as soon as healthy filaggrin expression is restored.

This reversibility of the pathological phenotype is possible because the *innate* immune responses triggered by the infiltrated pathogen display a *reversible*, switch like dose response behaviour (figure 3.2). As soon as the infiltrated stimulus is decreased below a threshold S^{-}, the immune responses cease and the barrier is restored. No *immunological memory* is kept from the past events of stimulus infiltration.

Advanced stages of the disease process, however, are characterized by allergic sensitization [160, 161, 27], that refers to the *irreversible* activation of impaired adaptive immune responses (mainly via Th2 cells) that are responsible for allergic reactions to infiltrating pathogens and chronic inflammation [39, 254, 160]. This is process is triggered by a cumulative history of innate immune responses and infiltrated pathogens [187].

It is clinically relevant to understand allergic sensitization in the context of AD, since this process is responsible for the *allergic* component that characterizes this disease [160, 161].

As shown in figures 2.3 A (control structure) and in 6.2 (cartoon representation), the onset of allergic sensitization and a pro-inflammatory micro-environment starts by the release of cytokines in response to activation of innate immune response pathways [111, 158]. Particularly important is TSLP, a cytokine that is produced by PAR2-mediated signalling pathways [39, 111] and has been show to play a key role in the onset of allergic inflammation that characterizes AD [257] (figure 6.2). TSLP induces the activation and migration of DC from the epidermis to the lymph nodes [158, 39] (figure 6.2, 2 and 2.3 A,II). Once in the lymph node, DC increase the levels of IL4 [9, 254, 158] (figure 6.2, 3). This triggers the differentiation of T cells from naïve

T cells into polarized Th2 cells, a process that involves Gata-3 mediated signalling [159, 189] (figure 6.2, 4), and is called T-cell polarization. Polarized Th2 cells migrate from the lymph node to the epidermis [159, 189] (figure 6.2, 5), where they contribute to the establishment to the allergic [158], pro-inflammatory micro-environment that characterizes the epidermis of patients with advanced [254] and severe [185, 186] forms of AD.
The establishment of this pro-inflammatory micro-environment in the epidermis of AD patients as a consequence of allergic sensitization further interferes with epidermal homeostasis, since pro-inflammatory cytokines released by polarized Th2 cells affect epidermal tissue remodelling by interfering with gene expression programs [137, 138, 29, 125]. The establishment of a pro-inflammatory and allergic micro-environment as a consequence of Th2 polarization is hence responsible for further worsening of the disease condition.

Furthermore, atopic sensitization is also the first step of the *atopic march*, defined as a progression from AD to other atopic diseases, namely asthma and allergic rhinitis [62, 25]. This sequential impairment of epithelial tissues (epidermis and airway epithelium) seems to be triggered by the increased levels of serum IgE and pro-inflammatory cytokines that result from Th2 cell polarization [258]. By circulating in the blood, these molecules are able to interfere not only with epidermal remodelling, but also with other epithelial tissues, including the airway epithelium [146]. This significantly increases the risk of developing asthma and allergic rhinitis [62, 258, 121]. Upon progression of the atopic march, loss of epithelial homeostasis is no longer confined to the epidermis, but spreads out to other epithelial systems to become *systemic*, since the rise in the levels of IgE and cytokines affects not only the epidermis, but also the serum that comes in contact with many other epithelial tissues [258, 62].
Early treatment (assessed in section 5) has the potential to prevent the advanced stages of AD, and avoid (1) the *chronicity* (associated to the irreversibility), (2) the *worsening* (associated to the impaired gene expression programs by pro-inflammatory cytokines) and (3) the *decentralization* of the loss of homeostasis from epidermis to other epithelial tissues the via the atopic march.
Shedding light on the mechanisms that underlie the onset of a pro-inflammatory micro-environment in the epidermis is the first step towards understanding the emergence of the aberrant gene expression patterns that characterize the epidermis of patients with severe forms of AD [134]. As observed for filaggrin, these impaired gene expression patterns can result from chronic exposure to cytokines without the need of ”hard coded” genetic defects, such as mutations or polymorphisms [36].
In this chapter, we build on the previous mathematical model that captured the early phases of AD (described in chapter 4), to encompass the processes that lead to allergic sensitization that characterizes advanced forms of AD. Our previous model considered following processes (depicted in figure 4.1):

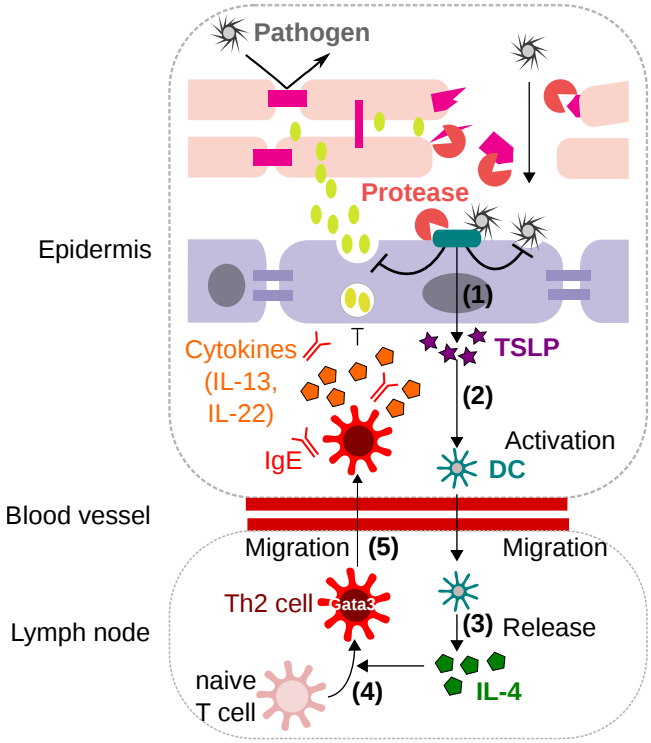

Figure 6.2: **Cartoon representation of the mechanisms leading to the onset of allergic sensitization and the establishment of a pro-inflammatory micro-environment that characterize the epidermis of AD patients with severe forms of AD** Onset of allergic sensitization and a pro-inflammatory micro-environment occurs through the polarization of T cells, a process that involves following steps: **(1)** Pathogen infiltration through a damaged skin barrier and the resulting activation of protease -mediated innate immune responses trigger the release of TSLP. **(2)** TSLP induces the activation and migration of DC from the infected epidermis to the lymph node. **(3)** There, DC increase the levels of IL4, a cytokine that **(4)** mediates the irreversible polarization of naïve T cells into Th-2 cells, in a Gata-3 dependent way. **(5)** Once polarized, Th-2 cells migrate back to the epidermis, where they play a protagonic role in the establishment of a allergic, pro-inflammatory micro-environment by rising the levels of cytokines.

- Infiltration of pathogens through the skin barrier.
- Switch-like activation of KLK networks in response to the infiltrated pathogen.
- KLK-mediated reduction of barrier function (through degradation of intercellular junctions and by reduction of the replenishment of skin barrier components).
- Self-recovery of the skin barrier function.
- KLK-mediated onset of innate immune responses, in the form of increase in AMPs and neutrophil recruitment.

- Persistence of neutrophils, even after the KLK activity has ceased.
- Elimination of pathogens by the immune responses.

To include the onset of allergic sensitization, in the model proposed in this chapter, we add following modules:

- Production of IL4 by DC that have migrated to the lymph nodes in response to TLSP stimulation. This module is simulated by the "persistence" network motif described in section 3.4.
- Irreversible polarization of T cells in response to IL4 levels in the lymph node. This module corresponds to the regulatory module presented in figure 2.3 G, and is simulated by the equation 3.2 proposed in [195]. The dose-response behaviour of this equation corresponds to a irreversible switch, as described in section 3.2.4 and shown in figure 3.2.

The migration of polarized Th2 cells from the lymph nodes to the epidermis is not considered in this model.

A schematic representation of the model of the onset of allergic sensitization, including the two added modules, is given in figure 6.3.

We use the resulting mathematical model (equations 6.1 and described in section 6.2) to assess whether environmental or genetic risk factors can potentially trigger the onset of allergic sensitization. We find that genetic (filaggrin mutation) and environmental (barrier perturbation) risk factors can trigger Th2 cell polarization, both alone and in combination (figure 6.5). These findings are congruent with different sets of experimental data, derived from different mouse models of AD in which the pathogenic process is triggered by only genetic [73], only environmental [258, 186, 255], or a combination of both [132] risk factors. For example, it has been observed that barrier perturbation, triggered by tape stripping and epicutaneous sensitization [258, 186], as well as repeated hapten exposure [255], leads to the development of an AD-like phenotype. A severe AD-like phenotype can also be triggered by a complete ablation of the filaggrin gene [73], and by a combination of filaggrin deficiency and repeated hapten challenges [132].

Our model conciliates these apparently disparate experimental observations by providing a coherent theoretical framework in which different mechanisms can trigger the onset of severe forms of AD.

It contributes to understanding risk-factor-dependent disease mechanisms, which is necessary to envision personalized treatment that considers the patient-specific pathogenic processes. Early therapeutic interventions can potentially prevent the onset of allergic sensitization, and

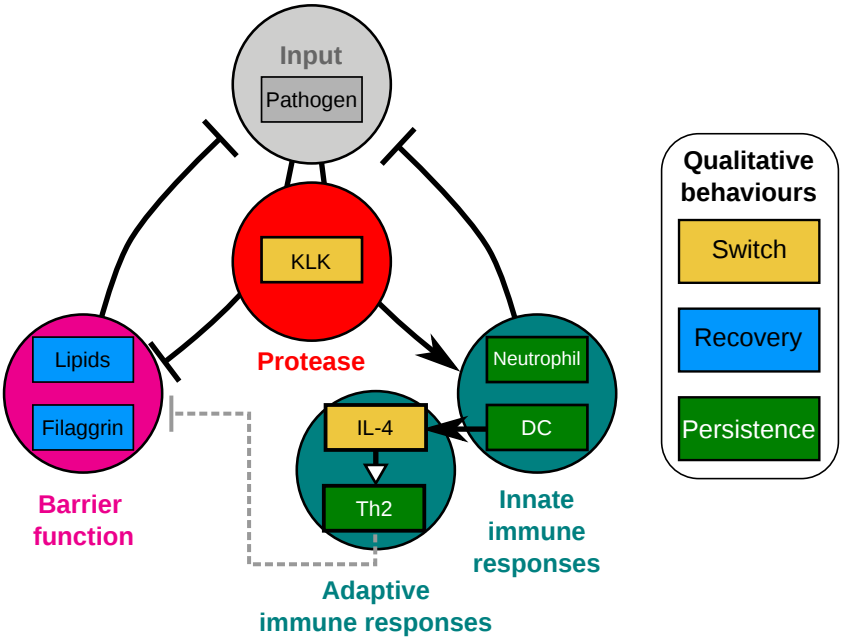

Figure 6.3: **Modular representation of the reaction network that underlies the onset of aberrant adaptive immune responses.** Infiltrating pathogens activate KLK networks in a switch-like manner. Active KLK reduce barrier function by degrading the barrier components and by reducing the lipid replenishment. Active KLK also triggers innate immune responses by inducing the recruitment of neutrophils that persist even after the KLK activity has ceased. Active KLK (via PAR2-induced TSLP) also triggers the activation and migration of DC from epidermis to the lymph nodes, where they increase the concentration of IL4. IL4 then mediates the polarization of Th2 cells via the switch like activation of the Gata3 pathway. Polarized Th2 cells are responsible for the establishment of an allergic and pro-inflammatory micro-environment that decreases the expression of filaggrin (represented by grey arrow, not considered in this model).

must be assessed in a systems-level dynamic framework that considers different stages of the disease.

6.2 Mathematical model of the advanced stages of AD

The mathematical model of the advanced stages of AD builds on the the mathematical model of the early stages of AD, described in section 4.
It considers the interplay between the barrier function and innate immune responses, mediated by the activation of protease (KLK) by the infiltrated pathogen (figure 4.1). The corresponding reaction network is modelled by the multi-scale system of ODEs (equations 4.1 and 4.2, reproduced for clarity in equations 6.1a-c), where $[\mathrm{PAR}^*]_s(\tau)$ and $[\mathrm{KLK}^*]_s(\tau)$ are the history-

dependent steady-state solutions of equations 3.1 (reproduced for clarity in equations 6.2), determined by the infiltrated pathogen load $S(\tau)$.

In this model, we add two additional components to represent the mechanisms leading to the onset of allergic sensitization via the induction of Th2 cell polarization: (1) Release of IL4 by DC that have been activated by proteases (via the PAR2-dependent induction of TSLP), and (2) Th2 cell polarization by the IL4 dependent induction of Gata3.
The PAR2-mediated increase in IL4 involves the activation and mobilization of a cellular component of the imune system (DC) in response to changes in cytokine levels (TSLP). It therefore corresponds to a *persistent* network motif described in section 3.4. To mathematically describe this process, we use the mechanistic description of the cytokine-mediated induction of cellular-level immune cells (equation 3.8, reproduced for clarity in equation 6.1 e, where $[IL4]$ is the concentration of IL4 in the lymph nodes, k_{IL4} is the rate of induction of IL4 by active PAR2, and d_{IL4} quantifies the rate of degradation of IL4.
T cell polarization occurs by the IL4- induced expression of Gata3 via the activation of the Stat6 signalling pathway [159]. The activation of the Stat6 signalling pathway involves biochemical interactions that stabilize quickly as compared to the slower, cellular processes leading to IL4. Further, Gata-3 mediated T cell polarization is *irreversible*, all-or-nothing process, since it involves major changes in gene expression programs [191]. Thus, the levels of Gata-3 as a function of IL4 correspond to a network motif that displays a *switch-like* dose response behaviour, as described in section 3.2. We use the mathematical description of the IL4-mediated Gata3 activation proposed in [195] equation 3.2 (reproduced for clarity in equation 6.1 e). The resulting dose response behaviour is a irreversible switchthat represents the irreversible differentiation of T cells: Once the levels of IL4 surpass the critical threshold value at which Gata3 switches from a low to a high value due to a saddle node bifurcation, Gata3 expression levels remain high, even if the IL4 levels completely cease afterwards (figure 3.2 D). We denote this

critical concentration of IL4 as the *threshold for T cell polarization* (figure 6.5).

$$\frac{d\mathrm{S}}{d\tau} = S_{\mathrm{out}}\frac{\widetilde{P}}{B+\varepsilon} - \mathrm{S}\left(f_{\mathrm{IP}}I_{\mathrm{P}} + I_0\right), \tag{6.1a}$$

$$\frac{d\mathrm{B}}{d\tau} = \frac{b_{\mathrm{pre}}}{1+k_{\mathrm{L}}[\mathrm{PAR2}^*]_{\mathrm{s}}}\left(1-\frac{\mathrm{B}}{\widetilde{B}}\right) - d_{\mathrm{K}}[\mathrm{KLK}^*]_{\mathrm{s}}\mathrm{B}, \tag{6.1b}$$

$$I_{\mathrm{P}} = \int_0^{\tau}[\mathrm{PAR2}^*]_{\mathrm{s}}e^{-\tau+x}\,\mathrm{d}x, \tag{6.1c}$$

$$\frac{d[\mathrm{IL4}](\tau)}{d\tau} = [PAR^*]_{\mathrm{s}}(\tau)k_{\mathrm{IL4}} - [\mathrm{IL4}](\tau)d_{\mathrm{IL4}}, \tag{6.1d}$$

$$\frac{d[\mathrm{Gata3(t)}]}{dt} = \alpha[[\mathrm{IL4}]] + \frac{\kappa_{\mathrm{G}}[\mathrm{Gata3(t)}]^2}{1+[\mathrm{Gata3(t)}]^2} - \kappa[\mathrm{Gata3(t)}]. \tag{6.1e}$$

$$\frac{d[\mathrm{KLK}^*\mathrm{LEKTI}]}{dt} = k_{\mathrm{a}}[\mathrm{KLK}^*][\mathrm{LEKTI}] - k_{\mathrm{d}}[\mathrm{KLK}^*\mathrm{LEKTI}] - \delta_{\mathrm{LK}}[\mathrm{KLK}^*\mathrm{LEKTI}], \tag{6.2a}$$

$$\frac{d[\mathrm{LEKTI}]}{dt} = -k_{\mathrm{a}}[\mathrm{KLK}^*][\mathrm{LEKTI}] + k_{\mathrm{d}}[\mathrm{KLK}^*\mathrm{LEKTI}] + t_{\mathrm{L}}(m_{\mathrm{L}} + f_{\mathrm{L}}[\mathrm{PAR2}^*]) - \delta_{\mathrm{L}}[\mathrm{LEKTI}], \tag{6.2b}$$

$$\frac{d[\mathrm{KLK}^*]}{dt} = -k_{\mathrm{a}}[\mathrm{KLK}^*][\mathrm{LEKTI}] + k_{\mathrm{d}}[\mathrm{KLK}^*\mathrm{LEKTI}] + k\frac{[\mathrm{KLK}^*][\mathrm{KLK}]}{[\mathrm{KLK}^*]+C_{\mathrm{K}}} - \delta_{\mathrm{K}^*}[\mathrm{KLK}^*], \tag{6.2c}$$

$$\frac{d[\mathrm{KLK}]}{dt} = -k\frac{[\mathrm{KLK}^*][\mathrm{KLK}]}{[\mathrm{KLK}^*]+C_{\mathrm{K}}} - \delta_{\mathrm{K}}[\mathrm{KLK}] + f_{\mathrm{KS}}S + f_{\mathrm{K}}[\mathrm{PAR2}^*], \tag{6.2d}$$

$$\frac{d[\mathrm{PAR2}]}{dt} = -k_{\mathrm{P}}\frac{[\mathrm{KLK}^*][\mathrm{PAR2}]}{[\mathrm{KLK}^*]+C_{\mathrm{P}}} - \delta_{\mathrm{P}}[\mathrm{PAR2}] + m_{\mathrm{P}}, \tag{6.2e}$$

$$\frac{d[\mathrm{PAR2}^*]}{dt} = f_{\mathrm{PS}}S[\mathrm{PAR2}] + k_{\mathrm{P}}\frac{[\mathrm{KLK}^*][\mathrm{PAR2}]}{[\mathrm{KLK}^*]+C_{\mathrm{P}}} - \delta_{\mathrm{P}^*}[\mathrm{PAR2}^*]. \tag{6.2f}$$

Unless otherwise stated, we used the nominal parameter values given in table 4.1 (for equations 6.1a-c), in [195] (for equation 6.1e, and in [84] (for equations 6.2). The parameters that quantify equation 6.1e are $k_{\mathrm{IL4}} = 0.04$, $d_{\mathrm{IL4}} = 0.05$, and the initial condition $\mathrm{IL4}(0) = 0$ (dimensionless and arbitrarily chosen).

A schematic representation of this model is given in figure 6.3.

6.3 Onset of adaptive immune responses can be triggered by both genetic and environmental risk factors

To determine if genetic, environmental or a combination of both risk factors can trigger the onset of allergic inflammation, we simulated the mathematical model of the advanced stages of AD (equations 6.1) for different concentrations of filaggrin (corresponding to different levels of genetically determined filaggrin deficiency) and severities of environmentally determined barrier damage.

Filaggrin deficiency was simulated as previously explained (section 4.2.3), by increasing the nominal skin permeability, $\widetilde{P}$, to represent the fact that a low filaggrin content increases the permeability of the skin barrier to external pathogens [73]. We considered three values of $\tilde{P}$, $\tilde{P} = 0.4$, $\tilde{P} = 0.6$, and $\tilde{P} = 1$, representing the healthy control ($FLG^{+/+}$), mild deficiency ($FLG^{+/-}$), and severe ($FLG^{-/-}$) filaggrin deficiency, respectively. These correspond to genetically encoded variations in filaggrin copy number [126].

Environmentally determined barrier damage, induced, for example, by acetone treatment, tape stripping or exposition to sodium-lauryl-sulphate, was modelled by changing the concentrations of barrier precursors b_{pre}, to mimic the fact that the expression of pro-filaggrin [140, 138, 163, 172, 142] and many other precursors of barrier components [173] are decreased upon barrier perturbation. We considered three values for b_{pre}, corresponding to a control ($b_{pre} = 0.05$), mild ($b_{pre} = 0.02$) and severe ($b_{pre} = 0.01$) barrier damage, representing different regimes of skin barrier perturbations (eg. tape stripping or acetone treatment with a particular frequency and intensity).

As we saw in section 4.2.5, particularly figure 4.6, our model suggests that increased skin barrier permeability caused by low *FLG* concentrations lead to oscillations in epidermal function (yellow area in figure 4.6, top) with an amplitude (figure 4.6, bottom) that increases with decreasing concentrations of *FLG*. As shown in figure 6.4, this dose-dependent severity of of the loss of epidermal homeostasis, caused in our model by low *FLG* expression, is also reflected in the frequency of PAR2-mediated release of TSLP. Very low levels of *FLG* ($FLG^{-/-}$) result to a higher frequency in the PAR2-mediated release of TSLP, as compared to mild forms of *FLG* deficiency ($FLG^{+/-}$). Only high frequency TSLP oscillations lead to a rapid increase in IL4 expression in the lymph nodes, because very short periods of relaxation (characterized by no TSLP expression) do not allow IL4 levels to decay before the subsequent period of induction of IL4 by TSLP. This results in a gradual accumulation of IL4 in the lymph nodes that eventually surpasses the threshold of Th2 cell polarization (figure 6.5 A, red line). Low frequency oscillations lead to a much slower increase in IL4 expression, stabilizing once the values of IL4 are equal between two periods of high TSLP expression (figure 6.5 B, blue line).

This dose-dependent effect of filaggrin expression on the risk of developing severe forms of

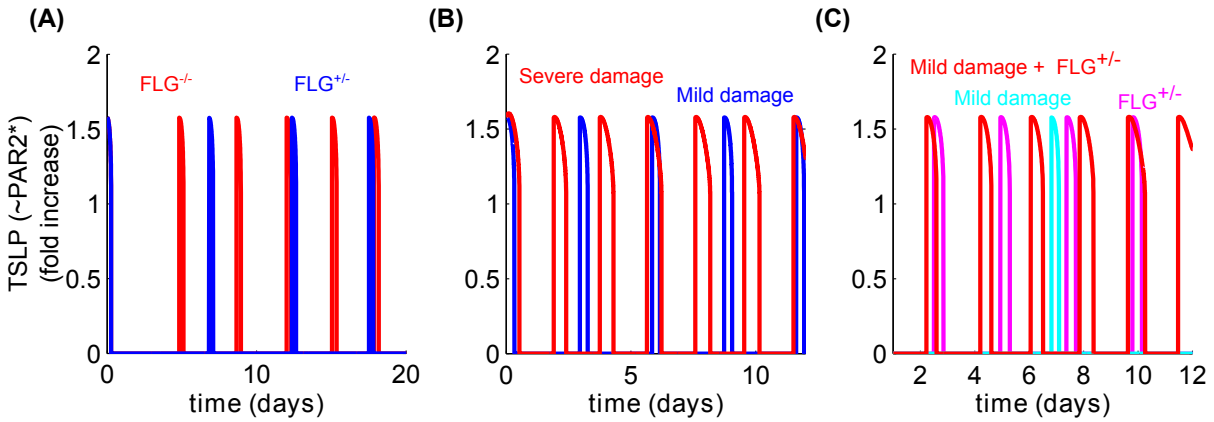

Figure 6.4: **Increased risk factor severity, given by low *FLG*, high barrier damage, or synergism between both, increases the frequency of the oscillations of the PAR2-mediated TSLP release** *(A)* Dynamic profiles for the levels of active PAR2-mediated release of TSLP for mild ($FLG^{+/-}$, simulated by setting $\tilde{P} = 0.6$) and severe ($FLG^{-/-}$, simulated by setting $\tilde{P} = 1$) filaggrin deficiency. Decreasing the levels of *FLG* increases the frequency of TSLP release. *(B)* Dynamic profiles for the levels active PAR2-mediated release of TSLP for mild ($b_{pre} = 0.02$) or severe ($b_{pre} = 0.01$) barrier damage. Severe barrier damage increases the frequency of TSLP release. *(C)* The combination of mild filaggrin deficiency ($FLG^{+/-}$, simulated by setting $\tilde{P} = 0.7$) and mild barrier damage (simulated by setting $b_{pre} = 0.02$) drastically increases the frequency of TSLP release that is triggered by a individual genetic ($FLG^{+/-}$, with $\tilde{P} = 0.4$ and $b_{pre} = 0.05$) or environmental ($b_{pre} = 0.02$ and $\tilde{P} = 0.4$), risk factor.
Unless otherwise stated, the parameters for these simulations correspond to the nominal values given in table 4.1. Parameters related to the KLK module correspond to the HC of [84]. Parameters related to the Gata3 module correspond to the nominal parameters given in [195]. The parameters quantifying the IL4 module are $k_{\mathrm{IL4}} = 0.04$, $d_{\mathrm{IL4}} = 0.05$, and the initial condition $IL4(0) = 0$.

AD is consistent with experimental and clinical findings, which have established a direct relation between filaggrin content (determined copy number variations, different forms of SNPs and null-mutations) and the severity of the disease [126, 125].
Our mathematical model also provides a plausible explanatory framework for murine models of AD, in which a AD-like phenotype is induced by manipulations in the genetic or environmental conditions of the mouse.
As reported in [73], genetic ablation of filaggrin results in the development of an AD-like phenotype in mice in a dose-dependent manner. Congruent with our results, only complete abrogation of filaggrin ($FLG^{-/-}$, but not $FLG^{-/+}$) results in allergic sensitization. Further increasing the penetration of environmental insults by subjecting the $FLG^{-/-}$ mice to a high concentration haptens augments the severity of the phenotype [73, 132]. Indeed, very frequent

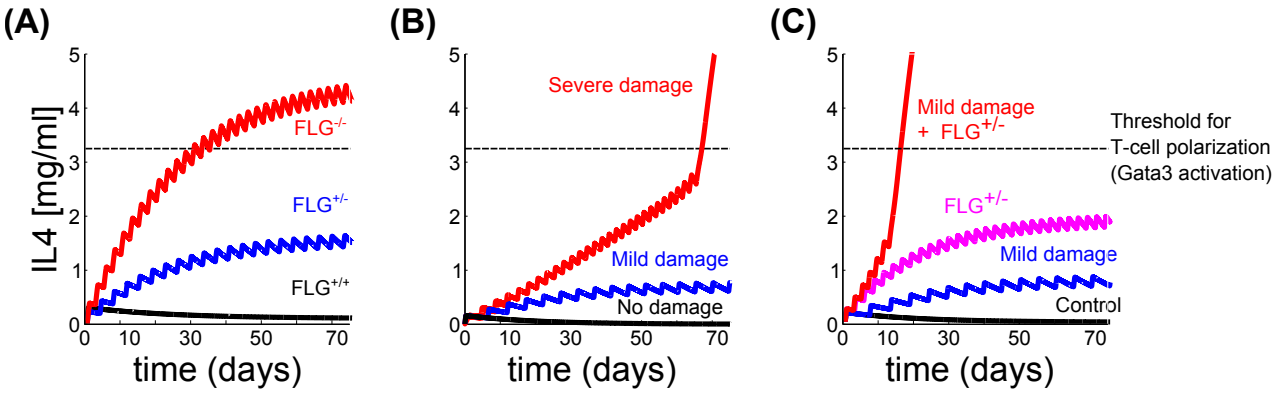

Figure 6.5: **The onset of aberrant adaptive immune responses can be triggered by severe forms of individual genetic (*FLG*) or environmental (*barrier damage*) risk factors. In combination, also *mild* forms of risk factors lead to allergic sensitization.** *(A)* Dynamic profiles for the levels of IL4 in the lymph node for different severities of genetically determined filaggrin deficiency. These are simulated by setting $\tilde{P} = 0.4$ ($FLG^{+/+}$, control), $\tilde{P} = 0.6$ ($FLG^{+/-}$, mild), and $\tilde{P} = 1$ ($FLG^{-/-}$, severe), corresponding to variations in *FLG* copy number. Only the most severe form of filaggrin deficiency results in a increase of IL4 above threshold for Th2 polarization, triggering in the onset of allergic sensitization. *(B)* Dynamic profiles for the levels of IL4 in the lymph node for different severities of environmentally determined barrier disturbances. These are simulated by setting $b_{pre} = 0.05$ (control), $b_{pre} = 0.02$ (mild barrier damage), $b_{pre} = 0.01$ (severe barrier damage), corresponding to the decreased amount of barrier precursors that result from sustained and frequent barrier damage. Only severe barrier damage triggers the onset of allergic sensitization, by leading a gradual rise in IL4 levels that eventually eventually surpass the threshold for Th2 polarization. *(C)* Alone, a mild form of genetic ($FLG^{+/-}$, simulated by setting $\tilde{P} = 0.7$ with $b_{pre} = 0.05$) or environmental (mild barrier damage, simulated by setting $b_{pre} = 0.02$ with $\tilde{P} = 0.4$) risk factor does not lead to the onset of allergic inflammation. However, in combination (simulated by setting $b_{pre} = 0.02$ and $\tilde{P} = 0.7$), even mild forms can result in the polarization of Th2 cells. Unless otherwise stated, the parameters for these simulations correspond to the nominal values given in table 4.1. Parameters related to the KLK module correspond to the HC of [84].

and severe hapten exposure can result in an AD-like phenotype, even in the absence of *FLG* mutations [255].

As shown in section 5, the use of emollients reduces the amplitude of the recurrent flares of PAR2 activation and immune responses caused by low *FLG* expression (figure 5.3 D). As we show in figure 6.5 A, reduced *FLG* expression seems to trigger the onset of adaptive immune responses by affecting the frequency of TSLP release, in a dose-dependent manner. These findings suggest that early use of emollient in high risk populations (eg. with *FLG* mutations) could

prevent the onset of advanced, severe and irreversible stages of AD. This model prediction is consistent with clinical findings, that suggest that a emollient therapy in neonates significantly reduces the risk for AD development [256].
The skin of neonates displays lower permeability barrier function that improves during the first year of life [211]. Partly, this weak barrier function can be attributed to the small corneocyte size [259] and low filaggrin content [211] that characterize the skin of neonates, increasing their propensity to develop AD. Hence, emollient treatment during the first year of life could be sufficient to prevent the onset of advanced stages of AD, by supporting the post-natal skin maturation process [259, 260].

Analogous to the results for filaggrin deficiency, our simulations suggest that severe forms of environmentally determined barrier damage can also result in T cell polarization.
As seen in figure 6.4 B, increasing severities in barrier damage result in increased frequency in active PAR2-mediated TSLP release, resulting in a rapid increase in the concentration of IL4 in the lymph nodes that eventually surpasses the threshold of T cell polarization (figure 6.5 B).

Our model suggests that the combined effect of filaggrin deficiency and environmentally determined barrier perturbation dramatically increases the risk of developing a severe AD phenotype. As seen in figure 6.5 C, the coincidence of filaggrin deficiency and barrier damage results in T cell polarization, even if the severity of the individual risk factors is not enough to trigger a increase of IL4 above the threshold of T cell polarization.
Our model predicts that this synergism between the environmental and genetic risk factor can be attributed to the dramatic increase in the frequency of TSLP oscillations caused by the simultaneous occurrence of barrier damage and filaggrin deficiency (figure 6.4 C).
This theoretical result is congruent with experimental observations. A severe AD phenotype can be reproduced in mice that have been subjected to prolonged exposure to high doses of haptens (increasing their penetration though the skin barrier) and tape stripping [258, 186]. Further, the development of an AD like phenotype requires that the frequency of the perturbations (hapten exposure and tape strip) are high [255], confirming our model predictions that suggest that high-frequency disturbances in epithelial function can result in severe forms of AD (figures 6.4 and 6.5).
This mechanism highlights the critical role of the *persistence* motif described in section 3.4, that acts as a *capacitor* that gradually stores the cyclic events of loss of barrier homeostasis in a frequency-dependent manner (figure 3.6).

6.4 Conclusions

In this chapter, we presented a model of the regulatory networks controlling epidermal function that can reproduce the onset of advanced stages of AD, triggered by genetic (*FLG* deficiency), environmental (barrier perturbation), or the synergism between both risk factors.
Our results agree with clinical [126, 125] and experimental data that describe the onset of an AD like phenotype that is caused by a severe increase in the permeability to environmental insults [258, 186, 255, 73, 132].
Our results also support the "outside-in hypothesis", stating that allergic inflammation can result from barrier defects [7].
Together with the results presented in section 5, our model predictions provide a plausible theoretical explanation of the mechanisms that underlie the preventive effect of early emollient treatment on AD development [256].
Taken together, this mathematical model effectively captures the dynamic process leading to the development of late stages of AD that has been observed in the clinic and in experiments. We will continue using this model to further explore the mechanisms that underlie the pathogenesis of AD. We hope that it will contribute to the design of better methods for early diagnosis, treatment and prevention of this socially relevant disease.

Chapter 7

Mathematical model of AD: Conclusions and future work

The mathematical model of AD proposed in this thesis is able to reproduce the two stages of the pathogenic dynamics that is triggered by different combinations and severities of genetic and environmental risk factors.

Based on the compilation of abundant but scattered experimental and clinical data, in chapter 2 we presented a manually curated reaction network responsible for controlling epidermal homeostasis. The network contains the most relevant biochemical and cellular effectors known to play a important role in the pathogenesis of AD. Specifically, it represents the regulatory interplay that exists between skin barrier function and inflammation, which are the two epithelial properties that are impaired in AD. It was previously known that the genetic and environmental risk factors predisposing to AD alter epidermal function by targeting individual components of this entangled network of biochemical and cellular interactions. However, the complexity of AD comes mainly from the fact that disturbances elicited on the strongly connected regulatory network components can eventually propagate, affecting different regions of the reaction network. This process is largely responsible for (1) the existence of many different potential triggers of the pathogenic process, (2) the synergy between risk factors, that appear in the clinic as a dramatic increase in the propensity to develop AD as a consequence of the co-occurrence of more than two risk factors, and (3) the gradual aggravation of the disease phenotype. This results in a wide spectrum of possible disease phenotypes, each of which might require a specific treatment. Decreasing the social burden of AD thus requires a systems-level approach, in which the effects of individual risk factors on the regulatory network are systematically assessed, alone and in combination, to entangle the complex pathogenesis of AD. Here, we provide such as systems-level framework, in the form of the first multi-scale mathematical model of AD. The model is a mechanistic representation of the previously described reaction network, that was assembled and carefully curated in chapter 2.

By simulating different risk factors, our model reproduces the main features of AD, providing an *in silico* representation of the different pathogenic processes that occur in different patient cohorts. Our model thus provides a plausible, mechanistic and integrative framework that can be used to study AD from a systems-level perspective.

Most of the experimental and clinical data describing the individual regulatory network components is qualitative. It clearly shows regulatory interactions and the different qualitative behaviours described in chapter 3, but fails to provide quantitative kinetic information. To account for this uncertainty, we use a qualitative modelling framework, in which the main experimentally described qualitative behaviours robustly arise from the underlying network topology without requiring accurate parameter choices. The resulting network motifs are then re-assembled into a multi-scale reaction network, which comprises the first multi-scale mathematical model of AD, proposed in this thesis.

We simulated virtual patient cohorts by altering the model components that are affected by the different risk factors. As a result, our mathematical model is able to display the different forms of loss of epidermal homeostasis that characterize early (chapter 4) and late (chapter 6) stages of AD.

This *in silico* reproduction of the pathogenic dynamics of AD, in which late and severe forms of AD emerge from specific early forms of the disease, pinpoints plausible mechanisms that underlie the gradual disease progression that affects some AD patients. Further, our framework allows us to map different forms of a worsening pathogenic dynamic trajectory to specific combinations and strengths of risk factors, that correspond to patient-specific pathogenic triggers of the disease.

This theoretical analysis can be used to inform new and more effective early treatment strategies that halt the progression of the pathogenic process. Indeed, as we showcased in chapter 5.3, using our mathematical model, we can explore the effects of different pharmacological treatments that are commonly used to control AD on the development of the disease in different cohorts of virtual patients. As we discuss in chapter 6, this analysis allows us propose preventive strategies that hinder the onset of severe forms of AD.

Our mathematical modelling results agree with different *in vivo* clinical and experimental datasets. Specifically, the sudden onset of allergic sensitization as a consequence of severe filaggrin deficiency, severe skin barrier damage, or a combination of mild filaggrin deficiency and mild barrier damage predicted in chapter 6 is congruent with different animal models of AD, in which abrupt skin barrier defects can be triggered by different combinations of filaggrin mutations, repeated hapten challenges and tape stripping. Also, the dynamical profiles discussed in chapter 4 resemble different disease phenotypes that have been observed in the clinic.

Our mathematical analysis predicts that the disease progresses from a mild to severe form of

AD, manifested as recurrent events of skin barrier damage and inflammation (discussed in chapter 4) that are suddenly transformed into a severe loss of barrier function resulting from the onset of allergic sensitization (chapter 6), only when the frequency of the early oscillations in barrier damage and inflammation are high enough. Further, we predicted that different types, severities and combinations of risk factors can be mapped onto specific pathological dynamical behaviours that appear as oscillating barrier function and inflammation with distinctive frequencies and amplitudes. Together, this suggests that there exists a risk-factor dependent onset of allergic sensitization. Validation of this theoretical result would mean that the pathogenic course in an individual patient, affected by a particular combination of risk factors, could potentially be predicted. This would enable early diagnosis and a pharmacological intervention that halts the incipient progression of AD in patients in which AD would eventually develop allergic sensitization.

The next steps are to validate the model predictions and to reach also a *quantitative* agreement between the model simulations and experimental and clinical data. For this, the proposed mathematical model of AD must be compared to *in vivo* datasets that dynamically describe different interacting components of the reaction network controlling epidermal homeostasis, and account for the different time-scales at which these different components operate.
Such datasets can be obtained from clinical analysis of AD patients, as well as from experimental analysis of animal models of AD.
Given that the epidermis is the most exposed (and hence, experimentally accessible) of all epithelial systems, several measurements can be taken, in a non invasive way, from AD patients. For example, optical methods such as Raman spectorscopy can be used to measure the content of several components of the skin barrier [261, 262, 263], and also the rate of epidermal proliferation [259].
In addition to this clinical data, detailed empirical description of the pathogenic process of AD can be obtained from murine models of AD. Together with our experimental collaborators (headed by Dr Mariko Okada, at RIKEN), we will use signalling activity profiles, quantifications of immune cell populations, dynamic gene expression profiles and quantification of histological sections to calibrate our mathematical model of AD.
We are confident that this will result in a experimentally validated and calibrated model of AD that can be used to make clinically relevant predictions and to devise optimal, patient specific treatment of AD.

To showcase the methodology to be followed to for the calibration of the mathematical model of AD, we present in the next chapter a experimentally calibrated mathematical model of epithelium homoeostasis.
The data-driven mathematical model presented in chapter 8 describes the host pathogen interactions between *Streptococcus pneumoniae* and the upper airway epithelium.
Similarly to the reaction network that controls *epidermal* homeostasis, *airway epithelium homeostasis* is also achieved by a balanced interplay between the two protective properties of the epithelium: immune responses and permeability barrier function.
Given this similarity, we can adapt the mathematical modelling framework that we developed for AD, based on a modular representation of the processes that control immune responses and barrier function, to explore the mechanisms that lead the commensal bacteria *Streptococcus pneumoniae* to become pathogenic as a consequence of a co-infection.
As we will see, our mathematical model of the host pathogen interactions between *Streptococcus pneumoniae* and the upper airway epithelium successfully captures the loss of epithelial homeostasis that results from co-infection, and agrees with experimental *in vivo* data.
This shows that our modelling framework to analyse the mechanisms responsible for the maintenance of epithelial homeostasis, inspired by the analysis of *epidermal* tissue, can be applied to uncover the mechanisms that control the functioning of other epithelial systems.

Thus far, we have used the mathematical model of the advanced stages of AD to explore how *"low FLG"* expression or a physical damage to the barrier results in the onset of allergic sensitization (figures 6.5). As a next step, we will explore the effect of other risk factors, such as *"low AMP"*, *low LEKTI* and *"high pH"* (assessed in terms of their role in the onset of early phases of AD in chapter 4) on the gradual aggravation of the disease phenotype.
For example, we saw in figure 4.5 that *"low AMP"* expression is associated to a persistent loss of barrier damage, accompanied with a chronic activation of innate immune responses. In this scenario, the levels of active PAR2 and TSLP remain elevated (figure 3.6 D), implying (equation 6.1d) that the levels of IL4 will increase constantly until the maximal, steady state value ($[\mathrm{IL4}]_{ss}^{high} = \frac{[PAR^*]_s^{high} k_{\mathrm{IL4}}}{d_{\mathrm{IL4}}}$) is reached (figure 3.4 D). Hence, as long as this steady state value $[\mathrm{IL4}]_{ss}^{high}$ is above the threshold of Th2 cell polarization, we expect that persistent activation of innate immune responses, given by low AMP expression, will inevitably result in the onset of aberrant adaptive immune responses.
This direct relation between persistent loss of homeostasis and the onset of adaptive immune responses also highlights the important role that early treatment can play in preventing allergic sensitization. As discussed in section 5.3, this can be achieved, under some circumstances, by a single dose of antibiotics or corticosteroids that reverse the persistent loss of homeostasis caused by risk factors such as *"low AMP"*.

By exploring the effect of these different risk factors on the development of allergic sensitization, we aim to provide a coherent framework that can explain the incidence of a severe AD-like phenotype that arises either by over-active proteases (equivalent to our *"high pH"* risk factor) [123] or *low LEKTI* [264, 265], *"low AMP"* (unpublished data from our collaborators), or combinations of *"low FLG"* and barrier damage (chapter 6).
To achieve this, we plan to carry out further analysis of the model proposed in chapter 6 (equations 6.1). This will be achieved by a combination of numerical simulations and a analytic exploration of the model behaviours. Particularly, we would like to quantitatively evaluate the relation between risk factor severity, the frequency of the TSLP oscillations, and the propensity to develop a severe form of AD.

Once we have quantitatively characterized the impact of different risk factors on the onset of allergic sensitization, we want to further expand our model to analyse the impact of the pro-inflammatory micro-environment that results from T cell polarization on epidermal function.
It is known that a pro-inflammatory micro-environment further impairs epidermal function by the interference of pro-inflammatory cytokines with the expression of skin barrier components [137, 138, 29, 125]. Modelling this requires "closing the loop" in the model proposed in chapter 6 (equations 6.1), by considering the inhibitory effect of Th2 induced cytokines on the expression of filaggrin and other barrier components (grey blunt arrow in figure 6.3). We expect that this further addition to the model will contribute to understand why low levels of filaggrin expression can *emerge* from a impaired control structure regulating epidermal function (represented in figure 2.3), even in the absence of "hard coded" genetic defects in the form of mutations or polymorphisms [138]. It will also help to understand the mechanisms that underlie the further aggravation of the AD condition that occurs upon allergic sensitization [185, 161, 160].

The mathematical model proposed here is able to reproduce the pathogenesis of AD, that is a disease that affects a particular type of epithelium, namely, the epidermis. However, the onset of several other diseases related to loss of epithelial function are caused by similar mechanisms as those that trigger AD, including asthma [266, 39, 266], allergic rhinitis [12], Crohn's disease [237, 1] and colon cancer [267].
This suggests that our modelling framework, derived from the analysis of the pathogenesis of AD, can be extrapolated to other epithelial systems, to explain the pathogenesis of other diseases related to loss of epithelial function.
In fact, as we will see in the next chapter (8), we can use modelling framework, based on a modular representation of the interplay between barrier function and immune responses, to successfully reproduce the loss of airway epithelium function that results from co-infection

with the commensal bacteria *Streptococcus pneumoniae* and the virus *Influenza*.

Chapter 8

Modelling host pathogen interactions between *Streptococcus pneumoniae* and the upper airway epithelium to understand co-infection

This work has been done in collaboration with our experimental collaborator Dr Thomas B Clarke (Faculty of Medicine, Imperial College London), who introduced us to this biological system and has contributed extensively to the understanding of the underlying biology. Currently, we are continuing this work with George Buckle (MRes is Molecular and Cellular Biosciences, Imperial College London).

8.1 Applying our modelling framework to understand the mechanisms that underlie infection by commensal bacteria

In the previous chapters, we presented our mathematical modelling framework, based on modularity and time-scale separation, and applied this framework to model the reaction networks controlling *epidermal* homeostasis, to uncover the mechanisms leading to the onset of Atopic Dermatitis (AD).

In this chapter, we extend this theoretical framework to analyse the functioning of another epithelial system: the host-pathogen interactions that occur in the *airway epithelium* in response to the bacterium *Streptococcus pneumoniae* (the pneumococcus), to understand the mechanisms that lead to infection by this pathogen that normally resides as a harmless commensal

organism.
In this epithelial system, homeostasis is achieved by a interplay between immune reactions (enacted by by neutrophils) and barrier function (given by intercellular junctions) that must be balanced to prevent the onset of infection (figure 8.1).
As discussed in previous chapters, this interplay is a key structural feature of the reaction networks controlling epidermal homeostasis, since loss of balance in this interaction results in the onset of AD.
Thus, the mathematical framework presented in the previous chapters, developed originally for understanding AD, can be naturally adapted to encompass the host-pathogen interactions that occur in the airway epithelium in response to *Streptococcus pneumoniae*.
Mechanistic and quantitative understanding the host-pathogen interactions between the airway epithelium and *Streptococcus pneumoniae* is fundamental to help preventing the yearly 14.5 million cases of severe infection and 820 000 deaths by *Streptococcus pneumoniae* [21], and find new and improved treatments that can circumvent antibiotic resistance [23].
Besides this clinical relevance, extrapolating our modelling framework to the host-pathogen interactions between the *airway epithelium* and *Streptococcus pneumoniae* also has two scientific objectives:
First, we want to show that our modelling framework for understanding epithelium function in health and disease is not specific for understanding epidermis, but can be naturally adapted to other disease that are triggered by a imbalance between the two protective properties of the epithelium: immune responses and permeability barrier function.
Second, we want to show how we can achieve a *quantitative*, not only a *qualitative* understanding of epithelial function, using our proposed modelling framework. The interactions between single-layered epithelial tissues (such as the airway epithelium), pathogens and neutrophils have been extensively characterized in experimental settings. This enables us to fit our mathematical model to empirical, quantitative data, and to make quantitative predictions.

8.2 Introduction

Steptococcus pneumoniae is a bacterium that normally resides in the upper airway epithelium as a commensal organism without causing infection. However, circumstances such as colonization of the airway epithelium by other pathogens such as the influenza virus, can trigger a infectious process that eventually can lead to severe disease [21]. In fact, most of the severe cases of infection by *Steptococcus pneumoniae* occur as a consequence of a previous infectious event [69].
Given the incipient problem of antibiotic resistance [23], it is necessary to devise new therapeutic strategies that minimize the use of antibiotics. Preventing a infection that requires extensive

use of antibiotics could be achieved by intervening the early stages of the infectious processes, namely the colonization or the upper airway epithelium by *Steptococcus pneumoniae*. This requires a mechanistic and quantitative understanding on how co-infection impairs the host-pathogen interactions between the upper airway epithelium and *Steptococcus pneumoniae*.

Co-infection can drive the infectious process by *Steptococcus pneumoniae* by different mechanisms, including the reduction in the immune responses [78], impairment of epithelial barrier function, and the increase in bacterial carrying capacity [69].
It is however still not clear how exactly these effects result in a loss of epithelial function that can lead to super-infection by the second pathogen (*Steptococcus pneumoniae*). Further, different pathogenic mechanisms might appear as different disease phenotypes that require specific pharmacological treatment. Clarifying the relation between disease mechanism and phenotype is important to devise adequate treatments that are specifically tailored to the patient-specific mechanism of infection. Here, we ask whether the different perturbations inflicted to the epithelium can be mapped to specific phenotypes.
To answer this question, a quantitative and mechanistic understanding of the host-pathogen interactions that occur between the airway epithelium and *Steptococcus pneumoniae* is necessary to systematically assess how different disturbances elicited by previous infectious events contribute to the development of super-infection.
Invasion of the bloodstream by *Steptococcus pneumoniae* is prevented by the airway epithelium by the combined effect of its two protective properties: A barrier function that physically hinders bacterial invasion, and immune responses that decrease the pathogen load by phagocyting and killing the bacterium.
Interestingly, these two protective properties inhibit each other. A competent barrier restricts not only the invasion of inhaled bacteria into the bloodstream, but also the transmigration of components of the immune systems (neutrophils) from the bloodstream to the epithelial tissue where bacteria reside. Further, immune responses elicited by transmigrating neutrophils are required for control of pathogen load, but also lead to barrier damage (figure 8.1 A).
Clarification of the relation between the pathogenic processes and the resulting disease phenotypes requires a quantitative systems-level view, that considers the complex interplay between barrier function, immune responses and pathogen (figure 8.1 B) load that must be balanced to maintain a healthy, non infected epithelium.
Here, we propose a quantitative systems level view of host-pathogen interactions between *Streptococcus pneumoniae* and the airway epithelium in the form of a mathematical model that considers all the relevant regulatory connections between the bacterium and the host.
The model builds on previous models of pneumococcal infection [91, 92, 93, 94], and considers, for the first time, the role of the epithelial barrier in mediating the infectious process, as

well as the complex interplay between barrier function and immune responses (figure 8.1 C).
We obtained the parameter values of the model by fitting the model to quantitative and dynamic experimental data (appendix B), and used the resulting calibrated model to assess the different pathogenic mechanisms.
Then, we analysed the different qualitative dynamic behaviours, corresponding to differential phenotypes, that can be displayed by the mathematical model.
Finally, we simulated the disturbances that the first pathogen (*influenza*) causes to the reaction network, and grouped the resulting dynamic behaviours into the different disease phenotypes.
Our preliminary results suggest that co-infection can trigger loss of epithelial homeostasis by at least four qualitatively different mechanisms that appear as four distinguishable phenotypes: (1) Increased carrying capacity leads to sepsis, but the epithelial barrier function remains intact (figure 8.11). (2) A strong decrease in barrier function is associated to a high immune cell infiltration and further barrier damage, but no infection (figure 8.12). The same qualitative behaviour is observed if immune cell infiltration is increased (figure 8.13, red trajectories). (3) Weakened strength in immune reactions lead to recurrent, low level flares of infection (figure 8.13, blue trajectories), and (4) Receptor desensitization leads to sepsis, but no associated barrier damage nor increased immune responses (figure 8.14).
This work contributes to understanding of the mechanisms and resulting disease phenotypes that are driven by *Streptococcus pneumoniae*, a bacterium that is normally a non-harmful commensal resident of the upper airway epithelium. It constitutes a first step towards devising better treatments that minimize the use of antibiotics.

8.2.1 Previous mathematical models of host-pathogen interactions that occur at epithelial tissues

This section reviews the mathematical models of the host-pathogen interactions that occur between different pathogens (including *Steptococcus pneumoniae*) and epithelial tissues (including airway epithelium).

Mathematical models of the interplay between immune responses and pathogens that do not consider epithelium function

There are numerous mathematical models on host-pathogen interactions. However, most of these focus on the immune responses, neglecting the role of the epithelium. For example, [268] propose a mathematical model of the interplay between HIV and immune cells, and the model of [100] examines the infection of mammary glands by *E coli*. The interplay between the bacterium *Helicobacter pylori* and immune response is explored in the model proposed in [101], that considers a dual effect of immune responses on infectious outcome: immune

responses not only eradicate the pathogen, but also trigger inflammation that rise the bacterial carrying capacity, by increasing the amount of nutrients that results from tissue damage. This dual effect was explored in a more abstract framework (i.e. not specific for a system) in [102], leading the authors to derive conditions that underlie two lethal forms of disease outcome of the host response to pathogen: septic (infected) or aseptic (uninfected, but chronically inflamed) death. In the model proposed in [103], the general mechanisms of interaction between innate immune responses and pathogens are systematically explored, to identify the conditions that trigger a persistent (pathological) vs a transient infection.

Mathematical models of viral infection of epithelial tissues consider the interplay between immune responses, viral load and epithelium-mediated viral replication

Host-pathogen interactions between virus and epithelial tissues are characterized by a dual role of the epithelial tissue. Epithelial cells form the basis for viral replication, but also enact a barrier that hinders the penetration of the virus into the bloodstream. This protective function of the epithelium mediates the between-host dynamics of the virus (eg. sexual transmission of HIV, which depends on the passage of the virus between cervix and bloodstream) [5], but thus far, has not be taken into account in mathematical models. Further, the clearance of viral infection by immune cells requires the killing of infected epithelial cells, resulting in significant tissue damage. Hence, a mathematical model that considers this complex interplay between barrier function, immune responses and pathogen load could be particularly relevant to understand the mechanisms of viral infection.

Thus far, the mathematical models of viral infection only consider the role of the epithelial cells in mediating viral replication, but not its barrier function. For example, using a system of ODE representing the interactions between Influenza A virus, epithelial cells and immune cells, the model in [104] explores the effects of initial viral load on the dynamic outcome of infection. Although the authors model the damaging effects of immune system on barrier function, the protective effects of epithelial tissue are not taken into consideration.

The mathematical model proposed in [106] analyses the different outcomes of Epstein Barr virus infection, considering that the virus can infect both immune cells (B cells) and epithelial cells. It uncovers the optimal strategies for the virus that maximise viral load and the probability of transmission to another host. This mathematical model considers both immune and epithelial cells, but the role of the epithelium is restricted to functioning as a substrate for viral replication, neglecting the barrier function.

The experimentally calibrated model of [105] quantitatively characterizes the dynamics of influenza A virus infection. The model considers the interplay between epithelial cells, virus and immune cells. In the model, the main role of the epithelial cells is as a substrate for viral replication, but the permeability barrier function is not considered.

Mathematical models of infection by *Steptococcus pneumoniae*

The first mathematical model of infection by *Steptococcus pneumoniae* was proposed in [91]. It focuses on the interplay between the pathogen and the immune response mediators. The epithelium is considered dynamically, but without having a regulatory effect neither on bacterial population, nor on the immune response. In their model, the role of the epithelium is restricted to mediating the immune responses triggered by bacteria (cytokine production is assumed to be proportional to epithelium that is associated to bacteria). It is further assumed that damage of epithelial cells, caused by immune responses, contribute to the debris production that positively contributes to the bacterial load by increasing the bacterial carrying capacity (as in [101]). The regulatory role of epithelium in mediating both the bacterial invasion and the immune responses was not assessed in this model.

Originally, the model proposed in [91] was used to assess the role of initial bacterial load on infectious outcome, but was expanded in [94] and [92] to study co-infection with influenza. The viral load was modelled dynamically, but, once again, the dual role of the epithelial barrier were not considered. The authors used the mathematical model to explore two mechanisms by which co-infection can drive pathogenicity of the commensal bacterium *Steptococcus pneumoniae*: (1) Increase in carrying capacity and (2) decreased phagocytosis of bacteria by immune cells.

A similar mathematical model, proposed in [94] and also based on [91], explores the effect of the time and size of inoculation with the first pathogen on the outcome of the host-pathogen interactions.

The model proposed in [93] considers for the first time the role of the epithelial barrier in mediating pneumococcal infection. It distinguishes two sub-populations of bacteria (but not of immune cells), separated by the airway epithelium. They use the model to assess the effects of variations between strains on the outcome of infection, represented in the model as differences in the strength of the immune mechanisms elicited by the host, on the outcome of the infection (clearance or sepsis). However, their model does not consider the interplay between barrier function and immune responses, given by the tissue damaging effects of infiltrating neutrophils and by the effect of the barrier in mediating the immune responses. Given that the tissue-damaging effects of neutrophil transmigration are responsible for a major component of the pathology of infection [31, 30], we believe that they are fundamental to consider in a model that is constructed to understand how loss of epithelial homeostasis results from impaired host-pathogen interactions.

Here, we build on the mathematical model of the host-pathogen interactions between *Steptococcus pneumoniae* and the airway epithelium proposed in [91, 94]. Specifically, our model focuses on the complex interplay between barrier function and immune responses. We follow [93] in considering apical and basal populations of bacteria, to explicitly consider the regula-

tory effect of the epithelial barrier in mediating the invasion of bacteria to the bloodstream. We further add apical and basal sub-populations of neutrophils, to explore the dual interplay between barrier function and neutrophil transmigration. Particularly, we use the model to clarify the different mechanism that drive the "lethal synergism" [69] that results from super-infection with a virus (typically influenza) and *Steptococcus pneumoniae*.

8.2.2 Novelty and timeliness of our approach

To our knowledge, this is the first mathematical model of the host-pathogen interactions between *Streptococcus pneumoniae* and the upper airway epithelium that focuses on the dynamic interplay between the epithelium barrier function and the immune responses.
Super-infection by *Streptococcus pneumoniae* arises from a loss of balance in the relation between pathogen load, barrier function and immune responses. Hence, a quantitative framework that explicitly considers the regulatory roles of barrier function and immune responses is necessary to clarify the mechanisms responsible for the loss of epithelial homeostasis that results from co-infection.

8.2.3 Aims and objectives

With our proposed mathematical model of the host-pathogen interactions between *Streptococcus pneumoniae* and the airway epithelium, we aim to:

- Increase our understanding on role of individual components on mediating the host response.
- Integrate and analyse scattered experimental data into a coherent quantitative framework to reconcile quantitative but partial *in vitro* with complete but qualitative *in vivo* datasets.
- Propose a calibrated, data-driven mathematical model of epithelium function that can be used to drive quantitative, and not only qualitative predictions.
- Generalize and extrapolate previous modelling results on epidermal homeostasis to a different epithelial system, to understand the emergence of another disease that is associated to loss of epithelial function.
- Clarify the different mechanisms that underlie lethal synergism between *Streptococcus pneumoniae* and another pathogen. This is the first step to devise novel treatment strategies that minimize the use of antibiotics.

- Minimize costly animal studies that are required for a systems-level analysis of the host-pathogens by informing the experimental design with predictions derived from *in silico* simulations.

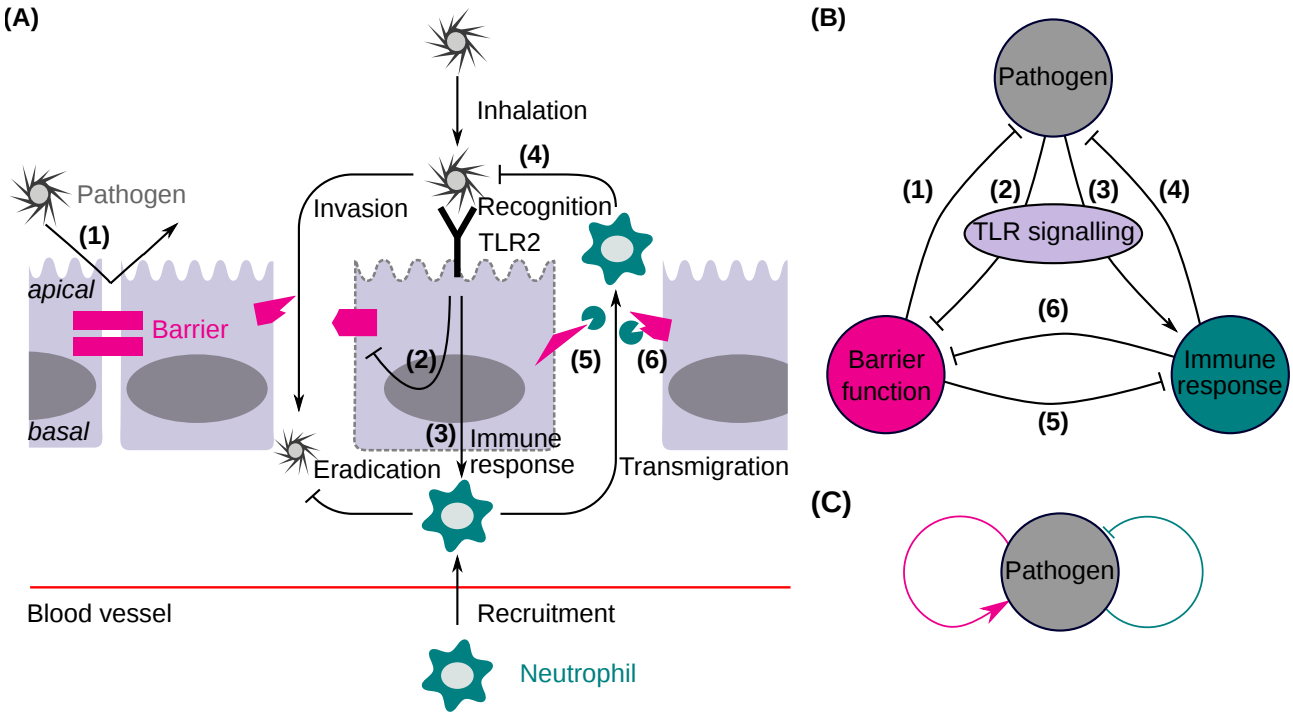

Figure 8.1: **Duality of the host-pathogen interactions between *Streptococcus pneumoniae* and the airway epithelium** *Cartoon (A) and regulatory structure representation (B) of the host-pathogen interactions between Streptococcus pneumoniae and the airway epithelium.* Upon inhalation, the pathogen *Streptococcus pneumoniae* comes in contact with the apical side of the upper airway epithelium. *(1)* A competent barrier hinders the infiltration of the pathogen to the basal aspect of the epithelium, preventing systemic infection (colonization of the blood vessel). Recognition of the pathogen by innate immune receptors (such as TLR) located on the apical side of the epithelial cell triggers *(2)* weakening of the barrier function and *(3)* immune responses in the form of neutrophil recruitment. A weaker barrier leads to the invasion of the pathogen to the basal side of the epithelium. *(4)* Neutrophils diminish the pathogen load by phagocytosis. To attack the apically located pathogens, neutrophils must transmigrate from the basal to the apical side of the epithelium, a process that requires barrier opening *(5)* and that further damages the barrier *(6)*. *(C)* The contact of the pathogen with epithelial cells trigger two opposing effects: diminishing barrier function increases, and immune responses reduce pathogen load, representing a dual host response.

8.3 The host-pathogen interactions that occur between *Streptococcus pneumoniae* and the upper airway epithelium

The airway epithelium consists of a single layer of polarized epithelial cells with a *apical* side that is exposed to inhaled pathogens, dust and other *environmental* components, and a *basal* side that faces the bloodstream. Passage of inhaled environmental insults from the apical to the basal side is restricted by inter-cellular junctions between the epithelial cells, that collectively determine the permeability barrier function of the epithelial tissue. Of particular relevance are the Tight Junctions (TJ), which are composed by claudin [38] and occludin [26], among other structural proteins [10]. *In vitro* barrier function of epithelial monolayers is commonly measured by Trans-Epithelial Electrical Resistance (TEER).

Under healthy conditions, a competent epithelial function restricts the location of *Streptococcus pneumoniae* to the apical side of the mucosa, where it resides as a non-pathogenic, commensal bacterium. Weak barrier function caused by barrier opening facilitates the invasion of bacteria from the apical to the basal side of the epithelium [68]. This is the first step in the infectious process. Contact of bacteria with the apical side of the epithelium can lead to a decrease in the barrier function, facilitating bacterial invasion [85, 68]. This tissue-level effect of bacterial contact with epithelial cells is triggered by the activation of TLR signalling by *Streptococcus pneumoniae*. Activation of TLR signalling increases expression of SNAIL1, a transcriptional repressor which inhibits the expression of the TJ component *claudin*, effectively leading to a decrease in permeability barrier function of the airway epithelium [38]. Also, the activation of host signalling cascades by the pathogen triggers the activation of proteases that reduce barrier function [269, 270, 271, 272].

Activation of TLR signalling by apically located bacteria also triggers immune responses in the form of neutrophil recruitment [273], via the NFκB-mediated release of IL-17 [231] that activates neutrophil -attracting interleukins IL-8 [274].

Neutrophils phagocytose the bacteria they encounter, contributing to the control the bacterial load in the mucosa [88, 89].

Effective immune responses require neutrophils to transmigrate from the basal to the apical side of the epithelium, a process that is restricted by the barrier function and requires the presence of apically located bacteria to guide the neutrophil movement (”chemeotaxis”) [86]. Neutrophil transmigration also causes reduction of permeability barrier function [30, 86, 87] through a release of barrier -degrading proteases that are released by transmigrating neutrophils [71].

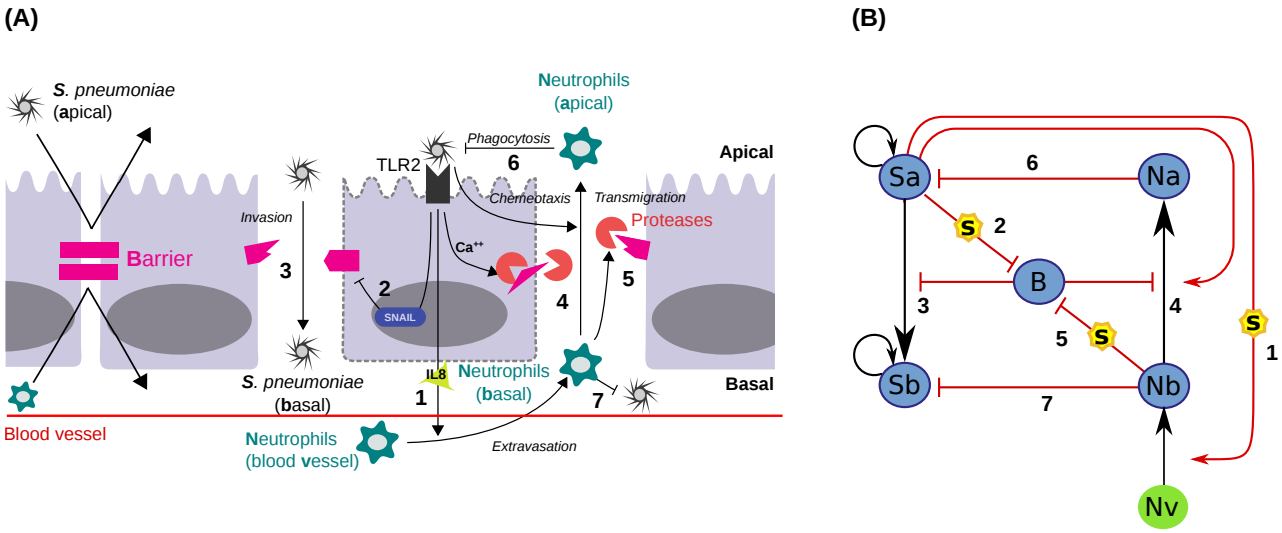

Figure 8.2: **Cartoon (A) and reaction network (B) of the host-pathogen interactions that occur between *Streptococcus pneumoniae* and the upper airway epithelium** Apically located *Streptococcus pneumoniae* (*Sa*) activate TLR pathway signalling, leading to **(1)** neutrophil recruitment from the blood vessel (*Nv*) but also to **(2)** a down-regulation of Barrier function (*B*). Competent barrier hinders **(3)** the invasion of bacteria to the basal side of the epithelium, but also **(4)** the transmigration of Neutrophils from the basal (*Nb*) to the apical (*Na*) compartment. **(5)** Transmigrating neutrophils reduce barrier function via the release of barrier-degrading proteases. Upon contact with *Streptococcus pneumoniae*, neutrophils phagocyte bacteria, both in the **(6)** apical and on the basal **(7)** side of the epithelium.

8.4 Mathematical model of host-pathogen interactions to understand the dual role of the epithelial barrier in determining the outcome of infectious processes

We represent the reaction network underlying the host-pathogen interactions between *Streptococcus pneumoniae* and the upper airway epithelium by the system of equations 8.1.

$$\frac{dSa(t)}{dt} = \left[\kappa_S\left(1-\frac{Sa(t)}{\mu_S}\right) - \frac{\kappa_{si}}{\varepsilon_S B(t)+1} - \phi_{NS}Na(t)\right]Sa(t), \tag{8.1a}$$

$$\frac{dSb(t)}{dt} = \frac{\kappa_{si}}{\varepsilon_S B(t)+1}Sa(t) + \left[\kappa_S\left(1-\frac{Sb(t)}{\mu_S}\right) - \phi_{NS}Nb(t)\right]Sb(t), \tag{8.1b}$$

$$\frac{dNa(t)}{dt} = \frac{\theta_{nt}}{\varepsilon_N B(t)+1}Sa(t)Nb(t) - \kappa_{Nd}Na(t), \tag{8.1c}$$

$$\frac{dNb(t)}{dt} = \theta_{Sanr}\mathrm{Nv}F(Sa(t)) - \left[\frac{\theta_{nt}}{\varepsilon_N B(t)+1}Sa(t) + \kappa_{Nd}\right]Nb(t) + \beta, \tag{8.1d}$$

$$\frac{dB(t)}{dt} = \frac{\kappa_{bp}(1-B(t))}{1+\lambda_{Sabp}F(Sa(t))} - \left[\theta_{Sabd}F(Sa(t)) + \phi_{Nbbd}F(Nb(t))\right]B(t), \tag{8.1e}$$

$$F(X(t)) = \frac{X(t)^{n_H}}{X(t)^{n_H} + K_M^{n_H}} \text{ (Switch function)}, \tag{8.1f}$$

where $S_a(t)$ and $S_b(t)$ represent the concentrations of apically and basally located bacteria, respectively, and are given in units of Colony-Forming Units (CFU) $\times 10^5/ml$, $B(t)$ represents the dimensionless barrier function, and $N_a(t)$ and $N_b(t)$ are the concentrations of apically and basally located neutrophils, respectively, given in units of [cells $\times 10^5/ml$].
The translation of the kinetic interactions between these species represented in the reaction network 8.2 B to the system of ODEs in 8.1 was done by using the Law of Mass Action (methodology described in section A).
In addition, our model has the assumptions detailed in the next section.

8.4.1 Model assumptions

Distinction between apical and basal sub-populations of bacteria and neutrophils

In our model, we distinguish between apical and basal sub-populations of bacteria and neutrophils to explore the role of the epithelial barrier in modulating the invasion of bacteria and the transmigration of neutrophils.
Accordingly, we follow up on the model proposed in [93], which distinguished between apical and basal sub-populations of bacteria, and add, for the first time, the distinction between apical

and basal neutrophils.

Unidirectional barrier crossings

Once bacteria have crossed from the apical to the basal side of the epithelial barrier and to the blood stream, circulating immune cells, the plasma flow and a low-nutrient environment rapidly decrease the local concentration of the bacteria in the basal side of the epithelium (*Sb*), dramatically reducing the probability of a re-colonization of the apical surface of the upper airway epithelium.
Analogously, neutrophil crossing through the epithelial barrier follows a chemeotactic gradient in the direction of the apically located bacteria [86, 72, 275], suggesting that reverse transmigration of neutrophils from the apical to the basal side of the epithelium is unlikely [276].
Accordingly, in our model, we assume that the crossings of both bacteria and of neutrophils through the barrier are unidirectional.

Logistic growth of bacteria

We follow [91] in modelling both apical and basal bacterial growth with a logistic equation, that considers that the growth of bacteria is limited by a carrying capacity μ_S, as observed experimentally [277], with a growth rate κ_S that is strongly dependent on growth medium and bacterial variant [278, 279, 277]. We assume that apical and basal growth rates of bacteria are undistinguishable.

Switch-like dose-response between apically located bacteria and the activation of the TLR signalling pathway

Sensing of bacteria by the host occurs by attachment of apically located bacteria to innate immune receptors such as TLR that are expressed on the apical side of the epithelium [280]. We follow [93] and assume that only apically located bacteria trigger the activation of TLR pathway.
Several experimental [193, 281, 194] papers have reported that the activation of TLR signalling by pathogens is switch-like. It involves fast biochemical events, but is triggered and also affects slower changing populations of cells (bacteria, neutrophils and epithelial cells). Given this difference in time-scales, the activation of TLR signalling by bacteria can be assumed to be in QSS, while the slower cellular processes are assumed to change dynamically, in a slower time-scale.
We model this switch-like dose-response behaviour of TLR activation by pathogens in a phenomenological way, with the Hill function $F(X(t))$ (equation 8.1 f) where $X(t)$ corresponds to the concentration of *Sa*, n_H is the Hill coefficient that quantifies the steepness of the switch,

and K_M is the concentration of bacteria at half maximal activity of TLR signalling. The function $F(X(t))$ describes the QSS concentration of biochemical effectors that are induced by the active TLR pathway (for example, *snail1* [38]).
The importance of a switch-like dose-response behaviour in mediating the immune responses has been discussed in section 3.2. In the case of the host-pathogen interactions between the airway epithelium and *Streptococcus pneumoniae*, a switch-like dose-response behaviour is particularly relevant, since *Streptococcus pneumoniae* normally resides on the airway epithelium as a commensal bacteria that does not trigger any immune responses.
In our model, TLR activity mediates both the immune responses (in the form of neutrophil recruitment) as well as the barrier damage (in the form of down-regulation of barrier production rate). Note that the model of [93] also assumes this dual effect of apically located bacteria, but without considering the switch-like dose-response behaviour of these rates. This is because the model of [93] focuses on the *bronchial* epithelium, that under healthy conditions does not have *any* resident *S. pneumoniae*. In contrast, we want to understand the host responses that occur in the *upper* airway epithelium, where *S. pneumoniae* normally resides as commensal bacterium.

No *de novo* production of neutrophils

We assume that neutrophils do not divide in the epithelial tissue, since it has been observed that *de novo* production of neutrophils does not occur outside the bone marrow [282]. Accordingly, in our model, apically and basally located neutrophils are subjected to death rate κ_{Nd}, but not to a proliferation rate.

Self-recovery of the barrier function upon perturbation

It has been consistently observed that epithelial monolayers [28, 283, 284] follow self-recovering dynamics upon perturbation.
We model this self-recovery in a phenomenological way (see section 3.3), with a first order logistic equation that has a nominal barrier production rate κ_{bp}.
The inhibition of barrier production by apically located bacteria was modelled in a phenomenological manner (see appendix A), by dividing κ_{bp} by the term $1+\lambda_{Sabp}F(Sa(t))$, where $F(Sa(t))$ is the Hill function that describes the switch-like activation of TLR signalling by bacteria, and λ_{Sabp} quantifies the inhibitory effect of TLR activation on barrier function.

Phagocytosis of bacteria by neutrophils

Upon contact with neutrophils, bacteria are eliminated with a rate ϕ_{NS} [88, 89]. We assume that this killing rate are not dependent on the location of the interaction (no distinction between basal

and apical killing rates). This pathogen elimination rate by neutrophils was also considered in the model of [91].

Switch-like barrier degradation by neutrophils

Barrier degradation by neutrophils occurs in a switch-like manner [87]. It is mediated by the release of proteases, corresponding to a fast biochemical process that can be approximated by the Hill function $F(X(t))$, where $X(t)$ corresponds to the concentration of Nb, and $F(X(t))$ is the resulting steady state concentration of barrier-damaging proteases.

8.4.2 Network motif representation

We identified three key regulatory modules in the reaction network controlling the host-pathogen interactions described in figure 8.2 and represented accordingly in the systems of equations 8.1:

- Switch-like activation of immune responses and barrier damage.
- Self-recovering dynamics of barrier function.
- Persistence of immune cells in the airway epithelium even after ceasing of the cytokine levels, resulting from the difference in time-scales between slow recruitment of neutrophils by fast activating TLR signalling.

These regulatory modules correspond to the network motifs that also mediate epithelial function, described in chapter 3, suggesting that our modelling framework, based on modularization (switching, self-recovery and persistence modules) and time-scale separation (interplay between fast biochemical and slow cellular level processes), can be applied to model other epithelial systems. The modular representation of the host-pathogen interactions are represented in figure 8.3.

8.4.3 Model parameters

All the the parameters of the model 8.1, except those involving the recruitment of neutrophils from the bloodstream, were estimated by extensively fitting the model to quantitative and dynamic experimental *in vitro* data that we gathered from the literature, as described in appendix B. The resulting set of nominal parameters is given in table 8.1.
Given that to date there is no systems-level experimental characterization of the reaction network modelled in this chapter, the dataset used for the calibration of our mathematical model was gathered from many different data-sources, in which different types of system components

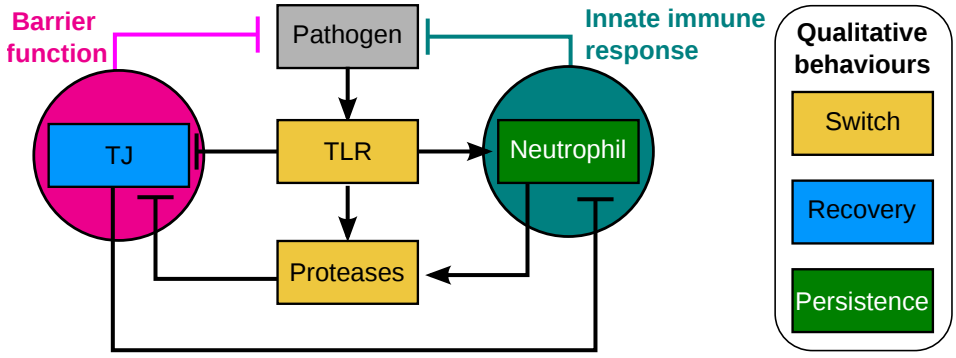

Figure 8.3: **Network motif representation of the mathematical model of the host-pathogen interactions occurring between *Streptococcus pneumoniae* and the airway epithelium.** Apically located pathogens lead to the activation of the TLR signalling pathway in a switch-like dose-response manner. Active TLR pathway triggers innate immune responses in the form of neutrophil recruitment from the bloodstream to the site of infection. Neutrophils degrade the pathogen, but also damage the barrier via the switch-like induction of barrier-degrading proteases, and persist in the epithelium tissue even after the production of cytokines has ceased. In turn, competent barrier hinders the transmigration of neutrophils from the basal to the apical side of the epithelium. Active TLR pathway also decreases the epithelial barrier function by interfering with its production and degradation rates. Neutrophil recruitment is modelled by a persistence motif, to represent the difference in time-scales between this slower cellular process that is triggered by a rise in TLR-induced cytokine levels. Barrier function, given by the amount of TJ, is modelled by a self-recovery motif. Both TJ and neutrophil concentrations reduce the pathogen load in the bloodstream by enacting the two protective properties of the epithelium: barrier function that prevents the invasion of bacteria to the bloodstream, and innate immune responses that eliminate the pathogen.

(eg. different epithelial tissues and bacterial strains) were empirically characterized under different experimental conditions. This results in a very heterogeneous dataset, with a strong variability between different measurements of the same process (see for example the different self-recovering dynamical behaviours observed for different epithelial tissues in figure B.2, or the different growth curves of *Streptococcus pnueumoniae* in different media, shown in figure B.3). Thus, although the parameter values presented in table 8.1 are biologically plausible, their exact values must be considered within a relatively large error margin that arises from the variability in the experimental system and the experimental conditions.
Hence, in addition to the determination of parameters (by optimization) presented in appendix B, it is necessary to further explore the effects of parameter variations on the system's behaviour. This is done in this chapter in section 8.6, and could be further complemented by a sensitivity analysis.

The parameters that quantify the basal (β) and TLR-dependent ($\theta_{Sanr}Nv$) rates of infiltration of the neutrophils from the blood can be estimated only from *in vivo* datasets that represent rather qualitative, but not quantitative dynamical behaviours of bacteria and neutrophils.

To obtain a rough estimate for these values, we adjusted our model simulations, by manually tuning the values for β and $\theta_{Sanr}Nv$, to qualitatively reproduce the dynamics of a *in vivo* dataset. Particularly, we used the *in vivo* data from [231]. It shows the the dynamics of the concentrations of apical bacteria $Sa(t)$ and neutrophils and macrophages, obtained from the analysis of the Broncheoalveolar Lavage Fluid (BALF) of mice that were colonized with *Streptococcus pneumoniae* (by direct instillation of the bacteria into the nares of the mice). These experiments were done for *wild type* (*wt*) and TLR mutant mice ($TLR2^{-/-}$).

Both neutrophils and macrophages are represented in our model by the variable $Na(t)$, that represents all the innate immune responses to the pathogen. We assume that our variable $Na(t)$ corresponds to the sum of the experimentally measured concentrations of neutrophils and macrophages.

To integrate the different *in vitro in vivo* datasets into a coherent and quantitative framework, we converted the *in vitro* experimental measurements -usually given in number of cells for neutrophils and CFUs for bacteria- to concentrations. This allowed us to directly compare the *in vitro* data to *in vivo* data, since the measurements of apical and basal neutrophils and bacteria in a mouse are usually accompanied with measurements of the volume of the solutions that contain neutrophils and bacteria (BALF and serum).

In addition to obtaining a first estimate for β and $\theta_{Sanr}Nv$, we also used this dataset to obtain a second value for the bacterial carrying capacity μ_s. As shown in section B, the value for μ_s can be estimated from *in vitro* data. However, we consider that *in vitro* estimates for the values of μ_s greatly over-estimate the *in vivo* conditions. Therefore, by comparing the model simulations with the *in vitro* data from [231], we roughly estimated a second, *in vivo* value for μ_s (table 8.1).

We acknowledge that the resulting parameter values for β, $\theta_{Sanr}Nv$ and μ_s are not accurate, and are used only as a starting point for the model simulations.

As shown in figure 8.4, simulations of our mathematical model (system of equations 8.1), using the nominal parameter set shown in table 8.1, show a qualitative agreement with the *in vivo* data from [231]. Both model simulations and the experimental data show that *wt* and also *TLR2* mutant mice effectively clear the infection, decreasing the pathogen load to a low, non-virulent value. This clearance occurs already within the first day post-infection for the *wt* mice, and is delayed in the *TLR2* mutant mice, as shown both by the experimental data and by the model simulations. Despite this qualitative agreement, the simulation results from our mathematical model do not agree quantitatively with the experimental data. Likely, this mismatch can be attributed to the fact that some of the processes that are involved *in vivo* in the bacterial clear-

ance are not considered in our simplified *in vitro* model. For example, the recruitment of other immune cells, such as macrophages, also play a important role in decreasing the pathogen load [231], but are not considered in our model.

The experimental results from [231] suggests that neither TLR-mediated immune responses nor TLR-mediated barrier damage play a major role in the determination of the pathogen load, since both the *wt* and the *TLR* mutant mice show a rapid clearance of the bacterial load.
These qualitative dynamics are also reflected in the model simulations of the *wt* and the *TLR mutant*. The initial high pathogen concentration $Sa(0)$ is rapidly decreased, for both of these virtual genetic conditions.
In our simulations, the concentration of $Sa(t)$ in the *wt* decreases quicker that in the *TLR mutant*, however, no experimental information is available for the fist hours of the host-pathogen interaction, when presumably these TLR-dependent immune responses occur.
Two possible mechanisms that could explain this TLR-independent control of the pathogen load are either a low bacterial carrying capacity (μ_s), or strong resident immune responses (represented in our model by the parameter β). Both correspond to basal, unstimulated conditions of the host that effectively controls pathogen load.
In the following section, we explore the consequences of changing these and other parameters on the model behaviours. To do so, we first present the *possible* dynamic behaviours that the model 8.1 can exhibit, and assess then the impact of parameters including μ_s and β that are affected by a previous episode of infection of the host.
The main aim of this analysis, that uses our quantitative mathematical model that his parametrized with *in vitro* experimental data and qualitatively reproduces *in vitro* data, is to help clarifying the mechanisms of co-infection. More generally, it will also serve as a tool for the analysis of the systems-level, but costly, inaccurate and incomplete *in vivo* datasets.
The qualitative agreement between our model simulations and *in vivo* experimental data from [231] (figure 8.4) is a first indication of the validity of our data-driven model. Further comparisons between our mathematical model simulations and other *in vivo* datasets will be performed in the future.

8.5 Qualitative dynamical behaviours

Healthy host-pathogen interactions, i.e. epithelial homeostasis, is defined by following conditions:

- A competent, undamaged **barrier** (”high permeability barrier function”).

Table 8.1: Parameters of the mucosal barrier model

Symbol	Name	Nominal value	Reference	Units
	System independent parameters: Natural production and decay rates			
κ_{bp}	Barrier production	0.45	[87]	h^{-1}
κ_s	Bacterial proliferation	0.45	[279]	h^{-1}
μ_s	Bacterial carrying capacity (*in vitro*)	$< 0.5 \times 10^4$	Dr Tom Clarke, personal communication	$\frac{CFU \times 10^5}{ml}$
	" (*in vivo*)	180	Arbitrary	$\frac{CFU \times 10^5}{ml}$
κ_{nd}	Neutrophil death	0.0831	[282]	h^{-1}
	Switch parameters: TLR activation			
k_m	Threshold of TLR2 activation by Sa	120	[285]	$\frac{CFU \times 10^5}{ml}$
n_h	Hill coefficient of TLR-activation	5.75	[285]	dimensionless
	Bacteria - neutrophil interactions			
ϕ_{NS}	Neutrophil-induced death of Bacteria	0.0019	[89]	$[h\frac{10^5 \times cells}{ml}]^{-1}$
	Bacteria - barrier interactions: Barrier damage by bacteria			
λ_{SaBp}	Active TLR on barrier production	0.18	[85]	dimensionless
θ_{sabd}	Active TLR-induced proteases on barrier degradation	0.8	[85]	h^{-1}
	Bacteria - barrier interactions: Invasion of bacteria through barrier			
κ_{si}	Bacterial invasion through barrier	0.05	[270]	h^{-1}
ε	Barrier-dependent inhibition of bacterial invasion	1	[270]	dimensionless
	Neutophil barrier interactions (1): Barrier damage by neutrophils			
ϕ_{Nbbd}	Neutrophil-induced barrier degradation	3.2	[86]	h^{-1}
K_{MN}	Concentration of the basal neutrophils at half maximal barrier degradation rate	9	[86]	$\frac{[cells] \times 10^{-5}}{h}$
n_{nH}	Hill coefficient of barrier degradation by neutrophils	5	[86]	dimensionless
	Neutophil barrier interactions (2): Infiltration of neutrophils through barrier			
θ_{nt}	Bacteria-induced neutrophil transmigration rate	14	[71]	$\frac{CFU \times 10^{-5}}{h}$
ε_S	Inhibition of neutrophil transmigration by barrier	81	[71]	dimensionless
	In vivo parameters			
θ_{SanrNv}	Bacteria-induced recruitment of neutrophils from blood vessels	100	Arbitrary	$\frac{CFU \times 10^{-5}}{h}$
β	Basal neutrophil extravasation rate	2	[231]	$\frac{[cells] \times 10^{-5}}{h}$

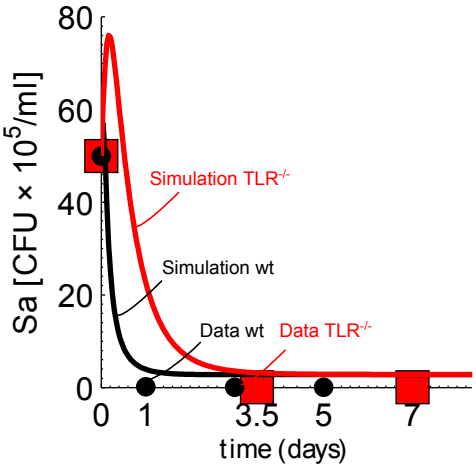

Figure 8.4: **Comparison of model simulations with *in vivo* data** Data-points reproduced from [231] ($TLR2^{-/-}$ data from figure 1, open circles, and and *wt* data from figure 6, closed circles). Simulations of model given by the system of equations 8.1, parametrized with the nominal parameter set shown in table 8.1. The *in vivo* parameters values are $\theta_{SanrNv} = 1000$ $\beta = 2$ and $\mu_s = 120$. The initial conditions are $Sa(0) = Sa_{exp}(0) = 50[\frac{CFU \times 10^5}{ml}]$, $Sb(0) = Nb(0) = B(0) = 0$, and $Na(0) = Na_{exp}(0) = 0$. We assumed that the simulated $Na(t)$ is equivalent to the sum of the experimentally measured neutrophils and macrophages in [231].

- Low **immune responses**.
- No infection (" low **pathogen** load").

To fulfil these conditions, it is necessary that, at steady state:

- The barrier is not damaged, neither by bacteria nor by neutrophils,
- the immune responses are not triggered by bacteria, and
- the bacterial load is maintained below its carrying capacity by the epithelial barrier and the basal immune responses.

Violation of these conditions results in different forms of loss of epithelial homeostasis, resulting from excessive pathogen load, activation of immune responses, or barrier damage.
To systematically characterize these different forms of loss of epidermal homeostasis, and how they result in *qualitative dynamical behaviours*, we recall that, in our model, barrier damage is mediated by switch-like activation of TLR signalling by apical pathogens, and by switch-like release of proteases by basal neutrophils dependent decrease in barrier function (figures 8.5 A,B).
Assuming perfect switching behaviours (which corresponds to setting the Hill coefficient to be infinitely large, i.e. $n_H \to \infty$, resulting in a Hill function $F(X(t))$ that resembles a perfect

step [286]), we can approximate the rates of Sa and Nb induced barrier degradation $F(X(t))$ in equation 8.1f by constant "low" or "high" rates of TLR or protease activities, depending if the concentration of apical bacteria or basal neutrophils is below or above the threshold concentration Sa^+ or Nb^+, respectively. The threshold concentration Sa^+ or Nb^+ correspond to k_m and K_{mn}, when $n_H \to \infty$ in $F(Sa(t))$ and $F(Nb(t))$, respectively. Formally, this corresponds to the Piece-Wise-Affine function (PWA):

$$\lim_{n_H \to \infty} F(X(t)) \sim F(x, x^+, y_{low}, y_{high}) = \begin{cases} y_{low}, & \text{if } x \geq x^+ \\ y_{high}, & \text{if } x < x^+, \end{cases} \tag{8.2}$$

where x corresponds to Sa or Nb, x^+ denotes the threshold values Sa^+ or Nb^+, respectively, y_{low} and y_{high} are the "low" and "high" values of TLR and protease activity, and n_H is the Hill coefficient of the Hill equation $F(X(t))$ (see section 3.2.6 for details on this PWA approximation).

This simplifying assumption allows us to discretize the projection of the phase plane of the concentrations of apically located pathogens and basally located neutrophils into four regions, corresponding to "high" or "low" concentrations of Sa and Nb, separated by the thresholds Sa^+ and Nb^+, respectively (figure 8.5 C).

Epithelium homeostasis requires that the steady state values of $Sa(t)$ and $Nb(t)$ are below their threshold concentrations Sa^+ and Nb^+, at which bacteria and neutrophil dependent barrier damage is negligibly low. This corresponds to the white the region of the phase plane projection $Sa \times Nb$ depicted in figure 8.5 C and figure 8.6.

Different forms of loss of epithelial homeostasis correspond to distinct trajectories on the regions of the phase plane projection $Sa \times Nb$. Defining Sa_{ss} and Nb_{ss} as the steady states of the variables $Sa(t)$ and $Nb(t)$, respectively, we can distinguish following dynamical behaviours, which depend on the position of Sa_{ss} and Nb_{ss} on the phase plane $Sa \times Nb$ [208], as follows:

- Convergence of apical bacteria and basal neutrophils towards the steady state concentrations $Sa_{ss} > Sa^+$ and $Nb_{ss} < Nb^+$, respectively (figure 8.9 A). This appears as bacteria-induced barrier damage and high pathogen load (figure 8.9 B).

- Convergence of apical bacteria and basal neutrophils towards the steady state concentrations $Nb_{ss} > Nb^+$ and $Sa_{ss} < Sa^+$, respectively (figure 8.8 A), resulting in neutrophil-induced barrier damage and high infiltration of immune cells (figure 8.8 B).

- Convergence of apical bacteria and basal neutrophils towards their "high" steady state concentrations $Nb_{ss} > Nb^+$, and $Sa_{ss} > Sa^+$ (figure 8.10 A). This condition is associated to barrier damage, high infiltration of immune cells, and high pathogen load (figure 8.10 B).

- Recurrent flares of barrier damage, pathogen invasion and high immune cell infiltration, depicted in figure 8.7 B, occur when the system of equations 8.1 has no global attractor (figure 8.7 A).

In the following sections, we present a systematic analysis of these different qualitative dynamic behaviours.
The possible qualitative behaviours of the PWA system, given by the approximation of equations 8.1 by 8.2, can be analysed by assessing the position of its *focal points* in relation to the four regions of the phase plane, depicted in figure 8.5 C.
The focal points are the steady state values of the mathematically simpler sub-system of equations resulting from setting $F(Sa(t))$ and $F(Nb(t))$ to a constant "high" or "low" value. Focal points are *attractors* of the whole system of equations only if all the trajectories (departing from any of the four regions of the phase plane) converge to this focal point [208].
In the following, we characterize each of the qualitative dynamic behaviours enlisted above. We follow [208] and present a mathematical analysis and simulations of the underlying, simplified PWA model, given by the step-like Hill function given by equations 8.2, and compare these to simulations of the original, continuous model given by the system of equations 8.1. In most of the cases, the PWA approximation retrieves a similar qualitative dynamical behaviour than the original, continuous model.

8.5.1 Epithelial homeostasis requires healthy clearance of a bacterial challenge

To achieve epithelial homeostasis, the focal point of the sub-system of equations given by $F(Sa)$="low" and $F(Nb)$="low" must be a *global attractor* of the system. I.e., all the trajectories must converge into the region of the phase-plane given by $Sa < Sa^+$ and $Nb < Nb^+$. Particularly relevant is the trajectory followed after a initial bacterial challenge to the system, when $Sa(0) > Sa^+$ (figure 8.6 A).
A *healthy clearance* of this initial bacterial load is achieved by a transient TLR mediated induction of immune responses leading to the increase of Nb (figure 8.6 B, left). The combination of TLR activation and the resulting increase in neutrophil concentrations leads to a transient decrease in barrier function (figure 8.6 B, center), which is restored again to a homeostatic value once the immune responses have cleared the infection (figure 8.6 B, center) and cease. Note that the homeostatic barrier slightly deviates from its nominal value, because in the continuous version of the model, barrier damage occurs even when $Sa < Sa^+$ and $Nb < Nb^+$. This is because $F(Sa) = low$ and $F(Nb) = low$ are small, but not always equal to zero in the continuous version of the model.
If TLR-mediated immune responses are sufficient to clear the infection without surpassing the

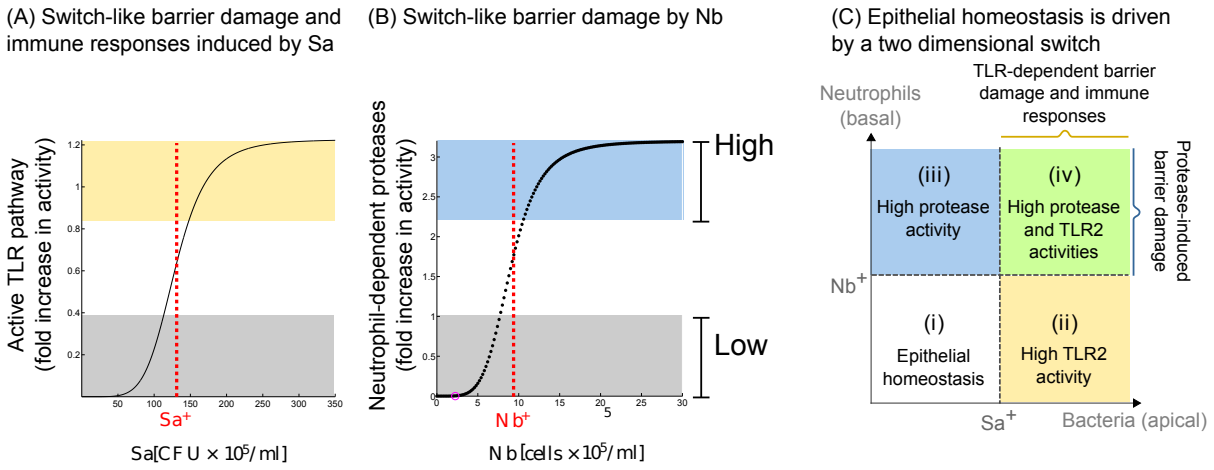

Figure 8.5: **Epithelial function is controlled by a two dimensional switch**. *[A]* Barrier damage and induction of immune responses by bacteria are mediated by a switch-like activation of TLR signalling pathway by apically located bacteria (Sa). Only values above the threshold of activation Sa^+ lead to a significant barrier damage and immune responses induced by bacteria. *[B]* Similarly, neutrophil dependent barrier damage is described by a switch that relates the basally located neutrophils (Nb) and the concentrations of barrier-damaging proteases. Only concentrations of Nb that are above threshold Nb^+ trigger significant barrier damage. *[C]* Together, these two switches determine different regions of the phase plane projection $Sa \times Nb$ corresponding to (i) homeostatic epithelium ($Sa < Sa^+$ and $Nb < Nb^+$), (ii) TLR-dependent barrier damage and immune responses ($Sa > Sa^+$ and $Nb < Nb^+$), (iii) neutrophil protease-dependent barrier damage ($Sa < Sa^+$ and $Nb > Nb^+$), or (iv) barrier damage and immune responses, induced by both bacteria-dependent TLR and neutrophil-dependent proteases ($Sa > Sa^+$ and $Nb > Nb^+$). Long term epithelium homeostasis, involving a competent barrier and resolution of the immune responses, requires thus that the steady state values of Sa and Nb are confined to the *(i)* region of the phase plane, in which no barrier damage occurs.

threshold values Nb^+, the transient barrier damage is lower (figure 8.6 B, center, blue line), but the transient infection is higher (figure 8.6 B, right, blue lines), as compared to strong immune responses that transiently surpass the threshold Nb^+ (red trajectories in figure 8.6).
When the initial concentration of bacteria is low ($Sa(0) < Sa^+$), the basal, unstimulated conditions of the host suffice to maintain the bacterial load below Sa^+.

This homeostatic dynamical behaviour, characterized by a healthy clearance of the infection, is consistent with the homeostatic behaviour observed in other mathematical models of the host-pathogen interactions between *Streptococcus pneumoniae* and the airway epithelium [94, 92, 93, 103].

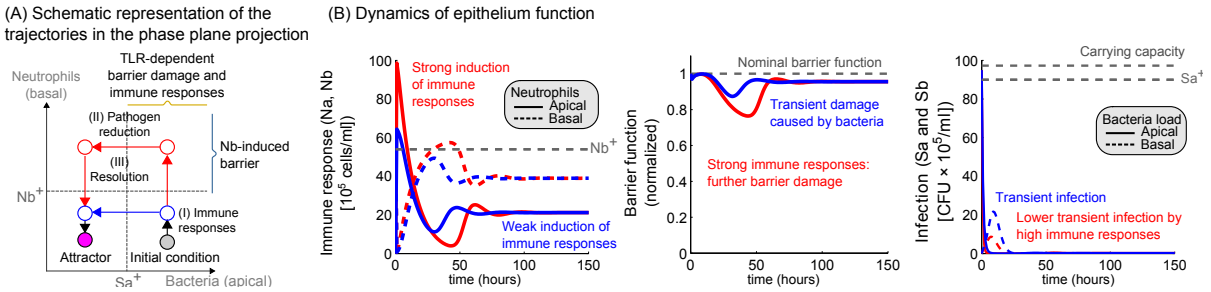

Figure 8.6: **Epithelial homeostasis requires healthy clearance of a bacterial challenge (A)** Epithelial homeostasis requires that the global attractor of the system is such that $Sa_{ss} < Sa^+$ and $Nb_{ss} < Nb^+$. Upon a pathogen challenge ($Sa(0) > Sa^+$), a healthy clearance is characterized by a transient induction of TLR-mediated immune responses *(B, left)*, accompanied by a transient decrease in barrier function *(B, center)*, and a transient infection *(B, right)*. Increase in immune responses leads to reduction of bacterial load ($Sa(t) < Sa^+$), followed by a resolution of the immune responses, resulting in homeostasis after a transient loss of barrier function and induction of immune responses. *(B)* shows the dynamics of epithelium, given by immune responses, barrier function and bacterial load. If the induction of immune responses are weak, i.e. such that $Nb < Nb^+ \forall t$, then the barrier damage is caused only by the transient bacterial challenge. Otherwise, infiltrating neutrophils lead to a further stronger, but equally transient reduction of barrier function.

These results were obtained by simulating the continuous system of equations 8.1 with the nominal parameters given in table 8.1, except for $\beta = 5$ (high basal immune responses) and $k_{MN} = 18$ (higher threshold for neutrophil activation, to compensate for higher β). High induction of immune responses (red trajectories) were simulating by increasing $\theta_{Sanr} Nv$ from 100 to 1000. The initial conditions are $Sa(0) = Sa^+ + 5$, $Sb(0) = Na(0) = 0$, $Nb(0) = 60$, and $B(0) = 1$.

8.5.2 Recurrent flares of immune responses, barrier damage and infection

Recurrent flares of barrier damage, immune responses and infection arise when *none* of the focal points is a *global attractor* of the system (figure 8.7 A).

In this scenario, a bacterial challenge $Sa(0) > Sa^+$ results in a transient induction of immune responses and the associated decrease in barrier function described in section 8.5.1. However, once the bacterial infection has been cleared and the immune responses cease, the pathogen load increases again until $Sa(t) > Sa^+$, initiating a new cycle of induction of immune responses (figure 8.7 B, left), decrease in barrier function (figure 8.7 B, center) and burst of infection (figure 8.7 B, right).

In the continuous version of the model, given by equations 8.1, these oscillations eventually

relax to a steady state value corresponding to moderate immune responses (figure 8.7 B, left), barrier damage (figure 8.7 B, center, blue line), and infection (figure 8.7 B, right).
Only in the discrete version of the model (given by the PWA resulting from the approximation in 8.2), the oscillations persist with constant frequency and amplitude, because the binary function $F(X(t))$ is not defined for the intermediate values towards which the continuous system relaxes (figure 8.7 B, center, red line) [208].
These results suggest that TLR-mediated immune responses alone cannot account for long term epithelial homeostasis, because homeostasis requires that, at steady state, TLR signalling is inactive (i.e. $Sa_{ss} < Sa^{+}$, figure 8.5). If clearance of infection is solely dependent on TLR mediated immune responses, the resulting dynamic behaviour corresponds to the non-homeostatic, recurrent flares of immune responses, barrier damage and infection described in figure 8.7. However, besides TLR-dependent immune responses, bacterial clearance is mediated also by basal levels of infiltration of immune cells, represented in the model by the parameter β. Resident immune cells can decrease Sa_{ss} below Sa^{+}, playing a pivotal role in determining the long-term behaviour of the host-pathogen interactions.
Understanding and preventing this cyclic behaviour that converges to a low level infection is clinically relevant, since frequent events of bacterial infiltration into the bloodstream can eventually result in the leakage of a particularly aggressive, or antibiotic resistant bacterial variant [279]. This relation between a sustained low level infection and the emergence of a sub-population of antimicrobial resistant pathogens has been addressed in the stochastic model of [287] for the host-pathogen interactions between *E coli* in the large intestine of cattle.

8.5.3 Aseptic loss of homeostasis is characterized by sustained high immune responses and barrier damage

Aseptic loss of homeostasis, characterized by sustained high immune responses and barrier damage, occurs when the focal point associated to the sub-system of equations given by $F(Sa)$="low" and $F(Nb)$="high" is a global attractor of the system, i.e., all the trajectories converge into the region of the phase-plane given by $Sa < Sa^{+}$ and $Nb > Nb^{+}$ (figure 8.8 A).
In this scenario, a pathogenic challenge (given by $Sa(0) > Sa^{+}$), leads to TLR-mediated induction of immune responses (figure 8.8 B, left) that eventually eradicate the pathogen (figure 8.8 B, right). However, the barrier damage that results from high ($Nb(t) > Nb^{+}$) immune responses persists (figure 8.8 B, center), even after the infection has been cleared ($Sa(t) < Sa^{+}$). This is because the basal, TLR-independent immune responses are high enough to surpass the Nb^{+} threshold, even when $Sa(t) < Sa^{+}$ (and hence, no TLR mediated immune responses are induced).
Hence, even in the absence of a pathogenic challenge, i.e. when $Sa(0) < Sa^{+}$, the basal im-

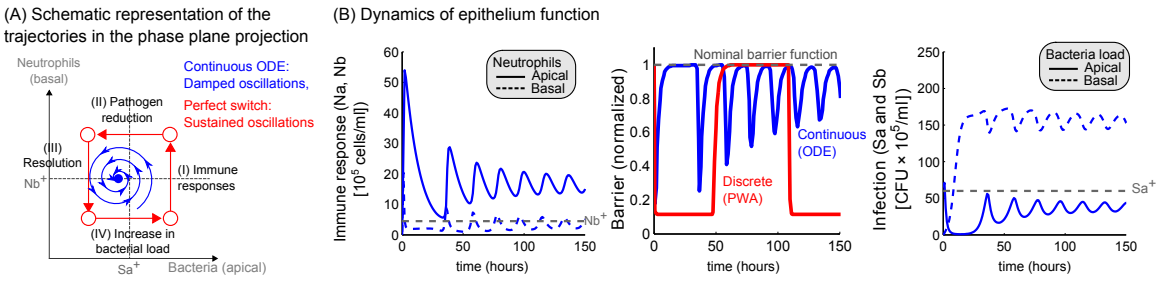

Figure 8.7: **Recurrent flares of immune responses, barrier damage and infection** *[A]* Cyclic loss of epithelial homeostasis and infection results from focal points being outside corresponding sub-domains of the $Sa \times Nb$ phase plane projection. A bacterial challenge ($Sa(0) > Sa^+$) leads to onset of TLR-mediated immune responses which effective reduce the bacterial load. Decreasing $Sa(t)$ below the threshold Sa^+ of TLR activation leads to remission of the immune responses. In the absence of TLR-induced neutrophil recruitment, bacterial load increases again to $Sa(t) > Sa^+$ and then $Nb(t) > Nb^+$, resulting the cycles of infection and accompanying barrier damage. *[B]* The corresponding recurrence dynamics for barrier function, immune responses and infection. In the continuous version of the model, the oscillations are damped and stabilize to a value corresponding to moderate immune responses, barrier damage and pathogen invasion.

These results were obtained by simulating model 8.1 with the nominal parameter set given in table 8.1, except for $\theta_{Sanr}Nv = 1000$, and $\theta_{nt} = 0.7$. The initial conditions are $Sa(0) = Sa^+ + 5$, $Sb(0) = Na(0) = 0$, $Nb(0) = 1$, and $B(0) = 1$. For the discrete (PWA) approximation, we defined $Sa^+ = 0.5k_m$ and $Nb^+ = 0.5k_{mn}$. The resulting discrete trajectories are shown only for the barrier function dynamics *([B], center, red curve)*. For the immune responses and pathogen load, only the continuous dynamics are displayed (red trajectories).

mune responses eventually surpass the threshold Nb^+ (figure 8.8 A, pink arrow), resulting in sustained barrier damage.

This qualitative dynamic behaviour has been observed in previous mathematical models of infection [103, 102]. However, these models do not consider epithelial barrier function, and could therefore not capture the long term tissue damage that results from persistent immune responses [31].

8.5.4 Sustained infection that fails to induce efficient immune responses

Sustained infection that fails to induce sufficiently strong immune responses occur when the global attractor of the system satisfies that $Sa_{ss} > Sa^+$ and $Nb_{ss} < Nb^+$ (figure 8.9 A).

Under these conditions, the immune responses induced by the high pathogen load (figure 8.9 B, left) are not strong enough to clear the pathogen (figure 8.9 B, right), resulting in a sustained

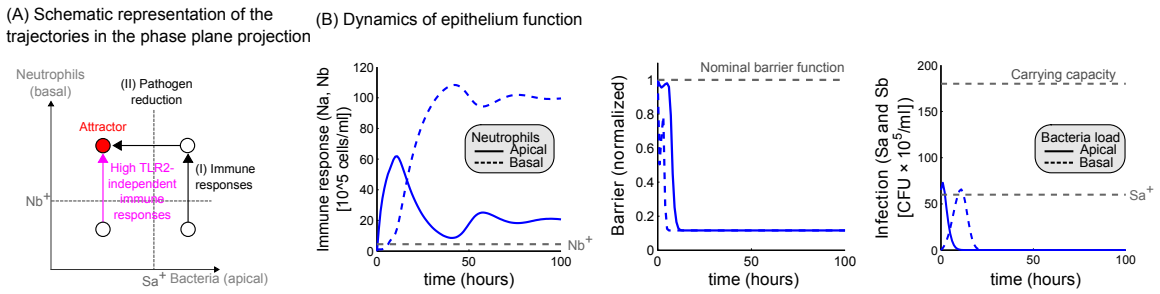

Figure 8.8: **Aseptic loss of homeostasis is characterized by sustained high immune responses and barrier damage** Aseptic loss of homeostasis occurs when the global attractor of the system of equations 8.1 is such that $Nb_{ss} > Nb^+$ and $Sa_{ss} > Sa^+$ (*[A]*), leading to persistent high immune responses (*[B], left*) that lead to chronic loss of barrier function (*[B], center*) and clearance of infection (*[B], right*).
These results were obtained by simulating model 8.1 with the nominal parameter set given in table 8.1, with a high basal rate of immune cell infiltration ($\beta = 10$), and initial conditions $Sa(0) = Sa^+ + 5$, $Sb(0) = Na(0) = 0$, $Nb(0) = 1$, and $B(0) = 1$.

infection and TLR- mediated barrier damage (figure 8.9 B, center).

8.5.5 Total loss of homeostasis is characterized by high infiltration of immune cells, loss of barrier function, and sustained infection

Inefficient immune responses can drive the global attractor of the system to the region of the phase plane where $Sa_{ss} > Sa^+$ and $Nb_{ss} > Nb^+$ (figure 8.10 A).
Under these conditions, a initial bacterial challenge ($Sa(0) < Sa^+$) triggers immune responses (figure 8.10 B, left) that fail to decease the bacterial load below the threshold value Sa^+ (figure 8.10 B, right), resulting in a sustained barrier damage elicited by both bacteria (because $Sa(t) < Sa^+$) and by neutrophils ($Nb(t) < Nb^+$) (figure 8.10 B, center).

8.6 Uncovering the mechanisms that drive the lethal synergism that results from co-infection

Having described the different possible qualitative behaviours that the model can display (section 8.5), we explore in this section how co-infection can drive these qualitative changes in the dynamic behaviour of the host response to a pathogenic challenge.
Infection by another pathogen, such as influenza, can drive a infectious process by the commensal bacterium *Streptococcus pneumoniae* by affecting following processes of the host-pathogen interactions between *Streptococcus pneumoniae* and the upper airway epithelium:

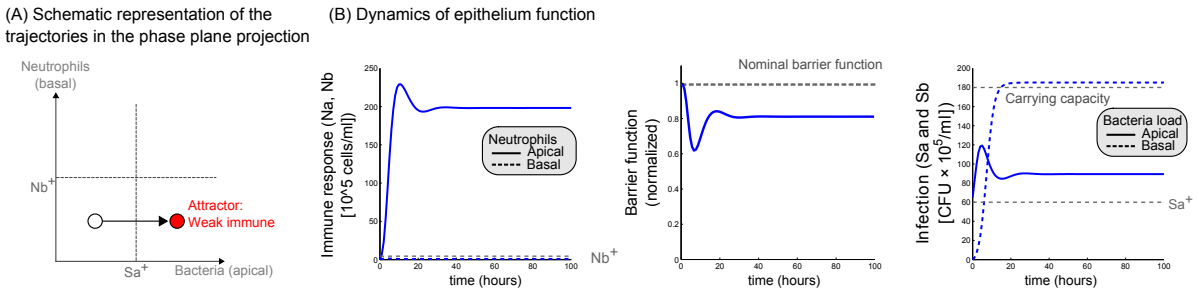

Figure 8.9: **Sustained infection that fails to induce efficient immune responses** When the global attractor of the system satisfies $Sa_{ss} > Sa^+$ and $Nb_{ss} < Nb^+$ *[A]*, then the immune responses induced by a pathogen challenge *[B], left* do not suffice to clear the pathogen load below the threshold concentration Sa^+ (*[B], right*, leading to a sustained infection *[B], right* and a constant damage to the barrier induced by TLR-mediated immune responses *[B], center*. These results were obtained by simulating model 8.1 with the nominal parameter set given in table 8.1, with a high basal rate of immune cell infiltration ($\beta = 10$), a weak pathogen eradication capacity $\phi_{NS} = 0.001$, and initial conditions $Sa(0) = Sa^+ + 5$, $Sb(0) = Na(0) = 0$, $Nb(0) = 1$, and $B(0) = 1$.

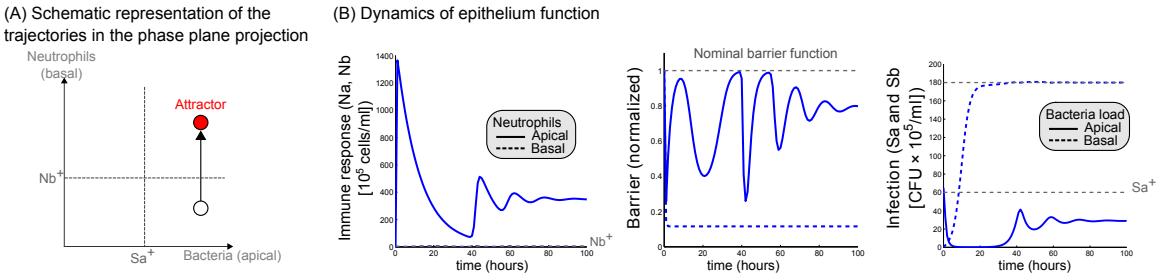

Figure 8.10: **Total loss of homeostasis is characterized by high infiltration of immune cells, loss of barrier function, and sustained infection** When the global attractor of the system is such that $Sa_{ss} > Sa^+$ and $Nb_{ss} > Nb^+$ *([A])*, immune responses elicited by a pathogenic challenge remain high (*[B], left*), leading to a sustained barrier damage (*[B], center*) that is further accentuated by the high pathogen load (*[B], left*) that cannot be decreased by the high but inefficient immune responses.
These results were obtained by simulating model 8.1 with the nominal parameter set given in table 8.1, with a weak pathogen eradication capacity ($\phi_{NS} = 0.005$), high TLR-mediated immune responses ($\theta_{Sanr}Nv = 100000$), a low threshold of neutrophil-induced barrier damage ($k_{MN} = 4.5$) and a low basal rate of neutrophil infiltration ($\beta = 1$). The initial conditions are $Sa(0) = Sa^+ + 5$, $Sb(0) = Na(0) = 0$, $Nb(0) = 1$, and $B(0) = 1$.

- Increase in the bacterial carrying capacity μ_s [69],
- increase in the epithelial permeability to both neutrophils and pathogens (ϕ_{nt} and κ_{si})

[69],

- increased load of resident neutrophils β [288, 69, 244], and
- desensitization of TLR receptor [78].

In the following, we will explore the effect of changing each of these model parameters on the qualitative dynamical behaviour of the system.

8.6.1 Increase in the carrying capacity leads high invasion of bacteria, but no associated barrier damage

The exposure of the airway epithelium to a first pathogen can result in a significant increase in the carrying capacity of *Streptococcus pneumoniae* as a result of the tissue-damaging immune responses that lead to an accumulation of debris [69].
This increase in the bacterial carrying capacity as a result of tissue-damaging immune responses has been modelled in [101, 91, 94, 104]. These models, however, do not explicitly consider the epithelial barrier function. Hence, they cannot be used to assess the potential impact of a increased carrying capacity on the epithelial permeability barrier function and on the resulting rate of bacterial invasion.
Numerical simulations of our model (figure 8.11) suggest that a increased carrying capacity μ_s results in a significant increase in the concentration of *infiltrated bacteria Sb*, but, interestingly, does not trigger a significant increase in the steady state concentrations of Sa_{ss} nor Nb_{ss}. Thus, μ_s does not seem to affect the position of the homeostatic global attractor of the system (given by $Sa_{ss} < Sa^+$ and $Nb_{ss} < Nb^+$, figure 8.11 A). In fact, increase in the carrying capacity μ_s seems to affect only the magnitude of the transient increase in immune responses (figure 8.11 B, left), barrier function (figure 8.11 B, center) and *apical* pathogen load (figure 8.11 B, right). The amount of bacteria that infiltrated to the bloodstream, however, suffers a considerable increases (figure 8.11 B, right, red dotted line).
It is interesting to note that only the basal concentration of bacteria seems to be affected by a increase in the carrying capacity. This suggests that the immune responses efficiently eradicate the increased concentration of apically located bacteria resulting from a increased carrying capacity, but fail to control the invading pathogen. Likely, this behaviour can be attributed to the fact that, in our model, neutrophil transmigration form the basal to the apical side of the epithelial monolayer is *Sa* dependent. Hence, increased bacterial load on the apical side of the epithelium can be compensated by a increasing transmigration of neutrophils. In contrast, the concentration of basal neutrophils that can eradicate the infiltrated bacteria (*Sb*) is not directly affected by the levels of *Sb*, resulting in a high concentration of basal bacteria that cannot be compensated by the neutrophils.

These results could have important clinical consequences, since they suggest that a high rate of bacterial invasion that can eventually lead to sepsis can occur even if the epithelium remains intact, and the apical concentrations of bacteria (commonly measured in experimental settings, in the BALF) and the concentrations of immune cell infiltrates are low.

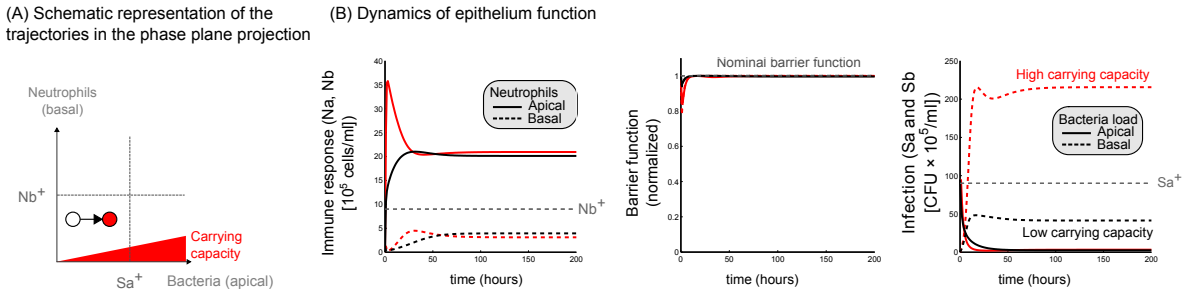

Figure 8.11: **Increase in the carrying capacity leads high invasion of bacteria, but no associated barrier damage** A increased carrying capacity μ_s, resulting from a first infectious event, does not affect the relative position of the global attractor of the system in the $Sa \times Nb$ phase plane projection *[A]*. It increases the amplitude of the *transient* induction of immune responses (*[B], left*) and leads to a *transient* reduction in barrier function (*[B], center*). Importantly, it significantly affects the steady state concentrations of infiltrated bacteria (*[B], left, red dotted line*).

These results were obtained by simulating the continuous system of equations 8.1 with the nominal parameters given in table 8.1, except for $k_{MN} = 18, \mu_s = 50$ (homeostasis, black trajectories) or $\mu_s = 250$ (sepsis, red trajectories). The initial conditions are given by $Sa(0) = Sa^+ + 5$, $Sb(0) = Na(0) = 0$, $Nb(0) = 60$, and $B(0) = 1$.

8.6.2 Decreased permeability barrier function leads to aseptic loss of homeostasis

A first infectious event can lead to epithelium-damaging inflammation, resulting in a decreased permeability barrier function of the epithelial monolayer to both immune cells and pathogens [69].

In our model, increased permeability of the epithelial monolayer can be represented by simultaneously increasing the rates of neutrophil transmigration (ϕ_{nt}) and of bacterial invasion (κ_{si}). As seen in figure 8.12, increased epithelial permeability can drive the system from a homeostatic state to an aseptic loss of homeostasis, characterized by a high degree of infiltration of immune cells to the apical side of the epithelial monolayer (figure 8.12 B, left) that results in persistent barrier damage by these neutrophils (figure 8.12 B, center). The bacterial load, however, is kept low by the increased immune responses, both in the basal and in the apical side of the epithelial monolayer (figure 8.12 B, right).

To our knowledge, this form of loss of epithelial homeostasis, driven by changes in the permeability barrier function that result from a host response to a first pathogen, has not been addressed previously. This is because none of the existing mathematical models of the host-pathogen interactions between *Streptococcus pneumoniae* and the upper airway epithelium considers the simultaneous movement of immune cells and pathogens across the epithelial monolayer that is responsible for the dynamic behaviour observed in figure 8.12.

Our results suggest that strengthening the epithelial barrier after a first infectious event, for example, by pharmacological increase in the concentration of calcium [289] or growth factors [290] on the basal side of the epithelial monolayer, can prevent a complete loss of barrier function that results from the increased amount transmigrating neutrophils and that leads to a high invasion of bacteria (*Sb*).

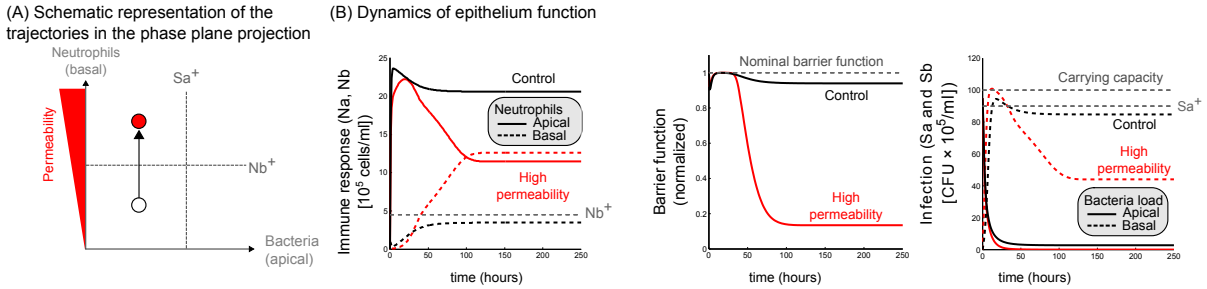

Figure 8.12: **Decreased permeability barrier function lead to an aseptic loss of homeostasis** Decreased permeability barrier function shifts the global attractor of the system from a homeostatic position on the $Sa \times Nb$ phase plane projection to a value such that $Nb > Nb^{+}$ *[A]*, resulting in a increased concentration of basal neutrophils (*[B], left*) that drive a persistent barrier damage (*[B], center*) but clear the invading pathogen (*[B], right*).

These results were obtained by simulating the continuous system of equations 8.1 with the nominal parameters given in table 8.1, except for $\mu_s = 100$ and the tuning parameters $\theta_{nt} = 14$ (control, black trajectories) or $\theta_{nt} = 140$ (decreased permeability barrier function, red trajectories), and $\kappa_{si} = 0.05$ (control, black trajectories) or $\kappa_{si} = 0.5$ (decreased permeability barrier function, red trajectories), and initial conditions $Sa(0) = Sa^{+} + 5$, $Sb(0) = Na(0) = 0$, $Nb(0) = 1$, and $B(0) = 1$.

8.6.3 Increased levels of resident neutrophils leads to aseptic loss of epithelial homeostasis

The host response the epithelium to a first infectious event results in a net *increase* in the total amount of neutrophils, resulting from the immune cell infiltration that was triggered by the first pathogen and persists even after the clearance of the infection [288, 69, 244].

In our model, increasing the amount of resident immune cells by increasing the basal rate of

neutrophil recruitment β increases the steady state concentration of basal neutophils, such that $Nb_{ss} > Nb^{+}$ (figure 8.13 A).

This increased neutrophil load (figure 8.13 B, left) leads to an aseptic loss of homeostasis, characterized by persistent barrier damage (figure 8.13 B, center) and clearance of the bacterial load (figure 8.13 B, right), both triggered by the high neutrophil load.

These results are consistent with experimental observations, in which a high load of resident immune cells is associated to acute injury to the epithelial tissue [30, 31, 244]. They are consistent with the ”aseptic death” proposed in other models of infection (eg. [102, 103]), although these models do not consider the epithelial damage that results from the persistent inflammation.

Besides co-infection, patients with a decreased amount of neutrophils (termed neutropenia) as a result from HIV infection or chemeotherapy also have a high risk of developing severe pneumonia [21]. This suggests that the effect of neutrophil numbers on the host response to a pathogen is *non-monotonic*: Both low and high concentrations of resident neutrophils, caused by neutropenia [21] or co-infection (figure 8.13), respectively, are associated to loss of epithelial homeostasis. This implies that the treatment for patients suffering from alterations in their neutrophil levels that result from co-infection must be carefully dosed, to avoid unwanted side-effects resulting from a excessive modulation of neutrophil concentrations.

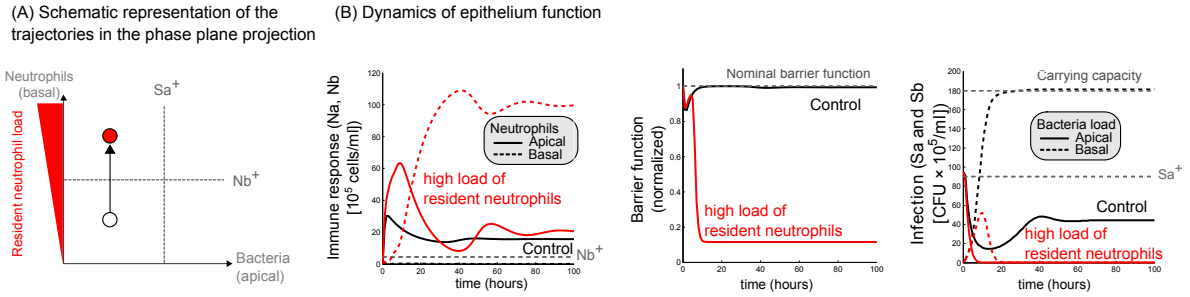

Figure 8.13: **Increased load of resident neutrophils results in loss of epidermal homeostasis** Increased levels of resident immune cells resulting from co-infection leads to an aseptic loss of homeostasis, characterized by a high immune cell infiltration that persistently decreases barrier function (*[B]*, center) and decreases the pathogen load (*[B]*, right).

These results were obtained by simulating the continuous system of equations 8.1 with the nominal parameters given in table 8.1, except for the the basal rates of neutrophil infiltration, corresponding to $\beta = 1$ (control, black) and $\beta = 10$ (high load of resident neutrophils, red) and the initial conditions $Sa(0) = Sa^{+} + 5$, $Sb(0) = Na(0) = 0$, $Nb(0) = 1$, and $B(0) = 1$.

8.6.4 Desensitization of the TLR receptor leads to sepsis

It has been reported that co-infection with influenza can lead to the de-sensitization of TLR-mediated immune responses [78].

To explore the effects of virus-mediated TLR desensitization, we considered a extreme case of TLR desensitization, corresponding to a TLR mutant, by setting $F(Sa) = 0 \; \forall \; Sa$ in our model (equations 8.1).

As seen in figure 8.14, simulations of the TLR mutant result in sepsis without associated barrier damage. Complete desensitization of the TLR shifts the threshold of apical bacterial concentrations required to induce significant TLR activity $Sa^+ \rightarrow \infty$ (figure 8.14 A). As a result, no immune responses can be triggered (figure 8.14 B, left), and the barrier remains intact (figure 8.14 B, center), but the levels of pathogen load are significantly increased (figure 8.14 B, right). These simulation results agree with the observation that patients with polymorphisms in TLR receptor tend to develop more severe forms of infections, often resulting in sepsis [46].

Our results are also consistent with the modelling results obtained in [93]. In their mathematical model, the authors also considered the reduction in the TLR-mediated neutrophil recruitment rate as a consequence of co-infection, and identified this mechanisms as key determinant of the lethal synergism between two pathogens.

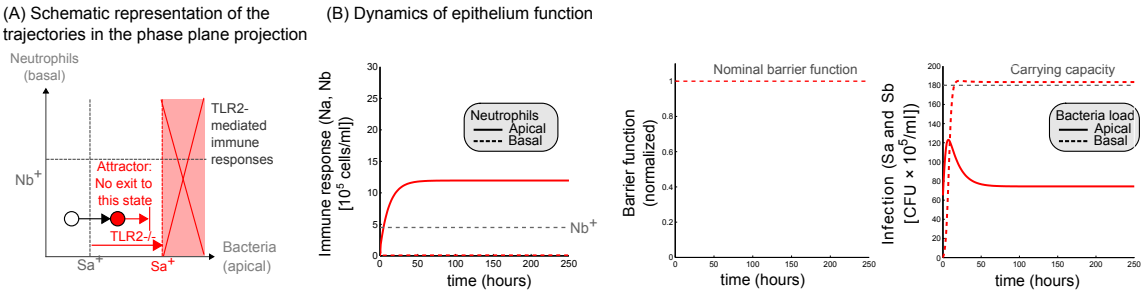

Figure 8.14: **Desensitization of the TLR receptor leads to sepsis** Complete desensitization of the TLR, corresponding to a TLR mutant ($TLR2^{-/-}$), shifts the threshold of apical bacterial concentrations required to induce significant TLR activity $Sa^+ \rightarrow \infty$ *[A]*. Under these conditions ($TLR2^{-/-}$), no immune responses can be triggered upon TLR stimulation (*[B]*, left). The barrier remains intact, since also $Sa-$ dependent barrier damage is TLR mediated (*[B]*, center), but the levels of pathogen load remain elevated (*[B]*, right).

These results were obtained by simulating the continuous system of equations 8.1 with the nominal parameters given in table 8.1, except for $\beta = 1$. The initial conditions are $Sa(0) = Sa^+ + 5$, $Sb(0) = Na(0) = 0$, $Nb(0) = 1$, and $B(0) = 1$. The TLR mutant is simulated by setting $F(Sa) = 0 \; \forall \; Sa(t)$.

8.7 Conclusions

In this chapter, we proposed a data-driven mathematical model of the host-pathogen interactions between *Streptococcus pneumoniae* and the upper airway epithelium. All the regulatory interactions and parameter values were carefully chosen, based on quantitative and dynamic experimental data (detailed in section 8.3 and appendix B, respectively).

Our model builds on previous mathematical models of the host response to *Streptococcus pneumoniae* [94, 92, 93] and considers, for the first time, the dual role of the epithelial monolayer in mediating the host response to a pathogenic challenge. On one hand, a intact epithelium prevents the invasion of bacteria to the bloodstream, but on the other, it hinders the neutrophil transmigration that is required for bacterial clearance. Further, barrier function is impaired by neutrophil transmigration. We believe that it is important to explicitly consider the interplay between epithelial barrier function and immune responses, since a major part of the pathology of infection is attributed to the damage to the epithelium that is inflicted by excessive immune responses [31, 30].

By considering this dual effects of both barrier function and immune responses, our model analysis strongly suggests that balance between the two protective properties of the epithelial tissue, namely the immune responses and the barrier function, is necessary to maintain epithelial homeostasis. Increased permeability of the epithelial monolayer (figure 8.12) and increased (figure 8.13) or decreased (figure 8.14) immune responses can result in a loss of epithelial homeostasis.

We used our model to explore the different mechanisms that are responsible for the onset of infection that results from the synergy between *Streptococcus pneumoniae* and another pathogen [69]. This co-infection is responsible for the vast majority of the severe cases of infection by *Streptococcus pneumoniae* [21, 69], but the exact mechanisms of the lethal synergism remain elusive.

With our model, we were able to map different effects of viral infection to qualitatively different ways of loss of homeostasis. For example, our findings suggest that decreased permeability barrier function, resulting from the tissue-damaging immune response to a previous infectious, leads to an aseptic loss of homeostasis, characterized by a high load of immune cell infiltration, barrier damage, but clearance of the pathogen (figure 8.12). In contrast, our model suggests that desensitization of TLR receptors resulting from a previous infectious event leads to sepsis, but without the associated barrier damage (figure 8.14).

Together, these findings have important clinical consequences in terms of devising optimal patient-specific treatment strategies that minimize the use of antibiotics [23], since they suggest that only a fraction of patients might benefit from antibiotics treatment, while others might require a pharmacological enhancement of the airway epithelium function. They correspond to

the patients in which the first infectious event increased the bacterial carrying capacity (figure 8.11) or desensitized the TLR receptor (figure 8.14), and those in which the first infectious event lead to a decreased permeability barrier function (figure 8.12) or a increased load of resident neutrophils (figure 8.13), respectively.
Our proposed modelling framework, that considers the interplay between immune responses and epithelial barrier function, uncovered the mechanisms that drive infection by other pathogens that attack epithelial tissues. Considering the dual role of the epithelial barrier in mediating infection could be particularly relevant for understanding the strongly convoluted host-pathogen interactions between virus and epithelial tissues. Epithelial tissues prevent severe infection by hindering the passage of virus into the bloodstream [5], but also act as a substrate for viral replication [106], and immune cells must attack the (infected) epithelial (and immune) cells to counteract the viral load [244]. The mathematical modelling approach proposed in this chapter considers the dual role of the barrier and the immune responses in mediating the pathogen load, and could therefore help to elucidate the mechanisms that result in viral infection.

8.8 Future work

In collaboration with Mr George Buckle (MRes is Molecular and Cellular Biosciences, Imperial College London) and Dr Thomas B Clarke (Faculty of Medicine, Imperial College London), we will continue the analysis of the host-pathogen interactions between *Streptococcus pneumoniae* and the upper airway epithelium discussed in this chapter.
First, we will conduct a more rigorous exploration of the qualitative changes of the model behaviours that are triggered by the different effects of co-infection on the host response to *Streptococcus pneumoniae*. We will do this by bifurcation analysis, which will allow us to identify the critical threshold values of the parameters that are affected by the first infectious event at which a qualitative change in the dynamic behaviour occurs. By extensive exploration of the parameter space, we will assess how these bifurcation diagrams are affected by different choices in the parameter values.
We will also compare our model predictions to other *in vivo* datasets, both from the literature (for example, [273]) and done by our experimental collaborators.
We will also assess the effects of assuming that the switch-like barrier damage elicited by neutrophils and bacteria is described by a *bistable* dose-response curve (described in section 3.2.1), rather than by the memory-less Hill function $F(X(t))$ in equations 8.1. A bistable dose-response relation between LPS (a bacterial PAMP) and active TLR4 pathway has been previously described [194]. It is relevant to consider this bistability, because thus far, our model cannot account for the long term clearance of bacteria induced by TLR signalling (see section 8.5.2). However, assuming that TLR activation is bistable could account for a long term clear-

ance of the infection by the TLR-dependent host responses, similarly to the PAR2 mediated immune responses explored in chapter 4.
Also, we could expand our current mathematical model to account for the long term consequences of a low level infection, by adding a ”persistence” motif (discussed in section 3.4) that stores the history of the infectious events and describes the probability of infiltration of a particularly pathogenic bacterial strain into the bloodstream.

Chapter 9

Concluding remarks

In this thesis, we developed a mathematical modelling framework to describe and analyse the reaction networks controlling epithelial function. Using this framework, we proposed mathematical models of the reaction networks that underlie the homeostasis of the epidermis and the airway epithelium, respectively. We used the resulting mathematical models to analyse the pathogenic mechanisms that are responsible for the development of AD and of infection by *Streptococcus pneumoniae*.
By focusing on understanding the mechanisms that trigger the loss of epithelial homeostasis, our theoretical analysis sheds light on the early events in the pathogenesis of AD and infection, respectively. Also, our model analysis uncovered several different potential mechanisms that can lead to the loss of epithelial homeostasis, corresponding to patient-specific triggers of the disease. Further, we used the mathematical model of AD to explore different treatment strategies that can potentially cure or at least prevent the onset of severe forms of AD.
Together, the findings contribute to the understanding of the mechanisms that cause diseases associated to the loss of epithelial homeostasis. This knowledge is fundamental to devise new treatment strategies that can prevent and cure these socially relevant diseases.

The modelling framework proposed in this thesis was originally developed to formally represent the regulatory networks controlling *epithelial* homeostasis (described in chapter 2). However, in chapter 8 we successfully applied this framework to for the representation and analysis of a different epithelial system -the host-pathogen interactions between *Streptococcus pneumoniae* and the upper airway epithelium that underlie pneumococcal infection, proving that the applicability of our framework is not restricted to a particular epithelial tissue.
The common feature that characterizes the regulatory networks that underlie the functioning of both the epidermis and the airway epithelium is the interplay between the permeability barrier function and the immune responses. Aberrant interactions between these two protective properties of the epithelium underlie many other diseases associated to the loss of epithelial

function, including lung infection by the fungus *Aspergilus fumigatus* [4], viral infection of the cervix [5], Crohn's disease [1], asthma [10, 11], allergic rhinitis [12], and different types of cancer [14, 15]. Thus, we are convinced that mathematical modelling framework proposed in this thesis can be used to analyse many other diseases that result from the loss of epithelial homeostasis.

Two key features of our proposed approach are the *multi-scale* and *modular* representation of the regulatory networks that control epithelial homeostasis.
With the multi-scale approach, we were able to represent the dynamic interplay between *biochemical* and *cellular* level processes that underlie the gradual loss of epithelial homeostasis. The interplay between a cell and its micro-environment is responsible for slow phenotype changes that characterize developmental and pathogenic processes. While the micro-environment is sensed by the biochemical signal processing machinery in the individual cells, the collective responses of the individual cells to the micro-environment drive tissue-level changes that, in turn, affect the micro-environment. Thus, our framework, based on the interplay between slowly changing micro-environments and quickly responding biochemical networks, could be adapted to model many other developmental and pathogenic processes that underlie phenotype transitions.
In terms of the modular representation, we were able to identify three qualitative *input-output* behaviours that control epithelial function: (1) A switch-like induction of cytokine release, (2) Self-recovery dynamics of epithelial permeability barrier components, and (3) Persistent dynamics of immune cells that are induced by a biochemical mediator (cytokine).
Having identified mechanisms that can cause these individual qualitative behaviours (corresponding to particular feedback control structures), we could abstract the description of the underlying network motif into simpler, phenomenological representations.
This qualitative approach allows us to suggest a core control structure that is responsible for the regulation of epithelial homeostasis [52]. It consists of the multi-scale regulatory network structure that is formed by the interplay between cytokine release, epithelial permeability and immune cells, and corresponds to a mesoscopic "template model" [291] to which mechanistic and quantitative detail can be added *a posteriori*.
The network motifs described in this thesis (switch-like dose response, self recovery and homeostasis) are not specific for the regulatory modules controlling epithelial homeostasis. For example, switch-like dose response behaviour has been observed in signalling networks involving caspases [292, 247] and mitogen-activated kinases [293, 205], and is thought to underlie embryonic differentiation programs [294]. Self-recovery dynamical behaviour characterizes the pheromone response pathway in *S. cerevisiae* [215, 216], the BMP4 signalling pathway in *X laevis* [217], and the hyperosmotic stress response in yeast [218, 219]. A persistent behaviour

plays a key role in determining the specificity in the gene expression controlled by the master regulator NFκB [232]. Thus, we believe that many other physiological processes can be represented by a combination of these regulatory modules, using the proposed multi-scale modelling framework.

There exist a overwhelming amount of experimental and clinical data describing biological processes that are believed to play important roles in pathological and developmental processes. However, most of these data characterize individual components of the reaction networks that underlie the healthy and pathological physiology. In many cases, however, a healthy or a disease phenotype results from the interplay between several biochemical, cellular and tissue level processes.
To uncover how normal developmental and aberrant pathological processes emerge from interactions between individual regulatory components, it is necessary to analyse the underlying reaction networks from a systems-level perspective.
This requires theoretical frameworks to integrate, organize and analyse the scattered clinical and experimental data.
The mathematical modelling framework proposed in this thesis provides such a theoretical framework. With it, we could uncover the mechanisms that underlie epithelial homeostasis. Due to its generality, it can be used to analyse many other relevant developmental processes underlying healthy and pathologic physiology.

Appendix A

Mathematical representation of reaction networks

This brief appendix gives an overview of the methodology by which we construct a mathematical model (based on systems of ODE) to represent the reaction networks of biochemical and cellular interactions analysed in this thesis.

To construct a mathematical model that represents the reaction network, each of the regulatory interactions must be translated into a mathematical expression -particularly, a rate. Collectively, these rates form a system of differential equations that describe the inter-dependent dynamics of the different components of the reaction network.

Here, we use ordinary differential equations (ODEs) to describe the dynamics of the system in a *deterministic* and *continuous* manner. Translating a reaction network into a system of ODE is a standard methodology in systems biology that has been discussed widely, for example in [295, 296, 297, 298]. Below, we give a brief description of this methodology. For details, please refer to the above mentioned publications. Particularly, we use the *law of mass action* to describe (most of) the rates of the system. We assume that the rate of change in the concentration of species X is proportional to the concentration of precursors X_{pre}, the effectors E and the kinetic rate constants k_i, thus for instance, a production reaction of X is represented by the term $\frac{dX}{dt} = X_{pre}k_{prod}E_{prod}$; degradation, by $\frac{dX}{dt} = -Xk_{deg}E_{deg}$, reversible dimerization of A and B, by $\frac{dAB}{dt} = [A][B]k_{dim}E_{dim} - [AB]k_{dis}E_{dis}$. Effectors are distinguished from precursors in that their concentrations are not affected by the reaction they catalyse.

Negative regulation is often represented in a phenomenological way, by multiplying the rate on which the repressor is acting by a function that decreases monotonically with the concentration of the repressor. It would also be possible to derive this sort of functions from basic biochemistry, by explicitly representing, with law of mass action, the mechanism by which the repressor exerts its action (depending on how the repressor acts: for instance, trapping the effector molecule). However, for convenience (less parameters and equations) this level of

mechanistic detail is omitted.
One of the main advantages of mathematical description of a reaction network is that *all* the reactions that affect X can be represented and studied simultaneously (this is why it is called a *systems biology approach*). Thus, if for example, X is being produced, degraded and also it forms a heterodimer with another molecule Y (reaction network depicted in figure A.1), then its full dynamics are described by simply adding up the individual reactions explained above. In this particular example, this procedure would retrieve the expression that describes X:

$$\frac{dX}{dt} = X_{pre}k_{prod}E_{prod} - X(t)k_{deg}E_{deg} - X(t)Y(t)k_{dim}E_{dim} + XY(t)k_{dis}E_{dis}. \tag{A.1}$$

The dynamics of X given by equation A.1 depend on *constant parameters*, such as k_{deg}, k_{dim} and k_{dis}, but also on other, time varying variables, such as $Y(t)$ and $XY(t)$. Collectively, the set of coupled equations that describe all the inter-dependent variables of the system form the system of differential equations describing the reaction network.
Once the reaction network has been represented by a system of ODEs, the resulting mathematical model can be analysed by numerical or analytical methods. For example, to analyse the dynamic evolution of the system, the system of ODE is integrated over the range of time of interest. In this thesis, numerical integration of ODEs is done using `Matlab R2012a`. To understand the dose response behaviour, a steady state analysis is performed. For this, we use `Maple 16` (analytical calculation of steady states and stability of non-linear systems of ODEs), `Matlab R2012a` (numerical calculation of steady states), `Oscill8` (found under `http://oscill8.sourceforge.net/`, used for bifurcation analysis).

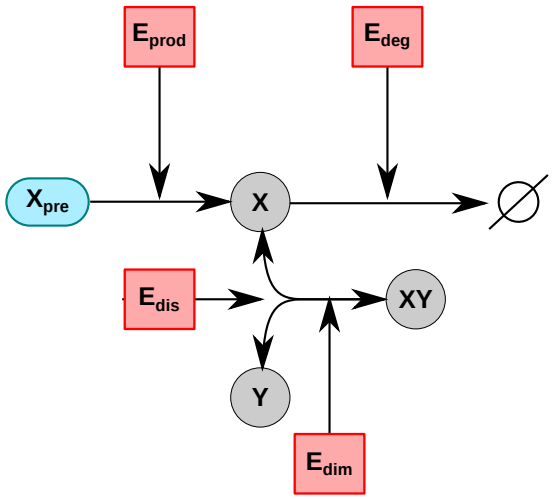

Figure A.1: **Example reaction network.** The reaction network is given by the interactions between the time-varying biochemical species X, Y and the heterodimer XY (shown in grey circles). The reactions of production of X from a (constant, in a blue oval) precursor X_{pre}, degradation of X and reversible formation of the heterodimer XY are catalysed by E_{prod}, E_{deg}, and E_{dis} and E_{dim} (red squares), respectively.

Appendix B

Parameter estimation of the mathematical model describing the host-pathogen interactions between airway epithelium and *Streptococcus pneumoniae*

This appendix describes the procedure used for deriving the parameter values of the mathematical model of the host-pathogen interactions between airway epithelium and Streptococcus pneumoniae given in equations 8.1 (described in chapter 8), from experimental in vitro data that we gathered from the literature. The resulting parameter set is summarized in table 8.1.
The parameters of the model 8.1 can be divided into following categories:

- **System-independent parameters** quantify the rates that are specific to a particular species. They correspond to natural (intrinsic) birth and death rates of barrier, pathogens and neutrophils that are measured by transwell experiments (barrier) and by tracking the population sizes of bacteria and neutrophils (figure B.1 I). They can be modelled by a one-dimensional linear ODE that be solved analytically. Hence, it is possible to derive an algebraic expression for these parameters as a function of the experimental values.

- **System-dependent parameters (*in vitro*)** characterize the interplay between subsets of the components of the system. They correspond to *modulations* of productions and degradations of one species by another, for example, bacterial killing by neutrophils. Experimentally, they are assessed by quantifying the barrier function and population sizes in co-cultures between neutrophils, bacteria and epithelial cells in a monolayer (figure B.1 II). We estimate these parameters by optimization, which involves the comparison of simulations from the corresponding system of equations 8.1 to experimental data.

- ***In vivo* parameters** quantify the rate of neutrophil recruitment from the blood stream, and are indirectly measured in *in vivo* experimental settings by quantification of neutrophil concentrations upon a bacterial challenge (figure B.1 III). These parameters are roughly estimated by comparing simulations of the full system of equations 8.1 to *in vivo* data, using the previously estimated *in vitro* parameters. Congruence between the model simulations using the estimated parameters from *in vitro* data and the *in vivo* data, shown in figure 8.4 is considered as a validation to our parameter estimation protocol.

Individual parameter calculations are detailed in the following subsections. All the parameter optimizations were done with `Matlab R2012a`, using the built in function `fminsearch`, using as a cost function the squared error between the simulations (given a parameter set) and the experimental data.

Barrier production rate (κ_{bp})

The barrier production rate κ_{bp} is assessed experimentally by following the dynamics of the TEER (given in units of electrical resistance per tissue area, i.e. in $\frac{\Omega}{cm^2}$) of an epithelial monolayer (represented in figure B.1 Ii) upon a perturbation [28, 283] and for intestinal epithelium [87].
Neither neutrophils nor bacteria are present in these experimental settings. This corresponds to assuming that $Na(t) = Nb(t) = Sa(t) = Sb(t) = 0$, which simplifies model 8.1 to $\dot{B}(t) = \kappa_{bp}(1 - B(t))$ with $B(0) = B_0$, which has the analytic solution:

$$B(t) = 1 + e^{-\kappa_{bp} t}\,(B_0 - 1)\,. \tag{B.1}$$

Given a experimental measurement at time t_{exp} and a initial condition B_0, κ_{bp} can be expressed analytically as:

$$\kappa_{bp} = \frac{-\ln\left(\frac{-1+B_{exp}(t_{exp})}{B_0-1}\right)}{t_{exp}}. \tag{B.2}$$

This expression (B.2) accepts only one data point, and retrieves one estimate for κ_{bp} that is used as a initial guess a optimization of equation B.1 using the experimental data from [87] (figure 5a), which measures the recovery of an epithelial monolayer (T84, intestinal epithelium) upon perturbation with cytokines. The data-points correspond to B_{exp} =[400, 750, 1100, 1400, 1500, 1400, 1200] (in $\frac{\Omega}{cm^2}$) at measured at times [70/60, 2, 4, 6, 8, 1, 0, 20] (in hours), which we normalized to its maximum value $\tilde{B}_{exp} = 1500$ to obtain a dimensionless quantity. This retrieved a value of $\kappa_{bp} = 0.45\frac{1}{h}$.
Using the same method but other experimental data, derived from airway epithelium, resulted in values for κ_{bp} that were one order of magnitude below ($\kappa_{bp} = 0.07$ [28]) or above ($\kappa_{bp} = 1.05$

[283]). The results of the optimization for the three datasets are shown in figure B.2. From these values, we chose the intermediate value $\kappa_{bp} = 0.45$, estimated from the data in [87], because it corresponds roughly to the average of the three values of κ_{bp} obtained by using the three different datasets.

Bacterial proliferation rate (κ_s) and carrying capacity (μ_s)

Bacterial proliferation rate is assessed experimentally by following bacterial cell cultures over time (figure B.1 Iii). In these experiments, no neutrophils nor epithelial cells are present. This condition can be reflected in the model 8.1 by assuming that $Na(t) = Nb(t) = B(t) = \kappa_{bp} = 0$, resulting in the system of equations B.3:

$$\dot{Sa}(t) = Sa(t)\kappa_s \left(1 - \frac{Sa(t)}{\mu_S}\right) - Sa(t)\kappa_{si}, \tag{B.3a}$$

$$\dot{Sb}(t) = Sb(t)\kappa_s \left(1 - \frac{Sb(t)}{\mu_S}\right) + Sa(t)\kappa_{si}. \tag{B.3b}$$

$$\tag{B.3c}$$

Defining $S(t) = Sa(t) + Sb(t)$, and given that $\dot{S}(t) = (Sa(t) \dot{+} Sb(t)) = \dot{Sa}(t) + \dot{Sb}(t)$, then:

$$\dot{S}(t) = Sa(t)\kappa_s \left(1 - \frac{Sa(t)}{\mu_S}\right) + Sb(t)\kappa_s \left(1 - \frac{Sb(t)}{\mu_S}\right). \tag{B.4}$$

Assuming that $Sa(0) = Sb(0)$, since there is no barrier separating Sa and Sb, equation B.4 can be simplified to:

$$\dot{S}(t) = S(t)\kappa_s \left(1 - \frac{S(t)}{\mu_S}\right). \tag{B.5}$$

Equation B.5 can be further simplified for bacterial concentrations such that $S(t) << \mu_s$. In this case, equation B.5 can be represented by the exponential growth model $\dot{S}(t) = S(t)\kappa_s$ that can be solved analytically ($S(t) = S(0)\exp^{(t\kappa_s)}$). From this analytic expression, κ_s can be directly calculated:

$$\kappa_s \sim \frac{log(\frac{S(t_{exp})}{S(0)})}{t_{exp}}. \tag{B.6}$$

We used expression B.6 and the experimental data from [279], corresponding to growth curves of *Streptococcus pneumoniae* in the low nutrient medium MLM that resembles the *in vivo* conditions of the epithelium. The two data points used to calculate κ_s from equation B.6 were $t_{exp} = 2.5h$, $S(0) = 0.1$ given in units of Optical Density of the bacterial colony at 450

nm (OD_{450nm}), and $S(t_{exp}) = 0.32\ OD_{450nm}$. Note that for the calculation of κ_s from equation B.6 requires the dimensionless ratio between $S(t_{exp})$ and $S(0)$. The resulting value $\kappa_s = .45\frac{1}{h}$ is given in table 8.1.
Following the same procedure but different datasets [278, 277] lead to slightly higher κ_s values ($\kappa_s = 0.92$ [277] and $\kappa_s = 1.1$ [278]. The resulting fit is shown in figure B.3. We chose the value derived from the data in [279], because the growth experiments were done in conditions that resemble the *in vivo* environment of the epithelium.

A maximal value for the carrying capacity μ_s was read out directly from the data in [277] (figures 2A and 4A, representing growth curves of *Streptococcus pneumoniae* in a glucose and lactose medium), by assuming that μ_s corresponds to the maximal concentration of bacteria, measured as $Sa_{max} = 0.55\ OD600$. To convert the units of $OD600$ to $[\frac{CFU\times 10^5}{ml}]$, we use the relation from [299]: $\frac{2\times 10^8 CFU}{50\mu l} \sim 0.63OD$, which results in a value of $\mu_s = 3.5\times 10^4[\frac{CFU\times 10^5}{ml}]$. Growth curves measured by our experimental collaborator Dr Tom Clarke (Imperial College London) retrieved a estimate for $\mu_s = .5\times 10^4[\frac{CFU\times 10^5}{ml}]$ (personal communication), which is one order of magnitude lower than the value for μ_s obtained from [277]. Given that both values for μ_s were estimated from ideal *in vitro* conditions, they both correspond to an over-estimation of the *in vivo* conditions of our model. Therefore, we chose the lower value of $\mu_s = .5\times 10^4[\frac{CFU\times 10^5}{ml}]$ (Dr Tom Clarke, personal communication) given in table 8.1 as a reference value.

Neutrophil death rate (κ_{nd})

The half life of neutrophils is commonly estimated by labelling neutrophils (for example, with a radioactive tracer) and following their fluorecence over time [282]. Assuming that neutrophil half lives are not affected by barrier and bacteria, their dynamics in the epithelium can be approximated by $\dot{N}(t) = -\kappa_{nd}N(t)$, where $N(t) = N_a(t) + N_b(t)$ corresponds to the total population of neutrophils in the epithelium. The ODE $\dot{N}(t)$ has a analytic solution $N(t)$, which can be solved analytically to express κ_{nd} as a function of a experimentally determined initial neutrophil concentration $N_{exp}(0)$, and the elapsed time t_{exp} and the neutrophil concentration at t_{exp}, as follows:

$$\kappa_{nd} = -\ln\left(\frac{N_{exp}(t_{exp})}{N_{exp}(0)}\right){t_{exp}}^{-1}. \tag{B.7}$$

Most of the datasets describing the effect of neutrophils on barrier or bacteria are derived from *in vitro* experiments that involve *human* neutrophils (for example, [72, 88, 89, 86, 275, 71, 300]). Thus, we estimated the neutrophil death rate using the data describing *human* neutrophil half lives in [282]. Substituting the average of the human neutrophil half lives (corresponding to the time t_{exp} at which $N(t_{exp}) = 0.5N(0)$) given in table 2 (control) of [282] ($t_{exp} = 8.3375h$)

in equation B.7, we obtain the nominal neutrophil death rate of $\kappa_{nd} = 0.08$ given in table 8.1. The resulting $N(t)$ simulations and the data-point from [282] are shown in figure B.4.

Switch-like activation of TLR pathway by bacteria (k_m and n_H)

The switch-like dose-response relation between the steady-state TLR pathway activity $F(Sa(t))$ and the concentration of apical bacteria $Sa(t)$ can be experimentally assessed in two ways. Directly, by measuring the output of TLR pathway activity (for example, in levels of NFκB activation) in response to a bacteria-derived ligand (like peptidoglycan) [285], or indirectly, by measuring the dose-dependent *effects* of TLR pathway activity (eg decreased barrier function [85]).

In the model, the activation of TLR pathway by bacteria is described by the Hill function $F(S_a(t)) = \frac{S_a(t)^{\mathrm{n_H}}}{S_a(t)^{\mathrm{n_H}} + k_{\mathrm{m}}^{\mathrm{n_H}}}$, where k_m is the concentration of $S_a(t)$ at half maximal TLR activation, and n_H is the Hill-coefficient that quantifies the steepness of the switch. Assuming very high values for n_H ($n_H \to \infty$) results in a perfect switch, where only values for $S_a(t)$ that are above threshold result in significant TLR activity (see section 3.2.6).

In [285] (figure 3A), direct relation between concentrations of bacterial ligand (corresponding to $[0, .125, .25, .50]$ $\frac{\mu g}{ml}$ of peptidoglican) and TLR activity (given by $[1, 1.25, 1.6, 2.3]$-fold expression of $NF\kappa B$ activity, measured in a reporter gene). Only the highest peptidoglycan concentrations ($.50\frac{\mu g}{ml}$) trigger a statistically significant increase in TLR activity. Slightly lower concentrations of peptidoglycan ($.25\frac{\mu g}{ml}$) trigger a small but not significant increase in TLR activity. We assume that, roughly, k_m corresponds to this value. To convert this concentration to our units $CFU \times 10^5/ml$, we follow [301], $1\mu g$ of peptidoglycan corresponds to $5 \times 10^7 CFU$ of *Streptococcus pneumoniae*. This results in the value of $k_m = 120[\frac{CFU \times 10^5}{ml}]$ given in table 8.1.

This estimation is consistent with the dataset from [85] (figure 1A), that relates concentrations of bacteria to barrier function. In this dataset, only concentrations of bacteria above $150[\frac{CFU \times 10^5}{ml}]$ result in barrier damage. Similarly, the data from [38] (figure 5A) state that a concentration of bacteria of $500[\frac{CFU \times 10^5}{ml}]$ (well above the k_m threshold) induces barrier damage. These qualitative results are shown in figure B.5.

A estimate of the Hill coefficient n_H was obtained by fitting the Hill equation $F(S_a(t))$ to the above mentioned data from [285]. The optimization resulted in a value for $n_H = 5.75$ given in table 8.1.

The resulting parametrized Hill equation and the data points from [285] are shown in figure B.6.

Neutrophil bacteria interactions: Neutrophil induced death of bacteria (ϕ_{NS})

The neutrophil-induced death of bacteria is assessed experimentally by a killing assay, in which the size of bacteria populations in a co-culture with neutrophils is assessed over time (figure B.1 IIii) [88, 89].

The measurements correspond to the fraction of bacteria present in the co-culture after t_{exp} units of time, in respect to the amount of bacteria present at t_{exp} when no neutrophils are applied [88, 89].

These experimental conditions, which involve no epithelial cells nor infiltration from neutrophils from the blood, can be mimicked by the mathematical model by setting $B(t) = \theta_{\mathrm{Sanr}}\mathrm{Nv} = \beta = \kappa_{bp} = 0$ in equations 8.1. Further, because there is no barrier, there is no distinction between apical and basal populations of bacteria and neutrophils. We reflect this condition in the model by defining $S(t) = Sa(t) + Sb(t)$ and $N(t) = Na(t) + Nb(t)$, and assuming that $Sa(0) = Sb(0)$ and $Na(0) = Nb(0)$. These assumption leads to the system of equations B.8:

$$\frac{dS(t)}{dt} = S(t)\kappa_{\mathrm{s}}\left(1 - \frac{S(t)}{\mu_{\mathrm{S}}}\right) - \phi_{NS}N(t)S(t), \tag{B.8a}$$

$$\frac{dN(t)}{dt} = -\kappa_{Nd}N(t). \tag{B.8b}$$

Equation B.8b is a uncoupled, first order linear ODE, hence, the system of equations B.8 can be simplified to equation B.9:

$$\frac{dS(t)}{dt} = S(t)\kappa_{\mathrm{s}}\left(1 - \frac{S(t)}{\mu_{\mathrm{S}}}\right) - \phi_{NS}N(0)e^{-\kappa_{Nd}t}S(t). \tag{B.9}$$

To compare the model simulations with the experimental conditions in [88] and [89], we define $S_0(t)$ as the control bacterial population (grown in the absence of neutrophils), and $S_E(t)$ as the population of bacteria that is grown in a co-culture with neutrophils (equations B.10). Then, the measured fraction of bacteria that survived neutrophil exposure corresponds to $S_M = \frac{S_E}{S_0}$, where:

$$\frac{dS_0(t)}{dt} = S_0(t)\kappa_{\mathrm{s}}\left(1 - \frac{S_0(t)}{\mu_{\mathrm{S}}}\right), \tag{B.10a}$$

$$\frac{dS_E(t)}{dt} = S_E(t)\kappa_{\mathrm{s}}\left(1 - \frac{S_E(t)}{\mu_{\mathrm{S}}}\right) - \underbrace{N(0)e^{-\kappa_{Nd}t}}_{\text{Analytic solution } N(t)}\phi_{NS}S_E(t). \tag{B.10b}$$

Further, assuming that $S(t) << \mu_S$, i.e. the bacteria population is in the linear growth phase,

leads to the expression for $\dot{S_M}$ given in equation B.11:

$$\frac{dS_M(t)}{dt} = \frac{d}{dt}\frac{S_E(t)}{S_0(t)} = \frac{S_0(t)\dot{S}_E(t) - S_E(t)\dot{S}_0(t)}{S_0(t)^2} \tag{B.11a}$$

$$= \frac{1}{S_0(t)^2}\left[S_0(t)\underbrace{S_E(t)\left(\kappa_{\mathrm{Sd}} - N(0)e^{-\kappa_{Nd}t}\phi_{NS}\right)}_{\dot{S}_E \text{ as in eq.B.10b}} - S_E(t)\underbrace{\kappa_{\mathrm{Sd}}S_0(t)}_{\dot{S}_0 \text{ as in eq.B.10a}}\right] \tag{B.11b}$$

$$= -S_M(t)N(0)e^{-\kappa_{Nd}t}\phi_{NS}. \tag{B.11c}$$

Equation B.11c is a first order ODE and hence has the analytic solution B.12:

$$S_M(t) = S_M(0)\,\mathrm{e}^{-\frac{N(0)\phi_{\mathrm{NS}}}{\kappa_{\mathrm{Nd}}}}\,\mathrm{e}^{\frac{N(0)\phi_{\mathrm{NS}}\,\mathrm{e}^{-\kappa_{\mathrm{Nd}}t}}{\kappa_{\mathrm{Nd}}}}. \tag{B.12}$$

From equation B.12, neutrophil- induced death of bacteria ϕ_{NS} can be expressed analytically as a function of the initial fraction of surviving bacteria $S_E(0)$, the initial concentration of applied neutrophils $N_{exp}(0)$, the time of exposure to neutrophils t_{exp} and the fraction of surviving bacteria after this exposure time ($S_E(t_{exp})$) (equation B.13):

$$\phi_{NS} = -\frac{\log\left(\frac{S_M(t_{exp})}{S_M(0)}\right)}{N_{exp}(0)\left(\frac{1}{\kappa_{Nd}} - \frac{e^{-\kappa_{Nd}t_{exp}}}{\kappa_{Nd}}\right)}. \tag{B.13}$$

Substituting the data from [89] (figure 1B, killing assay between human neutrophils and *Streptococcus pneumoniae*; $t_{exp} = 0.74h$, $S_E(0) = 1$, $S_E(t_{exp}) = .25$, and $N_{exp}(0) = 1000[cells] \times 10^{-5}T^{-1}$) in equation B.13 gives the nominal value $\phi_{NS} = .0019[T\frac{10^5 \times cells}{ml}]^{-1}$ given in table 8.1. Following the same technique but using a different dataset [88] retrieved an almost identical value ($\phi_{NS} = .00185$). The data-points of [89] and [88], as well as the simulations of equation B.12 with the calculated values of ϕ_{NS}, are shown in B.7.

Rates of barrier damage by bacteria (θ_{Sabd} and λ_{Sabp})

The damaging effects of *Streptococcus pneumoniae* on the epithelial tissue are experimentally assessed by dynamically measuring the permeability barrier function of a epithelial monolayer (corresponding to TEER) to which bacteria are added (see figure B.1IIi) [85, 68]. These experiments are carried out in the absence of neutrophils, and hence, can be described by setting $Na(t) = Nb(t) = \beta = \theta_{Sanr}Nv = 0$ our model (system of equations 8.1), resulting in the simpli-

fied system of equations describing the interactions between bacteria and barrier B.14:

$$\frac{dSa(t)}{dt} = \left[\kappa_S\left(1-\frac{Sa(t)}{\mu_S}\right) - \frac{\kappa_{si}}{\varepsilon_S B(t)+1}\right] Sa(t), \tag{B.14a}$$

$$\frac{dSb(t)}{dt} = Sb(t)\kappa_S\left(1-\frac{Sb(t)}{\mu_S}\right) + \frac{\kappa_{si}}{\varepsilon_S B(t)+1} Sa(t), \tag{B.14b}$$

$$\frac{dB(t)}{dt} = \frac{\kappa_{bp}(1-B(t))}{1+\lambda_{Sabp}F(Sa(t))} - \theta_{Sabd}F(Sa(t))B(t), \tag{B.14c}$$

$$F(Sa(t)) = \frac{Sa(t)^{\mathbf{n_H}}}{Sa(t)^{\mathbf{n_H}} + K_M^{\mathbf{n_H}}}. \tag{B.14d}$$

Recall that barrier damage by bacteria occurs via the switch-like activation of TLR signalling cascades. Thus, if the apical bacterial concentration is very high, then TLR signalling is activated to its maximum level for the whole duration of the experiment. If these conditions are met, then equations B.14 can be simplified by setting $Sa(t) = Sa^{high}$, where Sa^{high} is a arbitrary, constant and, importantly, above-threshold (k_m) concentration of apical bacteria. This simplification results in equation B.15.

$$\frac{dB(t)}{dt} = \frac{\kappa_{bp}(1-B(t))}{1+\lambda_{Sabp}\mathbf{Sa^{high}}} - \theta_{Sabd}\mathbf{Sa^{high}}B(t). \tag{B.15}$$

In [85] (figure 1a), the dynamics of the barrier function of a primary culture of human nasopharyngeal epithelium and of *Streptococcus pneumoniae* are tracked over time. We use the last three time-points for barrier function ([150, 60, 40] TEER (Ωcm^2), normalized to the mean barrier value of the untreated control), measured at times [0, 6, 13] h. The bacterial concentrations $Sa(t)$ are [100, 199, 316] (last two values well above threshold). We optimized B.15 to these experimental data to obtain the values for TLR-dependent barrier degradation $\theta_{Sabd} = 0.8T^{-1}$ and inhibition of barrier production $\lambda_{Sabp} = 0.18$ (dimensionless) shown in table 8.1.
The resulting dynamics for $B(t)$, described by B.15 and parametrized by the obtained values for θ_{Sabd} and λ_{Sabp} predict the independent dataset described in [68]. The results of the parameter optimization (with data from [85]) and validation (with data from [68]) are shown in figure B.8.

Invasion of bacteria through barrier (κ_{Si} and ε_S)

The rate of invasion of bacteria through barrier is estimated experimentally by tracking the populations of bacteria on the basal and on the apical side of an epithelial monolayer over time (figure B.1IIi) [270]. These experimental conditions do not involve neutrophils, and can hence be approximated by equation B.14. Further, if the apical bacterial concentrations are high, then

the Hill function describing the activation of TLR signalling by bacteria can be approximated by setting $F(Sa(t)) \sim F_{max}$.

We use data from [270] (fig. 5b), which measure the percentage of infiltration of *Streptococcus pneumoniae* through a monolayer of airway epithelial cells (A549). In their experiments, the initial concentration of apically located bacteria is $S_a(0) = 50000[\frac{CFU \times 10^5}{ml}]$, corresponding to a value well above threshold $k_m = 120[\frac{CFU \times 10^5}{ml}$ (table 8.1). Thus, the assumption $F(Sa(t)) \sim F_{max}$ is reasonable. The measured [270] percentage of bacterial invasion is [0, 3, 12, 20, 25, 30, 35, 38, 45, 50, 50] at time-points [0, 1, 2, 3, 4, 5, 6, 7, 8, 9, 10] (in h).

We used these data-points and equation B.14 (with $F(Sa(t)) \sim F_{max}$) to estimate the rate of invasion of bacteria though the monolayer (κ_{Si}), as well as the rate of inhibition of the infiltration by the barrier (ε_{S}) by optimization. The resulting values are $\kappa_{\mathrm{Si}} = 0.05T^{-1}$ and $\varepsilon_{\mathrm{S}} = 1$, shown in table 8.1. The fit of the resulting simulations for $\frac{Sb(t)}{Sa(t)+Sb(t)}$ (obtained by integrating equation B.14) to the data from [270] is shown in figure B.9 .

Neutrophil barrier interactions (1): Switch like damage of barrier by neutrophils (parameters k_{mn}, n_{hN} and ϕ_{nbBd})

Experimentally, the damaging effect of neutrophils on barrier function is commonly assessed by measuring the permeability barrier function of a inverted epithelial monolayer to which neutrophils are added on the basal side (figure B.1 IIiii). The apical chamber of the transwell device (below the inverted monolayer) also contains PAMPs that trigger the transmigration of the neutrophils [86, 87, 30].

In the mathematical model, these PAMPs can be represented by $\hat{S}(t)$ with $\frac{d\hat{S}(t)}{dt} = \frac{\kappa_{\mathrm{si}}}{\varepsilon_{\mathrm{S}} B(t) + 1}$, corresponding to the concentration of a biochemical molecule that is affected only by the infiltration through the barrier. In these *in vitro* experiments, no neutrophil infiltration occurs, corresponding to setting $\beta = \theta_{SanrNv} = 0$ in the system of equations 8.1. Together, setting $Sa(t) = \hat{S}(t)$ and $\beta = \theta_{SanrNv} = 0$ in the system of equations 8.1 results in the simplified system of equations B.16:

$$\frac{dNb(t)}{dt} = -\left[\frac{\theta_{\mathrm{nt}}}{\varepsilon_{\mathrm{N}} B(t) + 1} \hat{Sa(t)} + \kappa_{\mathrm{Nd}}\right] Nb(t), \tag{B.16a}$$

$$\frac{dB(t)}{dt} = \kappa_{\mathrm{bp}}(1 - B(t)) - \frac{\phi_{Nbbd} Nb(t)^{\mathbf{nH}}}{Nb(t)^{\mathbf{nH}} + K_{\mathrm{MN}}^{\mathbf{nH}}} B(t), \tag{B.16b}$$

$$\frac{d\hat{S}(t)}{dt} = \frac{\kappa_{\mathrm{si}}}{\varepsilon_{\mathrm{S}} B(t) + 1}. \tag{B.16c}$$

To obtain estimates for the parameters that quantify the switch-like dose-response relation

between the applied neutrophils and the resulting barrier damage (the concentration of neutrophils at half maximal barrier damage k_{mn}, the hill coefficient n_{hN} quantifying the sharpness of the switch, and the maximal strength of Nb induced barrier degradation ϕ_{nbBd}), we used experimental values from [86] (figure 4). These were obtained from transwell experiments, using a inverted monolayer (intestinal epithelium, T84), a fMLP gradient (corresponding to the PAMP) and varying concentrations of neutrophils. The experimental dose-response curve was obtained by measuring the concentrations of basal neutrophils and the barrier function $t_{exp} = 1h$ post- treatment. The resulting data are $Nb_{exp} = [0.01, 1, 10, 100]\ cells \times 10^5/ml$ and B_{exp} =[1, 0.95, 0.6, 0.1500].

We simulated these dose-response curves by numerically integrating equations B.16 for $t_{exp} = 1h$ and collecting the final values for B and Nb. This allowed us to estimate, by optimization, the parameter values $k_{mn} = 9\ [\frac{cells \times 10^5}{ml}]$, $n_{hN} = 5$ and $\phi_{nbBd} = 3.2$ shown in table 8.1, using the data from [86] and equations B.16.

Dose-response simulations of neutrophil concentrations vs barrier damage, using the resulting parametrized model (equations B.16), can reproduce two independent data-sets reported in [275] (damage of airway epithelium by human neutrophils) and in [71, 87] (damage of intestinal epithelium by human neutrophils). Results from the parameter optimization and validation are shown in figure B.10.

The resulting, parametrized dose-response relation between basal neutrophils and the rate of barrier damage, given by the scaled Hill function $\phi_{nbBd}F(Nb)$, is shown in figure B.11.

Neutrophil barrier interactions (2): Infiltration of neutrophils through barrier (θ_{nt} and ε_n)

Empirically, the rate of neutrophil transmigration through the barrier is assessed in a similar experimental setting as described above, by following the dynamics of apical neutrophils $Na(t)$ that have migrated from the basal side of a inverted epithelial monolayer in response to a gradient of PAMPs [71, 300] .

Mathematically, these experimental conditions can be represented as before (system of equations B.16), and adding a explicit description of $Na(t)$ dynamics, given by

$$\frac{dNa(t)}{dt} = \frac{\theta_{\mathrm{nt}}}{\varepsilon_{\mathrm{N}} B(t) + 1} \hat{Sa}(t) - \kappa_{\mathrm{Nd}} Na(t). \tag{B.17}$$

The data from [71] (figure 2b) shows the percentage of applied neutrophils that have transmigrated from the basal to the apical side of the epithelial monolayer (Na_{exp} =[0, 2.5, 30, 50, 70], in %, at times t_{exp} =[0, 0.5, 1, 1.5, 2], in hours), given a initial concentration of applied basal neutrophils $Nb_{exp}(0) = 50[\frac{cells \times 10^5}{ml}]$.

Using these data and our simplified model (equations B.16, with B.17), we obtained the opti-

mized parameter values $\theta_{nt} = 14\ [\frac{CFU \times 10^{-5}}{T}]$ and $\varepsilon_n = 81$, shown in table 8.1.
The parametrized model accurately predicts the independent experimental data-set of [300]. The results of the parameter optimization and the model predictions are shown in figure B.12.

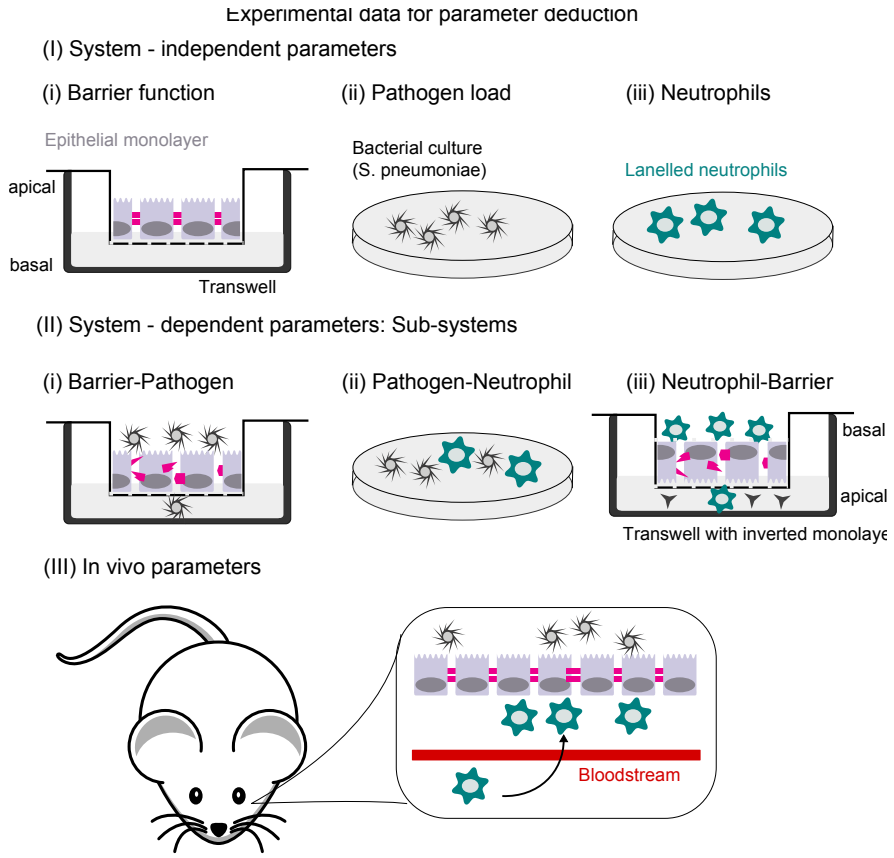

Figure B.1: **Experimental techniques leading to quantitative dynamic experimental data used for the parameter estimation and validation of the mathematical model of the host-pathogen interactions between the airway epithelium and *Streptococcus pneumoniae*.** *(I) System - independent parameters* quantify the rates that are specific to a particular species. (i) Barrier function of a given epithelial monolayer is assessed by transwell experiments that measure the electrical resistance between apical and basal chamber. (ii) Pathogen and (iii) neutrophil growth and death rates are quantified by tracking the changes of population sizes over time. *(II) System -dependent parameters that characterize interactions between a sub-set of model species* (i) The interplay between barrier function and pathogen load is assessed by transwell experiments, which are initialized by placing a population of pathogens in the apical chamber of the transwell device. Remaining apical and invading basal pathogen load, as well as barrier function, are then quantified over time. (ii) The interplay between pathogens and neutrophils is characterized by following the population size of these two species in a co-culture. (iii) The interplay between neutrophil and barrier is quantified by transwell experiments which are initialized by placing neutrophils in the basal side of a inverted monolayer, and tracking the remaining basal and transmigrated apical neutrophils, as well as the barrier function, over time. *(II) In vivo parameters* are calculated by inoculating a population of pathogens (bacterial challenge) into the nares of a mouse. Apically located pathogens and neutrophils are estimated by quantification of Broncheoalveolar lavage fluid (BALF). *In vivo* estimation of barrier function is not commonly performed.

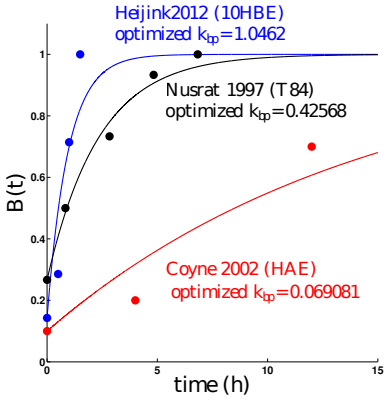

Figure B.2: Data-points and model fit for the calculation of the barrier production rate κ_{bp}. Data points were derived from airway [28] [283] and intestinal [87] epithelial monolayers.

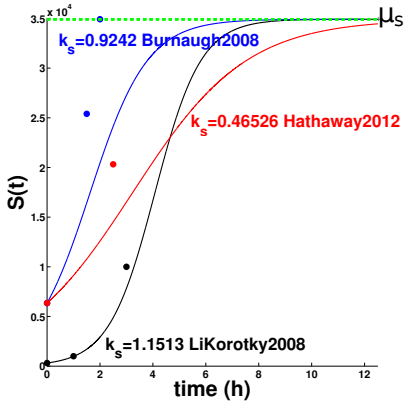

Figure B.3: Data-points and model fit for the calculation of the bacterial growth rate κ_s and carrying capacity μ_s, using equation B.6 and data from [277], [279] and [278].

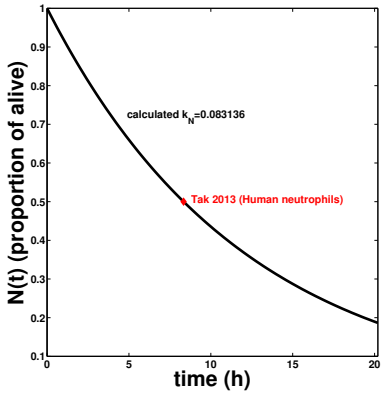

Figure B.4: Data-point and model fit for the calculation of the neutrophil death rate κ_{nd}, using equation B.7 and data from [282].

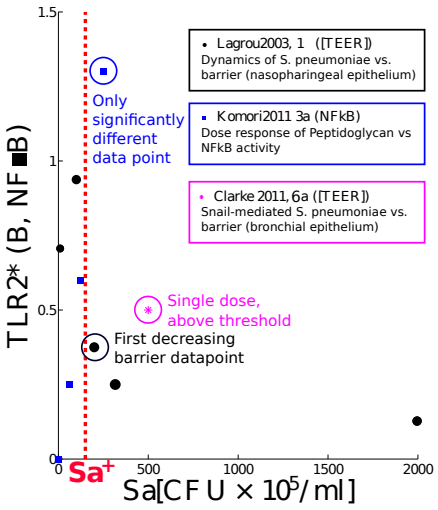

Figure B.5: **Determination of the minimal bacterial concentration required for a significant induction of TLR activity** According to data from [285], [85] and [38], concentrations of bacteria above $120 CFU \times 10^5/ml$ result in significant TLR2 activity. This roughly corresponds to the minimal concentration of bacteria Sa^+ that triggers TLR activation.

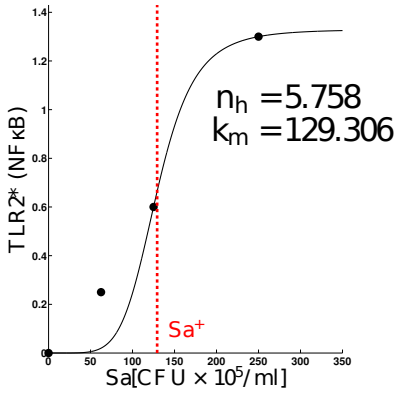

Figure B.6: **Data-points and fitted dose-response curve of bacteria-mediated TLR activation (parameters k_m and n_H).** Fit of the Hill function $F(S_a(t)) = \frac{S_a(t)^{\mathrm{n_H}}}{X(t)^{\mathrm{n_H}} + k_{\mathrm{m}}^{\mathrm{n_H}}}$ to the experimental data-points of [285].

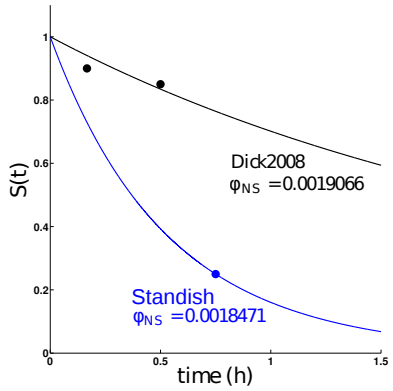

Figure B.7: **Data-points and model fit for the calculation of the neutrophil-induced death of bacteria (ϕ_{NS})** The parameter ϕ_{NS} was calculated using the equations B.13 and B.11, as well as the data from [88] and [89]. Note the almost perfect agreement between the obtained parameter values.

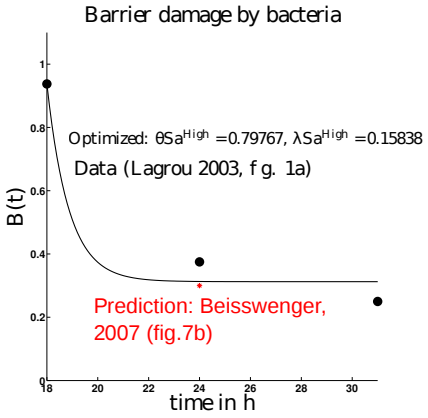

Figure B.8: **Data-points, model fit and validation for the calculation of the parameters quantifying barrier damage by bacteria (θ_{Sabd} and λ_{Sabp})** The TLR-dependent barrier degradation $\theta_{Sabd} = 0.8T^{-1}$ and inhibition of barrier production $\lambda_{Sabp} = 0.18$ (dimensionless) were estimated by fitting equation B.15 to data from [85] (fig. 1a). The resulting parametrized equation agrees well with the independent experimental data from [68].

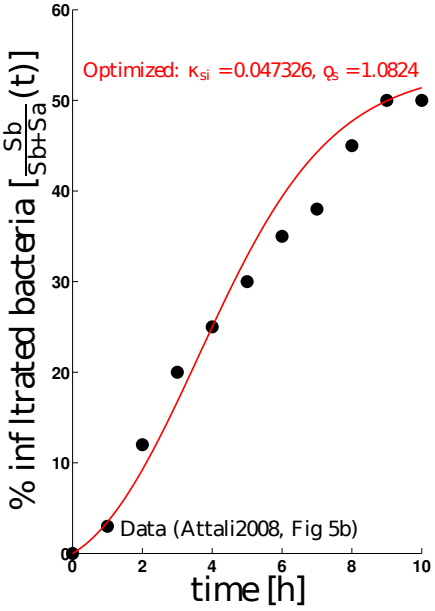

Figure B.9: Estimation of parameters that quantify the rate of invasion of bacteria through barrier (κ_{Si} and ε_S)

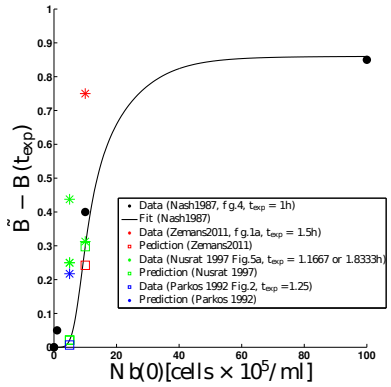

Figure B.10: **Estimation and validation of parameters quantifying the switch-like damage of barrier by neutrophils.** To obtain the values quantifying the switch-like damage of barrier by neutrophils (the concentration of neutrophils at half maximal barrier damage k_{mn}, the Hill coefficient n_{hN} quantifying the sharpness of the switch, and the maximal strength of Nb induced barrier degradation ϕ_{nbBd}), we used data from [86] representing dose-response behaviours of $Nb(0)$ vs $B(t_{exp})$ and *in silico* simulations of the system of equations B.16 from $t = 0$ to t_{exp} for different initial conditions $Nb(0)$. The resulting parametrized model agrees with other, independent datasets [275, 71, 87].

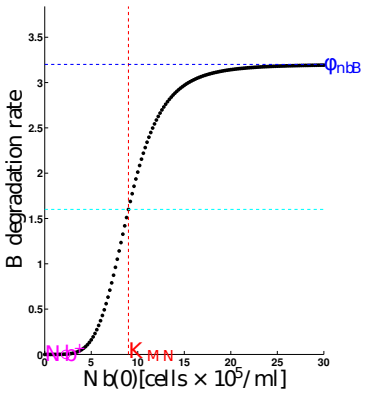

Figure B.11: **Switch-like dose response behaviour of barrier damage by basal neutrophils, given by the parametrized and scaled Hill function $\phi_{nbBd}F(Nb)$.**

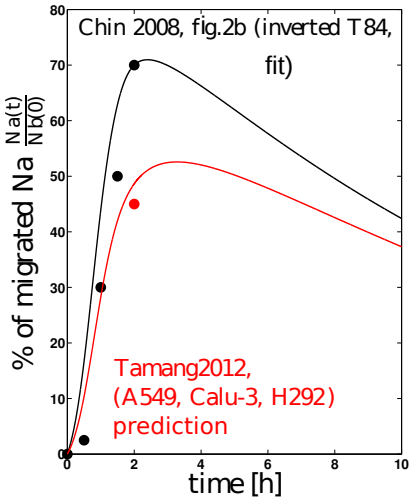

Figure B.12: **Model fit, model prediction and data-points showing the transmigration of neutrophils across a epithelial monolayer, parametrized by θ_{nt} and ε_n.** The parameters θ_{nt} and ε_n, quantifying the rate of transmigration of neutrophils through a epithelial monolayer, were calculated by fitting equations equations B.16, with B.17 to the experimental data from [71] (figure 2b). The resulting parametrized model accurately reproduces the independent dataset from [300].

Bibliography

[1] Amanda M Marchiando, W Vallen Graham, and Jerrold R Turner. Epithelial barriers in homeostasis and disease. *Annual review of pathology*, 5:119–44, January 2010.

[2] Ehrhardt Proksch, Johanna M. Brandner, and Jens-Michael Jensen. The skin: an indispensable barrier. *Experimental Dermatology*, 17(12):1063–1072, December 2008.

[3] David Verhoeven, Monica Nesselbush, and Michael E Pichichero. Lower nasopharyngeal epithelial cell repair and diminished innate inflammation responses contribute to the onset of acute otitis media in otitis-prone children. *Medical microbiology and immunology*, 202(4):295–302, August 2013.

[4] Elena Svirshchevskaya, Dmitrii Zubkov, Isabelle Mouyna, and Nadia Berkova. Innate Immunity and the Role of Epithelial Barrier During Aspergillus fumigatus Infection. *Current immunology reviews*, 8(3):254–261, August 2012.

[5] Ann M Carias, Scott McCoombe, Michael McRaven, Meegan Anderson, Nicole Galloway, Nathan Vandergrift, Angela J Fought, John Lurain, Maurice Duplantis, Ronald S Veazey, and Thomas J Hope. Defining the interaction of HIV-1 with the mucosal barriers of the female reproductive tract. *Journal of virology*, 87:11388–400, 2013.

[6] Laura Y McGirt and Lisa a Beck. Innate immune defects in atopic dermatitis. *The Journal of Allergy and Clinical Immunology*, 118(1):202–8, July 2006.

[7] Peter M Elias and Matthias Schmuth. Abnormal Skin Barrier in the Etiopathogenesis of Atopic Dermatitis. *Current Allergy and Asthma Reports*, 9:265–272, 2009.

[8] Peter M Elias and Martin Steinhoff. "Outside-to-inside" (and now back to "outside") pathogenic mechanisms in atopic dermatitis. *Journal of Investigative Dermatology*, 128(5):1067–70, May 2008.

[9] Stephen J Galli, Mindy Tsai, and Adrian M Piliponsky. The development of allergic inflammation. *Nature*, 454(7203):445–54, July 2008.

[10] Martijn C Nawijn, Tillie L Hackett, Dirkje S Postma, Antoon J M van Oosterhout, and Irene H Heijink. E-cadherin: gatekeeper of airway mucosa and allergic sensitization. *Trends in immunology*, 32(6):248–55, June 2011.

[11] William Cookson. The immunogenetics of asthma and eczema: a new focus on the epithelium. *Nature Reviews Immunology*, 4(12):978–88, December 2004.

[12] Alexander N Greiner, Peter W Hellings, Guiseppina Rotiroti, and Glenis K Scadding. Allergic rhinitis. *Lancet*, 378(9809):2112–22, December 2011.

[13] Anna De Benedetto, Akiharu Kubo, and Lisa a Beck. Skin barrier disruption: a requirement for allergen sensitization? *Journal of Investigative Dermatology*, 132(3 Pt 2):949–63, March 2012.

[14] Robert F Schwabe and Christian Jobin. The microbiome and cancer. *Nature reviews. Cancer*, 13(11):800–12, 2013.

[15] Eran Elinav, Roni Nowarski, Christoph a Thaiss, Bo Hu, Chengcheng Jin, and Richard a Flavell. Inflammation-induced cancer: crosstalk between tumours, immune cells and microorganisms. *Nature reviews. Cancer*, 13(11):759–71, November 2013.

[16] Ruby Pawankar. Allergic diseases and asthma: a global public health concern and a call to action. *The World Allergy Organization journal*, 7(1):12, 2014.

[17] Lionel Fry. *An atlas of atopic eczema*. Parthenon, 2003.

[18] B Ehlken, M Möhrenschlager, B Kugland, K Berger, K Quednau, and Johannes Ring. [Cost-of-illness study in patients suffering from atopic eczema in Germany]. *Der Hautarzt; Zeitschrift für Dermatologie, Venerologie, und verwandte Gebiete*, 56(12):1144–51, December 2005.

[19] N Wadonda-Kabondo, J A C Sterne, J Golding, C T C Kennedy, C B Archer, M G S Dunnill, T H E Alspac, and Study Team. Epidemiology and Health Services Research A prospective study of the prevalence and incidence of atopic dermatitis in children aged 0 âĂŞ 42 months. *British Journal of Dermatology*, 149:1023–1028, 2003.

[20] Edith N Nnoruka and Clin Derm Lond. Tropical medicine rounds Current epidemiology of atopic dermatitis in south-eastern Nigeria. pages 739–744, 2004.

[21] World Health Organization. Measuring impact of Streptococcus pneumoniae and Haemophilus influenzae type b conjugate vaccination. Technical report, 2012.

[22] Farin Kamangar, Graça M. Dores, and William F. Anderson. Patterns of cancer incidence, mortality, and prevalence across five continents: Defining priorities to reduce cancer disparities in different geographic regions of the world. *Journal of Clinical Oncology*, 24(14):2137–2150, 2006.

[23] World Health Organization. Antimicrobial resistance: Fact sheet Number 194, 2014.

[24] Johannes Ring, a Alomar, T Bieber, Mette Deleuran, a Fink-Wagner, C Gelmetti, U Gieler, J Lipozencic, Thomas a Luger, a P Oranje, T Schäfer, T Schwennesen, S Seidenari, D Simon, Sonja Ständer, G Stingl, S Szalai, J C Szepietowski, Alain Taïeb, Thomas Werfel, a. Wollenberg, and U Darsow. Guidelines for treatment of atopic eczema (atopic dermatitis) part I. *Journal of the European Academy of Dermatology and Venereology*, 26(8):1045–60, August 2012.

[25] Alain Taïeb, Julien Seneschal, and M Djavad Mossalayi. Biologics in atopic dermatitis. *Journal der Deutschen Dermatologischen Gesellschaft = Journal of the German Society of Dermatology : JDDG*, 10(Band 10):174–8, 2012.

[26] Jarin Chun and Alice S Prince. TLR2-induced calpain cleavage of epithelial junctional proteins facilitates leukocyte transmigration. *Cell host & microbe*, 5(1):47–58, January 2009.

[27] Akiharu Kubo, Keisuke Nagao, and Masayuki Amagai. Epidermal barrier dysfunction and cutaneous sensitization in atopic diseases. *The Journal of Clinical Investigation*, 122(2), 2012.

[28] Carolyn B Coyne, Miriam K Vanhook, Todd M Gambling, L Johnny, Richard C Boucher, Larry G Johnson, Chapel Hill, and North Carolina. Regulation of Airway Tight Junctions by Proinflammatory Cytokines. *Molecular Biology of the Cell*, 13(September):3218–3234, 2002.

[29] François-Xavier Bernard, Franck Morel, Magalie Camus, Nathalie Pedretti, Christine Barrault, Julien Garnier, and Jean-Claude Lecron. Keratinocytes under Fire of Proinflammatory Cytokines: Bona Fide Innate Immune Cells Involved in the Physiopathology of Chronic Atopic Dermatitis and Psoriasis. *Journal of allergy*, 2012:718725, January 2012.

[30] Rachel L Zemans, Sean P Colgan, and Gregory P Downey. Transepithelial migration of neutrophils: mechanisms and implications for acute lung injury. *American journal of respiratory cell and molecular biology*, 40(5):519–35, May 2009.

[31] Alex C Chin and Charles A Parkos. Pathobiology of neutrophil transepithelial migration: implications in mediating epithelial injury. *Annual Review of Pathology*, 2:111–143, 2007.

[32] Ryan F L O'Shaughnessy, Ishaan Choudhary, and John I Harper. Interleukin-1 alpha blockade prevents hyperkeratosis in an in vitro model of lamellar ichthyosis. *Human molecular genetics*, 19(13):2594–605, July 2010.

[33] Peter M Elias. Stratum corneum defensive functions: an integrated view. *Journal of Investigative Dermatology*, 125(2):183–200, August 2005.

[34] Karin M Aberg, Mao-Qiang Man, Richard L Gallo, Tomas Ganz, Debra Crumrine, Barbara E Brown, Eung-Ho Choi, Dong-Kun Kim, Jens M Schröder, Kenneth R Feingold, and Peter M Elias. Co-regulation and interdependence of the mammalian epidermal permeability and antimicrobial barriers. *Journal of Investigative Dermatology*, 128(4):917–25, April 2008.

[35] Nicolas Cenac, Alex C Chin, Rafael Garcia-Villar, Christel Salvador-Cartier, Laurent Ferrier, Nathalie Vergnolle, André G Buret, Jean Fioramonti, and Lionel Bueno. PAR2 activation alters colonic paracellular permeability in mice via IFN-gamma-dependent and -independent pathways. *The Journal of physiology*, 558(Pt 3):913–25, August 2004.

[36] Jacob P. Thyssen and Sanja Kezic. Causes of epidermal filaggrin reduction and their role in the pathogenesis of atopic dermatitis. *Journal of Allergy and Clinical Immunology*, 134(4):792–799, 2014.

[37] I-Hsin Kuo, Amanda Carpenter-Mendini, Takeshi Yoshida, Laura Y McGirt, Andrei I Ivanov, Kathleen C Barnes, Richard L Gallo, Andrew W Borkowski, Kenshi Yamasaki, Donald Y Leung, Steve N Georas, Anna De Benedetto, and Lisa a Beck. Activation of Epidermal Toll-Like Receptor 2 Enhances Tight Junction Function: Implications for Atopic Dermatitis and Skin Barrier Repair. *The Journal of investigative dermatology*, pages 1–11, December 2012.

[38] Thomas B Clarke, Nicholas Francella, Alyssa Huegel, and Jeffrey N Weiser. Invasive bacterial pathogens exploit TLR-mediated downregulation of tight junction components to facilitate translocation across the epithelium. *Cell host & microbe*, 9(5):404–14, May 2011.

[39] Hamida Hammad and Bart N Lambrecht. Dendritic cells and epithelial cells: linking innate and adaptive immunity in asthma. *Nature Reviews Immunology*, 8(3):193–204, March 2008.

[40] Michael J Cork, Darren a Robinson, Yiannis Vasilopoulos, Adam Ferguson, Manar Moustafa, Alice L Macgowan, Gordon W Duff, Simon J Ward, and Rachid Tazi-Ahnini. New perspectives on epidermal barrier dysfunction in atopic dermatitis: gene-environment interactions. *The Journal of Allergy and Clinical Immunology*, 118(1):3–21; quiz 22–3, July 2006.

[41] Judith G M Bergboer, Patrick L J M Zeeuwen, and Joost Schalkwijk. Genetics of psoriasis: evidence for epistatic interaction between skin barrier abnormalities and immune deviation. *Journal of Investigative Dermatology*, 132(10):2320–1, October 2012.

[42] Donata Vercelli. Discovering susceptibility genes for asthma and allergy. *Nature reviews. Immunology*, 8(3):169–82, March 2008.

[43] Gráinne M O'Regan, Aileen Sandilands, W H Irwin McLean, and Alan D Irvine. Filaggrin in atopic dermatitis. *The Journal of Allergy and Clinical Immunology*, 122(4):689–93, October 2008.

[44] S Chavanas, C Bodemer, A Rochat, D Hamel-Teillac, M Ali, Alan D Irvine, J L Bonafé, J Wilkinson, Alain Taïeb, Yann Barrandon, John I Harper, Y de Prost, and A Hovnanian. Mutations in SPINK5, encoding a serine protease inhibitor, cause Netherton syndrome. *Nature Genetics*, 25(2):141–2, June 2000.

[45] Magali Savignac, Anissa Edir, Marina Simon, and Alain Hovnanian. Darier disease : a disease model of impaired calcium homeostasis in the skin. *Biochimica et biophysica acta*, 1813(5):1111–7, May 2011.

[46] Irit Nachtigall, Andrey Tamarkin, Sascha Tafelski, Andreas Weimann, Andreas Rothbart, Susanne Heim, Klaus D Wernecke, and Claudia Spies. Polymorphisms of the toll-like receptor 2 and 4 genes are associated with faster progression and a more severe course of sepsis in critically ill patients. *The Journal of international medical research*, 42(1):93–110, March 2014.

[47] Barbara S Baker. The role of microorganisms in atopic dermatitis. *Clinical and experimental immunology*, 144(1):1–9, April 2006.

[48] Marsha Wills-karp, Joanna Santeliz, and Christopher L Karp. revisiting the hygiene hypothesis. *Nature Reviews Immunology*, 1(October):69–75, 2001.

[49] Daniel H Kaplan, Botond Z Igyártó, and Anthony a Gaspari. Early immune events in the induction of allergic contact dermatitis. *Nature reviews. Immunology*, 12(2):114–24, February 2012.

[50] Peter M Elias and Joan S. Wakefield. Therapeutic implications of a barrier-based pathogenesis of atopic dermatitis. *Clinical Reviews in Allergy and Immunology*, 41(3):282–295, 2011.

[51] Iu Lazebnik. Can a biologist fix a radio, or what I learned while studying apoptosis. *Biochemistry*, 12(12):166–71, January 2003.

[52] Olaf Wolkenhauer and Sara Green. The search for organizing principles as a cure against reductionism in systems medicine. *The FEBS journal*, 280(23):5938–48, December 2013.

[53] Yoram Vodovotz, Gary An, and Ioannis P Androulakis. A Systems Engineering Perspective on Homeostasis and Disease. *Frontiers in bioengineering and biotechnology*, 1(September):6, 2013.

[54] Mark D. a. van Logtestijn, Elisa Domínguez-Hüttinger, Georgios N. Stamatas, and Reiko J. Tanaka. Resistance to Water Diffusion in the Stratum Corneum Is Depth-Dependent. *Plos One*, 10:e0117292, 2015.

[55] Shinji Nakaoka and Kazuyuki Aihara. Stochastic simulation of structured skin cell population dynamics. *Journal of mathematical biology*, pages 1–7, December 2012.

[56] Niels Grabe and Karsten Neuber. A multicellular systems biology model predicts epidermal morphology, kinetics and Ca2+ flow. *Bioinformatics (Oxford, England)*, 21(17):3541–7, September 2005.

[57] Thomas Sütterlin, Simone Huber, Hartmut Dickhaus, and Niels Grabe. Modeling multicellular behavior in epidermal tissue homeostasis via finite state machines in multi-agent systems. *Bioinformatics (Oxford, England)*, 25(16):2057–63, August 2009.

[58] Thomas Sütterlin, Christoph Kolb, Hartmut Dickhaus, Dirk Jäger, and Niels Grabe. Bridging the scales: semantic integration of quantitative SBML in graphical multicellular models and simulations with EPISIM and COPASI. *Bioinformatics (Oxford, England)*, 29(2):223–9, January 2013.

[59] Paul a Orlando, Joel S Brown, Robert a Gatenby, and Anna R Guliano. The ecology of human papillomavirus-induced epithelial lesions and the role of somatic evolution in their progression. *The Journal of infectious diseases*, 208(3):394–402, August 2013.

[60] I M M van Leeuwen, H M Byrne, O E Jensen, and J R King. Crypt dynamics and colorectal cancer: advances in mathematical modelling. *Cell proliferation*, 39(3):157–81, June 2006.

[61] Philip J Murray, Jun-Won Kang, Gary R Mirams, Sung-Young Shin, Helen M Byrne, Philip K Maini, and Kwang-Hyun Cho. Modelling spatially regulated beta-catenin dynamics and invasion in intestinal crypts. *Biophysical journal*, 99(3):716–25, August 2010.

[62] Tao Zheng, Jinho Yu, Min Hee Oh, and Zhou Zhu. The atopic march: progression from atopic dermatitis to allergic rhinitis and asthma. *Allergy, asthma & immunology research*, 3(2):67–73, April 2011.

[63] Ting Seng Tang, Thomas Bieber, and Hywel C Williams. Are the concepts of induction of remission and treatment of subclinical inflammation in atopic dermatitis clinically useful ? *Journal of Allergy and Clinical Immunology*, pages 1–12, 2012.

[64] S G Danby, J Chittock, K Brown, L H Albenali, and M J Cork. The effect of tacrolimus compared to betamethasone valerate on the skin barrier in volunteers with quiescent atopic dermatitis. *The British journal of dermatology*, 170:914–921, 2014.

[65] Stefanie Schoepe, Heike Schäcke, Ekkehard May, and Khusru Asadullah. Glucocorticoid therapy-induced skin atrophy. *Experimental Dermatology*, 15(5):406–420, 2006.

[66] David a. Norris. Mechanisms of action of topical therapies and the rationale for combination therapy. *Journal of the American Academy of Dermatology*, 53:17–25, 2005.

[67] Peter M Elias. The skin barrier as an innate immune element. *Seminars in Immunopathology*, 29(1):3–14, March 2007.

[68] Christoph Beisswenger, Carolyn B Coyne, Mikhail Shchepetov, and Jeffrey N Weiser. Role of p38 MAP kinase and transforming growth factor-beta signaling in transepithelial migration of invasive bacterial pathogens. *The Journal of biological chemistry*, 282(39):28700–8, September 2007.

[69] Jonathan a McCullers. The co-pathogenesis of influenza viruses with bacteria in the lung. *Nature reviews. Microbiology*, 12(4):252–62, 2014.

[70] Anna De Benedetto, Ritesh Agnihothri, Laura Y McGirt, Lora G Bankova, and Lisa a Beck. Atopic dermatitis: a disease caused by innate immune defects? *The Journal of Investigative Dermatology*, 129(1):14–30, January 2009.

[71] Alex C Chin, Winston Y Lee, Asma Nusrat, Nathalie Vergnolle, and Charles a Parkos. Neutrophil-mediated activation of epithelial protease-activated receptors-1 and -2 regulates barrier function and transepithelial migration. *Journal of immunology (Baltimore, Md. : 1950)*, 181(8):5702–10, October 2008.

[72] Charles A Parkos, S P Colgan, C Delp, M a Arnaout, and James L Madara. Neutrophil migration across a cultured epithelial monolayer elicits a biphasic resistance response representing sequential effects on transcellular and paracellular pathways. *The Journal of cell biology*, 117(4):757–64, May 1992.

[73] Padraic G Fallon, Takashi Sasaki, Aileen Sandilands, Linda E Campbell, Sean P Saunders, Niamh E Mangan, John J Callanan, Hiroshi Kawasaki, Aiko Shiohama, Akiharu Kubo, John P Sundberg, Richard B Presland, Philip Fleckman, Nobuyoshi Shimizu, Jun Kudoh, Alan D Irvine, Masayuki Amagai, and W H Irwin McLean. A homozygous frameshift mutation in the mouse Flg gene facilitates enhanced percutaneous allergen priming. *Nature Genetics*, 41(5):602–8, May 2009.

[74] Alain Hovnanian. Netherton syndrome: skin inflammation and allergy by loss of protease inhibition. *Cell and tissue research*, 351(2):289–300, February 2013.

[75] D Roedl, C Traidl-Hoffmann, Johannes Ring, H Behrendt, and M Braun-Falco. Serine protease inhibitor lymphoepithelial Kazal type-related inhibitor tends to be decreased in atopic dermatitis. *Journal of the European Academy of Dermatology and Venereology*, 23(11):1263–6, November 2009.

[76] Nahoko Komatsu, Kiyofumi Saijoh, Cynthia Kuk, Amber C Liu, Saba Khan, Fumiaki Shirasaki, Kazuhiko Takehara, and Eleftherios P Diamandis. Human tissue kallikrein expression in the stratum corneum and serum of atopic dermatitis patients. *Experimental Dermatology*, 16:513–519, 2007.

[77] T Terui, T Hirao, Y Sato, T Uesugi, M Honda, M Iguchi, N Matsumura, K Kudoh, S Aiba, and H Tagami. An increased ratio of interleukin-1 receptor antagonist to interleukin-1alpha in inflammatory skin diseases. *Experimental dermatology*, 7(6):327–34, December 1998.

[78] Arnaud Didierlaurent, John Goulding, Seema Patel, Robert Snelgrove, Lionel Low, Magali Bebien, Toby Lawrence, Leonie S van Rijt, Bart N Lambrecht, Jean-Claude Sirard, and Tracy Hussell. Sustained desensitization to bacterial Toll-like receptor ligands after resolution of respiratory influenza infection. *The Journal of experimental medicine*, 205(2):323–329, 2008.

[79] Charles N. Ellis, Lynn a. Drake, Mary M. Prendergast, William Abramovits, Mark Boguniewicz, C. Ralph Daniel, Mark Lebwohl, Seth R. Stevens, Diane L. Whitaker-Worth, J. Wang Cheng, and Kuo B. Tong. Cost of atopic dermatitis and eczema in the United States. *Journal of the American Academy of Dermatology*, 46:361–370, 2002.

[80] Anthony J Mancini, Kellee Kaulback, and Sarah L Chamlin. The socioeconomic impact of atopic dermatitis in the United States: a systematic review. *Pediatric dermatology*, 25(1):1–6, 2008.

[81] Donald Y M Leung, Mark Boguniewicz, Michael D Howell, Ichiro Nomura, and Qutayba A Hamid. Science in Medicine: New insights into atopic dermatitis. *The Journal of Clinical Investigation*, 113:651–657, 2004.

[82] Donald Y M Leung and Emma Guttman-yassky. Deciphering the complexities of atopic dermatitis : Shifting paradigms in treatment approaches. *Journal of Allergy and Clinical Immunology*, 134(4):769–779, 2015.

[83] Reiko J Tanaka and Masahiro Ono. Skin Disease Modeling from a Mathematical Perspective. *Journal of Investigative Dermatology*, 133(6):1472–1478, 2013.

[84] Reiko J Tanaka, Masahiro Ono, and Heather a Harrington. Skin barrier homeostasis in atopic dermatitis: feedback regulation of kallikrein activity. *PloS one*, 6(5):e19895, January 2011.

[85] K Lagrou, W E Peetermans, J Verhaegen, M Jorissen, and J Van Eldere. Disruption of nasopharyngeal epithelium by pneumococci is density-linked. *European journal of clinical investigation*, 33(4):340–5, April 2003.

[86] Shirin Nash, Joan Stafford, and James L Madara. Effects of Polymorphonuclear Leukocyte Transmigration of Cultured Intestinal Epithelial Monolayers. *The Journal of Clinical Investigation*, 80(October):1104–1113, 1987.

[87] Asma Nusrat, Charles A Parkos, T W Liang, D K Carnes, and James L Madara. Neutrophil migration across model intestinal epithelia: monolayer disruption and subsequent events in epithelial repair. *Gastroenterology*, 113(5):1489–500, November 1997.

[88] Emily Patricia Dick, Lynne Rebecca Prince, and Ian Sabroe. Ex vivo-expanded bone marrow CD34+ derived neutrophils have limited bactericidal ability. *Stem cells (Dayton, Ohio)*, 26(10):2552–63, October 2008.

[89] Alistair J Standish and Jeffrey N Weiser. Human neutrophils kill Streptococcus pneumoniae via serine proteases. *Journal of immunology (Baltimore, Md. : 1950)*, 183(4):2602–9, August 2009.

[90] Arturo Casadevall and Liise-anne Pirofski. The damage-response framework of microbial pathogenesis. *Nature reviews. Microbiology*, 1(1):17–24, October 2003.

[91] Amber M Smith, Jonathan a McCullers, and Frederick R Adler. Mathematical model of a three-stage innate immune response to a pneumococcal lung infection. *Journal of theoretical biology*, 276(1):106–16, May 2011.

[92] Sourya Shrestha, Betsy Foxman, Suzanne Dawid, Allison E Aiello, Brian M Davis, Joshua Berus, and Pejman Rohani. Time and dose-dependent risk of pneumococcal pneumonia following influenza : a model for within-host interaction between influenza and Streptococcus pneumoniae. *Interface Focus*, 10:20130233, 2013.

[93] Ericka Mochan, David Swigon, Bard Ermentrout, Sarah Lukens, and Gilles Clermont. A mathematical model of intrahost pneumococcal pneumonia infection dynamics in murine strains. *Journal of Theoretical Biology*, 353:44–54, 2014.

[94] Amber M Smith, Frederick R Adler, Ruy M Ribeiro, Ryan N Gutenkunst, Julie L McAuley, Jonathan a McCullers, and Alan S Perelson. Kinetics of coinfection with influenza A virus and Streptococcus pneumoniae. *PLoS pathogens*, 9(3):e1003238, March 2013.

[95] Samir Mitragotri, Yuri G Anissimov, Annette L Bunge, H Frederick Frasch, Richard H Guy, Jonathan Hadgraft, Gerald B Kasting, Majella E Lane, and Michael S Roberts. Mathematical models of skin permeability: an overview. *International journal of pharmaceutics*, 418(1):115–29, October 2011.

[96] Sophie C Weatherhead, Peter M Farr, David Jamieson, Jennifer S Hallinan, James J Lloyd, Anil Wipat, and Nick J Reynolds. Keratinocyte Apoptosis in Epidermal Remodeling and Clearance of Psoriasis Induced by UV Radiation. *Journal of Investigative Dermatology*, 131(9):1916–1926, 2011.

[97] Niels Grabe and Karsten Neuber. Simulating psoriasis by altering transit amplifying cells. *Bioinformatics*, 23(11):1309–1312, 2007.

[98] Anna Ougrinovskaia, Rosemary S Thompson, and Mary R Myerscough. An ODE model of early stages of atherosclerosis: mechanisms of the inflammatory response. *Bulletin of mathematical biology*, 72(6):1534–61, August 2010.

[99] Najl V Valeyev, Christian Hundhausen, Yoshinori Umezawa, Nikolay V Kotov, Gareth Williams, Alex Clop, Crysanthi Ainali, Christos Ouzounis, Sophia Tsoka, and Frank O Nestle. A systems model for immune cell interactions unravels the mechanism of inflammation in human skin. *PLoS computational biology*, 6(12):e1001024, January 2010.

[100] Lisa J W Hite, Ynte H S Chukken, Belgin D Ogan, Laura G Reen, Mike J C Happell, and Graham F M Edley. Modelling the dynamics of intramammary E . coli infections in dairy

cows : understanding mechanisms that distinguish transient from persistent infections. *Veterinary Research*, 41(13), 2010.

[101] Denise E Kirschner and M J Blaser. The dynamics of Helicobacter pylori infection of the human stomach. *Journal of theoretical biology*, 176(2):281–90, September 1995.

[102] Angela Reynolds, Jonathan Rubin, Gilles Clermont, Judy Day, Yoram Vodovotz, and G Bard Ermentrout. A reduced mathematical model of the acute inflammatory response: I. Derivation of model and analysis of anti-inflammation. *Journal of theoretical biology*, 242(1):220–36, September 2006.

[103] Rukmini Kumar, Gilles Clermont, Yoram Vodovotz, and Carson C Chow. The dynamics of acute inflammation. *Journal of theoretical biology*, 230:145–155, 2004.

[104] Baris Hancioglu, David Swigon, and Gilles Clermont. A dynamical model of human immune response to influenza A virus infection. *Journal of theoretical biology*, 246(1):70–86, May 2007.

[105] Hongyu Miao, Joseph a Hollenbaugh, Martin S Zand, Jeanne Holden-Wiltse, Tim R Mosmann, Alan S Perelson, Hulin Wu, and David J Topham. Quantifying the early immune response and adaptive immune response kinetics in mice infected with influenza A virus. *Journal of virology*, 84(13):6687–98, July 2010.

[106] Giao T Huynh and Frederick R Adler. Alternating host cell tropism shapes the persistence, evolution and coexistence of epstein-barr virus infections in human. *Bulletin of mathematical biology*, 73(8):1754–73, August 2011.

[107] Richard Howey, Melvyn Quan, Nicholas J Savill, Louise Matthews, Sø ren Alexandersen, and Mark Woolhouse. Effect of the initial dose of foot-and-mouth disease virus on the early viral dynamics within pigs. *Journal of the Royal Society, Interface / the Royal Society*, 6(39):835–47, October 2009.

[108] Katherine Wendelsdorf, Josep Bassaganya-Riera, Raquel Hontecillas, and Stephen Eubank. Model of colonic inflammation: immune modulatory mechanisms in inflammatory bowel disease. *Journal of theoretical biology*, 264(4):1225–39, June 2010.

[109] Wing-Cheong Lo, Edward W Martin, Charles L Hitchcock, and Avner Friedman. Mathematical model of colitis-associated colon cancer. *Journal of theoretical biology*, 317:20–9, January 2013.

[110] Carla a Borgoño, Iacovos P Michael, Nahoko Komatsu, Arumugam Jayakumar, Ravi Kapadia, Gary L Clayman, Georgia Sotiropoulou, and Eleftherios P Diamandis. A potential role for multiple tissue kallikrein serine proteases in epidermal desquamation. *The Journal of Biological Chemistry*, 282(6):3640–52, February 2007.

[111] Anaïs Briot, Céline Deraison, Matthieu Lacroix, Chrystelle Bonnart, Aurélie Robin, Céline Besson, Pierre Dubus, and Alain Hovnanian. Kallikrein 5 induces atopic dermatitis-like lesions through PAR2-mediated thymic stromal lymphopoietin expression in Netherton syndrome. *The Journal of experimental medicine*, 206(5):1135–47, May 2009.

[112] Jörg Buddenkotte, Christopher Stroh, Ingo H Engels, Corinna Moormann, Victoria M Shpacovitch, Stephan Seeliger, Nathalie Vergnolle, Dietmar Vestweber, Thomas a Luger, Klaus Schulze-Osthoff, and Martin Steinhoff. Agonists of proteinase-activated receptor-2 stimulate upregulation of intercellular cell adhesion molecule-1 in primary human keratinocytes via activation of NF-kappa B. *The Journal of Investigative Dermatology*, 124(1):38–45, January 2005.

[113] Jean-Pierre Hachem, Debra Crumrine, Joachim W Fluhr, Barbara E Brown, Kenneth R Feingold, and Peter M Elias. pH directly regulates epidermal permeability barrier homeostasis, and stratum corneum integrity/cohesion. *The Journal of Investigative Dermatology*, 121(2):345–53, August 2003.

[114] Henrik Dommisch, Whasun O Chung, Maryam G Rohani, David Williams, Minnie Rangarajan, Mike a Curtis, and Beverly a Dale. Protease-activated receptor 2 mediates human beta-defensin 2 and CC chemokine ligand 20 mRNA expression in response to proteases secreted by Porphyromonas gingivalis. *Infection and immunity*, 75(9):4326–33, September 2007.

[115] Georgia Sotiropoulou, Georgios Pampalakis, and Eleftherios P Diamandis. Functional roles of human kallikrein-related peptidases. *The Journal of biological chemistry*, 284(48):32989–94, November 2009.

[116] Toby Lawrence. Inflammation and cancer: a failure of resolution? *Trends in pharmacological sciences*, 28(4):162–5, April 2007.

[117] Eleonora Candi, Rainer Schmidt, and Gerry Melino. The cornified envelope: a model of cell death in the skin. *Nature reviews. Molecular cell biology*, 6(4):328–40, April 2005.

[118] Kathi C. Madison. Barrier Function of the Skin: âĂŸâĂŸLa Raison dâĂŹEtreâĂŹâĂŹ of the Epidermis. *Journal of Investigative Dermatology*, 121:231–241, 2003.

[119] Jean-Pierre Hachem, Evi Houben, Debra Crumrine, Mao-Quiang Man, Nanna Y Schurer, Truus Roelandt, Eung-Ho Choi, Yoshikazu Uchida, Barbara E Brown, Kenneth R Feingold, and Peter M Elias. Serine protease signaling of epidermal permeability barrier homeostasis. *Journal of Investigative Dermatology*, 126(9):2074–86, September 2006.

[120] I-Hsin Kuo, Takeshi Yoshida, Anna De Benedetto, and Lisa a Beck. The cutaneous innate immune response in patients with atopic dermatitis. *The Journal of Allergy and Clinical Immunology*, 131(2):266–78, February 2013.

[121] Hannah J Gould and Brian J Sutton. IgE in allergy and asthma today. *Nature reviews. Immunology*, 8(3):205–17, March 2008.

[122] Ehsan Aliahmadi, Robert Gramlich, Andreas Grützkau, Manuel Hitzler, Melanie Krüger, Ria Baumgrass, Maximilian Schreiner, Burghardt Wittig, Reinhard Wanner, and Matthias Peiser. TLR2-activated human langerhans cells promote Th17 polarization via IL-1beta, TGF-beta and IL-23. *European journal of immunology*, 39(5):1221–30, May 2009.

[123] Lennart Hansson, Assar Bäckman, Annelii Ny, Michael Edlund, Elisabeth Ekholm, Barbro Ekstrand Hammarström, Jan Törnell, Pia Wallbrandt, Hå kan Wennbo, and Torbjörn Egelrud. Epidermal overexpression of stratum corneum chymotryptic enzyme in mice: a model for chronic itchy dermatitis. *The Journal of Investigative Dermatology*, 118(3):444–9, March 2002.

[124] Michael J Cork, Simon G Danby, Yiannis Vasilopoulos, Jonathan Hadgraft, Majella E Lane, Manar Moustafa, Richard H Guy, Alice L Macgowan, Rachid Tazi-Ahnini, and Simon J Ward. Epidermal barrier dysfunction in atopic dermatitis. *Journal of Investigative Dermatology*, 129(8):1892–908, August 2009.

[125] Maeve a McAleer and Alan D Irvine. The multifunctional role of filaggrin in allergic skin disease. *The Journal of Allergy and Clinical Immunology*, 131(2):280–91, February 2013.

[126] Sara J Brown, Karin Kroboth, Aileen Sandilands, Linda E Campbell, Elizabeth Pohler, Sanja Kezic, Heather J Cordell, W H Irwin McLean, and Alan D Irvine. Intragenic copy number variation within filaggrin contributes to the risk of atopic dermatitis with a dose-dependent effect. *The Journal of Investigative Dermatology*, 132(1):98–104, January 2012.

[127] Colin N a Palmer, Alan D Irvine, Ana Terron-Kwiatkowski, Yiwei Zhao, Haihui Liao, Simon P Lee, David R Goudie, Aileen Sandilands, Linda E Campbell, Frances J D Smith, Gráinne M O'Regan, Rosemarie M Watson, Jo E Cecil, Sherri J Bale, John G Compton, John J DiGiovanna, Philip Fleckman, Sue Lewis-Jones, Gehan Arseculeratne, Ann Sergeant, Colin S Munro, Brahim El Houate, Ken McElreavey, Liselotte B Halkjaer, Hans Bisgaard, Somnath Mukhopadhyay, and W H Irwin McLean. Common loss-of-function variants of the epidermal barrier protein filaggrin are a major predisposing factor for atopic dermatitis. *Nature genetics*, 38(4):441–6, April 2006.

[128] Maria Brattsand, Kristina Stefansson, Christine Lundh, Ylva Haasum, and Torbjörn Egelrud. A proteolytic cascade of kallikreins in the stratum corneum. *The Journal of Investigative Dermatology*, 124(1):198–203, January 2005.

[129] Heidi H Kong, Julia Oh, Clay Deming, Sean Conlan, Elizabeth a Grice, Melony Beatson, Effie Nomicos, Eric Polley, Hirsh D Komarow, Nisc Comparative Sequence Program, Patrick R Murray, Maria L Turner, and Julia a Segre. Temporal shifts in the skin microbiome associated with atopic dermatitis disease flares and treatment. *Genome research*, pages 850–859, February 2012.

[130] Sang Eun Lee, Ji-Min Kim, Se Kyoo Jeong, Jeong Eun Jeon, Hyun-Ju Yoon, Min-Kyung Jeong, and Seung Hun Lee. Protease-activated receptor-2 mediates the expression of inflammatory cytokines, antimicrobial peptides, and matrix metalloproteinases in keratinocytes in response to Propionibacterium acnes. *Archives of dermatological research*, 302(10):745–56, December 2010.

[131] Ikue Nemoto-Hasebe, Masashi Akiyama, Toshifumi Nomura, Aileen Sandilands, W H Irwin McLean, and Hiroshi Shimizu. Clinical severity correlates with impaired barrier in filaggrin-related eczema. *Journal of Investigative Dermatology*, 129(3):682–689, 2009.

[132] Tiffany C Scharschmidt, Mao-Qiang Man, Yutaka Hatano, Debra Crumrine, Roshan Gunathilake, John P Sundberg, Kathleen a Silva, Theodora M Mauro, Melanie Hupe, Soyun Cho, Yan Wu, Anna Celli, Matthias Schmuth, Kenneth R Feingold, and Peter M Elias. Filaggrin deficiency confers a paracellular barrier abnormality that reduces inflammatory thresholds to irritants and haptens. *The Journal of Allergy and Clinical Immunology*, 124(3):496–506, 506.e1–6, September 2009.

[133] Kevin O Kisich, Charles W Carspecken, Stephanie Fiéve, Mark Boguniewicz, and Donald Y M Leung. Defective killing of Staphylococcus aureus in atopic dermatitis is asso-

ciated with reduced mobilization of human beta-defensin-3. *The Journal of Allergy and Clinical Immunology*, 122(1):62–8, July 2008.

[134] Emma Guttman-Yassky, Mayte Suárez-Fariñas, Andrea Chiricozzi, Kristine E Nograles, Avner Shemer, Judilyn Fuentes-Duculan, Irma Cardinale, Peng Lin, Reuven Bergman, Anne M Bowcock, and James G Krueger. Broad defects in epidermal cornification in atopic dermatitis identified through genomic analysis. *The Journal of Allergy and Clinical Immunology*, 124(6):1235–1244.e58, December 2009.

[135] Mayte Suárez-Fariñas, Suzanne J Tintle, Avner Shemer, Andrea Chiricozzi, Kristine E Nograles, Irma Cardinale, Shenghui Duan, Anne M Bowcock, James G Krueger, and Emma Guttman-Yassky. Nonlesional atopic dermatitis skin is characterized by broad terminal differentiation defects and variable immune abnormalities. *The Journal of Allergy and Clinical Immunology*, 127(4):954–64.e1–4, April 2011.

[136] Aileen Sandilands, Calum Sutherland, Alan D Irvine, and W H Irwin McLean. Filaggrin in the frontline: role in skin barrier function and disease. *Journal of cell science*, 122(Pt 9):1285–94, May 2009.

[137] Kristine E Nograles, L C Zaba, Emma Guttman-Yassky, Judilyn Fuentes-Duculan, Mayte Suárez-Fariñas, I Cardinale, a Khatcherian, J Gonzalez, K C Pierson, T R White, C Pensabene, I Coats, I Novitskaya, M a Lowes, and James G Krueger. Th17 cytokines interleukin (IL)-17 and IL-22 modulate distinct inflammatory and keratinocyte-response pathways. *The British journal of dermatology*, 159(5):1092–102, November 2008.

[138] Michael D Howell, Byung Eui Kim, Peisong Gao, Audrey V Grant, Mark Boguniewicz, Anna Debenedetto, Lynda Schneider, Lisa a Beck, Kathleen C Barnes, and Donald Y M Leung. Cytokine modulation of atopic dermatitis filaggrin skin expression. *The Journal of Allergy and Clinical Immunology*, 120(1):150–5, July 2007.

[139] Marianne Demerjian, Jean-Pierre Hachem, Erwin Tschachler, Geertrui Denecker, Wim Declercq, Peter Vandenabeele, Theodora M Mauro, Melanie Hupe, Debra Crumrine, Truus Roelandt, Evi Houben, Peter M Elias, and Kenneth R Feingold. Acute modulations in permeability barrier function regulate epidermal cornification: role of caspase-14 and the protease-activated receptor type 2. *The American Journal of Pathology*, 172(1):86–97, January 2008.

[140] Peter M Elias, Sung Ku Ahn, Mitsuhiro Denda, Barbara E Brown, Debra Crumrine, Llewellyn K Kimutai, Laszlo Kömüves, Seung Hun Lee, and Kenneth R Feingold. Modulations in epidermal calcium regulate the expression of differentiation-specific markers. *Journal of Investigative Dermatology*, 119(5):1128–36, November 2002.

[141] Peter M Elias, Sung Ku Ahn, BarbaraE Brown, Debra Crumrine, and Kenneth R Feingold. Origin of the epidermal calcium gradient: regulation by barrier status and role of active vs passive mechanisms. *Journal of Investigative Dermatology*, 119(6):1269–74, December 2002.

[142] Chia-Ling Tu, Debra Crumrine, Mao-Qiang Man, Wenhan Chang, Hashem Elalieh, Michael You, Peter M Elias, and Daniel D Bikle. Ablation of the calcium-sensing receptor in keratinocytes impairs epidermal differentiation and barrier function. *Journal of Investigative Dermatology*, 132(10):2350–9, October 2012.

[143] Frank O Nestle, Paola Di Meglio, Jian-Zhong Qin, and Brian J Nickoloff. Skin immune sentinels in health and disease. *Nature reviews. Immunology*, 9(10):679–91, October 2009.

[144] Georgia Sotiropoulou and Georgios Pampalakis. Kallikrein-related peptidases: bridges between immune functions and extracellular matrix degradation. *Biological chemistry*, 391(4):321–31, April 2010.

[145] Cécile Caubet, Nathalie Jonca, Maria Brattsand, Marina Guerrin, Dominique Bernard, Rainer Schmidt, Torbjörn Egelrud, Michel Simon, and Guy Serre. Degradation of corneodesmosome proteins by two serine proteases of the kallikrein family, SCTE/KLK5/hK5 and SCCE/KLK7/hK7. *Journal of Investigative Dermatology*, 122(5):1235–1244, 2004.

[146] Jocelyn M. Biagini Myers, Lisa J. Martin, Melinda Butsch Kovacic, Tesfaye B. Mersha, Hua He, Valentina Pilipenko, Mark a. Lindsey, Mark B. Ericksen, David I. Bernstein, Grace K. LeMasters, James E. Lockey, and Gurjit K. Khurana Hershey. Epistasis between serine protease inhibitor Kazal-type 5 (SPINK5) and thymic stromal lymphopoietin (TSLP) genes contributes to childhood asthma. *Journal of Allergy and Clinical Immunology*, 134(4):891–899.e3, 2014.

[147] Ulrich Auf dem Keller, Anna Prudova, Ulrich Eckhard, Barbara Fingleton, and Christopher M Overall. Systems-level analysis of proteolytic events in increased vascular permeability and complement activation in skin inflammation. *Science signaling*, 6(258):rs2, January 2013.

[148] Kenshi Yamasaki, Kimberly Kanada, Daniel T Macleod, Andrew W Borkowski, Shin Morizane, Teruaki Nakatsuji, Anna L Cogen, and Richard L Gallo. TLR2 expression is increased in rosacea and stimulates enhanced serine protease production by keratinocytes. *Journal of Investigative Dermatology*, 131(3):688–97, March 2011.

[149] R. Voegeli, A V Rawlings, S. Doppler, and T. Schreier. Increased basal transepidermal water loss leads to elevation of some but not all stratum corneum serine proteases. *International Journal of Cosmetic Science*, 30(6):435–42, December 2008.

[150] G Grubauer, Peter M Elias, and Kenneth R Feingold. Transepidermal water loss: the signal for recovery of barrier structure and function. *Journal of lipid research*, 30(3):323–33, March 1989.

[151] Gopinathan K Menon, Kenneth R Feingold, Arthur H Moser, Barbara E Brown, and Peter M Elias. De novo sterologenesis in the skin. II. Regulation by cutaneous barrier requirements. *Journal of lipid research*, 26(5):418–427, 1985.

[152] Catarina Rosado, Pedro Pinto, and Luis Monteiro Rodrigues. Modeling TEWL-desorption curves: a new practical approach for the quantitative in vivo assessment of skin barrier. *Experimental dermatology*, 14(5):386–90, May 2005.

[153] Giampiero Pietrocola, Carla Renata Arciola, Simonetta Rindi, Antonella Di Poto, Antonino Missineo, Lucio Montanaro, and Pietro Speziale. Toll-like receptors (TLRs) in innate immune defense against Staphylococcus aureus. *The International journal of artificial organs*, 34:799–810, 2011.

[154] John E Sims and Dirk E Smith. The IL-1 family: regulators of immunity. *Nature Reviews Immunology*, 10(2):89–102, February 2010.

[155] Prasad Rallabhandi, Quan M Nhu, Vladimir Y Toshchakov, Wenji Piao, Andrei E Medvedev, Morley D Hollenberg, Alessio Fasano, and Stefanie N Vogel. Analysis of proteinase-activated receptor 2 and TLR4 signal transduction: a novel paradigm for receptor cooperativity. *The Journal of Biological Chemistry*, 283(36):24314–25, September 2008.

[156] Stephan Seeliger, Cllaudia K Derian, Nathalie Vergnolle, Nigel W Bunnett, Roman Nawroth, Martin Schmelz, Pierre-Yves Von Der Weid, Jörg Buddenkotte, Cord Sunderkötter, Dieter Metze, Patricia. Andrade-Gordon, Erik Harms, Dietmar Vestweber, Thomas a Luger, and Martin Steinhoff. Proinflammatory role of proteinase-activated receptor-2 in humans and mice during cutaneous inflammation in vivo. *FASEB journal : official publication of the Federation of American Societies for Experimental Biology*, 17(13):1871–85, October 2003.

[157] E R Sharlow, C S Paine, L Babiarz, M Eisinger, S Shapiro, and M Seiberg. The protease-activated receptor-2 upregulates keratinocyte phagocytosis. *Journal of Cell Science*, 113:3093–101, September 2000.

[158] Bart N Lambrecht and Hamida Hammad. The role of dendritic and epithelial cells as master regulators of allergic airway inflammation. *Lancet*, 376(9743):835–43, September 2010.

[159] Jyoti Das, Chang-hung Chen, Liyan Yang, Lauren Cohn, Prabir Ray, and Anuradha Ray. A critical role for NF- κ B in Gata3 expression and T H 2 differentiation in allergic airway inflammation. *Nature*, 2(1), 2001.

[160] Julia K Gittler, Avner Shemer, Mayte Suárez-Fariñas, Judilyn Fuentes-Duculan, Kara J Gulewicz, Claire Q F Wang, Hiroshi Mitsui, Irma Cardinale, Cristina de Guzman Strong, James G Krueger, and Emma Guttman-Yassky. Progressive activation of T(H)2/T(H)22 cytokines and selective epidermal proteins characterizes acute and chronic atopic dermatitis. *The Journal of Allergy and Clinical Immunology*, 130(6):1344–54, December 2012.

[161] Louise Newell, Marta E Polak, Jay Perera, Charlotte Owen, Peter Boyd, Christopher Pickard, Peter H Howarth, Eugene Healy, John W Holloway, Peter S Friedmann, and Michael R Ardern-Jones. Sensitization via healthy skin programs Th2 responses in individuals with atopic dermatitis. *Journal of Investigative Dermatology*, 133(10):2372–80, 2013.

[162] Toshiro Takai and Shigaku Ikeda. Barrier dysfunction caused by environmental proteases in the pathogenesis of allergic diseases. *Allergology international : official journal of the Japanese Society of Allergology*, 60(1):25–35, March 2011.

[163] Hans Törmä, Magnus Lindberg, and Berit Berne. Skin barrier disruption by sodium lauryl sulfate-exposure alters the expressions of involucrin, transglutaminase 1, profilaggrin, and kallikreins during the repair phase in human skin in vivo. *Journal of Investigative Dermatology*, 128(5):1212–9, May 2008.

[164] Shin Morizane, Kenshi Yamasaki, Filamer D Kabigting, and Richard L Gallo. Kallikrein expression and cathelicidin processing are independently controlled in keratinocytes by calcium, vitamin D(3), and retinoic acid. *Journal of Investigative Dermatology*, 130(5):1297–306, May 2010.

[165] Paola Fortugno, Alberto Bresciani, Chantal Paolini, Chiara Pazzagli, May El Hachem, Marina D'Alessio, and Giovanna Zambruno. Proteolytic activation cascade of the Netherton syndrome-defective protein, LEKTI, in the epidermis: implications for skin homeostasis. *Journal of Investigative Dermatology*, 131(11):2223–32, November 2011.

[166] Céline Deraison, Chrystelle Bonnart, Frederic Lopez, Celine Besson, Ross Robinson, Arumugam Jayakumar, Fredrik Wagberg, Maria Brattsand, Jean-Pierre Hachem, Göran Leonardsson, and Alain Hovnanian. LEKTI Fragments Specifically Inhibit KLK5 , KLK7 , and KLK14 and Control Desquamation through a pH-dependent Interaction. *Molecular Biology of the Cell*, 18(September):3607–3619, 2007.

[167] Akemi Ishida-Yamamoto, Satomi Igawa, and Mari Kishibe. Order and disorder in corneocyte adhesion. *Journal of Dermatology*, 38(January):645–654, 2011.

[168] Michelle Janssens, Jeroen van Smeden, Gert S Gooris, Wim Bras, Guiseppe Portale, Peter J Caspers, Rob J Vreeken, Thomas Hankemeier, Sanja Kezic, Ron Wolterbeek, Adriana P Lavrijsen, and Joke a Bouwstra. Increase in short-chain ceramides correlates with an altered lipid organization and decreased barrier function in atopic eczema patients. *Journal of lipid research*, 53(12):2755–66, December 2012.

[169] Peter M Elias. Epidermal barrier function: intercellular lamellar lipid structures, origin, composition and metabolism. *Journal of Controlled Release*, 15:199–208, 1991.

[170] Yutaka Hatano, Yasuko Adachi, Peter M Elias, Debra Crumrine, Takashi Sakai, Rieko Kurahashi, Kazumoto Katagiri, and Sakuhei Fujiwara. The Th2 cytokine, interleukin-4, abrogates the cohesion of normal stratum corneum in mice: implications for pathogenesis of atopic dermatitis. *Experimental dermatology*, 22(1):30–5, January 2013.

[171] Jens-Michael Jensen, Regina Fölster-Holst, Anke Baranowsky, Michael Schunck, Supandi Winoto-Morbach, Claudia Neumann, Stefan Schütze, and Ehrhardt Proksch. Impaired sphingomyelinase activity and epidermal differentiation in atopic dermatitis. *Journal of Investigative Dermatology*, 122(6):1423–31, June 2004.

[172] H D de Koning, E H van den Bogaard, J G M Bergboer, M Kamsteeg, I M J J van Vlijmen-Willems, K Hitomi, J Henry, M I Simon, N Takashita, Akemi Ishida-Yamamoto, Joost Schalkwijk, and P L J M Zeeuwen. Expression profile of cornified envelope structural proteins and keratinocyte differentiation-regulating proteins during skin barrier repair. *The British journal of dermatology*, 166(6):1245–54, June 2012.

[173] Piyush Koria, Daniel Brazeau, Keith Kirkwood, Patrick Hayden, Mitchell Klausner, and Stelios T Andreadis. Gene expression profile of tissue engineered skin subjected to acute barrier disruption. *Journal of Investigative Dermatology*, 121(2):368–82, August 2003.

[174] Gopinathan K Menon, Kenneth R Feingold, and Peter M Elias. Lamellar Body Secretory Response to Barrier Disruption. *Journal of Investigative Dermatology*, 98:279–289, 1992.

[175] E Proksch, W M Holleran, Gopinathan K Menon, Peter M Elias, and Kenneth R Feingold. Barrier function regulates epidermal lipid and DNA synthesis. *The British journal of dermatology*, 128(5):473–82, May 1993.

[176] Geertrui Denecker, Petra Ovaere, Peter Vandenabeele, and Wim Declercq. Caspase-14 reveals its secrets. *The Journal of cell biology*, 180(3):451–8, February 2008.

[177] Takeshi Matsui, Kenichi Miyamoto, Akiharu Kubo, Hiroshi Kawasaki, Tamotsu Ebihara, Kazuya Hata, Shinya Tanahashi, Shizuko Ichinose, Issei Imoto, Johji Inazawa, Jun Kudoh, and Masayuki Amagai. SASPase regulates stratum corneum hydration through profilaggrin-to-filaggrin processing. *EMBO molecular medicine*, 3(6):320–33, June 2011.

[178] Chrystelle Bonnart, Céline Deraison, Matthieu Lacroix, Yoshikazu Uchida, Céline Besson, Aurélie Robin, Anaïs Briot, Marie Gonthier, Laurence Lamant, Pierre Dubus, Bernard Monsarrat, and Alain Hovnanian. Elastase 2 is expressed in human and mouse epidermis and impairs skin barrier function in Netherton syndrome through filaggrin and lipid misprocessing. *The Journal of Clinical Investigation*, 120(3):871–882, 2010.

[179] Peck Y Ong, Takaaki Ohtake, Corinne Brandt, Ian Strickland, Mark Boguniewicz, Tomas Ganz, Richard L Gallo, and Donald Y M Leung. Endogenous antimicrobial peptides and skin infections in atopic dermatitis. *The New England journal of medicine*, 347(15):1151–60, October 2002.

[180] Volker Brinkmann, Ulrike Reichard, Christian Goosmann, Beatrix Fauler, Yvonne Uhlemann, David S Weiss, Yvette Weinrauch, and Arturo Zychlinsky. Neutrophil extracellular traps kill bacteria. *Science (New York, N.Y.)*, 303(5663):1532–5, March 2004.

[181] Sanja Kezic, Gráinne M O'Regan, René Lutter, Ivone Jakasa, Ellen S Koster, Sean P Saunders, Peter J Caspers, Patrick M J H Kemperman, Gerwin J Puppels, Aileen Sandilands, Huijia Chen, Linda E Campbell, Karin Kroboth, Rosemarie M Watson, Padraic G Fallon, W H Irwin McLean, and Alan D Irvine. Filaggrin loss-of-function mutations are associated with enhanced expression of IL-1 cytokines in the stratum corneum of patients with atopic dermatitis and in a murine model of filaggrin deficiency. *The Journal of Allergy and Clinical Immunology*, 129(4):1031–9.e1, April 2012.

[182] Cindy M de Jongh, Liubov Khrenova, Sanja Kezic, Thomas Rustemeyer, Maarten M Verberk, and Swen M John. Polymorphisms in the interleukin-1 gene influence the stratum corneum interleukin-1 alpha concentration in uninvolved skin of patients with chronic irritant contact dermatitis. *Contact dermatitis*, 58(5):263–8, May 2008.

[183] Parviz Ahmad-Nejad, Salima Mrabet-Dahbi, Kristine Breuer, Martina Klotz, Thomas Werfel, Udo Herz, Klaus Heeg, Michael Neumaier, and Harald Renz. The toll-like receptor 2 R753Q polymorphism defines a subgroup of patients with atopic dermatitis having severe phenotype. *The Journal of Allergy and Clinical Immunology*, 113(3):565–7, March 2004.

[184] Shizuo Akira and Kiyoshi Takeda. Toll-like receptor signalling. *Nature reviews. Immunology*, 4(7):499–511, July 2004.

[185] E. Vakirlis, E. Lazaridou, T. G. Tzellos, S. Gerou, D. Chatzidimitriou, and D. Ioannides. Investigation of cytokine levels and their association with SCORAD index in adults with acute atopic dermatitis. *Journal of the European Academy of Dermatology and Venereology*, 25:409–416, 2011.

[186] Haoli Jin, Rui He, Michiko Oyoshi, and Raif S Geha. Animal models of atopic dermatitis. *Journal of Investigative Dermatology*, 129(February 2008):31–40, 2009.

[187] Robin E Callard and John I Harper. The skin barrier, atopic dermatitis and allergy: a role for Langerhans cells? *Trends in immunology*, 28(7):294–8, July 2007.

[188] Jitlada Meephansan, Hidetoshi Tsuda, Mayumi Komine, Shin-Ichi Tominaga, and Mamitaro Ohtsuki. Regulation of IL-33 expression by IFN-γ and tumor necrosis factor-α in normal human epidermal keratinocytes. *Journal of Investigative Dermatology*, 132(11):2593–600, November 2012.

[189] William E Paul and Jinfang Zhu. How are T(H)2-type immune responses initiated and amplified? *Nature reviews. Immunology*, 10(4):225–235, 2010.

[190] W Zheng and R a Flavell. The transcription factor GATA-3 is necessary and sufficient for Th2 cytokine gene expression in CD4 T cells. *Cell*, 89:587–596, 1997.

[191] I-Cheng Ho, Tzong-Shyuan Tai, and Sung-Yun Pai. GATA3 and the T-cell lineage: essential functions before and after T-helper-2-cell differentiation. *Nature reviews. Immunology*, 9(feBRuARy):125–135, 2009.

[192] Sun-young Hwang, Kye-yeon Hur, Jeong-Rae Junil Kim, Kwang-hyun Cho, Seung-hwan Kim, and Joo-yeon Yoo. Biphasic RLR âĹŠ IFN- β Response Controls the Balance between Antiviral Immunity and Cell Damage. *The Journal of Immunology*, 190:1192–1200, 2013.

[193] Alex K Shalek, Rahul Satija, Xian Adiconis, Rona S Gertner, Jellert T Gaublomme, Raktima Raychowdhury, Schraga Schwartz, Nir Yosef, Christine Malboeuf, Diana Lu,

John J Trombetta, Dave Gennert, Andreas Gnirke, Alon Goren, Nir Hacohen, Joshua Z Levin, Hongkun Park, and Aviv Regev. Single-cell transcriptomics reveals bimodality in expression and splicing in immune cells. *Nature*, 498(7453):236–40, June 2013.

[194] Myong-Hee Sung, Ning Li, Qizong Lao, Rachel a Gottschalk, Gordon L Hager, and Iain D C Fraser. Switching of the Relative Dominance Between Feedback Mechanisms in Lipopolysaccharide-Induced NF-κB Signaling. *Science signaling*, 7(308):ra6, January 2014.

[195] Thomas Höfer, Holger Nathansen, Max Löhning, Andreas Radbruch, and Reinhart Heinrich. GATA-3 transcriptional imprinting in Th2 lymphocytes: a mathematical model. *PNAS*, 99(14):9364–8, July 2002.

[196] Johannes Müller and Thorsten Tjardes. Modeling the Cytokine Network In Vitro and In Vivo. *Journal of Theoretical Medicine*, 5(2):93–110, 2003.

[197] Panayiotis Christodoulides. Roles of combined positive and negative feedback control with time-delay in multi-scale biological control. Early Stage Assessment Report. Technical report, Imperial College London, 2014.

[198] a. Goldbeter and D. E. Koshland. Ultrasensitivity in biochemical systems controlled by covalent modification. Interplay between zero-order and multistep effects. *Journal of Biological Chemistry*, 259:14441–14447, 1984.

[199] Tomasz Lipniacki, Beata Hat, James R Faeder, and William S Hlavacek. Stochastic effects and bistability in T cell receptor signaling. *Journal of theoretical biology*, 254(1):110–22, September 2008.

[200] Qiang Zhang, Sudin Bhattacharya, Douglas E Kline, Robert B Crawford, Rory B Conolly, Russell S Thomas, Norbert E Kaminski, and Melvin E Andersen. Stochastic modeling of B lymphocyte terminal differentiation and its suppression by dioxin. *BMC systems biology*, 4:40, January 2010.

[201] Jin Nam, Baltazar D Aguda, Bjoern Rath, and Sudha Agarwal. Biomechanical thresholds regulate inflammation through the NF-kappaB pathway: experiments and modeling. *PloS one*, 4(4):e5262, January 2009.

[202] Najaf a Shah and Casim a Sarkar. Robust network topologies for generating switch-like cellular responses. *PLoS computational biology*, 7(6):e1002085, June 2011.

[203] Abhinav Tiwari, J Christian J Ray, Jatin Narula, and Oleg a Igoshin. Bistable responses in bacterial genetic networks: designs and dynamical consequences. *Mathematical biosciences*, 231(1):76–89, May 2011.

[204] Gheorghe Craciun, Yangzhong Tang, and Martin Feinberg. Understanding bistability in complex enzyme-driven reaction networks. *PNAS*, 103(23):8697–8702, 2006.

[205] J. E. Ferrell Jr. The Biochemical Basis of an All-or-None Cell Fate Switch in Xenopus Oocytes. *Science*, 280(5365):895–898, May 1998.

[206] James E Ferrell, Joseph R Pomerening, Sun Young Kim, Nikki B Trunnell, Wen Xiong, Chi-Ying Frederick Huang, and Eric M Machleder. Simple, realistic models of complex biological processes: positive feedback and bistability in a cell fate switch and a cell cycle oscillator. *FEBS letters*, 583(24):3999–4005, December 2009.

[207] Madalena Chaves and Jean-Luc Gouzé. Exact control of genetic networks in a qualitative framework: The bistable switch example. *Automatica*, 47(6):1105–1112, June 2011.

[208] Diego a Oyarzún, Madalena Chaves, and Marit Hoff-Hoffmeyer-Zlotnik. Multistability and oscillations in genetic control of metabolism. *Journal of theoretical biology*, 295:139–53, February 2012.

[209] Olaf Wolkenhauer, Mukhtar Ullah, Peter Wellstead, and Kwang-Hyun Cho. The dynamic systems approach to control and regulation of intracellular networks. *FEBS letters*, 579(8):1846–53, March 2005.

[210] Jörg Stelling, Uwe Sauer, Zoltan Szallasi, Francis J. Doyle, and John Doyle. Robustness of cellular functions. *Cell*, 118:675–685, 2004.

[211] Janeta Nikolovski, Georgios N Stamatas, Nikiforos Kollias, and Benjamin C Wiegand. Barrier function and water-holding and transport properties of infant stratum corneum are different from adult and continue to develop through the first year of life. *Journal of Investigative Dermatology*, 128(7):1728–36, July 2008.

[212] Mitsuhiro Denda, Sumiko Denda, Moe Tsutsumi, Makiko Goto, Junichi Kumamoto, Masashi Nakatani, Kentaro Takei, Hiroyuki Kitahata, Satoshi Nakata, Yusuke Sawabu, Yasuaki Kobayashi, and Masaharu Nagayama. Frontiers in epidermal barrier homeostasis - an approach to mathematical modelling of epidermal calcium dynamics. *Experimental dermatology*, 23(18):79–82, December 2013.

[213] a Becskei and L Serrano. Engineering stability in gene networks by autoregulation. *Nature*, 405(June):590–593, 2000.

[214] Dmitry Nevozhay, Rhys M Adams, Kevin F Murphy, Kresimir Josic, and Gábor Balázsi. Negative autoregulation linearizes the dose-response and suppresses the heterogeneity of gene expression. *PNAS*, 106(13):5123–5128, 2009.

[215] Alejandro Colman-lerner, Andrew Gordon, Eduard Serra, Tina Chin, Orna Resnekov, Drew Endy, C Gustavo Pesce, and Roger Brent. Regulated cell-to-cell variation in a cell-fate decision system. *Nature*, 437(September), 2005.

[216] Richard C Yu, C Gustavo Pesce, Alejandro Colman-lerner, Larry Lok, David Pincus, Eduard Serra, Mark Holl, Kirsten Benjamin, Andrew Gordon, and Roger Brent. Negative feedback that improves information transmission in yeast signalling. *Nature*, 456(December):755–761, 2008.

[217] Malte Paulsen, Stefan Legewie, Roland Eils, Emil Karaulanov, and Christof Niehrs. Negative feedback in the bone morphogenetic protein 4 (BMP4) synexpression group governs its dynamic signaling range and canalizes development. *PNAS*, 4, 2011.

[218] Dale Muzzey, Carlos a. Gómez-Uribe, Jerome T. Mettetal, and Alexander van Oudenaarden. A Systems-Level Analysis of Perfect Adaptation in Yeast Osmoregulation. *Cell*, 138:160–171, 2009.

[219] Jörg Schaber, Rodrigo Baltanás, Alan Bush, Edda Klipp, and Alejandro Colman-Lerner. Modelling reveals novel roles of two parallel signalling pathways and homeostatic feedbacks in yeast. *Molecular systems biology*, 8(622):622, 2012.

[220] Diana Clausznitzer, Olga Oleksiuk, Linda Lø vdok, Victor Sourjik, and Robert G. Endres. Chemotactic response and adaptation dynamics in Escherichia coli. *PLoS Computational Biology*, 6(5):1–11, 2010.

[221] Uri Alon, M G Surette, Naama Barkai, and S Leibler. Robustness in bacterial chemotaxis. *Nature*, 397(6715):168–71, January 1999.

[222] Alan M Weinstein. Modeling epithelial cell homeostasis: assessing recovery and control mechanisms. *Bulletin of mathematical biology*, 66(5):1201–40, September 2004.

[223] T M Yi, Y Huang, M I Simon, and John Doyle. Robust perfect adaptation in bacterial chemotaxis through integral feedback control. *PNAS*, 97(9):4649–4653, 2000.

[224] Wenzhe Ma, Ala Trusina, Hana El-Samad, Wendell a Lim, and Chao Tang. Defining network topologies that can achieve biochemical adaptation. *Cell*, 138(4):760–73, August 2009.

[225] D. R. Hoffman, L. M. Kroll, a. Basehoar, B. Reece, C. T. Cunningham, and D. W. Koenig. Immediate and extended effects of sodium lauryl sulphate exposure on stratum corneum natural moisturizing factor. *International Journal of Cosmetic Science*, 36:93–101, 2014.

[226] Danuta Gutowska-Owsiak, Anna L Schaupp, Maryam Salimi, Tharini a Selvakumar, Tess McPherson, Stephen Taylor, and Graham S Ogg. IL-17 downregulates filaggrin and affects keratinocyte expression of genes associated with cellular adhesion. *Experimental dermatology*, 21(2):104–10, February 2012.

[227] Malene Hvid, Christian Vestergaard, Kaare Kemp, Gitte B Christensen, Bent Deleuran, and Mette Deleuran. IL-25 in atopic dermatitis: a possible link between inflammation and skin barrier dysfunction? *Journal of Investigative Dermatology*, 131(1):150–7, January 2011.

[228] Dongsan Kim, Yung-Keun Kwon, and Kwang-Hyun Cho. Coupled positive and negative feedback circuits form an essential building block of cellular signaling pathways. *BioEssays : news and reviews in molecular, cellular and developmental biology*, 29(1):85–90, January 2007.

[229] Kim Newton and Vishva M Dixit. Signaling in innate immunity and inflammation. *Cold Spring Harbor perspectives in biology*, 4(3), March 2012.

[230] N. C J Filewod, Jelena Pistolic, and R. E W Hancock. Low concentrations of LL-37 alter IL-8 production by keratinocytes and bronchial epithelial cells in response to proinflammatory stimuli. *FEMS Immunology and Medical Microbiology*, 56:233–240, 2009.

[231] Zhe Zhang, Thomas B Clarke, and Jeffrey N Weiser. Cellular effectors mediating Th17-dependent clearance of pneumococcal colonization in mice. *The Journal of Clinical Investigation*, 119(7):1899–1909, 2009.

[232] Benedicte Mengel, Alexander Hunziker, Lykke Pedersen, Ala Trusina, Mogens H Jensen, and Sandeep Krishna. Modeling oscillatory control in NF-κB, p53 and Wnt signaling. *Current opinion in genetics & development*, 20(6):656–64, December 2010.

[233] D. E. Nelson. Oscillations in NF-ÂăB Signaling Control the Dynamics of Gene Expression. *Science*, 306(October):704–708, 2004.

[234] Raymond Cheong, Alexander Hoffmann, and Andre Levchenko. Understanding NF-kappaB signaling via mathematical modeling. *Molecular systems biology*, 4(192):192, January 2008.

[235] Reiko J Tanaka, Masahiro Ono, and Heather a Harrington. Skin barrier homeostasis in atopic dermatitis: feedback regulation of kallikrein activity. *PloS one*, 6(5):e19895, January 2011.

[236] Elisa Domínguez-Hüttinger, Masahiro Ono, Mauricio Barahona, and Reiko J Tanaka. Risk factor-dependent dynamics of atopic dermatitis : modelling multi-scale regulation of epithelium homeostasis. *Interface Focus*, 3(February):20120090, 2013.

[237] Jerrold R Turner. Intestinal mucosal barrier function in health and disease. *Nature reviews. Immunology*, 9(11):799–809, November 2009.

[238] J S Alexander and John W Elrod. Extracellular matrix, junctional integrity and matrix metalloproteinase interactions in endothelial permeability regulation. *Journal of anatomy*, 200(6):561–74, June 2002.

[239] Johannes Witt, Sandra Barisic, Eva Schumann, Frank Allgöwer, Oliver Sawodny, Thomas Sauter, and Dagmar Kulms. Mechanism of PP2A-mediated IKK beta dephosphorylation: a systems biological approach. *BMC systems biology*, 3:71, January 2009.

[240] L Olsen, J a Sherratt, and Philip K Maini. A mathematical model for fibro-proliferative wound healing disorders. *Bulletin of mathematical biology*, 58(4):787–808, July 1996.

[241] S Mrabet-Dahbi and M Maurer. Does allergy impair innate immunity? Leads and lessons from atopic dermatitis. *Allergy*, 65(11):1351–6, November 2010.

[242] Kazuyuki Aihara and Hideyuki Suzuki. Theory of hybrid dynamical systems and its applications to biological and medical systems. *Philosophical transactions. Series A, Mathematical, physical, and engineering sciences*, 368(1930):4893–914, November 2010.

[243] B Liu, J Willette-Brown, S Liu, X Chen, S M Fischer, and Yinling Hu. IKKα represses a network of inflammation and proliferation pathways and elevates c-Myc antagonists and differentiation in a dose-dependent manner in the skin. *Cell death and differentiation*, 18(12):1854–64, December 2011.

[244] Nicole L La Gruta, Katherine Kedzierska, John Stambas, and Peter C Doherty. A question of self-preservation: immunopathology in influenza virus infection. *Immunology and cell biology*, 85(October 2006):85–92, 2007.

[245] Jennifer M Lund, Lianne Hsing, Thuy T Pham, and Alexander Y Rudensky. Coordination of early protective immunity to viral infection by regulatory T cells. *Science (New York, N.Y.)*, 320(2008):1220–1224, 2008.

[246] Donald Y M Leung. Immunopathology of atopic dermatitis. *Springer Seminars in Immunopahtology*, 2:427–440, 1992.

[247] Heather A Harrington, Kenneth L Ho, Samik Ghosh, and K C Tung. Construction and analysis of a modular model of caspase activation in apoptosis. *Theoretical biology & medical modelling*, 5:26, January 2008.

[248] Liselotte E Jensen. Targeting the IL-1 family members in skin inflammation. *Curr Opin Investig Drugs*, 11(11):1211–1220, 2011.

[249] Ronina a Covar, Robert Strunk, Robert S Zeiger, Laura a Wilson, Andrew H Liu, Scott Weiss, James Tonascia, Joseph D Spahn, and Stanley J Szefler. Predictors of remitting, periodic, and persistent childhood asthma. *The Journal of Allergy and Clinical Immunology*, 125(2):359–366.e3, February 2010.

[250] Georgios N Stamatas, Charles Zerweck, Gary Grove, and Katharine M Martin. Documentation of impaired epidermal barrier in mild and moderate diaper dermatitis in vivo using noninvasive methods. *Pediatric dermatology*, 28(2):99–107, 2011.

[251] Thora Pommerencke, Kathi Westphal, Claudia Ernst, Kai Safferling, Hartmut Dickhaus, Thorsten Steinberg, Pascal Tomakidi, and Niels Grabe. Spatial quantification and classification of skin response following perturbation using organotypic skin cultures. *Bioinformatics (Oxford, England)*, 26(21):2760–6, November 2010.

[252] Malene Hvid, Claus Johansen, Bent Deleuran, Kaare Kemp, Mette Deleuran, and Christian Vestergaard. Regulation of caspase 14 expression in keratinocytes by inflammatory cytokines–a possible link between reduced skin barrier function and inflammation? *Experimental dermatology*, 20(8):633–6, August 2011.

[253] Jennifer Y Zhang, Cheryl L Green, Shiying Tao, and Paul a Khavari. NF-kappaB RelA opposes epidermal proliferation driven by TNFR1 and JNK. *Genes & development*, 18(1):17–22, January 2004.

[254] Sabina a Islam and Andrew D Luster. T cell homing to epithelial barriers in allergic disease. *Nature Medicine*, 18(5):705–715, 2012.

[255] Mao-Qiang Man, Yutaka Hatano, Seung Hun Lee, Mona Man, Sandra Chang, Kenneth R Feingold, Donald Y M Leung, Walter Holleran, Yoshikazu Uchida, and Peter M Elias. Characterization of a hapten-induced, murine model with multiple features of atopic dermatitis: structural, immunologic, and biochemical changes following single versus multiple oxazolone challenges. *Journal of Investigative Dermatology*, 128(1):79–86, January 2008.

[256] Eric L Simpson, Joanne R Chalmers, Jon M Hanifin, Kim S Thomas, Michael J Cork, W H Irwin Mclean, Sara J Brown, Zunqiu Chen, and Simpson E T Al. Emollient enhancement of the skin barrier from birth offers effective atopic dermatitis prevention. *Journal of Allergy and Clinical Immunology*, 134(4):818–823, 2014.

[257] Jane Yoo, Miyuki Omori, Dora Gyarmati, Baohua Zhou, Theingi Aye, Avery Brewer, Michael R Comeau, Daniel J Campbell, and Steven F Ziegler. Spontaneous atopic dermatitis in mice expressing an inducible thymic stromal lymphopoietin transgene specifically in the skin. *The Journal of experimental medicine*, 202(4):541–9, August 2005.

[258] Jonathan M. Spergel, Emiko Mizoguchi, Joanne P. Brewer, Thomas R. Martin, Atul K. Bhan, and Raif S. Geha. Epicutaneous sensitization with protein antigen induces localized allergic dermatitis and hyperresponsiveness to methacholine after single exposure to aerosolized antigen in mice. *Journal of Clinical Investigation*, 101:1614–1622, 1998.

[259] Georgios N Stamatas, Janeta Nikolovski, Michael a Luedtke, Nikiforos Kollias, and Benjamin C Wiegand. Infant skin microstructure assessed in vivo differs from adult skin in organization and at the cellular level. *Pediatric dermatology*, 27(2):125–31, 2010.

[260] Georgios N Stamatas. The Structural and Functional Development of Skin During the First Year of Life: Investigations Using Non-invasive Methods. In Miranda A. Farage, Kenneth W. Miller, and Howard I. Maibach, editors, *Textbook of Aging Skin*, chapter 69: The St, pages 715–724. Springer Berlin Heidelberg, Berlin, Heidelberg, 2010.

[261] Peter J Caspers, G W Lucassen, and G J Puppels. Combined in vivo confocal Raman spectroscopy and confocal microscopy of human skin. *Biophysical journal*, 85(1):572–80, July 2003.

[262] Gráinne M O'Regan, Patrick M J H Kemperman, Aileen Sandilands, Huijia Chen, Linda E Campbell, Karin Kroboth, Rosemarie M Watson, Marion Rowland, Gerwin J Puppels, W H Irwin McLean, Peter J Caspers, and Alan D Irvine. Raman profiles of the stratum corneum define 3 filaggrin genotype-determined atopic dermatitis endophenotypes. *The Journal of Allergy and Clinical Immunology*, 126(3):574–80.e1, September 2010.

[263] Nikiforos Kollias and Georgios N Stamatas. Optical non-invasive approaches to diagnosis of skin diseases. *The journal of investigative dermatology. Symposium proceedings / the Society for Investigative Dermatology, Inc. [and] European Society for Dermatological Research*, 7(1):64–75, December 2002.

[264] Duncan R Hewett, Alison L Simons, Niamh E Mangan, Helen E Jolin, Shelia M Green, Padraic G Fallon, and Andrew N J McKenzie. Lethal, neonatal ichthyosis with increased proteolytic processing of filaggrin in a mouse model of Netherton syndrome. *Human molecular genetics*, 14(2):335–46, January 2005.

[265] Chrystelle Bonnart, Maaike Kreft, Mari Kishibe, Pascal Descargues, Akemi Ishida-yamamoto, Peter M Elias, Yann Barrandon, Giovanna Zambruno, Arnoud Sonnenberg, and Alain Hovnanian. Spink5 -deficient mice mimic Netherton syndrome through degradation of desmoglein 1 by epidermal protease hyperactivity. *Nature Genetics*, 37(1):56–65, 2005.

[266] David H Broide, Toby Lawrence, Taylor Doherty, Jae Youn Cho, Marina Miller, Kirsti Mcelwain, Shauna Mcelwain, Michael Karin, and Michael Karints. Allergen-Induced Peribronchial Fibrosis and Mucus Production Mediated by IκB Kinase β- Dependent Genes in Airway Epithelium. *PNAS*, 102(49):17723–17728, 2005.

[267] Anna Velcich, WanCai Yang, Joerg Heyer, Alessandra Fragale, Courtney Nicholas, Stephanie Viani, Raju Kucherlapati, Martin Lipkin, Kan Yang, and Leonard Augenlicht. Colorectal cancer in mice genetically deficient in the mucin Muc2. *Science (New York, N.Y.)*, 295(5560):1726–9, March 2002.

[268] Guy-Bart V Stan, F Belmudes, R Fonteneau, F Zeggwagh, M-a Lefebvre, C Michelet, and D Ernst. Modelling the influence of activation-induced apoptosis of CD4+ and CD8+ T-cells on the immune system response of a HIV-infected patient. *IET systems biology*, 2(2):94–102, March 2008.

[269] Bernd Schmeck, Ralph Gross, Phillipe Dje N Guessan, Andreas C Hocke, Sven Hammerschmidt, Tim J Mitchell, Simone Rosseau, Norbert Suttorp, Stefan Hippenstiel, and Phillipe Dje N ĐĹ Guessan. Streptococcus pneumoniae- Induced Caspase 6-Dependent Apoptosis in Lung Epithelium Streptococcus pneumoniae- Induced Caspase 6-Dependent Apoptosis in Lung Epithelium. *Infection and immunity*, 72(9):4940–4947, 2004.

[270] Cécile Attali, Claire Durmort, Thierry Vernet, and Anne Marie Di Guilmi. The interaction of Streptococcus pneumoniae with plasmin mediates transmigration across endothelial and epithelial monolayers by intercellular junction cleavage. *Infection and immunity*, 76(11):5350–6, November 2008.

[271] David D Tieu, Robert C Kern, and Robert P Schleimer. Alterations in epithelial barrier function and host defense responses in chronic rhinosinusitis. *The Journal of Allergy and Clinical Immunology*, 124(1):37–42, July 2009.

[272] Marco R. Oggioni, Guido Memmi, Tiziana Maggi, Damiana Chiavolini, Francesco Iannelli, and Gianni Pozzi. Pneumococcal zinc metalloproteinase ZmpC cleaves human matrix metalloproteinase 9 and is a virulence factor in experimental pneumonia. *Molecular Microbiology*, 49(3):795–805, January 2004.

[273] Jörg Reutershan, Abdul Basit, Elena V Galkina, and Klaus Ley. Sequential recruitment of neutrophils into lung and bronchoalveolar lavage fluid in LPS-induced acute lung injury. *American journal of physiology. Lung cellular and molecular physiology*, 289:L807–L815, 2005.

[274] a Lindén. Role of interleukin-17 and the neutrophil in asthma. *International archives of allergy and immunology*, 126(3):179–84, November 2001.

[275] Rachel L Zemans, Natalie Briones, Megan Campbell, Jazalle McClendon, Scott K Young, Tomoko Suzuki, Ivana V Yang, Stijn De Langhe, Susan D Reynolds, Robert J Mason, Michael Kahn, P M Henson, Sean P Colgan, and Gregory P Downey. Neutrophil transmigration triggers repair of the lung epithelium via beta-catenin signaling. *PNAS*, 108(38):15990–5, September 2011.

[276] Elzbieta Kolaczkowska and Paul Kubes. Neutrophil recruitment and function in health and inflammation. *Nature reviews. Immunology*, 13(3):159–75, March 2013.

[277] Amanda M Burnaugh, Laura J Frantz, and Samantha J King. Growth of Streptococcus pneumoniae on human glycoconjugates is dependent upon the sequential activity of bacterial exoglycosidases. *Journal of bacteriology*, 190(1):221–30, January 2008.

[278] Ha-Sheng Li-Korotky, Juliane M Banks, Chia-Yee Lo, Fan-Rui Zeng, Donna B Stolz, J Douglas Swarts, and William J Doyle. Interaction of pneumococcal phase variation and middle ear pressure/gas composition: an in vitro model of simulated otitis media. *Microbial pathogenesis*, 45(3):201–6, September 2008.

[279] Lucy J Hathaway, Silvio D Brugger, Brigitte Morand, Mathieu Bangert, Jeannine U Rotzetter, Christoph Hauser, Werner a Graber, Suzanna Gore, Aras Kadioglu, and Kathrin Mühlemann. Capsule type of Streptococcus pneumoniae determines growth phenotype. *PLoS pathogens*, 8(3):e1002574, January 2012.

[280] Tamene Melkamu, Diane Squillace, Hirohito Kita, and Scott M O'Grady. Regulation of TLR2 expression and function in human airway epithelial cells. *The Journal of membrane biology*, 229(2):101–13, May 2009.

[281] Donghong He, Yanlin Su, Peter V Usatyuk, Ernst Wm Spannhake, Paul Kogut, Julian Solway, Viswanathan Natarajan, and Yutong Zhao. Lysophosphatidic acid enhances

pulmonary epithelial barrier integrity and protects endotoxin-induced epithelial barrier disruption and lung injury. *The Journal of biological chemistry*, 284(36):24123–32, September 2009.

[282] Tamar Tak, Kiki Tesselaar, Janesh Pillay, José a M Borghans, and Leo Koenderman. What's your age again? Determination of human neutrophil half-lives revisited. *Journal of leukocyte biology*, 94(4):595–601, October 2013.

[283] I H Heijink, S M Brandenburg, D S Postma, and Antoon J M van Oosterhout. Cigarette smoke impairs airway epithelial barrier function and cell-cell contact recovery. *The European respiratory journal*, 39(2):419–28, March 2012.

[284] a Nusrat, C a Parkos, T W Liang, D K Carnes, and J L Madara. Neutrophil migration across model intestinal epithelia: monolayer disruption and subsequent events in epithelial repair. *Gastroenterology*, 113(5):1489–500, November 1997.

[285] Masahiro Komori, Yoshihisa Nakamura, Jesse Ping, Ling Feng, Katsuhiro Toyama, Youngki Kim, Patricia Ferrieri, and Jizhen Lin. Receptor 2 in the Mouse Middle Ear Epithelial Cells. *Pediatric research*, 69(2):101–105, 2011.

[286] Jacques-A Sepulchre, Sylvie Reverchon, and William Nasser. Modeling the onset of virulence in a pectinolytic bacterium. *Journal of theoretical biology*, 244(2):239–57, January 2007.

[287] Victoriya V. Volkova, Zhao Lu, Cristina Lanzas, H. Morgan Scott, and Yrjö T. Gröhn. Modelling dynamics of plasmid-gene mediated antimicrobial resistance in enteric bacteria using stochastic differential equations. *Scientific Reports*, 3, August 2013.

[288] Lu Yin, Shuoyu Xu, Jierong Cheng, Dahai Zheng, Gino V Limmon, Nicola H N Leung, Jagath C Rajapakse, Vincent T K Chow, Jianzhu Chen, and Hanry Yu. Spatiotemporal quantification of cell dynamics in the lung following influenza virus infection. *Journal of biomedical optics*, 18(4):046001, April 2013.

[289] L Gonzalez-Mariscal, R G Contreras, J J Bolívar, a Ponce, B Chávez De Ramirez, and M Cereijido. Role of calcium in tight junction formation between epithelial cells. *The American journal of physiology*, 259:C978–C986, 1990.

[290] D Flores-Benítez, a Ruiz-Cabrera, C Flores-Maldonado, L Shoshani, M Cereijido, and R G Contreras. Control of tight junctional sealing: role of epidermal growth factor. *American journal of physiology. Renal physiology*, 292:F828–F836, 2007.

[291] Eberhard O. Voit. Mesoscopic modeling as a starting point for computational analyses of cystic fibrosis as a systemic disease. *Biochimica et Biophysica Acta - Proteins and Proteomics*, 1844(1):258–270, 2014.

[292] Kenneth L Ho and Heather a Harrington. Bistability in apoptosis by receptor clustering. *PLoS computational biology*, 6(10):e1000956, January 2010.

[293] Nick I Markevich, Jan B Hoek, and Boris N Kholodenko. Signaling switches and bistability arising from multisite phosphorylation in protein kinase cascades. *The Journal of cell biology*, 164(3):353–9, February 2004.

[294] Vijay Chickarmane, Carl Troein, Ulrike a Nuber, Herbert M Sauro, and Carsten Peterson. Transcriptional dynamics of the embryonic stem cell switch. *PLoS computational biology*, 2(9):e123, September 2006.

[295] Zoltan Szallasi, Vipul Periwal, and Jörg Stelling. *System Modeling in Cellular Biology: From Concepts to Nuts and Bolts*. The MIT Press, 2006.

[296] Carlo Cosentino and Declan Bates. *Feedback Control in Systems Biology*. CRC Press, 2012.

[297] Steven Strogatz. *Nonlinear dynamics and chaos*. 2000.

[298] J D Murray. *Mathematical biology*. 3 edition, 2003.

[299] Graciela Andonegui, Kim Goring, Dan Liu, Donna-Marie McCafferty, and Brent W Winston. Characterization of S. pneumoniae pneumonia-induced multiple organ dysfunction syndrome: an experimental mouse model of gram-positive sepsis. *Shock (Augusta, Ga.)*, 31(4):423–8, April 2009.

[300] David L Tamang, Waheed Pirzai, Gregory P Priebe, David C Traficante, Gerald B Pier, John R Falck, Christophe Morisseau, Bruce D Hammock, Beth a McCormick, Karsten Gronert, and Bryan P Hurley. Hepoxilin A(3) facilitates neutrophilic breach of lipoxygenase-expressing airway epithelial barriers. *Journal of immunology (Baltimore, Md. : 1950)*, 189(10):4960–9, November 2012.

[301] Leonardo H Travassos, Stephen E Girardin, Dana J Philpott, Didier Blanot, Marie-Anne Nahori, Catherine Werts, and Ivo G Boneca. Toll-like receptor 2-dependent bacterial sensing does not occur via peptidoglycan recognition. *EMBO reports*, 5(10):1000–6, October 2004.